Ontwerp van coöperatieve zuur-base-katalysatoren
voor aldolcondensaties

Design of Cooperative Acid-Base Catalysts for Aldol Condensations

Jeroen Lauwaert

Promotoren: prof. dr. ir. J. W. Thybaut, prof. dr. ir. G. B. Marin
Proefschrift ingediend tot het behalen van de graad van
Doctor in de Ingenieurswetenschappen: Chemische Technologie

Vakgroep Chemische Proceskunde en Technische Chemie
Voorzitter: prof. dr. ir. G. B. Marin
Faculteit Ingenieurswetenschappen en Architectuur
Academiejaar 2014 - 2015

UNIVERSITEIT
GENT

ISBN 978-90-8578-824-9
NUR 913, 952
Wettelijk depot: D/2015/10.500/68

Promotoren:

Prof. Dr. Ir. Joris W. Thybaut	Universiteit Gent
Prof. Dr. Ir. Guy B. Marin	Universiteit Gent

Examencommissie:

Prof. Dr. Ir. Patrick De Baets, voorzitter	Universiteit Gent
Prof. Dr. Marie-Françoise Reyniers*, secretaris	Universiteit Gent
Prof. Dr. Pegie Cool	Universiteit Antwerpen
Prof. Dr. Ir. Christopher W. Jones*	Georgia Institute of Technology
Prof. Dr. Ir. Sven Mangelinckx	Universiteit Gent
Prof. Dr. Ir. Guy B. Marin, promotor	Universiteit Gent
Prof. Dr. Ir. Joris W. Thybaut*, promotor	Universiteit Gent
Prof. Dr. Pascal Van Der Voort*	Universiteit Gent

* leescommissie

Universiteit Gent
Faculteit Ingenieurswetenschappen en Architectuur
Vakgroep Chemische Proceskunde en Technische Chemie
Laboratorium voor Chemische Techniek
Technologiepark 914
B-9052 Gent
België
Tel.: +32 (0)9 331 17 57
Fax: +32 (0)9 331 17 59
http://www.lct.ugent.be

This work was supported by the Long Term Structural Methusalem Funding by the Flemish Government, the U.S. Department of Energy Office of Basic Energy Sciences through Catalysis Contract Number DEFG02-03ER15459, the Fund for Scientific Research Flanders (FWO) through Grant Number 3G006813 and a travel grant for a long stay abroad (Grant Number V428614N).

Dankwoord

Acknowledgments

Het lijkt alsof het gisteren was dat Joris mij tijdens de tussentijdse posterpresentatie van mijn masterthesis vroeg of ik eventueel wou doctoreren. Dit is ondertussen reeds meer dan vier jaar geleden en als ik er nu op terugkijk ben ik zeker en vast tevreden dat ik deze uitdaging heb aangenomen. De voorbije vier jaar was een periode waarin ik mij zowel op wetenschappelijk vlak als op persoonlijk vlak heb kunnen ontplooien. Nu het einde in zicht is, had ik graag de volgende personen bedankt voor hun directe en indirecte bijdrage tot dit werk.

Allereerst wil ik professor Guy B. Marin bedanken om mij de kans te bieden om aan het LCT te doctoreren. Het nalezen van mijn manuscripten en het houden van de bijhorende wetenschappelijke discussies was uitermate nuttig om de kwaliteit van dit werk op te krikken.

Als tweede persoon wil ik prof. Joris Thybaut bedanken. Eerst en vooral om in mij te geloven en mij te overhalen dat een doctoraat voor mij de beste keuze was. Daarnaast ook omdat u mij geleerd hebt om mijn grenzen te verleggen en, natuurlijk ook, voor alle wetenschappelijke discussies die we doorheen de jaren gehad hebben.

Bedankt prof. Pascal Van Der Voort om mij in de COMOC groep op te nemen. Toen ik vier jaar geleden aan mijn doctoraat begon, was mijn kennis omtrent katalysatorsynthese eerder beperkt. Maar dankzij uw hulp is daar heel snel verandering in gekomen.

Additionally, I would like to thank three other key persons of the COMOC group, namely Els De Canck, Dolores Esquivel and Judith Ouwehand. Els, eerst en vooral, heel erg bedankt om mij als beginnende doctoraatstudent “de kneepjes van de katalysatorsynthese” aan te leren. Maar daarnaast ook voor de goede en leuke samenwerking die we de jaren daarna nog gehad hebben. *Dolores, many thanks for all the help with and discussions on the synthesis of*

the catalysts and the interpretation of the NMR spectra. Judith, onze samenwerking is nog maar net gestart maar ik denk dat er ondertussen toch al mooi werk op tafel ligt. Veel succes met het vervolg van jouw doctoraat.

I would like to thank prof. Chris Jones for hosting my research stay at Georgia Tech. It was a very pleasant and instructive experience. Also many thanks to dr. Eric Moschetta for all the support and the interesting discussions. I think it turned out to be a fruitful collaboration.

Bedankt aan alle thesisstudenten die een bijdrage leverden aan dit werk: Eli Van de Perre, Lara François, Yu Yan To, Handan Nalli, Jonathan De Vydt en Elien Laforce.

I would like to express my gratitude to the members of my examination committee. Thanks for all your valuable comments and suggestions on the PhD dissertation.

Mijn appreciatie gaat ook uit naar het technisch personeel en het secretariaat van het LCT. Wanneer ik een probleem had stonden jullie steeds klaar om mij uit de nood te helpen. Bedankt ook Tom Planckaert van de vakgroep anorganische en fysische chemie voor het uitvoeren van de stikstofsorptie en CHNS elementaire analyse experimenten.

Bedankt professor Geraldine Heynderickx voor de interessante samenwerking. Ik denk dat we met trots mogen terugkijken naar de lessen Stoftransport.

I would also like to thank all my colleagues and friends of LCT, COMOC and Georgia Tech for all the scientific and non-scientific talks and the amusing after-school activities. I wish you all the best in your personal lives and your careers. In het bijzonder zou ik nog Bart, Kenneth, Kristof, Aaron, Kae, Jonas en Jolien willen bedanken voor de gezellige middagpauzes. Jullie absurde gevoel voor humor zorgde ervoor dat de sfeer steeds dik in orde was.

Tenslotte wil ik mijn ouders, mijn twee broers en hun gezinnetjes bedanken omdat ze hun jongste zoon en hun kleine broertje onvoorwaardelijk blijven steunen. En, *last but not least*, mijn allerliefste schatje, Eline. Bedankt om er altijd te zijn voor mij. Dikke kus!

Jeroen

Gent, Mei 2015

Table of Contents

List of figures

List of schemes

List of tables

List of symbols

Roman symbols

a	thermodynamic activity	[mol mol^{-1} or mol l^{-1}]
A	parameter in the Hayden-O'Connell equation of state	[-]
A_i	pre exponential factor of step i	[variable]
a_{ij}	interaction parameter 1 in the NRTL model	[-]
B	the second virial coefficient	[cm³ mol^{-1}]
b_0	equivalent hard-sphere volume of molecules	[cm³ mol^{-1}]
b_{ij}	interaction parameter 2 in the NRTL model	[K]
C_i	concentration of component *i*	[mol l^{-1}]
c_{ij}	interaction parameter 3 in the NRTL model	[-]
E_a	activation energy	[J mol^{-1}]
EE	experimental error in percentage	[-]
f	fugacity	[Pa]
G_{ij}	binary interaction as described in the NRTL model	[-]
ΔH	enthalpy change	[J mol^{-1}]
k	rate coefficient	[variable]
K_{ads}	adsorption equilibrium coefficient	[variable]
k_B	Boltzmann constant = 1.3806 x 10^{-23}	[m² kg s^{-2} K^{-1}]
K_i^{CT}	equilibirum constant for the chemical theory of vapor imperfections	[atm^{-1}]
l_i	quantity in the UNIQUAC model	[-]
n_i	number of moles of component *i*	[mol]
N	number of experiments	[-]
N_0	Avogadro's number = 6.0225 x 10^{23}	[molecules mol^{-1}]

P	pressure	[Pa]
pK_a	the logartihmic acid dissociation constant	[-]
q_i	measure of the molecular surface area	[-]
R	universal gas constant	[J mol^{-1} K^{-1}]
r_i	measure of the molecular van der Waals volume	[-]
R_i	net rate of formation of component *i*	[mol s^{-1} gcat^{-1}]
ΔS	entropy change	[J mol^{-1} K^{-1}]
T	temperature	[K]
t	time	[s]
$T^{*\prime}$	reduced temperature	[-]
TOF	turnover frequency	[s^{-1}]
Δu_{ij}	binary interaction parameter	[J mol^{-1}]
v	molar volume	[cm³ mol^{-1}]
X	conversion	[-]
x_i	mole fraction of component i	[-]
y	dependent variable	[variable]
$\hat{y}$	simulated value	[variable]
z	coordination number in the UNIQUAC model, typically equal to 10	[-]
Z	compressibility factor	[-]

Greek symbols

α_{ij}	nonrandomness factor in the NRTL model	[-]
β	parameter in the model	[variable]
γ_i	activity coefficient	[-]
γ_i^C	combinatorial part of the activity coefficient	[-]
γ_i^R	residual part of the activity coefficient	[-]
ε	experimental error	[variable]
ϵ	energy parameter in the HOC equation of state	[ergs molecule^{-1}]
θ_i	area fraction	[-]

μ	molecular dipole moment	[D]
ξ	angle averaged polar effect in the HOC equation of state	[-]
σ	standard deviation	[variable]
σ	molecular size parameter in the HOC equation of state	[Å]
τ_{ij}	measure of the binary interaction	[-]
Φ_i	segment fraction in the UNIQUAC model	[-]
Φ_i	vapor fugacity coefficient	[-]
ω	acentric factor	[-]

Superscripts

0	initial condition
°	at the standard state
G	gas phase
L	liquid phase
S	saturation

Subscripts

ace	acetone
ads	adsorption
av	average
benz	4-nitrobenzaldehyde
boun	bound pair contribution
c	critical property
chem	chemically bound pair contribution
free	free unbound pair contribution
furf	furfural
i	component *i*

ij	interaction of species *i* with species *j*
im	imine
metastable	metastable bound pair contribution
nC_6	*n*-hexane
OH	silanol
prom	promoted
sat	at saturation conditions
total	sum of all contributions
unprom	unpromoted
water	water

List of structures

acetone 

alcohol 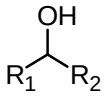

amine 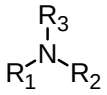

(3-aminopropyl)dimethylethoxysilane (APDMES) 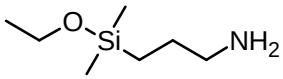

(3-aminopropyl)triethoxysilane (APTES) 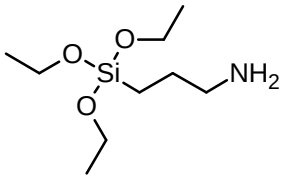

benzene 

1,4-bis(triethoxysilyl)benzene (BTEB) 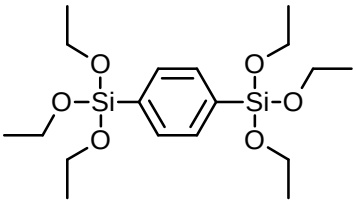

1,2-bis(triethoxysilyl)ethane (BTEE) 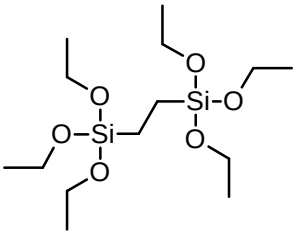

carbinolamine 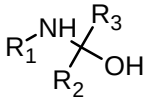

carboxylic acid 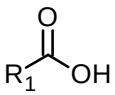

citral 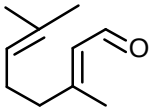

N-cyclohexylaminopropyltrimethoxysilane (CAPTMS)

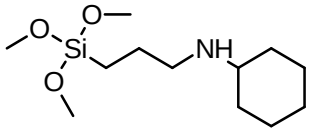

cysteamine

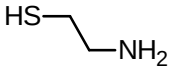

cysteine

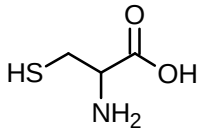

diethyl aminomethylphosphonate

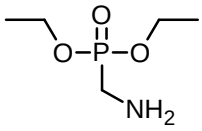

(N,N-diethyl-3-aminopropyl)trimethoxysilane (DEAPTMS)

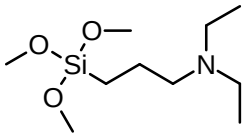

diisopropylethylamine (DIPEA)

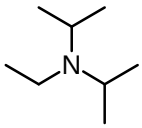

1,4-dimethoxybenzene

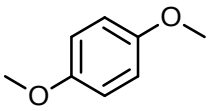

dimethyl sulfoxide (DMSO)

enamine

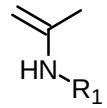

enol

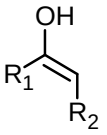

enolate

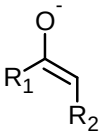

ethanol

ethanolamine

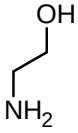

ethylamine

fructose

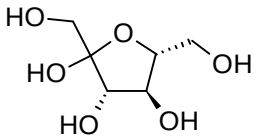

2-furaldehyde (furfural)

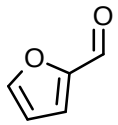

4-(furan-2-yl)-4-hydroxybutan-2-one (aldol)

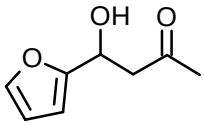

4-(furan-2-yl)but-3-en-2-one (ketone)

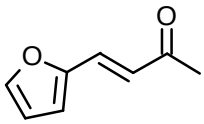

glucose

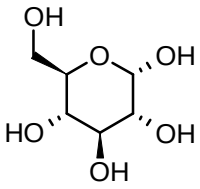

glycine

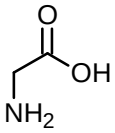

heterocycle

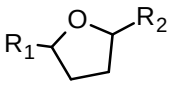

1,1,1,3,3,3-hexamethyldisilazane (HMDS)

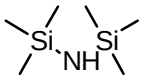

n-hexane

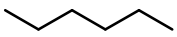

β-hydroxy carbonyl (aldol)

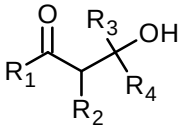

4-hydroxy-3-methyl-4-(4-nitrophenyl)butane-2-one (aldol)

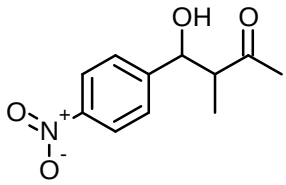

4-hydroxy-4-(4-nitrophenyl)butane-2-one (aldol)

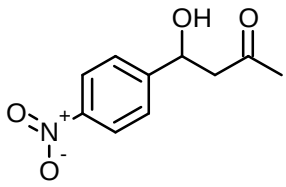

2-hydroxy-4’-(2-hydroxyethoxy)-2-methylpropiophenone)

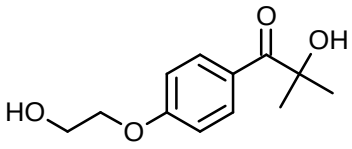

5-hydroxymethyl)furfural (HMF)

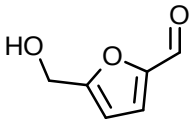

imine

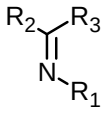

iminium ion

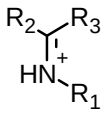

(3-iodopropyl)trimethoxysilane

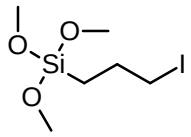

α-ionone

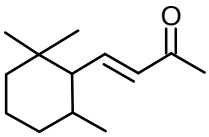

ketone

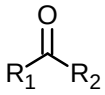

methyl 2-aminoacetate

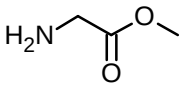

methyl 4-nitrobenzoate

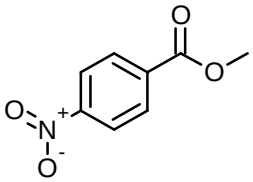

N-methylaminopropyltrimethoxysilane (MAPTMS)

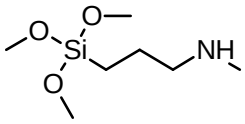

4-nitrobenzaldehyde

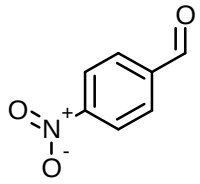

4-(4-nitrophenyl)-3-buten-2-one (ketone)

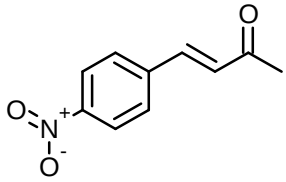

6-oxoheptanal

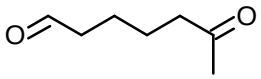

1,4-pentandien-3-on-1,5-di-2-furanyl

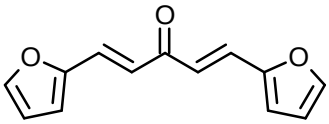

N-phenylaminopropyltrimethoxysilane (PAPTMS)

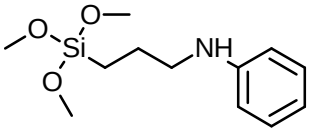

phosphoric acid

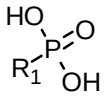

proline

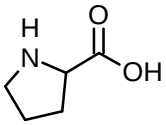

n-propylamine

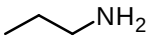

tetraethyl orthosilicate (TEOS)

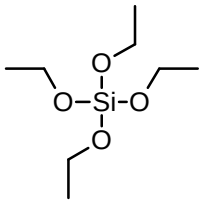

toluene

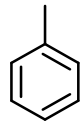

α,β-unsaturated carbonyl

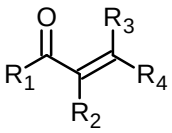

vinyltriethoxysilane (VTES)

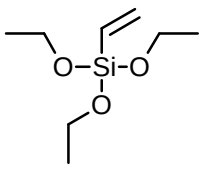

xylose

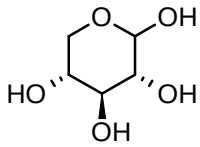

Glossary of terms

Acid strength	The ability or tendency of a functional group to lose a proton.
Activation energy	For an elementary step, the difference in internal energy between transition state and reactants. A measure for the temperature dependence of the rate coefficient.
Active site	Functional group at the surface of a solid support or on an enzyme which is responsible for the catalytic activity.
Activity coefficient	Coefficient explicitly accounting for the non-ideality of the liquid phase, often denoted as γ.
Activity library	Set of kinetic data obtained with the catalysts in the catalyst library.
Aldol condensation	C-C coupling reaction between two carbonyl components yielding a β-hydroxy carbonyl component which can, subsequently, lose water with formation of a α,β-unsaturated carbonyl component.
Arrhenius relation	Relationship that expresses the dependence of a rate coefficient k on the temperature T and activation energy, Ea: $k=A \exp(Ea/RT)$ with R is the universal gas constant, T the temperature and A the pre-exponential factor.
Base strength	The ability or tendency of a functional group to receive a proton.
Catalyst	A source of active centers regenerated at the

	end of a closed reaction sequence.
Catalyst descriptor	Parameter in the kinetic model which specifically account for the effect of the catalyst properties on the kinetics.
Catalyst library	Set of catalysts.
CHNS elemental analysis	Method based on the combustion of organic components to determine the weight percentage of carbon, hydrogen, nitrogen and sulfur in a sample.
Conversion	Measure for the amount of a reactant that has been transformed into products as a result of a chemical reaction.
Cooperativity	The interaction process by which binding of a reactant to one site, *i.e.* the promoting site, influences binding at a second site, *i.e.* the active site.
Delplot technique	Method for reaction pathway analysis.
Diastereoisomer or diastereomer	One of a pair of stereoisomers which are not related as mirror images. Diastereoisomers are characterized by differences in physical properties, and by some differences in chemical behavior towards achiral as well as chiral reagents.
Diffuse Reflectance Infrared Fourier Transform (DRIFT) spectroscopy	Infrared spectroscopic technique used to identify chemical functional groups present in porous solid materials.
Elementary step	The irreducible act of reaction in which reactants are transformed into products directly, i.e., without passing through an intermediate that is susceptible to isolation.
Enantiomer	One of a pair of molecular entities which are

	mirror images of each other and non-superposable.
Group contribution method	A technique to estimate and predict thermodynamic and other properties from molecular structures, i.e., atoms, atomic groups, bond type etc.
High performance liquid chromatography (HPLC)	The process in which the components of a liquid mixture are separated from one another by injecting the sample into a carrier liquid which is passing through a high-density packed column with different affinities for adsorption of the components to be separated.
Inhibition	The decrease in rate of reaction due to the addition of a substance, *i.e.*, inhibitor, by virtue of its effect on the concentration of a reactant, catalyst or reaction intermediate.
Kinetic descriptor	Parameter in the kinetic model which solely depend on the reaction mechanism.
Lignocellulosic biomass	Non-edible biomass composed of carbohydrate polymers (cellulose, hemicellulose), and an aromatic polymer (lignin).
Mesopores	Pores of intermediate size, i.e. between 2 nm and 50 nm.
Nitrogen adsorption-desorption measurments	Experimental method to determine the specific surface, average pore size and pore size distribution of a porous solid material.
NMR spectroscopy	Technique that exploits the magnetic properties of atomic nuclei in order to determine the physical and chemical properties of the atoms or molecules in which they are contained.
Nucleophile	Reactant that forms a bond to its reaction

	partner, *i.e.*, the electrophile, by donating both bonding electrons.
Parameter estimation	Process of estimating the parameters of a relation between independent and dependent variables as to describe a chemical reaction as good as possible.
Pre-exponential factor	The temperature-independent factor of a rate, also called the frequency factor.
Promoting site	Functional group at the surface of a solid support or on an enzyme which influences the interactions of the reactants with the catalytically active site.
Raman spectroscopy	Technique based on inelastic scattering of photons for the identification of chemical function groups.
Reaction mechanism	A sequence of elementary steps in which reactants are converted into products, through the formation of intermediates.
Reaction rate	The number of moles of a component created by a chemical reaction per unit of time and catalyst mass.
Silanol	Hydroxy group bonded to a silicon atom.
Stereoselectivity	The preferential formation in a chemical reaction of one stereoisomer over another. When the stereoisomers are enantiomers, the phenomenon is called enantioselectivity and is quantitatively expressed by the enantiomer excess; when they are diastereoisomers, it is called diastereoselectivity and is quantitatively expressed by the diastereoisomer excess.
Support	Also called carrier material, usually of high

	surface area, on which the active catalytic material, present as the minor component, is dispersed. The support may contribute to the overall catalytic activity.
Turnover frequency	The number of molecules of a component reacting per active site in unit of time.

Summary

As fossil resources are facing depletion due to an increasing world population and the associated energy and chemicals demand, it is of strategic importance to search for renewable alternatives. An example of a promising renewable resource for the production of liquid hydrocarbon fuels and chemicals is lignocellulosic biomass. This type of non-edible biomass can, *e.g.*, be converted into aqueous furan mixtures, comprising compounds such as 2-furaldehyde (furfural) and 5-(hydroxymethyl)furfural (HMF) [1-4]. Subsequently, the carbonyl group in the furan components can be used to perform an aldol condensation with molecules such as acetone, in order to produce components of an adequate carbon number for further use [1, 5-7]. After the (partial) removal of the oxygen atoms in the obtained molecules liquid hydrocarbon fuels and/or desired chemicals are obtained. The above demonstrates how C-C coupling reactions, such as aldol condensations, will potentially play a crucial role in the transition from a fossil resource based towards a more sustainable society.

At present, at the industrial scale, aldol condensations are typically catalyzed by strong, homogeneous base catalysts such as KOH, $Ca(OH)_2$, NaOH, or Na_2CO_3. However, in a pursuit towards more sustainable chemical processes, heterogeneous alternatives for these homogenous catalysts are being developed. Class I aldolases are enzymes which are found in nature and contain both an amine site (base) as well as an acid site [8]. These two sites are able to cooperatively catalyze aldol condensations in a very efficient way [9]. This observation has led to an increasing interest in heterogeneous cooperative acid-base catalysts and provided the necessary inspiration for the design of novel catalysts in this respect.

In the present work, a series of cooperative acid-base catalysts (type AB) has been synthesized by functionalizing a commercially available mesoporous silica, *i.e.*, silicagel 60, with various amounts of a primary amine-containing silane, (3-aminopropyl)triethoxysilane (APTES). Unpromoted base (type B) versions of the cooperative catalysts were prepared by

treating them with hexamethyldisilazane (HMDS) to endcap the silanols on the silica surface. The catalytic performance of all materials is tested in the aldol condensation of 4-nitrobenzaldehyde with acetone, see Figure 1. Irrespective of the amine density, identical, moderate turnover frequencies (TOF) are obtained if the silica exclusively has amines on its surface. Comparison of the turnover frequencies of the other materials confirms that the silanols, which are intrinsically present in silica materials, have a promoting effect on the activity of the actually active sites, *i.e.*, the amines. This promotion does not affect the product selectivity.

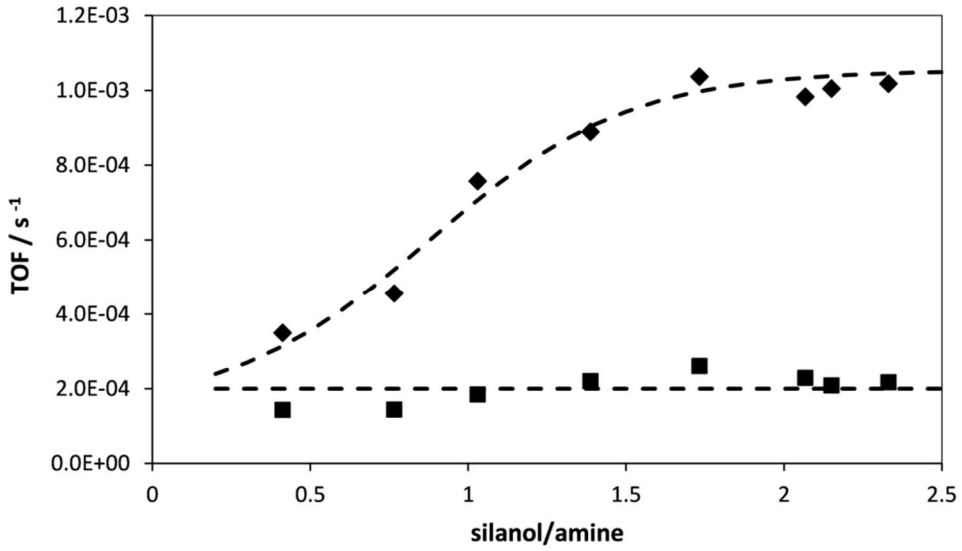

Figure 1. Turnover frequencies (TOFs) in the aldol condensation of 4-nitrobenzaldehyde with acetone of the cooperative catalysts (type AB, ◆) as a function of their molar silanol-to-amine ratio and the hexamethyldisilazane-treated catalysts (type B, ■) as a function of the molar silanol-to-amine ratios of their parent catalysts; the dashed lines are intended as visual aids only.

The overall observed cooperativity between both types of sites does not only depend on their concentrations but also on their spatial arrangement with respect to each other. The surface arrangement and corresponding effect on the observed behavior has been rationalized by means of computer simulations. It was found that if primary amines are grafted from a dilute synthesis mixture, a random positioning occurs whereas if more concentrated synthesis mixtures are employed, the primary amines are grafted as clusters on the silica surface because of the preferential propylamine–propylamine interactions by means of hydrogen bonding, compared to propylamine–solvent interactions. The occurrence of the latter interactions could be demonstrated by thermodynamic calculations.

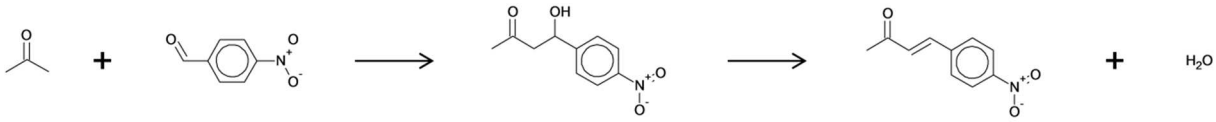

Scheme 1. Aldol condensation of acetone and 4-nitrobenzaldehyde towards 4-hydroxy-4-(4-nitrophenyl)butane-2-one and 4-(4-nitrophenyl)-3-buten-2-one, the aldol and ketone, respectively.

Based on the delplot technique [10] it has been shown that in the aldol condensation between 4-nitrobenzaldehyde and acetone, 4-hydroxy-4-(4-nitrophenyl)butane-2-one (aldol) is a primary product and 4-(4-nitrophenyl)-3-buten-2-one (ketone) is a secondary one, see Scheme 1. Additionally, in situ Raman spectroscopy of the homogeneous reaction between acetone and *n*-propylamine provided evidence for the formation of an enamine via a carbinolamine intermediate. Hence, a reaction mechanism is proposed, see Scheme 2, in which acetone first forms an enamine with the amine site that subsequently reacts with 4-nitrobenzaldehyde from the liquid phase yielding an iminium ion. The primary reaction product, *i.e.*, the aldol species, is formed by a water-assisted desorption of this iminium ion. Finally, the aldol product releases water and forms the secondary reaction product, *i.e.*, the unsaturated ketone. The promotion by silanol groups originates from hydrogen-bridge interactions between the carbonyl moiety of the reactants and these silanol groups, which makes the former more susceptible to nucleophilic reactions.

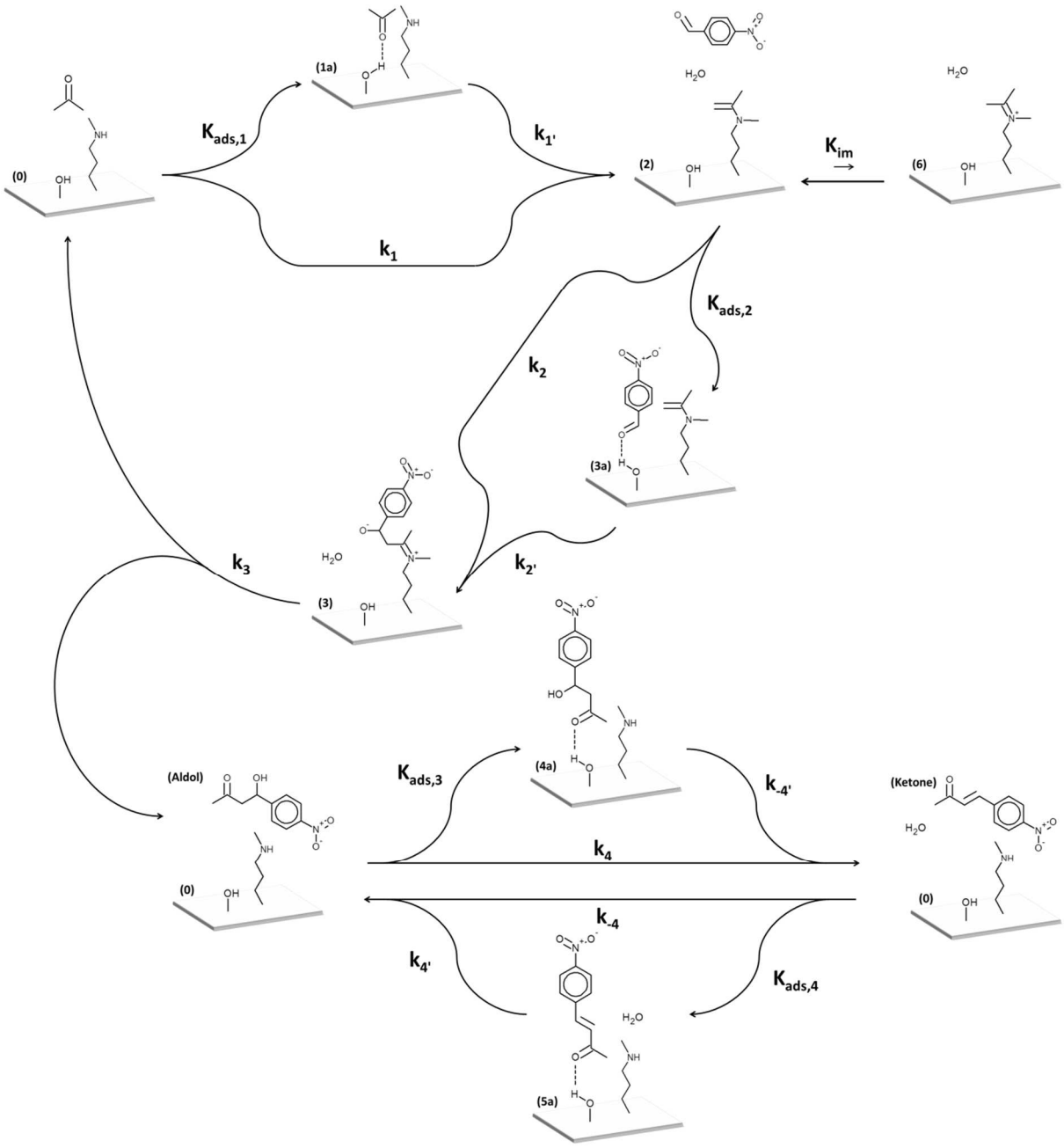

Scheme 2. Proposed reaction mechanism for the aldol condensation of 4-nitrobenzaldehyde with acetone

Alternative cooperative acid-base (type AB) and unpromoted base (type B) catalysts are synthesized by grafting of N-methylaminopropyltrimethoxysilane (MAPTMS), N-cyclohexylaminopropyltrimethoxysilane (CAPTMS), N-phenylaminopropyltrimethoxysilane (PAPTMS) and (N,N-diethyl-3-aminopropyl)trimethoxysilane (DEAPTMS) on silicagel 60. It is shown both experimentally as by means of thermodynamic calculations that, in contrast to primary amines, secondary amines have a lower tendency to cluster in the catalyst synthesis mixture and, hence, are grafted in a random manner on the catalyst surface. These catalysts allowed assessing amine structure and base strength effects both experimentally and by

means of kinetic modeling. The low basicity of molecules such as phenylaminopropane, resulting from the stabilization of the nitrogen lone electron pair by conjugation with the aromatic π cloud, limits its suitability for catalyzing nucleophilic reactions and, hence, a low TOF is obtained with this active site. However, the limited differences in basicity of the other amines are insufficient to explain the experimentally observed variations in TOFs, see Figure 2. Factors such as the possibility of forming a reactive enamine intermediate and inhibiting imine species with the amine active site and steric hindrance cannot be neglected. The crucial enamine reactive intermediate cannot be formed on a tertiary amine and, hence, the turnover frequency observed with tertiary amines is extremely low. Inhibiting imine species can only be formed on primary amine active sites. As a result, a secondary amine active site which can yield the reactive enamine intermediate without forming the inhibiting imine (species 6 in Scheme 2) will exhibit the highest turnover frequencies, provided that it is not subject to steric hindrance or unfavorable basicity effects. Both the base strength of the amine site as the steric effects depend on the substituent of the secondary amine. In the kinetic model the effects of the base strength are quantified via differences in both the activation entropies and energies of all adsorption and desorption steps involving the lone electron pair of the nitrogen atom, *i.e.*, the enamine formation, the water assisted desorption with the product aldol formation, the product ketone formation and the reverse reaction with product aldol formation. A final factor which is considered in the kinetic model is steric hindrance. A cyclohexyl substituent on the amine active site results in an increase in activation energy of about 17 kJ/mol. Moreover, the turnover frequency obtained with a SBA-15 support functionalized with an ethyl substituted secondary amine (SBA-A in Figure 2) suggests that steric hindrance matters even for relatively small substituents. Hence, it seems that a methyl substituted secondary amine is the best amine type to catalyze the aldol condensation.

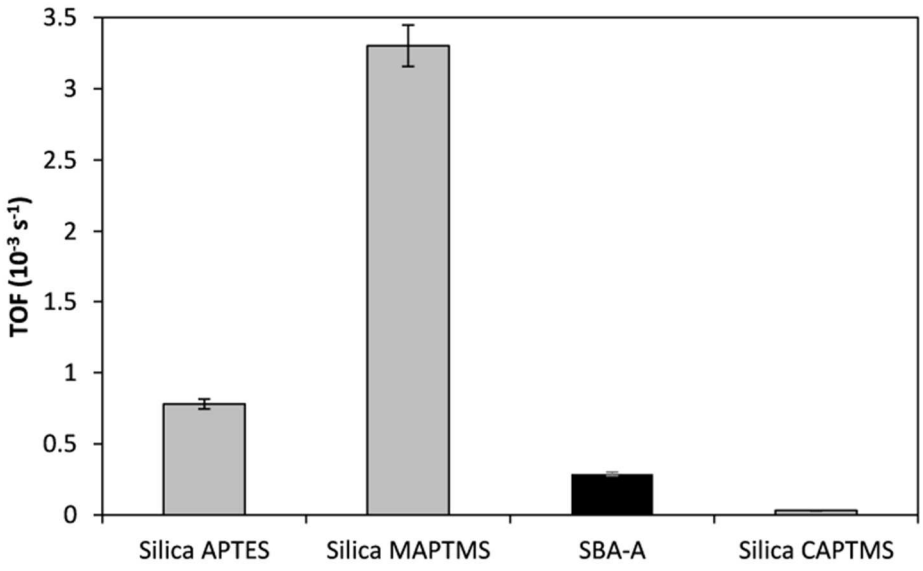

Figure 2. Turnover frequency (TOF) of SBA-A (black), (3-aminopropyl)triethoxysilane (APTES), N-methylaminopropyltrimethoxysilane (MAPTMS) and N-cyclohexylaminopropyltrimethoxysilane (CAPTMS) grafted on Silicagel 60 (grey) in the aldol condensation of 4-nitrobenzaldehyde with acetone at 45 °C using 4 mol% of amines with respect to the concentration of 4-nitrobenzaldehyde; the error bars indicate the 95% confidence interval

In a next step, the effects of acid strength and arrangement of the promoting site with respect to a secondary amine are investigated. For this purpose a new catalyst library comprising different acid-base catalysts was synthesized by functionalizing an SBA-15 support with (3-iodopropyl)trimethoxysilane. The iodo-group is subsequently replaced with the desired functional groups, *i.e.*, a secondary amine and an acid site separated by one carbon atom. As the iodosilane cannot form hydrogen bonds, it does not have any tendency to be grafted in a clustered manner. In addition, the grafting procedure of the iodosilane aims at a low loading, *i.e.*, 0.3 mmol Iodo/g silica, resulting in isolated sites. This procedure makes it possible to study the intramolecular interactions between the acid and the amine site independent of the intermolecular interactions between sites on different linkers. Intermolecular interactions between the amine site and surface silanols remain possible, of course. The effect of these interactions is studied by endcapping the surface silanols using HMDS. By comparing the turnover frequencies obtained with these materials, see Figure 3, it was shown that an intramolecular OH function, provided by a primary alcohol incorporated on the β-carbon of the amine substituent is as efficient as an intermolecular OH function provided by neighboring surface silanols as promoting site for the aldol

condensation. However, incorporating stronger acids in the catalyst demonstrated that intermolecular amine-silanol cooperativity or intramolecular amine-alcohol cooperativity resulted in higher reaction rates than intramolecular amine-carboxylic acid or amine-phosphoric acid cooperativity. Nevertheless, intramolecularly promoted catalysts retain up to 83% of their original activity when the intermolecular promotional effects are cancelled by endcapping the surface silanol groups, while the activity of a conventional amine reduces by a factor of four upon endcapping the surface silanols. These results further support the notion that the optimal promoting sites for the aldol condensation are H-bond donors and not strong acid sites [11] but also demonstrate that, indeed, stronger acids do exert a promoting effect on the activity of the amines, albeit less pronounced than that by silanols. A maximum activity was achieved when the secondary amine with a primary alcohol containing substituent was surrounded by surface silanols. This observation can be attributed to the concerted movement of the amine and intramolecularly promoting alcohol function. Due to this concerted movement the amine and alcohol can bend together towards a neighboring silanol on the silica surface, resulting in two promoting sites in the vicinity of the amine active site, *i.e.*, the intramolecular alcohol function and the intermolecular surface silanol. This results in a simultaneous activation of both reactants by the formation of a hydrogen bond and an increase in activity compared to the consecutive activation when there is only one promoting site in the vicinity of the amine. This suggests that a methyl-substituted secondary amine with one or more intramolecular alcohol functions on the β-carbons would be optimal for the aldol condensation, provided that the inclusion of such intramolecular alcohol functions does not significantly increase steric hindrance.

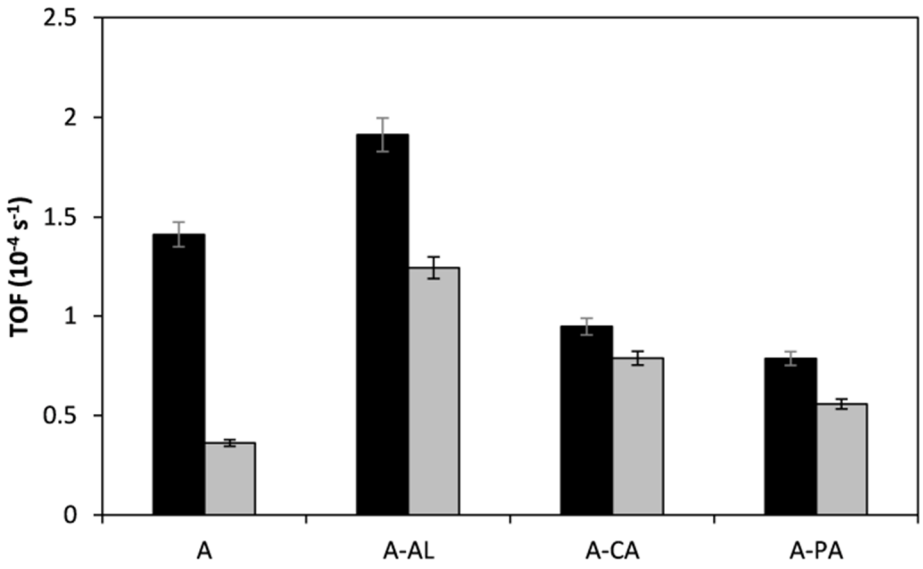

Figure 3. Turnover frequencies in the aldol condensation of 4-nitrobenzaldehyde with acetone at 45 °C using 15 mol% of amines with respect to the concentration of 4-nitrobenzaldehyde; black: catalysts without HMDS treatment combining intra- and intermolecular cooperativity (SBA-X), grey: catalysts treated with HMDS exhibiting exclusively intramolecular cooperativity (SBA-HMDS-X); the error bars indicate the 95% confidence interval

In the framework of the transition from a fossil resources based towards a more sustainable society, the aldol condensation of furfural with acetone catalyzed by a methyl substituted secondary amine grafted on silicagel 60 was studied. In contrast to 4-nitrobenzaldehyde, furfural does not contain an electron withdrawing group such as the nitro function, which makes the carbonyl group of furfural less susceptible for nucleophilic reactions and, hence, relatively higher temperatures are necessary to obtain measurable reaction rates. As a result, the aldol product dehydration becomes more pronounced and the main observed reaction product is the α,β-unsaturated ketone. It also appears that the absence of an electron withdrawing group on furfural, gives rise to a predominance of furfural bounded to the silanols. As a result, at high furfural concentrations, acetone is unable to reach the silanols and the enamine is formed directly rather than via the promoted route. As a result, correspondingly lower TOFs are obtained. This is in strong contrast with the increased TOFs obtained when increasing the 4-nitrobenzaldehyde concentration in the reactant mixture. If 2 vol% water is added to the reaction mixture the catalytic activity of a hydrophilic catalyst support drastically decreases. This can be related to a protonation of the lone electron pair of the amine after which it is no longer available for reaction with the reactants. Because

furfural is typically produced from lignocellulosic biomass in an aqueous solution and water has a negative effect on the catalytic performance of hydrophilic aminated silica materials it is interesting to investigate other types of supports. Therefore, the performance of two types of organosilicas functionalized with cysteine were assessed via the aldol condensation of 4-nitrobenzaldehyde and acetone. The organosilica comprising benzene bridges in its structure exhibits a TOF which is an order of magnitude lower than that exhibited by an organosilica comprising ethane bridges. This could be due to a strong physisorption of 4-nitrobenzaldehyde originating from the 'like-likes-like' principle [12, 13], which results in a decrease in acetone concentration in the pores and, subsequently, a decrease in TOF.

Concluding, in the framework of the design of optimal, heterogeneous, cooperative acid-base catalysts for aldol condensations, this work has focused on the establishment of fundamental relations between catalyst properties and their performance. It was found that the overall observed cooperativity between the two types of sites does not only depend on their nature and concentrations but also on their spatial arrangement with respect to each other. The reaction mechanism of amine-catalyzed aldol condensations is elucidated in more detail and allows explaining the effect of the amine structure and base strength on the observed activity. An investigation of the effects of the acid strength of the promoting site supported the notion that the optimal promoting sites for the aldol condensation are H-bond donors and not strong acid sites. The incorporation of a second promoting site, *i.e.*, an intramolecular alcohol function, results in a simultaneous activation of both reactants by the formation of a hydrogen bond and an increase in activity compared to the consecutive activation when there is only a single promoting site in the vicinity of the amine. The information gained based on the selected model reaction is translated to a more relevant one in the framework of renewables valorization, *i.e.*, the aldol condensation of furfural with acetone. The presence or absence of an electron withdrawing group in the aromatic aldehyde and, hence, the electronegativity of the oxygen atom in the carbonyl function, has a major effect on the reactivity of that component. Additionally, an increase in water content in the feed drastically decreases the TOF. Finally, it was shown that at identical operating conditions in the aldol condensation of 4-nitrobenzaldehyde and acetone, organosilicas comprising different bridge types in their structure exhibit significant differences in TOFs originating from differences in reactant physisorption.

In the near future, the catalyst support hydrophobicity will be tuned by co-condensation of tetraethyl orthosilicate and bridged organosilanes and the investigation of the effects of water in the feed will be continued. Additionally, the fundamental effects that give rise to the steric hindrance for secondary amines with relatively small substituents are not yet fully understood. This could be further investigated by performing ab initio calculations which are aimed at clarifying the interaction of acetone with the various types of amines. Synthesizing and assessing the performance of a series of methyl-substituted secondary amines with several intramolecular alcohol functions on the β-carbons could confirm the effect of the simultaneous activation of the reactants and reveal the potential steric hindrance of the inclusion of multiple alcohol functions.

References

1. J. C. Serrano-Ruiz, J. A. Dumesic, Energy Environ. Sci., **2011**, 4, 83-99
2. K. J. Zeitsch, *The chemistry and technology of furfural and its many by-products*, Sugar series, Elsevier, Amsterdam ; New York, **2000**, xv, 358 p.
3. J. N. Chheda, G. W. Huber, J. A. Dumesic, Angew. Chem.-Int. Edit., **2007**, 46, 7164-7183
4. C. Moreau, M. N. Belgacem, A. Gandini, Top. Catal., **2004**, 27, 11-30
5. D. T. Jones, D. R. Woods, Microbiol. Rev., **1986**, 50, 484-524
6. M. Sasaki, K. Goto, K. Tajima, T. Adschiri, K. Arai, Green Chem, **2002**, 4, 285-287
7. H. Olcay, A. V. Subrahmanyam, R. Xing, J. Lajoie, J. A. Dumesic, G. W. Huber, Energy Environ. Sci., **2013**, 6, 205-216
8. S. Huh, H. T. Chen, J. W. Wiench, M. Pruski, V. S. Y. Lin, Angew. Chem.-Int. Edit., **2005**, 44, 1826-1830
9. R. Cammack, *Oxford dictionary of biochemistry and molecular biology*, Oxford University Press, Oxford ; New York, **2006**, 720
10. N. A. Bhore, M. T. Klein, K. B. Bischoff, Ind. Eng. Chem. Res., **1990**, 29, 313-316
11. N. A. Brunelli, K. Venkatasubbaiah, C. W. Jones, Chem Mater, **2012**, 24, 2433-2442
12. R. P. Feynman, R. Leighton, M. Sands, *The Feynman Lectures on Physics*, Addison-Wesley, Reading, MA, USA, **1970**, 1552

13. K. L. Williamson, K. M. Masters, *Macroscale and Microscale Organic Experiments*, (Eds.: S. Kiselica), Hartford, C., Bemont, CA, USA, **2011**, 802

Samenvatting

Door de groeiende wereldbevolking en de bijhorende stijgende vraag naar energie en chemicaliën raken de fossiele grondstoffen uitgeput. Daarom is het belangrijk om op zoek te gaan naar alternatieve grondstoffen, bij voorkeur van een hernieuwbare oorsprong. Een voorbeeld van een veelbelovende hernieuwbare grondstof voor de productie van vloeibare brandstoffen is lignocellulose bevattende biomassa. Dit type van niet-eetbare biomassa kan, b.v., omgezet worden naar waterige furaanmengsels, die componenten zoals 2-furaldehyde (furfural) en 5-(hydroxymethyl)furfural (HMF) bevatten [1-4]. Vervolgens kan de carbonylgroep van de furaancomponenten via een aldolcondensatie met aceton componenten vormen met langere koolstofketens [1, 5-7]. Na het verwijderen van (een deel van) de zuurstofatomen worden vloeibare brandstoffen en/of chemicaliën verkregen. Derhalve kan geconcludeerd worden dat C-C koppelingsreacties, zoals aldolcondensaties een cruciale rol kunnen spelen in de overgang van fossiele grondstoffen gebaseerde naar een duurzamere samenleving.

Vandaag worden aldolcondensaties industrieel doorgaans gekatalyseerd door middel van homogene, basische katalysatoren zoals KOH, $Ca(OH)_2$, NaOH, of Na_2CO_3. Echter, in een zoektocht naar meer duurzame chemische processen, worden heterogene alternatieven voor deze homogene katalysatoren nagestreefd. Klasse I aldolasen zijn enzymen die in de natuur worden aangetroffen en zowel amine (basische) als zure centra bevatten [8]. Deze twee types van centra zijn in staat om door middel van coöperatieve katalyse, aldolcondensaties op een efficiënte manier uit te voeren [9]. Deze waarneming heeft geleid tot een toenemende belangstelling voor heterogene coöperatieve zuur-base-katalysatoren en zorgde tevens voor inspiratie bij de ontwikkeling van nieuwe, dergelijke katalysatoren.

In dit werk werd een reeks van coöperatieve zuur-base-katalysatoren (type AB) gesynthetiseerd door een commercieel mesoporeus silicamateriaal, nl. silicagel 60, te functionaliseren met verschillende hoeveelheden van een primair amineprecursor, (3-aminopropyl)triethoxysilaan (APTES). Niet-coöperatieve basische (type B) versies van de

coöperatieve katalysatoren werden bereid door ze met hexamethyldisilazaan (HMDS) te behandeld om de oppervlaksilanolgroepen te blokkeren. De katalytische prestaties in de aldolcondensatie van 4-nitrobenzaldehyde met aceton werden voor deze materialen bepaald, zie Figuur 1. Indien er uitsluitend amines aanwezig zijn op het katalysatoroppervlak worden er, ongeacht de aminedichtheid, identieke, matige omzetfrequenties (OZFs) verkregen. Vergelijking van de omzetfrequenties van de andere materialen bevestigt dat de silanolgroepen, die intrinsiek aanwezig zijn in silicamaterialen, een promotend effect hebben op de activiteit van de eigenlijke actieve centra, d.w.z., de amines. De promotie heeft geen effect op de productdistributie.

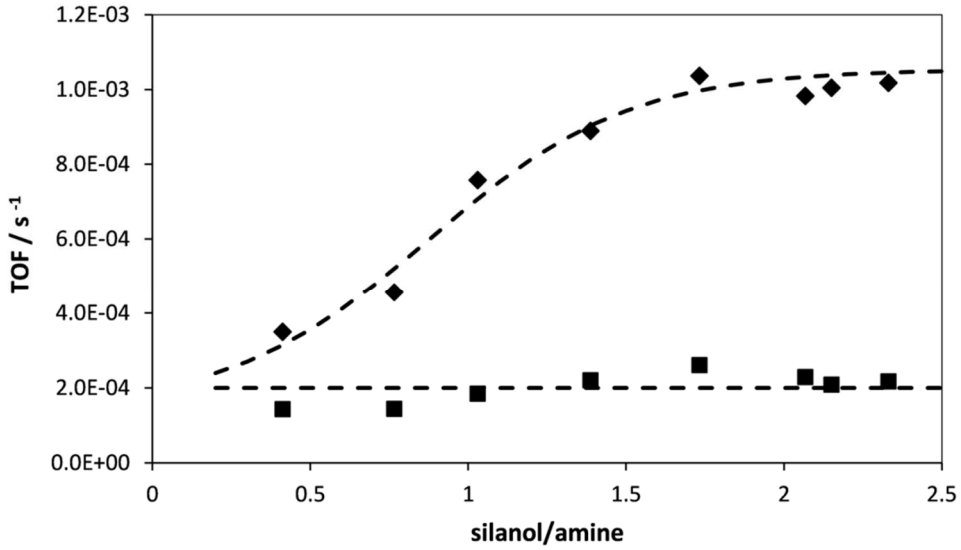

Figuur 1. Omzetfrequenties (OZFs) in de aldolcondensatie van 4-nitrobenzaldehyde met aceton van de coöperatieve katalysatoren (type AB, ◆) als functie van hun molaire silanol-op-amine verhouding en de met hexamethyldisilazaan-behandelde katalysatoren (type B, ■) als functie van de molaire silanol-op-amine verhouding van het moedermateriaal; de stippellijnen zijn enkel bedoelt als visuele hulpmiddelen.

De globaal waargenomen coöperativiteit tussen de twee types centra hangt niet enkel af van hun concentraties maar ook van de ruimtelijke positionering ten opzicht van elkaar. De ruimtelijke positionering en het resulterende effect op het waargenomen gedrag werden a.h.v. computersimulaties gerationaliseerd. Het kon worden aangetoond dat, indien primaire amines vanuit een verdunde oplossing op het oppervlak geënt worden, ze willekeurig gepositioneerd worden terwijl geconcentreerde synthesemengsels aanleiding geven tot clusters van amines op het katalysatoroppervlak. Dit wordt veroorzaakt door de preferentiële propylamine-propylamine interacties d.m.v. waterstofbrugvorming, in

vergelijking met de propylamine-solvent interacties, een fenomeen dat werd bevestigd a.h.v. thermodynamische berekeningen.

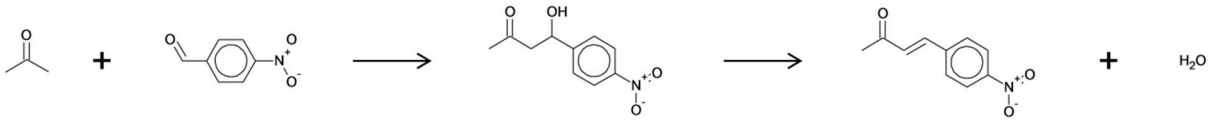

Schema 1. Aldolcondensatie van aceton met 4-nitrobenzaldehyde met vorming van dat 4-hydroxy-4-(4-nitrofenyl)butaan-2-on en 4-(4-nitrofenyl)-3-buten-2-on, respectievelijk, het aldol en keton

Aan de hand van de delplot techniek [10] werd aangetoond dat 4-hydroxy-4-(4-nitrofenyl)butaan-2-on (aldol) een primair product is van de aldolcondensantie tussen 4-nitrobenzaldehyde en aceton terwijl 4-(4-nitrofenyl)-3-buten-2-on (keton) een secundair product is, zie Schema 1. Bovendien, werd met behulp van in situ Raman spectroscopie van de homogene reactie tussen aceton en *n*-propylamine, de vorming van een enamine met een carbinolamine als intermediair aangetoond. In het corresponderende reactiemechanisme dat werd voorgesteld, zie Schema 2, vormt aceton eerst een enamine met het aminecentrum vooraleer te reageren met 4-nitrobenzaldehyde afkomstig uit de bulkfase met vorming van een iminium ion. Het primaire reactieproduct, nl., het aldol, wordt gevormd door middel van een door water geassisteerde desorptie van het iminium ion. Tenslotte, kan dit aldol water afsplitsen met vorming van het secundaire product, nl., het onverzadigde keton. Het promotend effect van de silanolgroepen vindt zijn oorsprong in de waterstofbruginteracties tussen de carbonylgroep van de reactanten en de silanolgroepen, waardoor de reactanten vatbaarder worden voor nucleofiele reacties.

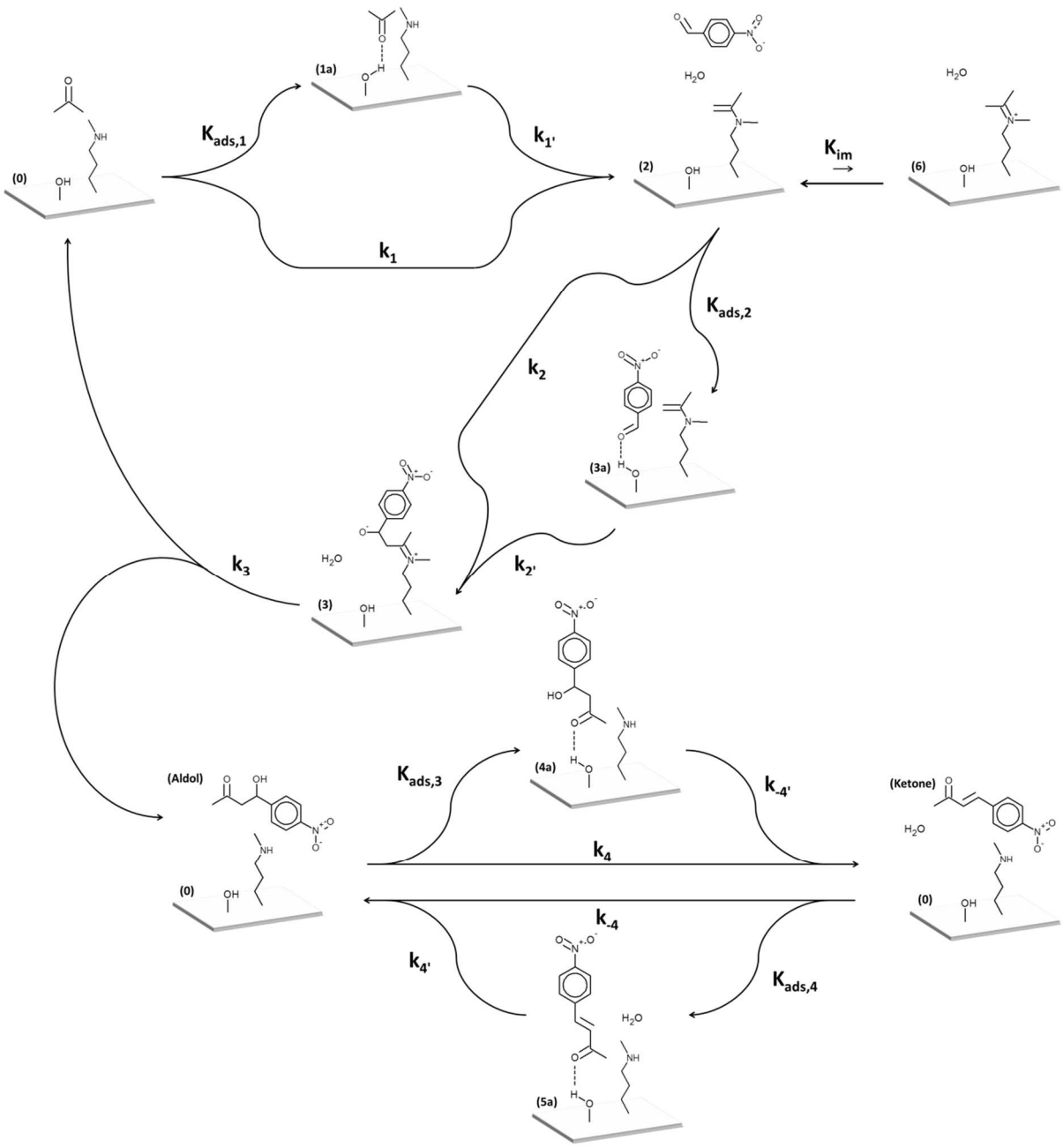

Schema 2. Reactiemechanisme voor de aldolcondensatie van 4-nitrobenzaldehyde met aceton

Een alternatieve reeks coöperatieve zuur-base (type AB) en uitsluitend basische (type B) katalysatoren werd gesynthetiseerd door N-methylaminopropyltrimethoxysilaan (MAPTMS), N-cyclohexyl-aminopropyltrimethoxysilaan (CAPTMS), N-phenylaminopropyltrimethoxy-silaan (PAPTMS) en (N,N-diethyl-3-aminopropyl)trimethoxysilaan (DEAPTMS) op silicagel 60 te enten. Zowel experimenteel als door middel van thermodynamische berekeningen werd er aangetoond dat, in tegenstelling tot primaire amines, secundaire amines minder neiging hebben om te groeperen in het synthesemengsel en, vandaar, op een willekeurige manier op het katalysatoroppervlak geënt worden. De katalysatoren werden gebruikt om het effect

van het amine structuur en basesterkte zowel experimenteel als door middel van kinetische modellering te onderzoeken. De lage basesterkte van moleculen zoals fenylaminopropaan als gevolg van de stabilisatie van het vrije elektronenpaar van het stikstofatoom door conjugatie met de aromatische π wolk maakt deze functie minder geschikt voor nucleofiele reacties en derhalve wordt een lage OZF verkregen met dit actief centrum. De beperkte verschillen in basesterkte tussen de andere amines zijn onvoldoende om de experimenteel waargenomen OZFs verklaren, zie Figuur 2. In dit geval domineren factoren zoals de mogelijkheid om het reactief enamine intermediair en inhiberende imines te vormen en sterische hinder. Een tertiair amine kan het cruciale enamine intermediair niet vormen en daarom worden lage omzetfrequenties waargenomen met tertiaire amines. De inhiberende imines kunnen enkel met primaire amines gevormd worden. Vandaar dat een secundair amine dat het reactieve enamine intermediair zonder inhibirende imines (component 6 in Schema 2) kan vormen de hoogste omzetfrequenties vertoont, indien deze tenminste niet belemmerd wordt door sterische hinder of ongunstige basesterkte effecten. Zowel de basesterkte van het aminecentrum als de sterische effecten zijn afhankelijk van de substituent op het secundaire amine. In het kinetische model wordt de basesterkte gekwantificeerd door verschillen in zowel de activeringsentropieën als de -energieën van alle adsorptie- en desorptiestappen waarbij het vrije elektronenpaar van het stikstofatoom betrokken is, namelijk de enaminevorming, de watergeassisteerde desorptie met de vorming van het aldolproduct, de vorming van het ketonproduct en de terugwaarte reactie met de vorming van het aldolproduct. Een laatste factor die wordt beschouwd in het kinetische model is sterische hinder. Een cyclohexylgroep gesubstitueerd op een amine leidt tot een toename van de activeringsenergie van ongeveer 17 kJ / mol. Bovendien blijkt uit de omzetfrequentie verkregen met een SBA-15 drager gefunctionaliseerd met een ethyl gesubstitueerd secundair amine (SBA-A in Figuur 2) dat sterische hinder reeds belangrijk is voor relatief kleine substituenten. Daarom lijkt een methylgroep gesubstitueerd secundair amine het beste amine type om de aldolcondensatie te katalyseren.

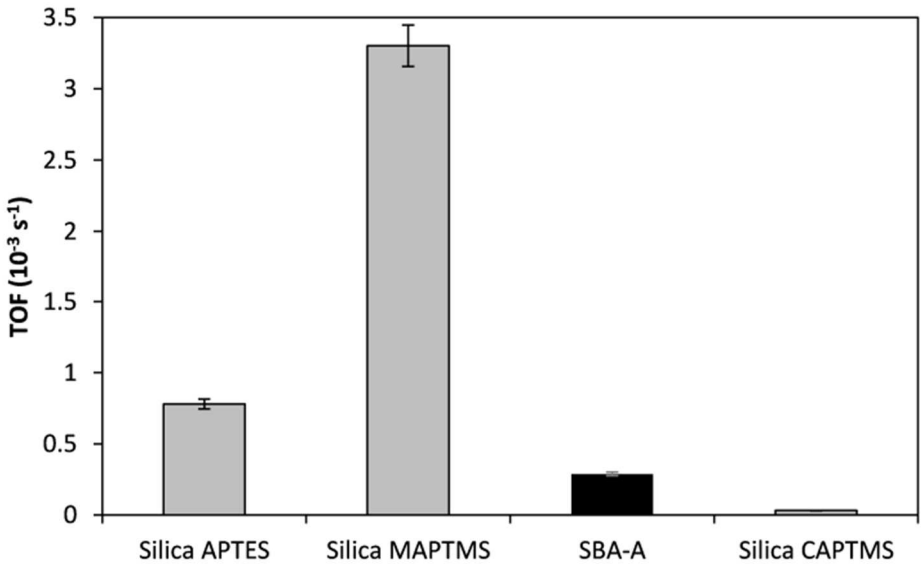

Figuur 2. Omzetfrequentie van SBA-A (zwart), (3-aminopropyl)triethoxysilaan (APTES), N-methylaminopropyltrimethoxysilaan (MAPTMS) and Ncyclohexylaminopropyl-trimethoxysilaan (CAPTMS) geënt op Silicagel 60 (grijs) in de aldolcondensatie van 4-nitrobenzaldehyde met aceton op 45 °C gebruikmakend van 4 mol% of amines ten opzichte van de concentratie van 4-nitrobenzaldehyde; de foutenbalken geven het 95% betrouwbaarheidsinterval weer

In een volgende stap is het effect van de zuursterkte en de positionering van het zure centrum ten opzichte van een secundair amine onderzocht. Hiervoor werd een nieuwe katalysatorbibliotheek bestaande uit verschillende zuur-base-katalysatoren gesynthetiseerd door een SBA-15 drager te functionaliseren met (3-joodpropyl)trimethoxysilaan. De jood-groep wordt vervolgens vervangen door de gewenste functionele groepen, nl., een secundair amine en een zuur centrum gescheiden door één koolstofatoom. Aangezien het joodsilaan geen waterstofbruggen kan vormen, is het niet geneigd om op een gegroepeerde wijze te worden geënt. Bovendien werd slechts een lage concentratie, nl., 0,3 mmol jood/g silica, beoogd tijdens de entprocedure van het joodsilaan, hetgeen aanleiding geeft tot geïsoleerde centra. Deze procedure maakt het mogelijk om de intramoleculaire interacties tussen het zuur en het aminecentrum onafhankelijk van de intermoleculaire interacties tussen centra op verschillende linkers te bestuderen. Intermoleculaire interacties tussen het aminecentrum en een silanolgroep op de drager blijven uiteraard steeds mogelijk. Het effect van deze interacties wordt bestudeerd door de silanolgroepen op de drager m.b.v. HMDS te blokkeren. Bij vergelijking van de OZFs, zie Figuur 3, werd aangetoond dat een intramoleculaire OH functionaliteit verschaft door een primair alcohol gesubstitueerd op het

β-koolstofatoom, de activiteit van het amine even efficiënt bevordert als een intermoleculaire OH functie van een silanolgroep op de drager. Na integratie van sterkere zuren in de katalysator bleek dat intermoleculaire amine-silanol coöperativiteit of intramoleculaire amine-alcohol coöperativiteit aanleiding geeft tot hogere reactiesnelheden dan intramoleculaire amine-carbonzuur of amine-fosforzuur coöperativiteit. Niettemin, behouden de katalysatoren die een intramoleculaire coöperativiteit vertonen na het blokkeren van de silanolen 68% tot 83% van hun originele activiteit, terwijl de activiteit van het gebruikelijke secundaire amine met een factor vier gereduceerd wordt. Deze resultaten ondersteunen het idee dat de optimale promotende centra voor de aldolcondensatie H-bond donoren zijn en geen sterk zure centra [11]. Daarnaast geven de resultaten ook aan dat ook sterkere zuren nog steeds een bevorderend effect uitoefenen op de activiteit van de amines, zij het minder uitgesproken dan door de zwak zure silanolgroepen. Een maximale activiteit werd bereikt wanneer het secundaire amine met een primair alcohol bevattende substituent omringd wordt door silanolgroepen op de drager. Deze observatie kan worden toegeschreven aan de gezamenlijke beweging van het amine en het alcohol wanneer zij op dezelfde linker gelokaliseerd zijn. Door deze gezamenlijke beweging kunnen het amine en het alcohol samen naar een naburige silanolgroep op de drager buigen, resulterend in twee promotende centra in de nabijheid van het aminecentrum, nl., de intramoleculaire alcoholgroep en de intermoleculaire silanolgroep op de drager. Dit resulteert in een gelijktijdige activering van beide reactanten door de vorming van een waterstofbinding en een toename van de activiteit vergeleken met de consecutieve activering wanneer er zich slechts één promotend centrum in de nabijheid van het amine bevindt. Dit suggereert dat een methylgesubstitueerd secundair amine met één of meer intramoleculaire alcohol functies verbonden aan β-koolstofatomen optimaal zou zijn voor de aldolcondensatie, op voorwaarde dat dergelijke bijkomende intramoleculaire alcoholfuncties geen significante toename van sterische hinder zou veroorzaken.

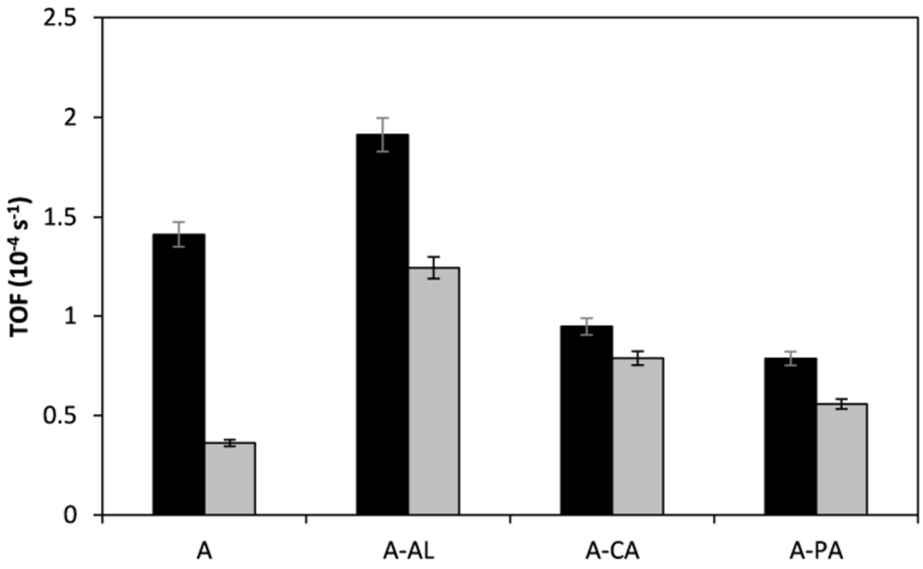

Figuur 3. Omzetfrequentie in de aldolcondensatie van 4-nitrobenzaldehyde met aceton verkregen op 45 °C gebruikmakend van 15 mol% amines ten opzichte van de concentratie van 4-nitrobenzaldehyde; zwart: katalysatoren die niet met HMDS behandeld warden en dus intra- en intermoleculaire coöperativiteit combineren (SBA-X), grijs: katalysatoren die wel met HMDS behandeld werden en enkel intramoleculaire coöperativiteit bevatten (SBA-HMDS-X); de foutenbalken geven het 95% betrouwbaarheidsinterval weer

In het kader van de overgang van een op fossiele grondstoffen gebaseerde naar een meer duurzame samenleving, wordt de aldolcondensatie van furfural met aceton gekatalyseerd door een methylgroep gesubstitueerd secundair amine geënt op silicagel 60 bestudeerd. In tegenstelling tot 4-nitrobenzaldehyde met zijn nitro groep, bevat furfural geen elektronenzuigende groep, waardoor de carbonylgroep van furfural minder geneigd is om nucleofiele reacties te ondergaan en er dus relatief hogere temperaturen nodig zijn om meetbare reactiesnelheden te verkrijgen. Daardoor wint tevens de dehydratatie van het aldol product aan belang en is het α,β-onverzadigd keton het meest gevormde product. Ook blijkt dat het ontbreken van een elektronenzuigende groep in furfural leidt tot belangrijke hoeveelheden van furfural die gebonden zijn aan de silanolgroepen op de drager. Hierdoor is aceton niet in staat om, bij hoge furfuralconcentraties, de silanolgroepen te bereiken en verloopt de enaminevorming eerder via de tragere, directe route dan via de coöperatieve route. Dit resulteert dan ook in een verlaging van de OZF, hetgeen in sterk contrast staat met de hogere OZFs waargenomen als gevolg van een toename van de 4-nitrobenzaldehyde concentratie. Wanneer 2 vol% water wordt toegevoegd aan het reactiemengsel neemt de katalytische activiteit van een katalysator met een hydrofiele drager drastisch af. Dit kan te

wijten zijn aan protonering van het vrije elektronenpaar van het amine, waarna het niet langer beschikbaar is voor reactie. Omdat de furfural geproduceerd uit lignocellulose bevattende biomassa als een waterige oplossing verkregen wordt en water een negatief effect heeft op de katalytische prestatie van hydrofiele geamineerde silicamaterialen is het interessant om andere soorten dragers te bestuderen. Daarom is het gedrag van twee types organosilicamaterialen getest via aldolcondensatie van 4-nitrobenzaldehyde. Deze werden gefunctionaliseerd met cysteïne. Een benzeenbruggen bevattende organosilica vertoont een OZF die een grootteorde lager is dan die van een organosilica die ethaanbruggen bevat. Dit kan te wijten zijn aan een sterke fysisorptie van 4-nitrobenzaldehyde afkomstig van het '*like-likes-like'* principe [12, 13], hetgeen resulteert in een afname van de acetonconcentratie in de poriën en vervolgens een afname van de OZF.

Afsluitend, in het kader van het ontwerp van optimale heterogene coöperatieve zuur-base-katalysatoren voor aldolcondensaties, werd in dit werk gefocust op de ontrafeling van fundamentele verbanden tussen de katalysatoreigenschappen en de bijhorende katalytische prestaties. Het bleek dat de globaal waargenomen coöperativiteit tussen de twee centra niet enkel afhankelijk is van hun concentraties, maar ook van hun ruimtelijke positionering ten opzichte van elkaar. Het reactiemechanisme van aminegekatalyseerde aldolcondensaties werd opgehelderd en liet toe om de waargenomen effecten van de basesterkte en aminestructuur te verklaren. Een studie over de effecten van de zuursterkte van het promotende centrum ondersteunt het idee dat de optimale promotende centra voor de aldolcondensatie H-bond donoren zijn en geen sterk zure centra. De opname van een tweede promotend centrum, d.w.z. een intramoleculaire alcoholgroep, resulteert in een gelijktijdige activering van beide reactanten door de vorming van een waterstofbinding en een toename van de activiteit vergeleken met de consecutieve activering wanneer er zich slechts één promotend centrum in de nabijheid van het amine bevindt. De informatie die uit de modelreactie verkregen werd, werd vervolgens vertaald naar een meer relevante reactie, namelijk de aldolcondensatie van furfural met aceton. De aan- of afwezigheid van een elektronenzuigende groep in het aromatische aldehyde heeft een grote invloed op de reactiviteit van die component. Bovendien leidt een toename van het watergehalte in de voeding tot een drastische vermindering van de waargenomen OZF. Tot slot werd aangetoond dat bij identieke reactiecondities in de aldolcondensatie van 4-

nitrobenzaldehyde en aceton, cysteine gefunctionaliseerde organosilica die verschillende organische bruggen in hun structuur bevatten, significante verschillen in OZFs vertonen. Deze verschillenkunnen te wijten zijn aan verschillen in reactantfysisorptie.

In de nabije toekomst zal de hydrofobiciteit van de katalysatordrager geregeld worden doormiddel van co-condensaties van tetraethylorthosilicaat en gebrugde organosilanen. Met deze materialen zal het onderzoek naar de effecten van het water in het voeding voortgezet worden. Bovendien zijn de fundamentele effecten die aanleiding geven tot de sterische hinder van secundaire aminen met relatief kleine substituenten nog niet volledig begrepen. Dit kan verder onderzocht worden door ab initio berekeningen uit te voeren die de zich focussen op het ophelderen van de interacties tussen aceton en de verschillende amines. Synthese en testen van een reeks methyl gesubstitueerde secondaire amines met meerdere intramoleculaire alcohol functies op de β-koolstofatomen kan het effect van de gelijktijdige activering van de reactanten bevestigen en verder inzicht geven in het effect van deze alcoholfuncties op de sterische hinder.

Referenties

1. J. C. Serrano-Ruiz, J. A. Dumesic, Energy Environ. Sci., **2011**, 4, 83-99
2. K. J. Zeitsch, *The chemistry and technology of furfural and its many by-products*, Sugar series, Elsevier, Amsterdam ; New York, **2000**, xv, 358 p.
3. J. N. Chheda, G. W. Huber, J. A. Dumesic, Angew. Chem.-Int. Edit., **2007**, 46, 7164-7183
4. C. Moreau, M. N. Belgacem, A. Gandini, Top. Catal., **2004**, 27, 11-30
5. D. T. Jones, D. R. Woods, Microbiol. Rev., **1986**, 50, 484-524
6. M. Sasaki, K. Goto, K. Tajima, T. Adschiri, K. Arai, Green Chem, **2002**, 4, 285-287
7. H. Olcay, A. V. Subrahmanyam, R. Xing, J. Lajoie, J. A. Dumesic, G. W. Huber, Energy Environ. Sci., **2013**, 6, 205-216
8. S. Huh, H. T. Chen, J. W. Wiench, M. Pruski, V. S. Y. Lin, Angew. Chem.-Int. Edit., **2005**, 44, 1826-1830
9. R. Cammack, *Oxford dictionary of biochemistry and molecular biology*, Oxford University Press, Oxford ; New York, **2006**, 720
10. N. A. Bhore, M. T. Klein, K. B. Bischoff, Ind. Eng. Chem. Res., **1990**, 29, 313-316

11. N. A. Brunelli, K. Venkatasubbaiah, C. W. Jones, Chem Mater, **2012**, 24, 2433-2442

12. R. P. Feynman, R. Leighton, M. Sands, *The Feynman Lectures on Physics*, Addison-Wesley, Reading, MA, USA, **1970**, 1552

13. K. L. Williamson, K. M. Masters, *Macroscale and Microscale Organic Experiments*, (Eds.: S. Kiselica), Hartford, C., Bemont, CA, USA, **2011**, 802

Chapter 1

Introduction

Fossil resources, such as coal, crude oil and natural gas constitute the world main supply of energy, see Figure 1-1, and also of building blocks for chemicals and polymers. Due to the ever increasing world population and the associated demand for energy and products, the fossil resources are depleting faster than ever before. Additionally, environmental concerns exist about the use of these fossil resources and, more particularly, of the concomitant emissions of CO_2, SO_x, NO_x and other harmful gasses. Therefore, it is important to investigate the exploitation of alternative feedstocks, preferable of a renewable origin, that, potentially, may replace the fossil resources.

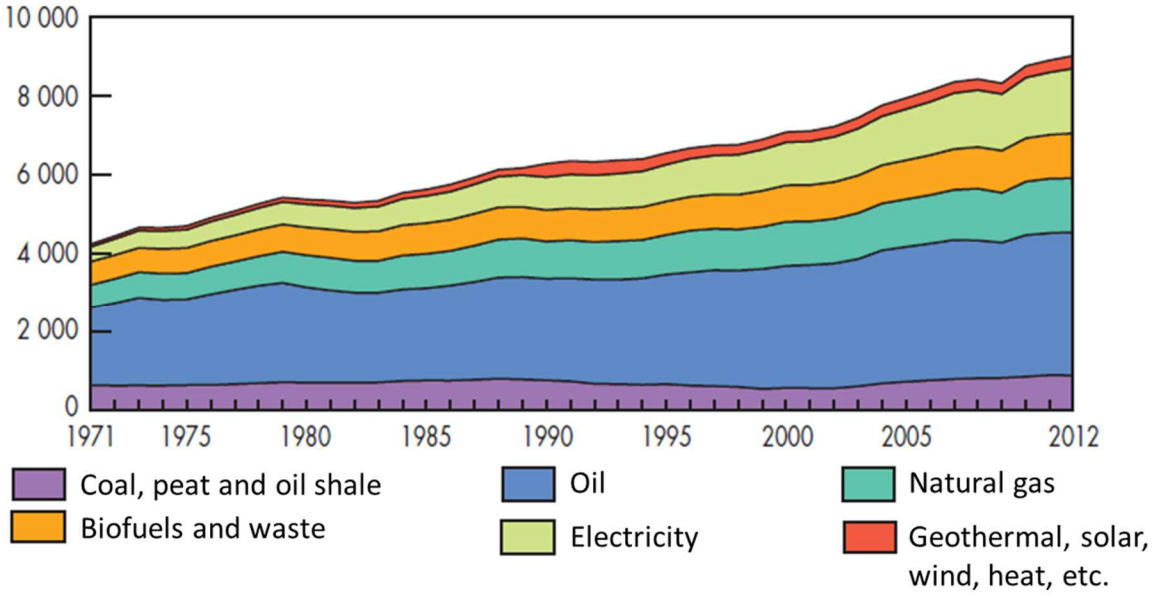

Figure 1-1. World energy consumption (in million tonnes oil equivalent) from 1971 to 2012 [1]

Biomass constitutes a viable option for the sustainable production of both energy and chemicals, because it is renewable, *i.e.,* it is replenished at the same rate of its consumption, the CO_2 emissions corresponding with the consumption are compensated during the

biomass growth and the emissions of harmful gasses are typically lower. Various types of biomass exist. A major concern with respect to the use of edible biomass, such as corn or sugar cane, for the large-scale production of fuels and chemicals is the (potential) competition with food production. This has led to the development of new technologies for processing non-edible renewables, such as lignocellulosic biomass, to produce so-called second generation biofuels without interfering with the food supply chain. Lignocellulose consist of three major constituent, *i.e.,* cellulose (40-50%), hemicellulose (15-20%) and lignin (15-25%) [2]. Cellulose is a polymer of glucose units that are linearly connected via β-1,4-glycoside linkages. This arrangement contributes to the material crystallinity and, hence, its rigidity and high resistance against degradation. The cellulose bundles are connected by hemicellulose, which is an amorphous polymer of five different C_5 and C_6 sugars which disintegrates more easily than cellulose. Cellulose and hemicellulose are surrounded by a three-dimensional polymer, called lignin, that essentially consists of propyl-phenol building blocks [2, 3].

This introductory chapter starts with a discussion of two of the main routes to produce liquid hydrocarbon fuels from lignocellulosic biomass. Subsequently, the aldol condensation reaction, which is a crucial reaction step in each of these routes and the main focus of this research, is further elaborated upon. Both aldol condensation as a reaction and the state-of-the-art in aldol condensation catalysts are reviewed. Afterwards, the model based catalyst design methodology, which will be exploited as part of this work to optimize these aldol condensation catalysts is explained. Finally, the scope of this work is discussed.

1.1 Biomass conversion routes into liquid hydrocarbon fuels

Two main pathways for liquid hydrocarbon fuels production from lignocellulosic biomass are illustrated in Figure 1-2 [3]. First lignocellulose is pretreated to weaken the lignin protective layer and increase the susceptibility of the crystalline cellulose to degradation, followed by a hydrolysis step to depolymerize the cellulose and hemicellulose with the release of sugar units.

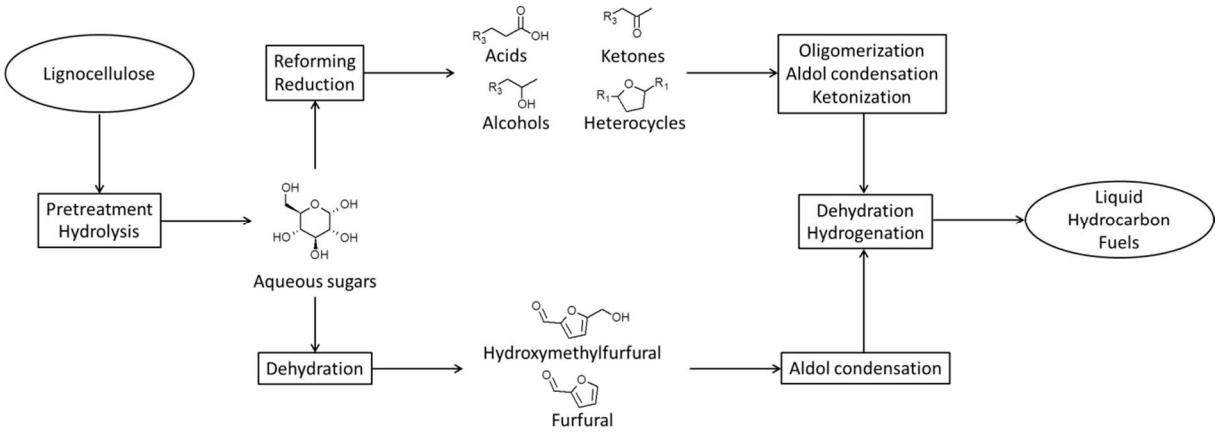

Figure 1-2. Conversion of lignocellulose into liquid hydrocarbon fuels [3]

By means of a reforming and reduction step, these sugars can be transformed into monofunctional components, *e.g.*, acids, alcohols, ketones and heterocyclic compounds, see the upper route in Figure 1-2 [3, 4]. These components typically contain four to six carbon atoms and are immiscible with water. As the desired hydrocarbon fuels consist of heavier alkanes, i.e., C_6-C_{12} for gasoline, C_9-C_{16} for jet fuel, and C_{10}-C_{22} for diesel applications, the carbon number of the different components has to increase [5]. This can be achieved through a selected C-C coupling reaction depending on the functionality of the reactants, *e.g.*, oligomerization, aldol condensation or ketonization. Finally, the oxygen is (partially) removed through dehydration and hydrogenation reactions, yielding the desired liquid hydrocarbon fuels.

Alternatively, furan components such as furfural or hydroxymethylfurfural (HMF) can be obtained by sugar dehydration, see the lower route in Figure 1-2 [3]. Furfural is obtained by dehydration of C_5 sugars such as xylose, while HMF is produced from C_6 sugars such as glycose or fructose [6-8]. Subsequently, thanks to the carbonyl group in the furan components they can be used to perform an aldol condensation with molecules such as acetone, which can be obtained from biomass-derived sources as well, in order to produce heavier components [9-11]. The last step of the process involves the removal of oxygen by means of dehydration and hydrogenation with formation of liquid hydrocarbon fuels.

1.2 Aldol condensation

As demonstrated above, aldol condensations may play a crucial role in the conversion of lignocellulosic biomass into hydrocarbon fuels as they provoke C-C bound coupling and,

hence, yield larger and more complex molecules from relatively simple ones. Two carbonyl compounds, *i.e.*, ketones or aldehydes, are involved in this reaction which was discovered in 1872 by Charles Adolphe Wurtz [12]. The product, a β-hydroxy carbonyl compound, is called an aldol because it contains both an aldehyde and an alcohol function. Apart from the combination of two molecules, a small molecule, *c.q.*, water, is eliminated during a condensation reaction, leading to the final α,β-unsaturated carbonyl compound, see Scheme 1-1.

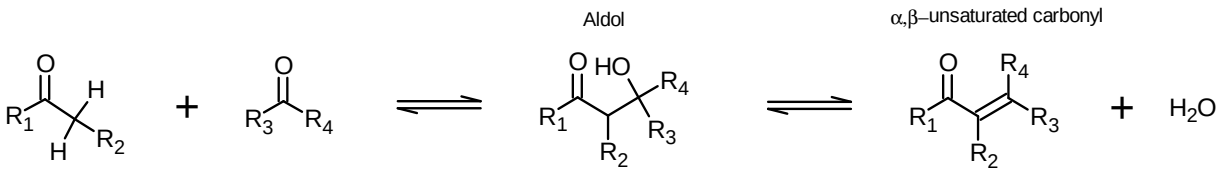

Scheme 1-1. Generalized example of an aldol condensation

The aldol condensation is not only useful for the creation of new C-C bonds, the products also contain functional groups, *i.e.*, a carbonyl and an alcohol, which provide opportunities for further upgrading of the obtained products [13, 14]. This reaction is, therefore, typically employed in the pharmaceutical and fine chemicals industry for the production of specifically tailored components. The production of ionones, see Scheme 1-2, is only one of the many industrial applications of aldol condensations [15]. β-Ionone is a costly specialty chemical that is used in the manufacture of vitamin A and carotenoids such as β-carotene [15]. Also large quantities of both α-ionone and β-ionone are used as additives in fragrances and flavorings. α-Ionone and β-ionone are important flavor substances for all kinds of fruit flavors, especially berry flavors such as raspberry, but also for a violet note [15].

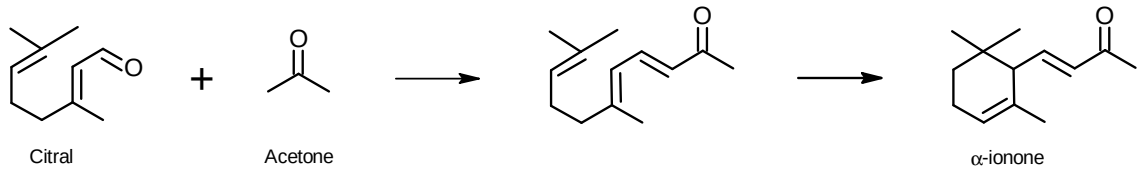

Scheme 1-2. Synthesis of α-ionone from citral and acetone [15]

1.2.1 Reaction mechanism

Aldol condensations are typically catalyzed by means of strong homogeneous bases or acids. The necessary and sufficient condition for an aldol condensation to proceed is the presence of an α-hydrogen in at least one of the reactants. The reaction mechanism, *i.e.*, the enol or enolate mechanism, depends on the acid or base character of the catalyst. The names of the two alternative reaction mechanisms refer to the most important corresponding intermediate.

A ketone with an α-hydrogen is susceptible to keto-enol tautomerism. This phenomenon entails the interconversion of the ketone into the corresponding enol via a proton transfer. The ketone is in thermodynamic equilibrium with the enol, see Scheme 1-3. Generally, the thermodynamics are such that the ketone is favored over the enol.

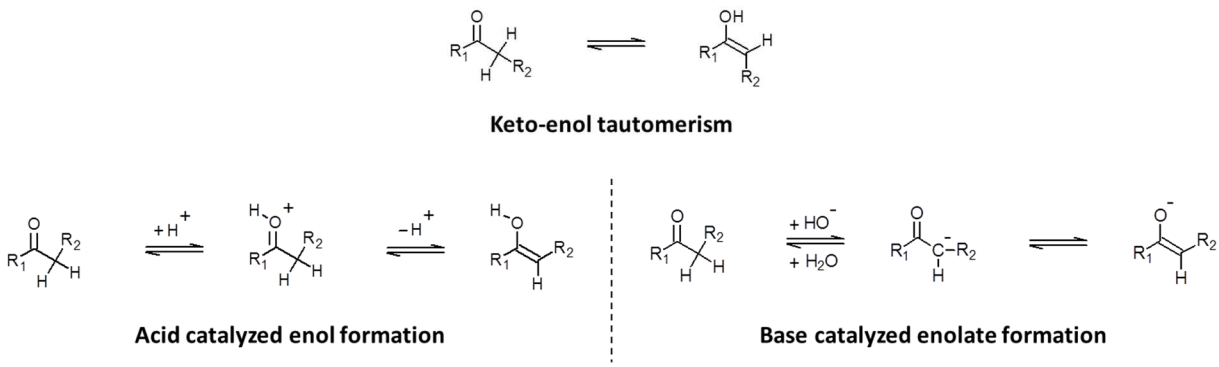

Scheme 1-3. Acid catalyzed enol (left) and base catalyzed enolate (right) formation

In an acidic environment, the carbonyl function is protonated, followed by the elimination of the acid α-hydrogen with formation of the enol. In the presence of a base, an enolate is formed by removing the acidic α-hydrogen from the ketone followed by a shift of the electrons to the oxygen atom. In contrast to the enol, the enolate is more stable due to existence of resonance and the inductive effect.

1.2.1.1 Acid catalyzed aldol condensation: enol mechanism

The acid catalyzed aldol condensation follows the reaction mechanism involving the enol intermediate, see Schemes 1-3 and 1-4. The first step in this reaction mechanism is the already discussed acid catalyzed enol formation from one of reactants containing an α-hydrogen with respect to the carbonyl group **(1)**. The second reactant enters the reaction mechanism in its protonated form **(2)**. Afterwards, both species undergo a nucleophilic

addition with the aldol formation and subsequent proton release **(3 and 4)**. The α,β-unsaturated ketone can be obtained through the dehydration of the aldol **(5 and 6)**. This dehydration reaction can also be acid catalyzed.

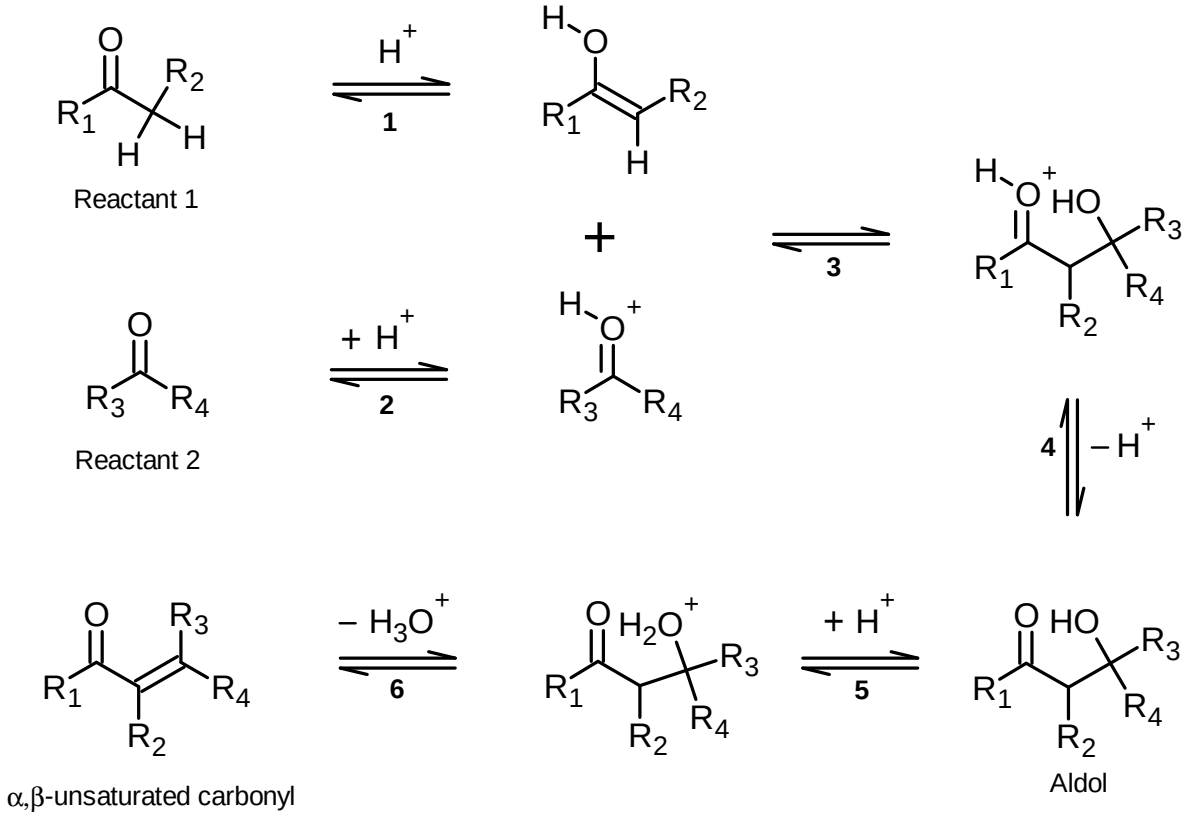

Scheme 1-4. Acid catalyzed aldol condensation reaction mechanism

1.2.1.2 Base catalyzed aldol condensation: enolate mechanism

If the catalyst is a strong base, the reaction starts with the removal of an α-hydrogen from a carbonyl group of one of the reactants to form an enolate ion **(1)**, see Schemes 1-3 and 1-5. Afterwards a nucleophilic addition of the enolate ion, which is a strong nucleophile, to the carbonyl group of the second reactant occurs **(2)**. Protonation of the formed alkoxide gives the aldol product **(3)**. In a similar manner to the enol reaction mechanism, the α,β-unsaturated ketone can be obtained via aldol dehydration, which can also be base catalyzed **(4 and 5)**.

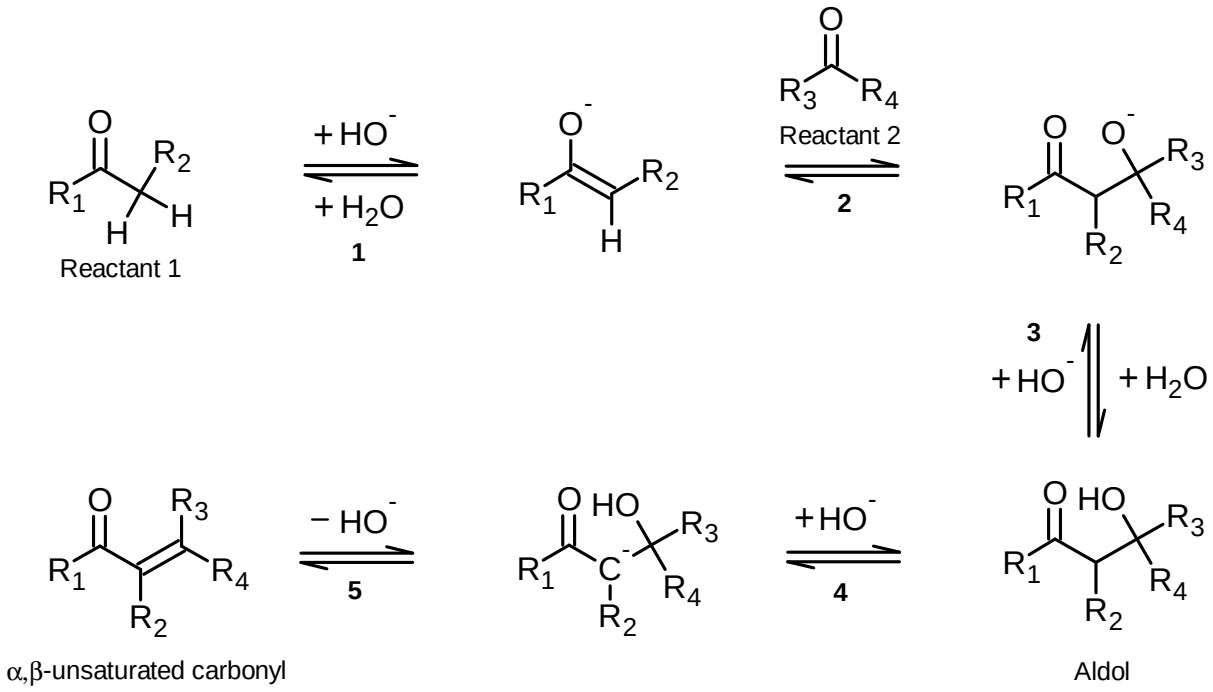

Scheme 1-5. Base catalyzed aldol condensation reaction mechanism

1.2.2 Aldol condensation product spectrum and model reaction

Two types of aldol condensations can be distinguished, *i.e.*, the self-condensation of two identical molecules and the cross-condensation of two different molecules. The relevance of self-condensations depends on the reactivity of the carbonyl moiety, the availability of α-hydrogen atoms and the catalyst proton affinity. As a result, the aldol condensation product spectrum can range from very simple to extremely complex.

Ketones have a reduced reactivity in nucleophilic additions compared to aldehydes due to steric hindrance and the electron donating effect of the carbon chains. Therefore, the self-condensation of ketones is less pronounced than that of aldehydes. Moreover, a carbonyl component which does not contain any α-hydrogens can only participate in cross-condensations because the presence of an α-hydrogen in at least one of the reactants is a prerequisite for an aldol condensation to occur. The catalyst base or acid strength is important for the (de)-protonation of the α-hydrogen containing component. If this component is not fully protonated or deprotonated, the formed enol or enolate can perform a nucleophilic addition on another unaltered molecule. Also the symmetry of the α-hydrogen containing component affects the complexity of the product spectrum. If the α-

hydrogen containing component is symmetrical only a single cross-condensation aldol product can be formed, while an unsymmetrical α-hydrogen containing component leads to two cross-condensation aldol products. Additionally, intramolecular aldol condensations can occur if dicarbonyl components are present in the reaction mixture. These kind of reactions yield cyclic aldol or unsaturated ketone products, see Scheme 1-6 and are often used to produce five- or six-membered ring components.

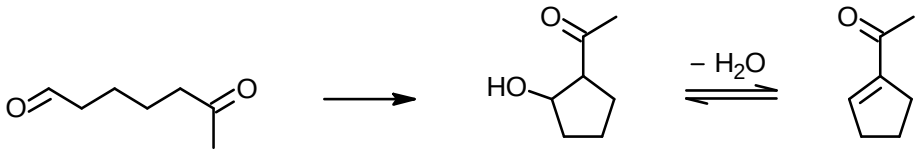

Scheme 1-6. Intramolecular aldol condensation of 6-oxoheptanal

The aldol condensation of acetone with furfural, see Scheme 1-7, is a relevant reaction from an environmental and industrial point of view, see section 1.1. Additionally, it is also an interesting model reaction for research purposes because the reactants meet the above-mentioned specifications to keep the product spectrum within acceptable limits. However, temperatures exceeding the boiling point of acetone are necessary to establish measurable reaction rates for catalyst screening and comparison. A more frequently used model reaction for aldol condensation is that of 4-nitrobenzaldehyde with acetone, see Scheme 1-8. The electron withdrawing nitro group present in 4-nitrobenzaldehyde results in a less pronounced partial, negative charge on the oxygen atom of the carbonyl function and, hence, leads to increased reaction rates. It allows working at more moderate reaction temperature than necessary for the aldol condensation of furfural with acetone.

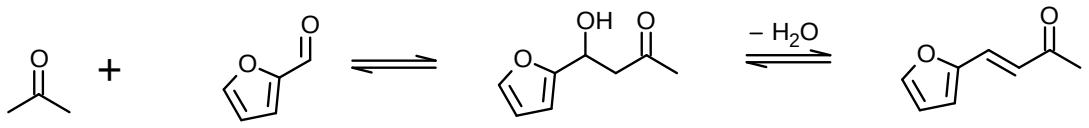

Scheme 1-7. Cross aldol condensation of acetone with furfural

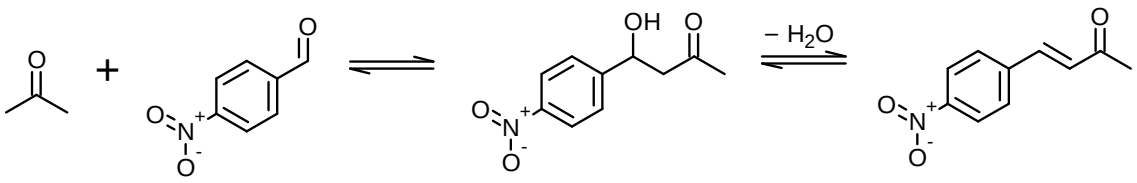

Scheme 1-8. Cross aldol condensation of acetone with 4-nitrobenzaldehyde

1.2.3 Stereoselectivity

In some cases, aldol condensations can exhibit stereoselectivity. This is particularly relevant for pharmaceutical purposes because stereoisomers, see Scheme 1-9, can behave very differently in biological applications. Stereoselective reactions can be separated into two types: diastereoselective and enantioselective reactions [16]. Diastereoselective reactions can occur due to an element controlling the stereochemistry. For example, the use of metals such as boron and lithium in combination with a trisubstituted enolate in the aldol condensation could result in different diastereomers [17]. In enantioselective reactions a chiral catalyst is used to control the stereochemistry.

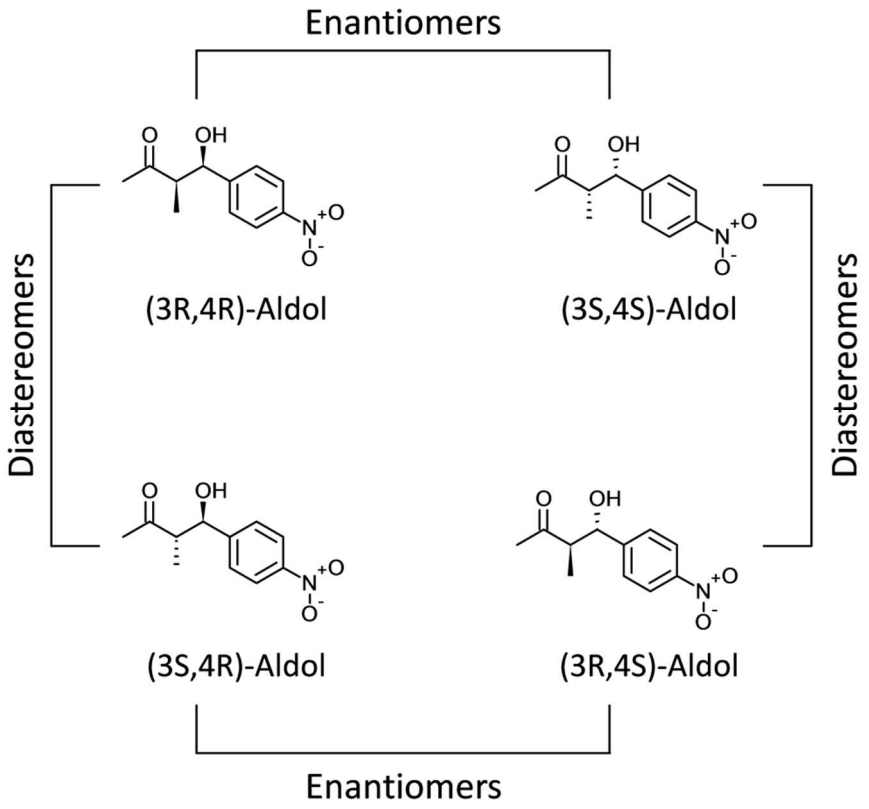

Scheme 1-9. Stereoisomers of 4-hydroxy-3-methyl-4-(4-nitrophenyl)butane-2-one

1.3 Aldol condensation catalyst innovation

As already mentioned above, strong homogeneous bases and acids are efficient aldol condensation catalysts. In present-day industrial applications strong, homogeneous base catalysts such as KOH, $Ca(OH)_2$, NaOH, or Na_2CO_3 are generally employed. However, homogeneous catalysis is frequently regarded as incompatible with sustainability due to

inherent disadvantages such as (i) the necessity of energy intensive separation steps to recuperate the products from the catalyst, (ii) a short catalyst life time and (iii) its low reusability, (iv) important waste streams and (v) intensive equipment corrosion [18, 19]. Hence, in search of greener chemical processes, heterogeneous alternatives need to be explored. In this section, some alternative types of aldol condensation catalysts are discussed.

1.3.1 Enzymatic biocatalysts

Many chemical reactions can be catalyzed by natural enzymes. The reaction conditions at which enzymatic catalysis occurs are typically very moderate. Moreover, enzymes are often more selective than synthetic catalysts. Hence, they can provide the necessary inspiration for the design of new and innovative catalyst generations, despite the typically lower turnover frequencies obtained with such biocatalysts compared to synthetic catalysts. Aldolases are an example of such enzymes which are able to catalyze aldol condensations [20, 21].

Aldolases are enzymes belonging to the category of the lyases, which occur in the muscles of humans and animals, where they play an important role in the conversion of sugars into energy. Lyases cleave C-C, C-O or C-N bonds via a mechanism which does not involve hydrolysis or oxidation. Most often, the bonds are cleaved by an elimination reaction and the resulting products contain a double bond. The enzymes are also able to catalyze the reverse reaction in which a new bond is formed [22].

Depending on the reaction mechanism employed by the aldolase to catalyze aldol condensations, they are classified into class I or class II aldolases. The former utilize an enamine as reaction intermediate, while class II aldolases use a zinc cofactor [21]. The class I aldolases contain both an amine site as well as an acid site, which leads to a cooperative catalytic mechanism [23]. The amine site acts as the actual, active site which forms the enamine intermediate while the acid site forms a hydrogen bond with the carbonyl group of the reactant in order to make the reactant more susceptible for the nucleophilic attack of the amine and, hence, acts as a promoting site, see Scheme 1-10. This observation has led to an increasing interest in the design of new bifunctional, also denoted as ‘cooperative’, acid-base catalysts, first by means of homogeneous amino acids, such as L-proline and

derivatives [21], see Scheme 1-10, and later by incorporating them into porous materials [24-30].

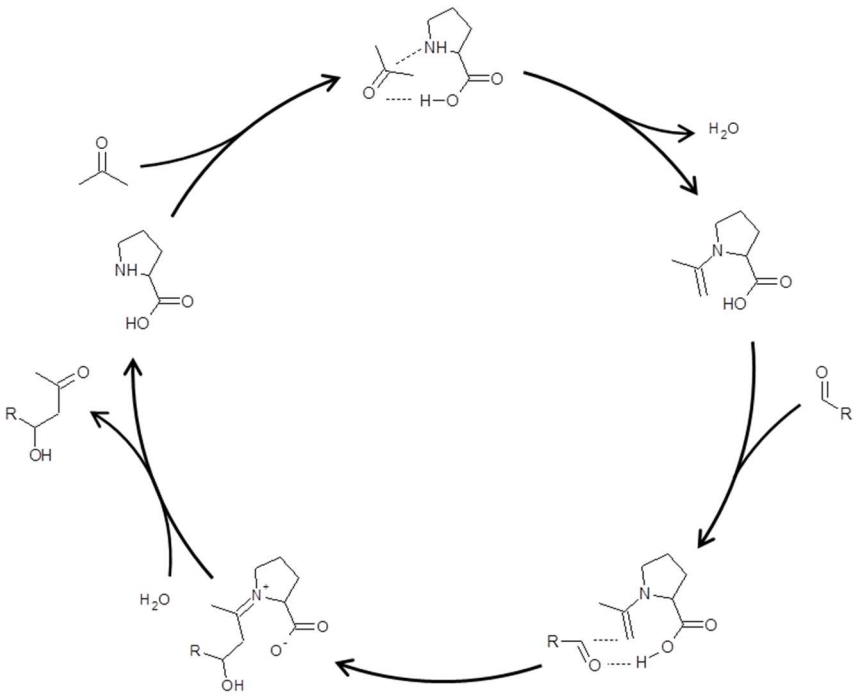

Scheme 1-10. Enamine mechanism of the Proline-catalyzed aldol condensation [21]

1.3.2 Supported aldol condensation catalysts

During the last two decades, research on heterogeneous catalysts for aldol condensations have received increasing attention, see Figure 1-3. This section provides an overview of the literature in this respect focusing on functionalized mesoporous silicas, functionalized periodic mesoporous organosilicas (PMOs) and layered double hydroxides. All these types of materials can contain both acid and base sites which act cooperatively on the reactants exposed to them and, hence, are relevant for aldol condensations.

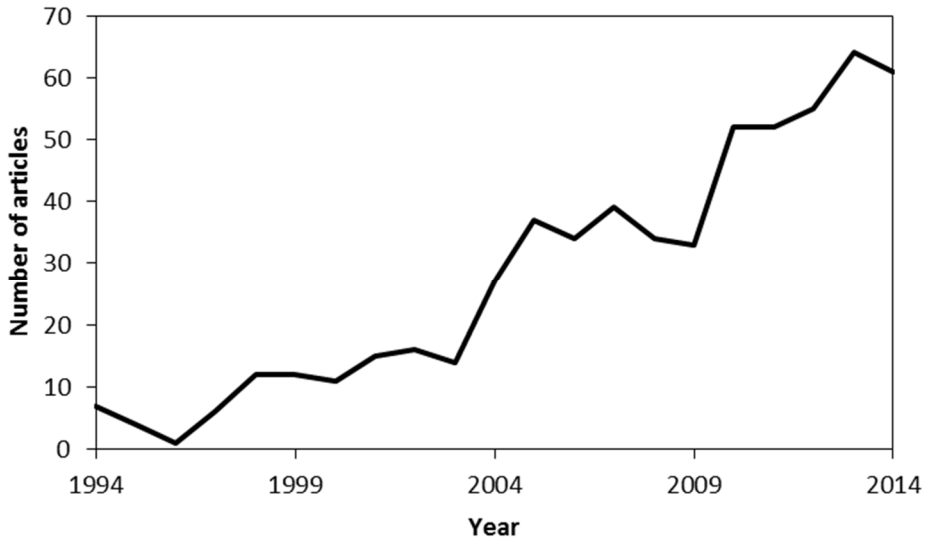

Figure 1-3. Number of articles published in year with respect to heterogeneously catalyzed aldol condensations; literature survey performed at Web of Science using the key words: TOPIC: ((heterogeneous OR silica OR alumina OR PMO OR organosilica OR layered double hydroxides OR hydrotalcite) AND aldol condensation) as accessed on April 14th 2015

1.3.2.1 Mesoporous silicas

According to the IUPAC definition, materials with pores between 2-50 nm are considered mesoporous materials. These materials consist mostly of silica and alumina and are typically amorphous. Until 1990's, no ordered mesoporous materials existed and broad pore size distributions were typically obtained [31, 32]. In 1992, a new family of mesoporous materials, called MCM, was synthesized by researchers at Mobil Research and Development Corporation. In the same year, researchers at the University of Santa Barbara also developed mesoporous silica materials, called SBA. Both the MCM and the SBA materials have regular pore structures similar to zeolites. However, zeolites are microporous materials (<20 Å) and are crystalline in contrast to the conventional mesoporous materials at that time having amorphous walls. MCM-41 was one of the first ordered mesoporous materials that has been discovered. This material has an ordered hexagonal pore structure, a uniform pore size, high surface area (>700 m^2/g) and other desirable properties, such as the ability to tune the pore size [31].

Apart from the structure, also the preparation of these mesoporous materials is similar to that of zeolites, *e.g.*, in both cases, a template is used. The major difference between both preparation methods is that the template used in zeolite synthesis is limited to a single

molecule whereas the templates used in the synthesis of ordered mesoporous materials are molecular aggregates [33]. The synthesis is performed in a solution. The molecular aggregates are formed by adding a surfactant, *i.e.*, a component with a hydrophilic head and a hydrophobic tail, to the solution. These surfactants form micelles, which subsequently serve as a template around which the material is formed. Depending on the surfactant and the shape of the micelles, different structures, *c.q.*, arrangements, can be obtained, *i.e.*, hexagonal arrangement, cubic arrangement or laminar structure, see Figure 1-4 [34].

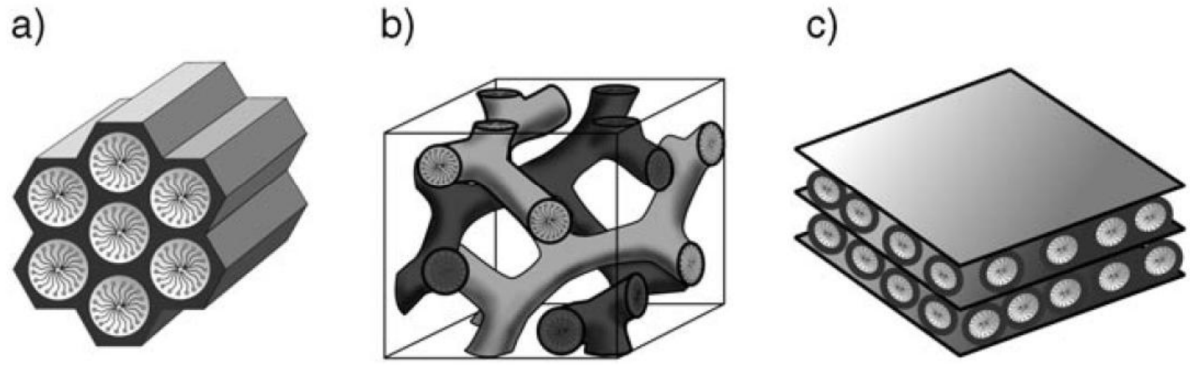

Figure 1-4. Structure of mesoporous silica materials: a) MCM-41, MCM-48 and c) MCM-50 [34]

The surface of mesoporous silicas

At the surface of mesoporous silica materials, the bulk structure terminates in either a siloxane group (≡Si-o-Si≡) which has an oxygen on the surface, or one of several forms of silanol groups (≡Si-OH). The silanol groups can be classified into isolated, vicinal and geminal silanols, as shown in Figure 1-5 [35]. The first type of silanol comprises a surface silicon atom that has three bonds into the bulk structure. Vicinal silanols refer to silanols from which the silicon atoms are separated by a single oxygen bridge. As a result the OH groups are sufficiently close to each other such that a hydrogen bond may develop. The third type of silanols occurs when two hydroxyl groups are attached to a single silicon atom. The geminal silanols are too close to form a hydrogen bond whereas the isolated hydroxyl groups are too far from each other to interact.

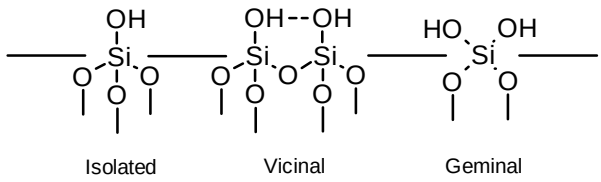

Figure 1-5. Types of surface silanols [35]

The calcination temperature of the silica material has been identified as the key factor to tune the total number of silanols and the relative distribution of the three types [35]. Figure 1-6 shows the average distribution of the silanol types as a function of the calcination temperature. Although the number of silanols depends on the type of silica material and even differs between samples of the same type, Figure 1-6 can be used as an estimate of the actual number and distribution.

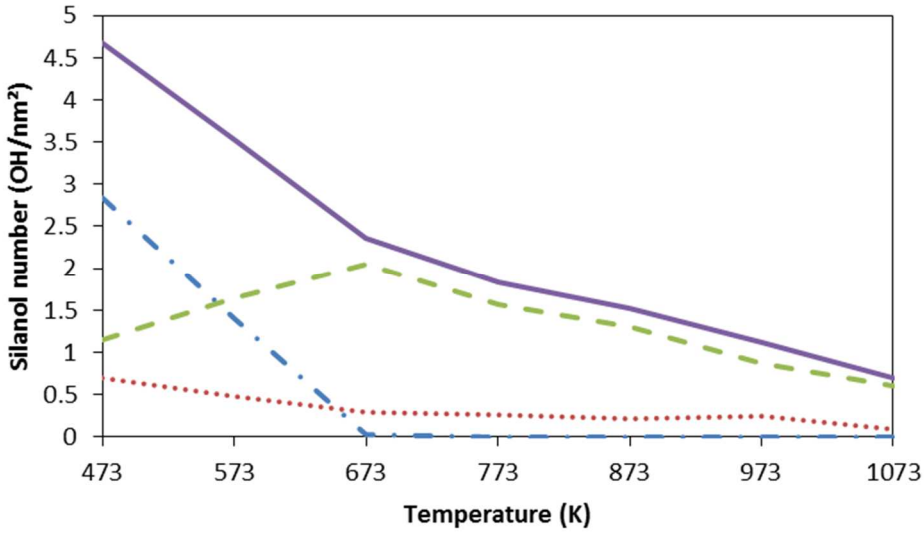

Figure 1-6. Silanol type distribution as a function of calcination temperature; green dashed line: isolated silanols; blue dashed-dotted line: vicinal silanols; red dotted line: geminal silanols; purple full line: total number of silanols [35]

The surface silanols can be deactivated, by reaction with 1,1,1,3,3,3-hexamethyldisilazane (HMDS), an operation which is also denoted as 'endcapping'. As shown in Scheme 1-11, one HMDS molecule reacts with two surface silanols resulting in the formation of two trimethylsilyl species and one ammonia molecule. Because, the stoichiometry of this reaction is well-known, it can be used to determine the number of surface silanols. However, due to sterical effects the trimethylsilyl coverage has an upper limit. Experimentally it was found that this upper limit is in the ranges from 2.2 to 2.7 groups per nm² [36]. Hence, using this method it is impossible to accurately determine the exact number of silanols on silica materials which are calcined at low temperature.

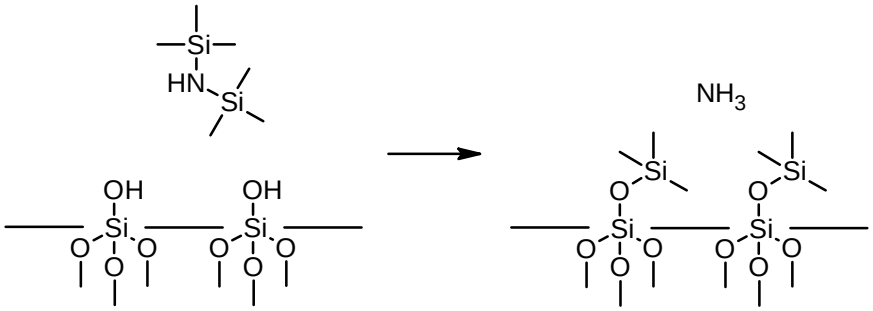

Scheme 1-11. Reaction of HMDS with surface silanols [37]

Functionalization of silica materials

Mesoporous silica on its own is not suitable as an aldol condensation catalyst. To this purpose the silica surface needs to be functionalized with an appropriate functional group, *e.g.*, an amine. This can be achieved via a post-synthesis functionalization or via co-condensation.

Post-synthetic grafting by means of a stirring or reflux procedure is a popular method to functionalize silica materials with amines [35]. In this method an amine-containing silane reacts with a surface silanol after which it is connected to the surface of the silica material, as shown in Scheme 1-12. If water is present in the mixture, the amine-containing silane will be hydrolyzed and releases one or more of its alkoxy groups with the formation of new hydroxyl groups. Afterwards, the silanes can polymerize and form a multilayer on the surface. Hence, if the formation of a multilayer is undesirable the grafting should be performed in the absence of water. Note that if the surface silanols are located close enough to each other, silanes which contain several alkoxy groups are able to form multiple connections with the silica surface.

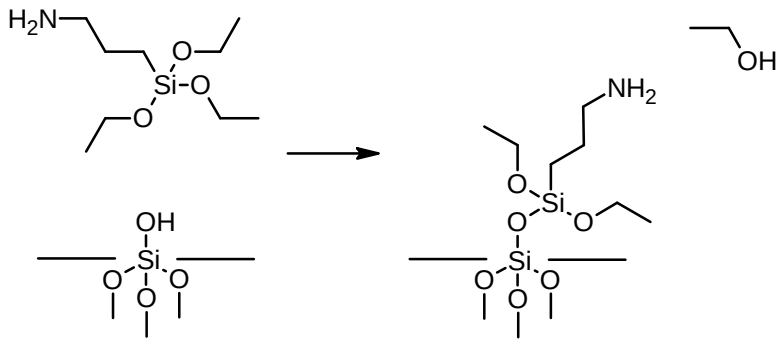

Scheme 1-12. Grafting of 3-aminopropyltriethoxysilane on a silica surface

An alternative method to functionalize silica materials with amines occurs via a one-pot-synthesis, namely by means of co-condensation of the silica precursor and the amine-

containing silane around the surfactant. Since the organic functionalities are direct components of the silica matrix, pore size reduction, and in the most extreme case blocking is less pronounced when using co-condensation. Furthermore, the organic units are generally more homogeneously distributed than in materials which are functionalized by means of post grafting. However, co-condensation has also some disadvantages, *e.g.*, the degree of mesoscopic order of the obtained materials decreases with increasing concentration of organic groups in the reaction mixture. Additionally, it is more difficult to completely remove the template surfactant from the material. The residual template complicates the determination of the organic loading via thermogravimetric analysis, which is a typical method used to assess the loading of organic active sites on the silica surface [26, 34].

1.3.2.2 Periodic mesoporous organosilicas

After the development of the MCM and SBA-materials, the interest to develop hybrid organic-inorganic ordered mesoporous materials with a high concentration of organic groups, wherein the organic and inorganic units are uniformly distributed in the structure has strongly increased. Such Periodic Mesoporous Organosilica materials (PMOs) are obtained through the direct condensation of bridged organosilanes, *e.g.*, $(R'O)_3$-Si-R-Si-$(OR')_3$, in the presence of a template surfactant, see Figure 1-7 [34, 38]. In addition to the high amount and uniform distribution of the organic groups in the pore walls, PMOs are also characterized by a high specific surface areas, thick pore walls, large pores, high pore volumes and an improved thermal stability compared to mesoporous silicas [34, 39]. Because the organic functions are embedded in the walls of the channels, pore blocking is avoided. Additionally, post synthetic tailoring of the organic functions allows further manipulations of the chemical and physical properties without losing the stability of the porous structure [38].

The first PMO materials were synthesized in 1999 by three independent research groups [40-42]. During the first years, only a few precursors (methane, ethane, ethene and benzene bissilanes) were frequently used. Nowadays, however, there is a lot of research on the incorporation of all kinds of bridged organic components [34, 38]. It is also possible to incorporate several types of organic bridges into a single support, which allows to tune the hydrophobicity of the material [43] and, subsequently, also the interactions of the support

with the reactants. This property of PMOs could be interesting in the context of the conversion of aqueous sugars into liquid hydrocarbon fuels, see section 1.1.

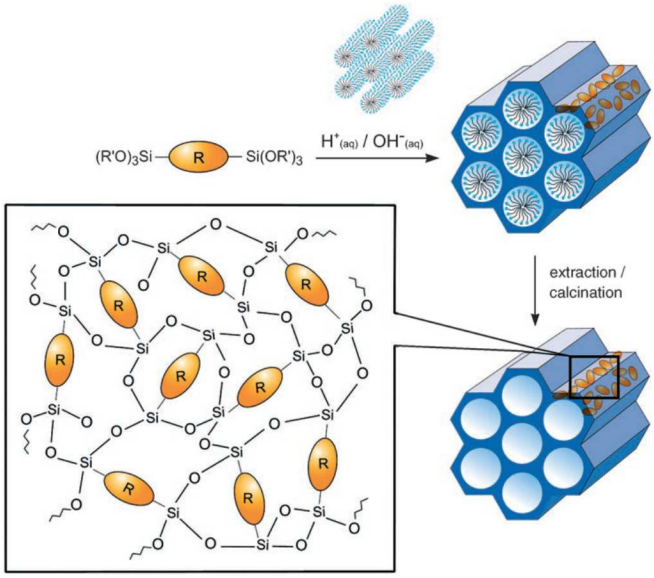

Figure 1-7. Synthesis of a PMO material via the condensation of a bissilane in the presence of a surfactant and an acidic or base environment [34]

1.3.2.3 Layered double hydroxides

Layered double hydroxides consist of positively charged layers which are held together by weak bonds. Water molecules and exchangeable negative ions, are situated between the positive layers to provide charge compensation, see Figure 1-8. These materials occur naturally but can also be synthesized [44].

Generally, a layered double hydroxide material can be represented by $[M^{2+}_{1-x}M^{3+}_{x}(OH)_2]^{x+}[A_{x/n}]^{n-}.mH_2O$ and possesses both acid as base sites. In this notation, M^{2+} and M^{3+} are cations, such as Mn^{2+}, Ca^{2+} or Al^{3+} which act as Lewis acid sites. The nature, strength and relative amount of the acid and base sites depend mainly on the nature and molar ratio of the cations, which usually ranges from 1.5 to 4. The anions are represented by A and are often Cl^-, CO_3^{2-}, O^{2-} or even organic anions which act as Lewis base sites. The OH^- anions present in the material act as Brønsted base sites. One of the most well-known layered double hydroxide is hydrotalcite, which can be represented by the chemical formula $[Mg_3Al(OH)_8][(CO_3)_{1/2}.\ 2H_2O]$ [45-47].

Layered double hydroxide are able to catalyze aldol condensations. The base sites deprotonate the reactants with formation of an enolate ion. The metal ions and acid sites have a stabilizing effect on the reaction intermediates. Additionally, the positively charged metal ions are able to dehydrate the aldol product with formation of a α,β-unsaturated carbonyl compound. Hence, cations as well as the anions have an important effect on the reaction [44, 48, 49].

Pressures around 10 bar and temperatures up to 800 K are necessary to perform aldol condensations using layered double hydroxides [50, 51], which are more severe reaction conditions than necessary using functionalized silica or PMO materials.

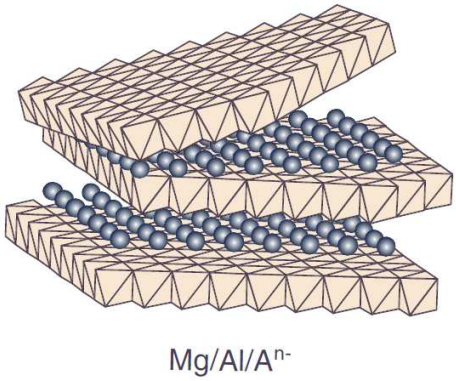

Figure 1-8. Representation of a Mg/Al/A^{n-} layered double hydroxide [44]

1.4 Catalyst design

Catalyst development has been a trial-and-error process for a long time [52]. However, since about a decade, so-called high-throughput technologies have emerged in order to speed up the catalyst innovation, development and optimization process [52, 53]. Complementary to an increased catalyst synthesis, characterization and testing capacity, an adequate feedback from the properties and performance towards the synthesis of a next catalyst generation is pursued via a dedicated design step [52, 54]. Quantitative structure–activity relationships (QSAR) which are empirical in nature and relate the catalyst composition and/or synthesis conditions to its performance, are typically used for this purpose [55]. However, a more fundamental description of the physical and chemical phenomena occurring inside the catalyst is expected to lead towards a more efficient feedback and correspondingly more informed and reliable catalyst design. In particular, microkinetic modeling, *i.e.*, a modeling

based on elementary steps considering each step as (potentially) kinetically relevant, will contribute to reaction mechanism elucidation and the establishment of fundamental relations between catalyst properties and behavior.

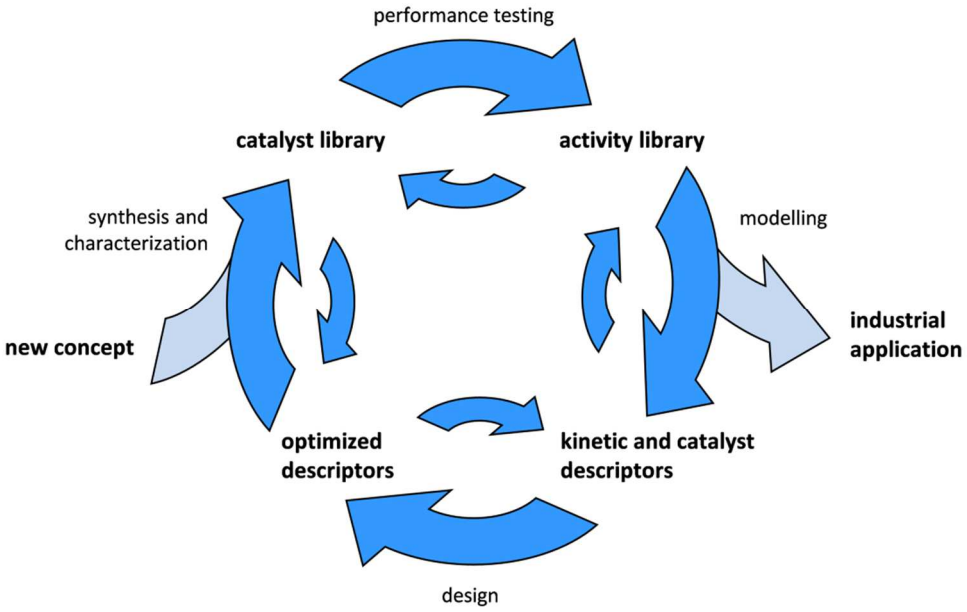

0Figure 1-9. Model based catalyst design methodology [52]

0Figure 1-9 shows a methodology for a model based catalyst design [52]. The first step of the methodology is the synthesis and characterization of a well-selected set of heterogeneous catalysts, which constitutes *the catalyst library* (1st generation). In a second step the catalysts' performance is assessed via a test reaction, *e.g.*, an aldol condensation in the present framework. The effect of the reaction conditions on the catalytic activity is investigated by systematically varying the reaction temperature and the initial reactant concentrations. The resulting kinetics data constitute *the activity library*. Based on an in depth analysis of the activity library a reaction mechanism can be proposed, which is the basis for kinetic model construction. The model contains two types of parameters: *kinetic descriptors* which solely depend on the reaction mechanism and *catalyst descriptors* which specifically account for the effect of the catalyst properties on the kinetics. All descriptors, both kinetic and catalyst, are either determined from independent catalyst characterization measurements or estimated by minimization of the residual sum of squares when simulating the activity library. In a final step the model is used to determine optimal catalyst descriptor values, which can be used to provide feedback to the synthesis step of a subsequent catalyst generation.

1.5 Scope of this thesis

The aim of the present thesis is to investigate the cooperativity between acids and bases during the aldol condensation catalysis and to establish fundamental relations between catalyst properties and performance in order to design optimal heterogeneous cooperative acid-base catalysts for aldol condensations. Due to the moderate reaction conditions which are necessary when the aldol condensation is catalyzed using enzymes and their derivatives, heterogeneous silica and PMO materials functionalized with active sites similar to those of enzymes will constitute the prime focus of the work. In the main part of this work, the aldol condensation of 4-nitrobenzaldehyde and acetone is used as a model reaction.

First, the effect of the weak acid sites inherently present on the silica support in the form of silanols, on amine-catalyzed aldol condensations is investigated. The surface arrangement, more specifically the proximity of the silanols to the amines, is an important catalyst property affecting the cooperativety between the two types of sites. This is rationalized by computer simulations. The reaction mechanism of amine-catalyzed aldol condensations is elucidated in more detail and allows explaining the effect of the amine structure and base strength on the observed activity. This is demonstrated in an integrated manner by kinetic modeling of experimental data acquired on catalysts that were synthesized using commercially available precursors to graft primary, secondary and tertiary amines on the silica surface. Afterwards, the study is expanded towards acid strength effects on acid-base cooperatively catalyzed aldol condensations by systematically varying the strength of the acid site incorporated in the catalyst. The spatial arrangement of the sites with respect to each other is also carefully controlled, providing more insights into the effects on the catalyst behavior. Finally, the information gained based on the selected model reaction is translated to a more relevant reaction, *i.e.*, the aldol condensation of furfural with acetone. This 'translation' also invokes an assessment of the water content in the feed as well as support hydrophobicity effects.

1.6 References

1. International Energy Agency, *Key World Energy Statistics 2014*, **2014**
2. D. L. Klass, *Biomass for renewable energy, fuels, and chemicals*, Academic Press, San Diego, **1998**, xv, 651 p.

3. J. C. Serrano-Ruiz, J. A. Dumesic, Energy Environ. Sci., **2011**, 4, 83-99
4. E. L. Kunkes, D. A. Simonetti, R. M. West, J. C. Serrano-Ruiz, C. A. Gartner, J. A. Dumesic, Science, **2008**, 322, 417-421
5. D. A. Simonetti, J. A. Dumesic, Catal. Rev.-Sci. Eng., **2009**, 51, 441-484
6. K. J. Zeitsch, *The chemistry and technology of furfural and its many by-products*, Sugar series, Elsevier, Amsterdam ; New York, **2000**, xv, 358 p.
7. J. N. Chheda, G. W. Huber, J. A. Dumesic, Angew. Chem.-Int. Edit., **2007**, 46, 7164-7183
8. C. Moreau, M. N. Belgacem, A. Gandini, Top. Catal., **2004**, 27, 11-30
9. D. T. Jones, D. R. Woods, Microbiol. Rev., **1986**, 50, 484-524
10. M. Sasaki, K. Goto, K. Tajima, T. Adschiri, K. Arai, Green Chem, **2002**, 4, 285-287
11. H. Olcay, A. V. Subrahmanyam, R. Xing, J. Lajoie, J. A. Dumesic, G. W. Huber, Energy Environ. Sci., **2013**, 6, 205-216
12. C. A. Wurtz, Comp. Rend., **1872**, 74, 1361
13. L. G. Wade, *Organic chemistry*, Pearson Prentice Hall, Upper Saddle River, N.J., **2006**, xli, 1262, 7, 1, 14 p.
14. G. S. Zweifel, M. H. Nantz, *Modern organic synthesis : an introduction*, W.H. Freeman, New York, **2007**, x, 477 p.
15. R. G. Berger, *Flavours and Fragrances: Chemistry, Bioprocessing and Sustainability*, Springer, **2007**
16. E. M. Carreira, A. Fettes, C. Martl, *Catalytic enantioselective aldol addition reactions*, **2006**
17. D. A. Evans, *Advanced Organic Chemistry: the Aldol Reaction*, **2006**
18. C. Lucarelli, A. Vaccari, Green Chem, **2011**, 13, 1941-1949
19. K. Tanabe, W. F. Holderich, Appl. Catal. A-Gen., **1999**, 181, 399-434
20. F. Tanaka, R. Thayumanavan, N. Mase, C. F. Barbas, Tetrahedron Lett., **2004**, 45, 325-328
21. B. List, R. A. Lerner, C. F. Barbas, J. Am. Chem. Soc., **2000**, 122, 2395-2396
22. R. Cammack, *Oxford dictionary of biochemistry and molecular biology*, Oxford University Press, Oxford ; New York, **2006**, 720
23. S. Huh, H. T. Chen, J. W. Wiench, M. Pruski, V. S. Y. Lin, Angew. Chem.-Int. Edit., **2005**, 44, 1826-1830

24. K. Kandel, S. M. Althaus, C. Peeraphatdit, T. Kobayashi, B. G. Trewyn, M. Pruski, I. I. Slowing, ACS Catal., **2013**, 3, 265-271
25. K. Kandel, S. M. Althaus, C. Peeraphatdit, T. Kobayashi, B. G. Trewyn, M. Pruski, I. I. Slowing, J. Catal., **2012**, 291, 63-68
26. N. A. Brunelli, K. Venkatasubbaiah, C. W. Jones, Chem Mater, **2012**, 24, 2433-2442
27. N. A. Brunelli, C. W. Jones, J. Catal., **2013**, 308, 60-72
28. N. A. Brunelli, S. A. Didas, K. Venkatasubbaiah, C. W. Jones, J. Am. Chem. Soc., **2012**, 134, 13950-13953
29. R. K. Zeidan, M. E. Davis, J. Catal., **2007**, 247, 379-382
30. R. K. Zeidan, S. J. Hwang, M. E. Davis, Angew. Chem.-Int. Edit., **2006**, 45, 6332-6335
31. J. S. Beck, J. C. Vartuli, W. J. Roth, M. E. Leonowicz, C. T. Kresge, K. D. Schmitt, C. T. W. Chu, D. H. Olson, E. W. Sheppard, S. B. Mccullen, J. B. Higgins, J. L. Schlenker, J. Am. Chem. Soc., **1992**, 114, 10834-10843
32. R. Iler, *The Chemistry of Silica: Solubility, Polymerization, Colloid and Surface Properties and Biochemistry of Silica*, John Wiley & Sons, **1978**
33. J. Y. Ying, C. P. Mehnert, M. S. Wong, Angew. Chem.-Int. Edit., **1999**, 38, 56-77
34. F. Hoffmann, M. Cornelius, J. Morell, M. Froba, Angew. Chem.-Int. Edit., **2006**, 45, 3216-3251
35. P. Van Der Voort, E. F. Vansant, J. Liq. Chromatogr. Relat. Technol., **1996**, 19, 2723-2752
36. E. F. Vansant, P. Van Der Voort, *Characterization and Chemical Modification of the Silica Surface. 2 ed. Studies in Surface Science and Catalysis*, **1997**
37. R. Anwander, I. Nagl, M. Widenmeyer, G. Engelhardt, O. Groeger, C. Palm, T. Roser, J Phys Chem B, **2000**, 104, 3532-3544
38. P. Van der Voort, C. Vercaemst, D. Schaubroeck, F. Verpoort, Phys. Chem. Chem. Phys., **2008**, 10, 347-360
39. D. A. Loy, K. J. Shea, Chem. Rev., **1995**, 95, 1431-1442
40. B. J. Melde, B. T. Holland, C. F. Blanford, A. Stein, Chem Mater, **1999**, 11, 3302-3308
41. S. Inagaki, S. Guan, Y. Fukushima, T. Ohsuna, O. Terasaki, J. Am. Chem. Soc., **1999**, 121, 9611-9614
42. T. Asefa, M. J. MacLachlan, N. Coombs, G. A. Ozin, Nature, **1999**, 402, 867-871
43. Z. An, Y. Guo, L. W. Zhao, Z. Li, J. He, ACS Catal., **2014**, 4, 2566-2576

44. D. Tichit, B. Coq, Cattech, **2003**, 7, 206-217

45. C. N. Perez, C. A. Perez, C. A. Henriques, J. L. F. Monteiro, Appl. Catal. A-Gen., **2004**, 272, 229-240

46. K. K. Rao, M. Gravelle, J. S. Valente, F. Figueras, J. Catal., **1998**, 173, 115-121

47. S. Abello, D. Vijaya-Shankar, J. Perez-Ramirez, Appl. Catal. A-Gen., **2008**, 342, 119-125

48. D. Tichit, M. H. Lhouty, A. Guida, B. H. Chiche, F. Figueras, A. Auroux, D. Bartalini, E. Garrone, J. Catal., **1995**, 151, 50-59

49. E. Suzuki, Y. Ono, Bull. Chem. Soc. Jpn., **1988**, 61, 1008-1010

50. S. Ordonez, E. Diaz, M. Leon, L. Faba, Catal Today, **2011**, 167, 71-76

51. W. Kagunya, W. Jones, Appl. Clay Sci., **1995**, 10, 95-102

52. J. W. Thybaut, G. B. Marin, J. Catal., **2013**, 308, 352-362

53. R. A. Potyrailo, W. F. Maier, *Combinatorial and High-throughput Discovery and Optimization of Catalysts and Materials*, CRC Taylor & Francis, Boca Raton, FL, **2007**

54. J. W. Thybaut, I. R. Choudhury, J. F. Denayer, G. V. Baron, P. A. Jacobs, J. A. Martens, G. B. Marin, Top. Catal., **2009**, 52, 1251-1260

55. X. Z. Wang, B. Perston, Y. Yang, T. Lin, J. A. Darr, Chem. Eng. Res. Des., **2009**, 87, 1420-1429

Chapter 2

Functional Group Positioning Effects on Cooperative Catalysis

Free silanol groups are known to enhance the activity of aminated silica materials for aldol condensation. In this chapter the effect of the silanol-to-amine ratio on the reaction of 4-nitrobenzaldehyde and acetone is investigated in a range from 0 to 2.4. Irrespective of the amine density, identical, moderate turnover frequencies are obtained if the silica exclusively has amines on its surface, *i.e.*, when the silanols were endcapped. The turnover frequency increases with increasing silanol-to-amine ratio until an upper limit is reached at a silanol-to-amine ratio of 1.7. At this upper limit the turnover frequency exceeds the turnover frequencies obtained with the unpromoted amine-based catalysts by a factor 5. This increase is ascribed to hydrogen-bridge interactions between the silanols and the carbonyl moiety of the reactants. As a result the reactants become more susceptible to nucleophilic reactions with the amine as required for the aldol condensation. The observation that values for the silanol-to-amine ratio exceeding one are required, can be rationalized by computer simulations. It was found that amine groups were grafted on the silica surface in a clustered manner, originating from positive deviations from thermodynamic ideality in the synthesis mixture, *i.e.*, from clustering of the amine precursor in the liquid synthesis mixture.

2.1 Introduction

Owing to their large pore sizes, large surface areas and the easy incorporation of different types of active sites, mesoporous silica materials are very useful as model catalysts for research purposes. It has been concluded recently [1-5] that amine groups, grafted as active sites on a silica support, perform well in aldol condensation. Most often, the silica surface is grafted with a silane, such as (3-aminopropyl)triethoxysilane (APTES), through stirring or refluxing. The catalytic activity of amines in aldol condensations and other important C-C coupling reactions can be improved by incorporating weak acid sites [2, 4-16]. This promoting effect is interesting because the silica material already inherently possesses such sites, *i.e.*, the silanol groups. Kubota et al. [4] demonstrated that these weakly acidic silanol groups indeed have a promoting effect on the activity of the amine groups. However, a systematic investigation of the effect of the surface silanol groups on amine-catalyzed aldol condensations has never been performed. Recently, Brunelli et al. [6] reported that the replacement of the silanols by carboxylic acids has a negative impact on the activity of the catalyst. The lower activity of amines, when combined with stronger acid sites compared to silanol groups, could be the result of a pronounced shift in the equilibrium from the free acid and free base towards the resulting neutralized ion pair. Furthermore, ambiguity exists about the actual reaction mechanism of amine-catalyzed aldol condensations. Some authors attribute the activity to the presence of different species during catalysis such as an imine [5], an enolate, the formation of which is possibly assisted through imine formation [2], an enamine [4, 15], or a carbanion [17]. The exact type of intermediate may depend on the type of amine used as active site. However, recent literature [8, 9] indicates that the formation of an imine is not responsible for the activity of the catalyst but rather constitutes an inhibition pathway.

In this chapter, the ratio of acid and base active sites has been systematically varied to unravel the effects exerted by silanol groups on the activity and the selectivity of aminated silica catalysts in the well-known test reaction of acetone and 4-nitrobenzaldehyde. APTES was chosen as a precursor for the active amine groups because, according to Brunelli et al. [7], the catalytic cooperativity between silanols and amines increases with the linker length up to a propyl chain. No additional benefit is gained with longer carbon chains whereas shorter ones such as C_1 and C_2, limit the cooperativity. Furthermore, the catalytic reaction

mechanism including the promoting effect was elucidated, among others, by analyzing the reaction between acetone and propyl amine by means of in situ Raman spectroscopy. In the final part of this chapter, a detailed analysis of the positioning of the amine groups on the catalyst surface was performed, which allowed for a quantitative explanation of the promotional effect of the silanol groups as a function of the silanol-to-amine ratio. Additionally, a series of cooperative catalysts were synthesized using (3-aminopropyl)dimethylethoxysilane (APDMES) as a precursor in order to investigate the effects of the ethoxy groups of the precursor on the positioning of the amines.

2.2 Procedures

2.2.1 Catalysts synthesis

2.2.1.1 Grafting of amines on Silicagel 60

The catalysts were prepared by using a commercially available mesoporous silica, *i.e.* silicagel 60 (grade 7734, Sigma–Aldrich). First, the silica is heated to 700°C with a heating rate of 2°C min^{-1} and maintained at this temperature for 6 h. After this pretreatment, the material is slowly cooled to a temperature of approximately 150°C. The pretreated material (5 g) is diluted in toluene (30 mL, extra dry, Acros) while still hot to avoid rehydration of the samples. The amine-containing silane, APTES (98%, ABCR) or APDMES (97 %, ABCR), is subsequently added. The added volume of the amine precursor is varied between several batches to silylate the silica with different amounts of amine groups (APTES 1–8 and APDMES 1–5). The molar ratio of added precursor to free silanols is varied in the range of 0.1–5. The necessary volume of the precursor is calculated by assuming the number of free silanols is equal to 1.1 $OHnm^{-2}$, see Figure 1-6 [18]. Caution is required as the silica, even after a treatment at 700°C can still readsorb water, and variations up to 25% are possible upon comparison of different kinds of silica [19, 20]. In this chapter, these deviations could be kept below 10%. However, as long as the amines are able to reach the surface silanols it is the silanol-to-amine ratio which is decisive for the obtained turnover frequencies. After adding the precursor, the mixture is heated to reflux under an argon atmosphere at 110°C for 24 h. The solid is recovered by filtration and washed with chloroform (>99.8%, Roth) for

3 h. After drying in vacuo at room temperature (RT) for 24 h the cooperative catalysts (samples AB) are ready for kinetic testing.

2.2.1.2 Endcapping the silanol groups with HMDS

Approximately half of the amount produced of each of the cooperative acid-base catalysts (type AB) is subsequently treated with 1,1,1,3,3,3-hexamethyldisilazane (HMDS, 98 %, ABCR) to prepare the unpromoted base catalysts (type B). The dry material (2.5 g) is added to a flask and completely covered with HMDS. The mixture is vigorously stirred at RT for 3 h and, subsequently, the mixture is filtered and thoroughly washed with chloroform for 3 h. Finally, the solids are dried in vacuo at room temperature for 24 h. HMDS quantitatively reacts with the surface silanols of silicagel if the silica is pretreated at a temperature above 400°C [21, 22]. Hence, this HMDS treatment endcaps all remaining silanols on the surface by replacing them with a trimethylsilyl function. A blank silica (sample 0), before (type AB) and after HMDS treatment (type B), is also studied as a reference. Thus, in total 28 different catalysts are prepared: samples prior to (type AB) and after (type B) HMDS treatment of catalysts without grafted amines (0), with amines grafted using a triethoxy-precursor (APTES 1–8), and with amines grafted using a monoethoxy-precursor (APDMES 1-5).

2.2.2 Catalyst characterization

Nitrogen adsorption–desorption measurements are conducted at 77 K by using a Belsorp Mini II gas analyzer. Samples are degassed at 120°C for 17 h prior to measurement and are measured immediately afterwards, without any re-exposure to air. The specific surface area and pore volume are determined by using the Brunauer-Emmett-Teller (BET) method [23]. The average pore size of the silica is obtained by using the Barrett–Joyner–Halenda (BJH) method [24].

The pretreatment of the silica results in an initial free silanol number (before the grafting of amines) of 1.1 OH nm^{-2} [18]. Experimental variations in the treatment could result in small deviations in the silanol content and, therefore, it is important to experimentally determine both the number of grafted amines and the number of remaining silanols on the surface. 1,1,1,3,3,3-hexamethyldisilazane (HMDS) has been demonstrated to react completely up to a silanol loading of 2.2 OHnm^{-2}, above which sterical hinderance becomes important [21]. Because precautions are needed when using silanes as a silanol titrator [22], an HMDS

treatment was preferred to 'remove', *c.q.*, endcap, all surface silanols. The concentrations of amine and endcapped silanol groups are determined by using elemental (CHNS) analysis. These experiments are performed on a Thermo Flash 2000 elemental analyser using V_2O_5 as catalyst. Sample cups are tightened and the analysis waiting time is kept as short as possible to avoid or minimize water readsorption, influencing the weight and elemental composition of the samples. This is especially important for the non-hydrophobized samples, *i.e.*, the samples of type AB.

The presence of amine groups after grafting and silanol removal through HMDS treatment is demonstrated by means of Diffuse Reflectance Infrared Fourier Transform (DRIFT) spectroscopy. These measurements are performed on a Nicolet 6700 of Thermo Scientific with a nitrogen cooled MCT-A detector. The DRIFT spectra are obtained using a Graseby Specac diffuse reactant cell, operating *in vacuo* at 140°C.

The ^{13}C CP/MAS NMR spectra are recorded at 100.6 MHz on a Bruker AVANCE-400 WB spectrometer at RT. The samples are spun at 13000 Hz. An overall 10000 free-induction decays were accumulated with 4 s of recycle time. Chemical shifts are measured relative to a tetramethylsilane standard.

2.2.3 Enamine detection

An in situ Raman experiment is performed on a Kaiser Raman RXN1 analyzer using an Invictus 532 nm VIS laser. Acetone (0.5 mL) and *n*-propylamine (0.5 mL) are mixed in a 1 mL vial. The reaction at RT between these two components was monitored for 3 h by taking a spectrum every 5 min.

2.2.4 Aldol condensation kinetics

The aldol condensation of acetone (99.6%, Acros) with 4-nitrobenzaldehyde (99 %, Acros) (Scheme 2-2) is performed in *n*-hexane as a solvent. Literature shows that the polarity and protic character of the solvent strongly affect the aldol condensation kinetics [3]. It was found that nonpolar, aprotic solvents, such as *n*-hexane are beneficial [3]. The experiments are performed in a Parr 4560 mini reactor, which is of the batch type and has a 300 mL volume. The reactor temperature is maintained using a thermocouple and a PID controller (CAL 9500P controller). The PID controller is connected to the reactor heating jacket and an

additional cooling unit (DLK 402 circulating cooler). The reaction mixture is stirred with a mechanical stirrer rotating at 500 rpm. The reactor is first loaded with an amount of catalyst corresponding to 0.114 mmol primary amines, *n*-hexane (36.0 g, Extra Pure, Acros) as a solvent, and methyl 4-nitrobenzoate as an internal standard (0.264 g, >99 %, Aldrich). Then, the mixture is heated to the reaction temperature. Acetone (46.0 g) is separately heated to the reaction temperature and used to dissolve 4-nitrobenzaldehyde (0.504 g) before injection in the reactor. The injection time is taken as the start of the reaction (t=0). The reaction is monitored for 200 min by taking a 0.5 mL samples of the reaction mixture every 20 min. These samples are analyzed by using a reversed-phased high-performance liquid chromatograph (RP–HPLC), from Agilent (1100 series). The HPLC is operated at a column temperature of 30°C and by using a gradient method with water (0.1% trifluoroacetic acid, Acros) and acetonitrile (HPLC grade, Acros) as solvents. In this gradient method the volumetric percentage of acetonitrile is varied from 30% to 62% over a period of 7 min in order to obtain a good separation of the peaks. The components are identified by using a UV detector. The wavelength of the UV source is varied as a function of time such that each component is detected using the wavelength it adsorbs the most, see Table 2-1. Quantification of the different components in the reaction mixture is performed by relating the peak surface areas to the amount of the internal standard, methyl 4-nitrobenzoate, see eq. 1. The calibration factors (CF_i) shown in Table 2-1, are determined from calibration mixtures where the composition has been determined by means of liquid phase H-NMR.

$$C_i = CF_i \frac{A_i}{A_{IS}} C_{IS} \quad (1)$$

Because of the low UV absorbance by acetone, which is reflected in the large calibration factor, a molar balance based on the aromatic components is made rather than a conventional mass balance, see eq. 2. For each experiment, this balance is closed within ± 5% and, subsequently, the concentrations are normalized assuming a closed balance.

$$n_{benz}^0 = n_{benz}^t + n_{aldol}^t + n_{ketone}^t \quad (2)$$

The activity of the catalysts is described by their turnover frequency (TOF), which could be determined from the slope of the initial linear part of the 4-nitrobenzaldehyde conversion profile as a function of time, the concentration of amine active sites and the initial 4-nitrobenzaldehyde concentration, see eq. 3 [25]. The concentration of the silanol groups is

not considered in the calculation of the TOF because the silanol groups only act as promoters and not as actual, catalytically active sites.

$$TOF = \frac{dX_{benz}/dt|_{t=0}\, C^0_{benz}}{C_{amines}} \quad (3)$$

Table 2-1. Wavelength of maximum adsorption and calibration factor for each component

Component	Wavelength (nm)	Calibration Factor
Acetone	265	786.69
Aldol product	272	1.29
4-nitrobenzaldehyde	265	0.87
Ketone product	305	0.53
Methyl 4-nitrobenzoate	260	1.0

2.2.5 Modeling of the arrangement of active sites

The modeling part of this chapter was done by using an in-house written Fortran code. This code simulates the amine grafting on a catalyst surface based upon random number generation and a grafting 'probability', see Scheme 2-1. This grafting probability depends on the type of clustering, *i.e.*, random positioning, clustering upon grafting or clustering in the synthesis mixture, and represents the probability that an amine is grafted on a position neighboring a given number of amines. More details about the grafting probabilities used in this work can be found in Appendix A. The percentage of promoted amines can be calculated from these generated surfaces.

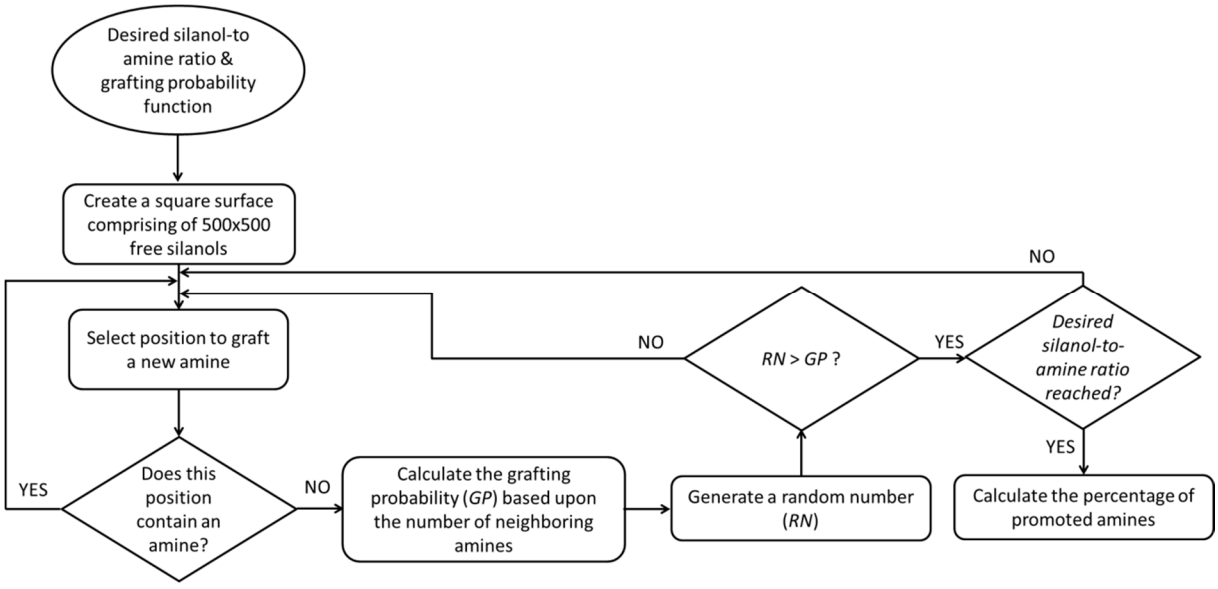

Scheme 2-1. Surface generation algorithm

2.2.6 Thermodynamic liquid-phase non-ideality calculations

The thermodynamic non-ideality of the liquid synthesis mixture was assessed by using the UNIFAC method [26, 27] to calculate the activity coefficients. As the required information for complex molecules such as APTES was not available, a model mixture comprising toluene and propylamine was used for this purpose. These calculations are performed using the commercial simulation software Aspen Plus.

2.3 Results and Discussion

2.3.1 Catalyst characterization and validation of the synthesis procedure

A nitrogen adsorption–desorption isotherm of type IV was obtained for the silicagel 60 material, pretreated at 700°C, see Figure 2-1. The material has a specific BET surface of 497 m^2g^{-1}, a total pore volume of 0.69 cm^3g^{-1}, and an average pore diameter of 5.6 nm.

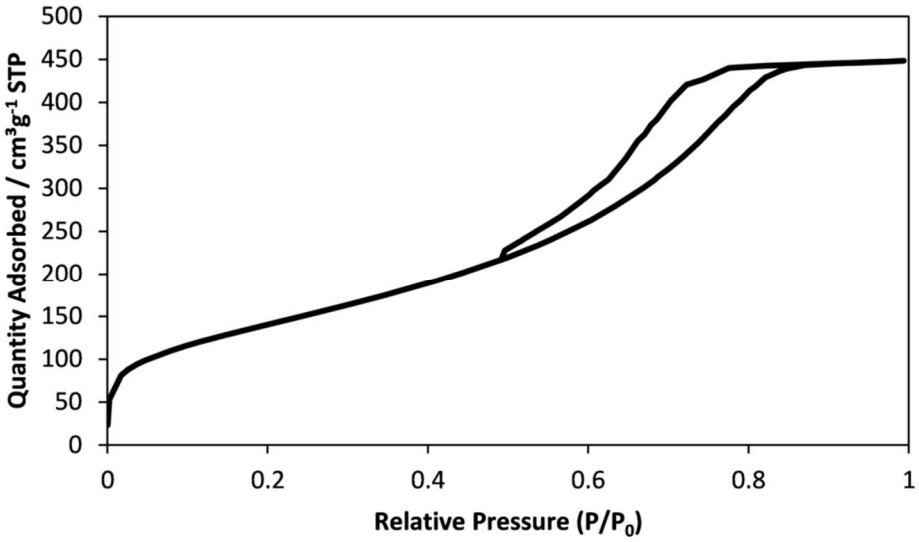

Figure 2-1. Adsorption-desorption isotherm from Silicagel 60, pretreated at 700°C

The presence of amine groups after grafting with APTES and silanol endcapping by HMDS treatment is demonstrated by using diffuse reflectance infrared Fourier transform (DRIFT) measurements. Note that the DRIFT spectra shown in Figure 2-2 are not scaled to the peaks originating from the silica structure, *i.e.*, the peaks in the range of 1000-2000, in order to clearly show the peaks which are important for the characterization of the materials. Prior

to grafting of the amine groups with APTES, the pretreated silica exhibited a narrow vibration band at 3745 cm^{-1}, characteristic for the free silanol groups (Si-OH), see Figure 2-2a. After treatment with APTES, see Figure 2-2b, the sample exhibited several bands in the range of 2800–2960 cm^{-1}, which can be attributed to the C-H stretching vibrations of the propyl or ethoxy groups of the grafted APTES. Two additional bands at 3314 and 3380 cm^{-1}, which are small but significant, specifically confirm the presence of amine groups. A signal remained at 3745 cm^{-1}, indicating that free silanol groups are preserved after grafting with APTES. Finally, after treatment with HMDS, see Figure 2-2c, the –OH stretching band at 3745 cm^{-1} disappeared completely, which confirms that all surface silanols were successfully endcapped. The additional C-H stretching vibrations of the trimethylsilyl group originating from the HMDS treatment explain the different patterns in the spectra b and c in the range of 2800–2960 cm^{-1}. These DRIFT results agree with what is reported in the literature. [28-32]

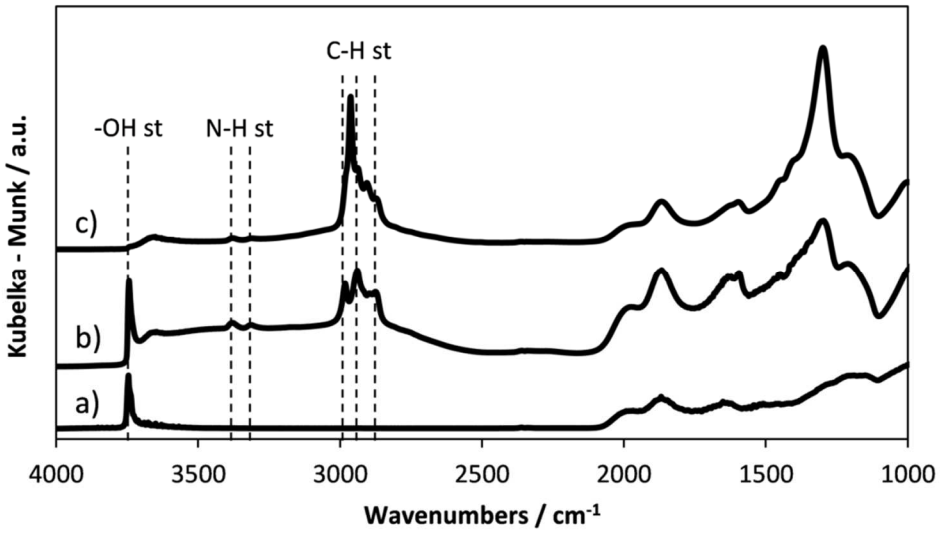

Figure 2-2. Typical DRIFT spectra of a) pretreated silica; b) APTES 6 (type AB); c) APTES 6 (type B)

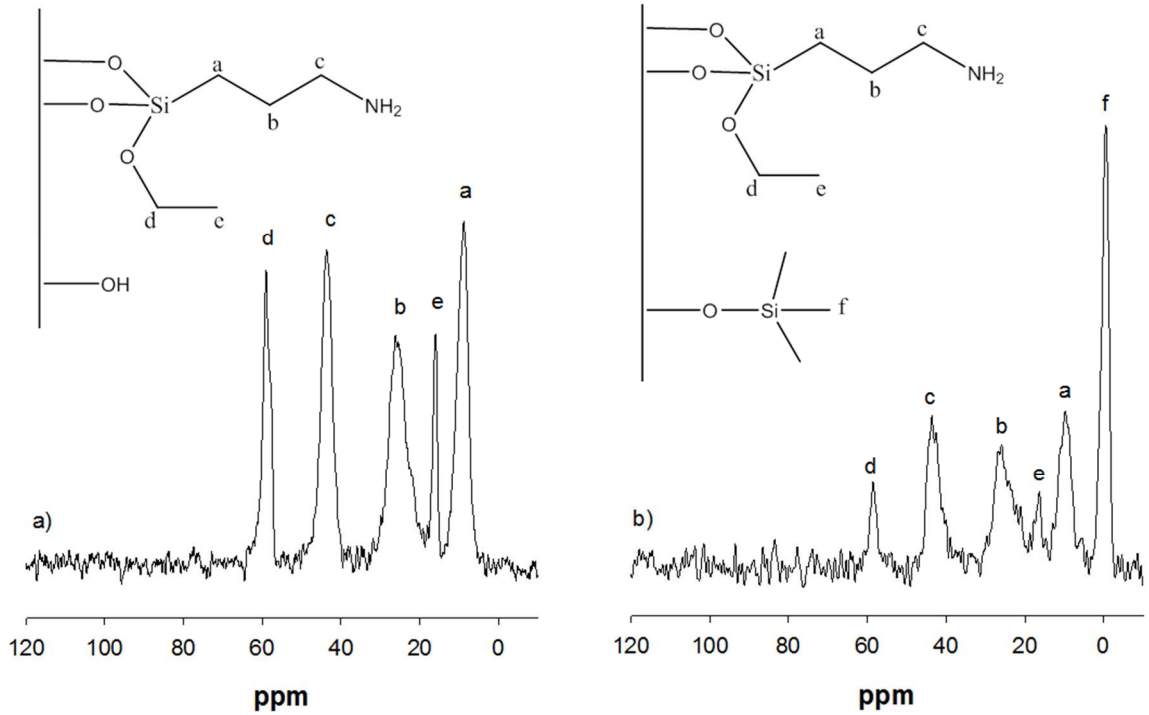

Figure 2-3. ^{13}C CP/MAS NMR spectra and assignment to chemical groups of a) cooperative acid-base catalyst APTES 6 (type AB); and b) unpromoted base catalyst APTES 6 (type B)

The presence of amine groups was also confirmed by ^{13}C cross-polarization/magic-angle-spinning (CP/MAS) NMR spectroscopy. After grafting with APTES, see Figure 2-3a, the silica exhibited three peaks at **(a)** 9, **(b)** 26, **(c)** 43 ppm, which can be associated to the sp^3 carbon atoms of the amine-containing propyl chains. Two more signals at **(e)** 16 and **(d)** 58 ppm can be assigned to ethoxy groups (-O-CH_2-CH_3), which did not react with a surface silanol. After HMDS treatment, see Figure 2-3b, the spectrum revealed an additional signal centered at approximately 0 ppm, which corresponds to the CH_3- signal of trimethylsilyl groups.

The active-site concentrations have been determined by using CHNS elemental analysis, see Table 2-2. The concentrations of amine groups on cooperative acid-base (type AB), as well as on unpromoted base (type B), samples were calculated from the obtained nitrogen weight percentage and found to be identical. The concentrations of free silanol groups on the cooperative samples were determined from the increase in carbon content after HMDS treatment, as one silanol is capped by one trimethylsilyl moiety and, hence, is equivalent with a mass increase corresponding to three carbon atoms. The experimental error was found to be independent of concentration and active site type and equal to 0.02 wt.%. By applying the rules of error propagation, it was found that the experimental error in the molar silanol-to-amine ratio decreases with decreasing ratios. Except for the reference

catalysts, all catalysts were synthesized in the molar silanol-to-amine ratio range from 0.4 to 2.4.

Table 2-2. Number of active sites determined through CHNS elemental analysis for the APTES-functionalized silica materials

Catalyst	Amine[a] [mmol g^{-1}]	Silanol[b] [mmol g^{-1}]	Silanol/amine[c]
Silica 0	0.00	0.91	∞
APTES 1	0.29	0.67	2.33 ± 0.13
APTES 2	0.32	0.69	2.15 ± 0.11
APTES 3	0.33	0.67	2.07 ± 0.11
APTES 4	0.35	0.61	1.73 ± 0.09
APTES 5	0.40	0.56	1.39 ± 0.07
APTES 6	0.49	0.50	1.03 ± 0.04
APTES 7	0.59	0.45	0.77 ± 0.04
APTES 8	0.65	0.27	0.42 ± 0.03

[a] The amine concentrations on the catalysts is equal for catalysts of type AB and type B. The error on this measurement amounts for all samples to ±0.01 $mmolg^{-1}$. [b] The silanol concentrations given in the table is only valid for catalysts of type AB, catalysts of type B have no silanols on the surface. The error on this measurement is for all samples ±0.01 $mmolg^{-1}$. [c] The ratio of silanols to amines given in the table is only valid for catalysts type AB, catalysts of type B have a silanol-to-amine ratio equal to zero.

2.3.2 The promoting effect of silanol groups on amine-catalyzed aldol condensation

The catalysts' performance was assessed through aldol condensation experiments with 4-nitrobenzaldehyde and acetone as reactants, see Scheme 2-2. The experiments were performed at 55 °C with an excess of acetone, *n*-hexane as the solvent, and methyl 4-nitrobenzoate as an internal standard. No conversion was observed if the reference materials, on which no amine groups had been grafted, were used as the catalysts. This means that neither pristine, *i.e.*, silica 0 (type AB), nor endcapped silica, *i.e.*, silica 0 (type B), are active in aldol condensation and that the incorporation of other functional groups is necessary to catalyze the reaction. Note that according to Davis and coworkers, the best catalytic results are obtained if the functional groups are effectively grafted on the surface of a silica material [3].

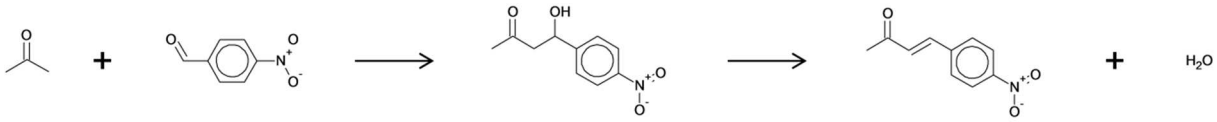

Scheme 2-2. Aldol condensation of acetone and 4-nitrobenzaldehyde towards 4-hydroxy-4-(4-nitrophenyl)butane-2-one and 4-(4-nitrophenyl)-3-buten-2-one, the aldol and ketone, respectively

In Figure 2-4, the evolution of the turnover frequencies (TOFs) obtained with the different catalysts as a function of their silanol-to-amine ratio is shown. All turnover frequencies were calculated with respect to the amine groups because the silanol groups only act as promoters and not as actual, catalytically active sites. The HMDS-treated catalysts (type B) all exhibited a similar catalytic activity, corresponding with a TOF of 1.94 x 10^{-4} s^{-1}. This activity is solely caused by the primary amines, *i.e.*, silanol groups are not necessary to catalyze the aldol condensation. The results also show that the TOFs of the unpromoted base catalysts (type B) are independent of the amount of trimethylsilyl moieties on the catalyst surface. The TOFs obtained with the cooperative catalysts (type AB) are higher and exhibit an S-shaped relation as a function the molar silanol-to-amine ratio. The trend starts with an intercept that is identical to the TOF of a unpromoted base catalyst (type B) because at a silanol-to-amine ratio of 0 the catalyst is unpromoted. At low silanol-to-amine ratios, the observed TOF only increases moderately. However, in the range from 0.5 to 1.1 it increases more rapidly with the molar silanol-to-amine ratio, after which the increase becomes again more moderate. The TOF reaches a plateau at a silanol-to-amine ratio of approximately 1.7. From this ratio onwards a further increase in silanol concentration does not lead to an increase in the activity of the amines, which is caused by the excess of silanol groups, *i.e.*, no amines are left that are not promoted yet. The TOFs obtained at the plateau are equal to 1.04 x 10^{-3} s^{-1}, which exceed the TOFs obtained with the unpromoted, HMDS-treated catalysts (type B) by a factor of 5 and which is in the same order of magnitude as reported in the literature [4].

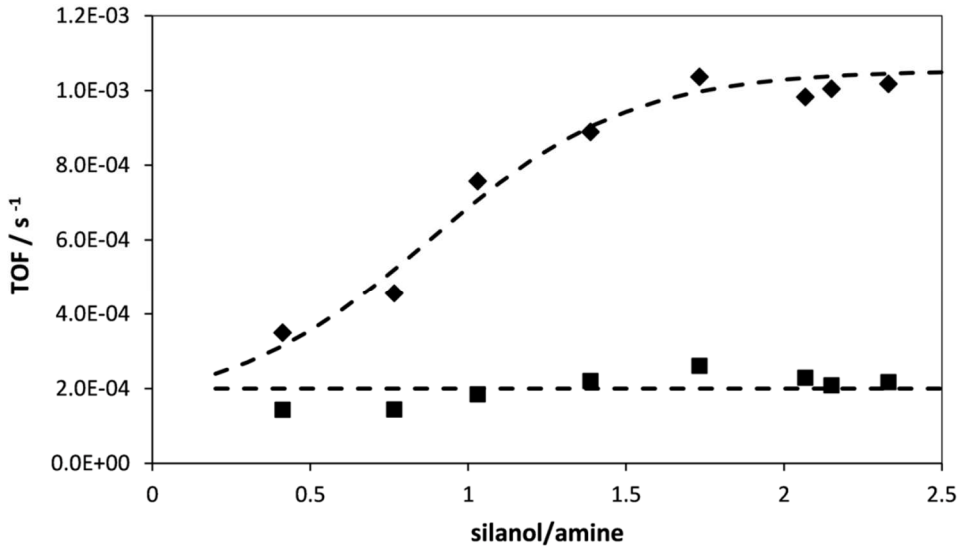

Figure 2-4. TOFs of the catalysts (type AB, ◆) as a function of their molar silanol-to-amine ratio and the HMDS-treated catalysts (type B, ■) as a function of the molar silanol-to-amine ratios of their parent catalysts; the dashed lines are intended as visual aids only

2.3.3 Reaction mechanism

Based on the delplot technique, as presented by Bhore et al. [33], it is shown that 4-hydroxy-4-(4-nitrophenyl)butane-2-one (aldol) is a primary product and 4-(4-nitrophenyl)-3-buten-2-one (ketone) a secondary one. In Figure 2-5 a and c, the first-order delplot chart representing the product selectivities, and in Figure 2-5b and d the second-order deplot chart representing the product selectivities divided by 4-nitrobenzaldehyde conversion versus the 4-nitrobenzaldehyde conversion are shown for both reaction products. The curve of the aldol product in the first-order delplot chart (a) clearly exhibits a nonzero intercept whereas the corresponding curve in the second-order delplot chart (b) exhibits an asymptote towards infinity at zero conversion. This result clearly demonstrates the primary nature of this reaction product. The secondary nature of the ketone product is indicated by the zero intercept in the first-order deplot chart and the finite, nonzero intercept in the second-order delplot chart (curves c and d, respectively). These results are consistent with the generally accepted reaction sequence for aldol condensation, which comprises the formation of the aldol product and its subsequent dehydration into an unsaturated ketone [2, 17, 34-39]. Although the catalyst activity is enhanced by the presence of silanol groups, it seems that the product distribution is not significantly affected. In all experiments, the

selectivities follow very similar trends. Also the unpromoted base catalysts (type B) follow this trend (not shown in the figure). This is consistent with silanol groups serving as promoters but not as the actual, catalytically active sites.

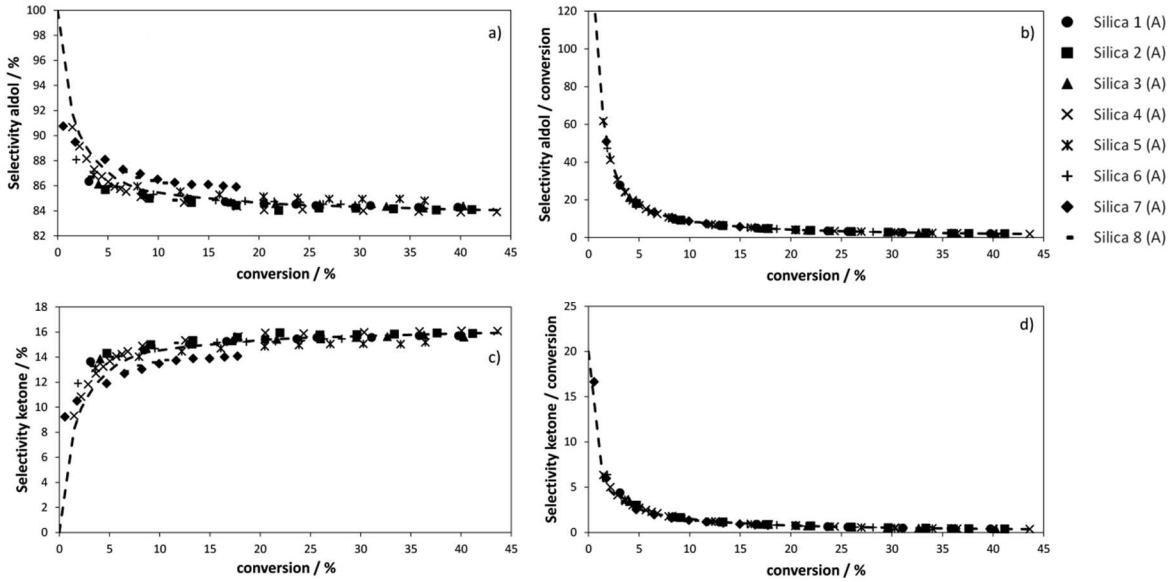

Figure 2-5. First-order (a,c) and second-order (b,d) delplot charts for the aldol (a,b) and the ketone (c,d) products

To obtain a better understanding of the heterogeneously catalyzed reaction between acetone and 4-nitrobenzaldehyde, more particularly, of surface intermediates that are potentially formed, the homogeneous reaction between acetone and *n*-propylamine was investigated via in situ Raman spectroscopy. The reaction was monitored at room temperature for 3 h by taking a spectrum every 5 min. In Figure 2-6, the Raman spectra at the start and the end of the experiment are shown. The peaks at 3314 and 3380 cm^{-1}, corresponding to the amine group of n-propylamine, decrease during the experiment. At the same time the peak at 1700 cm^{-1}, corresponding with the carbonyl group of acetone, decreases. New peaks at 1666, 1377, and 3680 cm^{-1} (very small) appear, corresponding with C=C stretching, -OH bending, and -OH stretching vibrations, respectively. These results suggest that acetone reacts with a primary amine yielding an enamine and with a carbinolamine formed as an intermediate. The presence of the enamine is also reported in the aldol condensation catalyzed by the homogeneous catalyst, L-proline [35, 40].

Based upon the experimental observations as described above, a reaction mechanism is proposed for the primary amine-catalyzed aldol condensation. In the absence of promoting silanol groups, the reaction mechanism comprises the reactions represented in Scheme 2-3a. In a first step an alcohol **(1)** is formed through nucleophilic addition of acetone to the amine group on the surface, after which it dehydrates with formation of an enamine **(2)**. The exact intermediate **(3)** formed from this enamine and 4-nitrobenzaldehyde depends on the possibility of a hydrogen transfer to take place. If hydrogen transfer is indeed possible in the transition state an iminium ion **(3)** will be obtained [34, 41] while an oxetane will be formed otherwise [41]. The primary aldol product is formed in a water-assisted desorption of the intermediate **(3)**. Subsequently, the aldol product may release water and forms the secondary ketone product, which is illustrated and discussed in more detail in the next chapter, see Scheme 3-2. When promoted by silanols, the reaction is enhanced by the hydrogen-bridge interactions between the carbonyl moieties in the reactants and the silanol groups. The correspondingly proposed mechanism is shown in Scheme 2-3b. The promoting effect is represented by the species indicated by **(1a)** and **(3a)**. As a result the reactants become more susceptible to nucleophilic reactions [4, 38, 42] and the formation of intermediates **(1b)** and **(3b)** is facilitated.

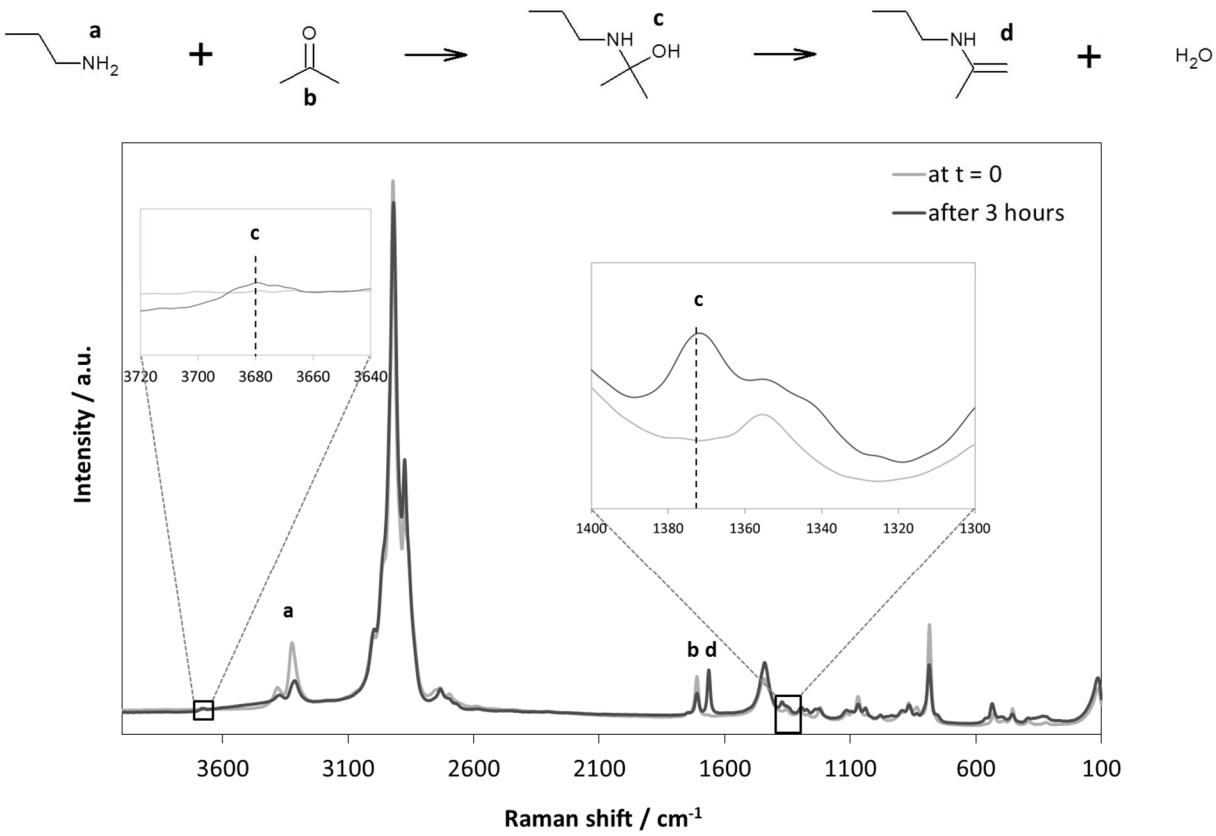

Figure 2-6. Reaction scheme and in situ Raman spectra of the reaction between acetone and *n*-propylamine

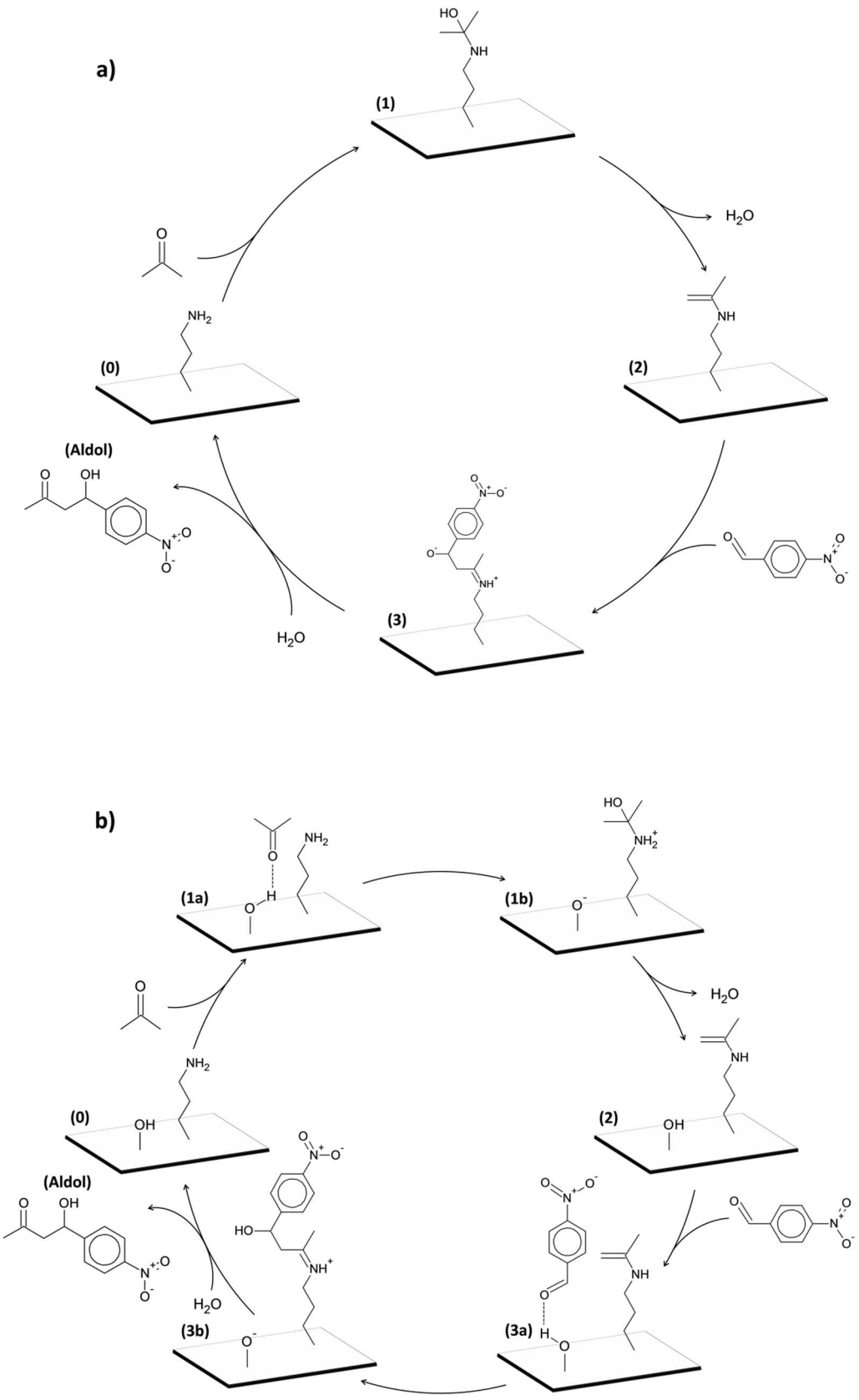

Scheme 2-3. Reaction mechanism for the aldol condensation of 4-nitrobenzaldehyde with acetone; a) unpromoted reaction mechanism; b) promoted reaction mechanism

2.3.4 Assessment of the active site positioning

The reaction mechanism, see Scheme 2-3, illustrates that if all amines have one neighboring silanol, the activity of all amines is promoted. In that case, an additional increase of silanol groups does not lead to further promotion. As shown in Figure 2-4, the catalytic activity does not reach such a plateau at a molar silanol-to-amine ratio of 1, but only at a higher ratio of 1.7. This means that, at a silanol-to-amine ratio of 1, not every amine has a neighboring silanol and the actual arrangement on the surface deviates from the ideal checkerboard pattern. To understand the factors affecting the positioning of the amines on the silica surface, catalytic surfaces with different silanol-to-amine ratios were mathematically generated using three alternative principles, *i.e.*, (i) random positioning, (ii) clustering upon grafting, and (iii) clustering in the synthesis mixture. In what follows, the promotional effects as calculated using these three methods are discussed and compared to the experimentally obtained results.

2.3.4.1 Random positioning

A square surface comprising 500x500 free silanol groups, all having 8 neighbors, was considered. A number of silanols was replaced by amines in a random manner such that a surface with a specific silanol-to-amine ratio was obtained. The number of promoted amines was then determined from the number of silanols neighboring the amines, accounting for the possibility that a silanol may be neighboring more than one amine. As a result, the number of neighboring silanols is not necessarily an integer, but can also be a fractional number. The distributions of the number of neighboring silanols to amine groups for various silanol-to-amine ratios are shown in Figure 2-7. The gray areas in Figure 2-7 indicate the amines that are surrounded by less than one silanol. These amines are considered to be promoted to an extent that is identical to the "fraction" of neighboring silanols. Consequently, the white areas correspond to the amines that are surrounded by at least one silanol and, hence, are considered to be fully promoted. The fraction of fully promoted amines is rather low at low molar silanol-to-amine ratios: only 7.7% of the amines have one or more neighboring silanols on a surface with a silanol-to-amine ratio of 0.5. For higher silanol-to-amine ratios the average number of neighboring silanols increases and the distribution broadens. From Figure 2-7b it can be seen that a catalyst upon which an equal amount of amines and silanols are randomly distributed will not exhibit the maximum

possible activity because only 41.8% of the amines is fully promoted. If the silanol-to-amine ratio further increases, the activity of the catalyst will keep on increasing until all amines are surrounded by one or more silanols.

The correspondingly simulated percentage of promoted amines and the theoretical maximum percentage of promoted amines, *i.e.*, in the case of a checkerboard pattern, is shown in Figure 2-8 by the dotted and full line, respectively, together with the experimentally obtained data represented by the diamonds. Although the percentage of promoted amines according to a random positioning of the amines is clearly below the theoretical maximum at intermediate values for the silanol-to-amine ratio, it only well describes the experimentally observed plateau at higher silanol-to-amine ratios. At lower silanol-to-amine ratios the promotion calculated according to a random pattern clearly exceeds that observed experimentally. Apparently, catalysts with a high number amines have less promoted amine groups than expected if the amines could be grafted in a random manner. This suggests that, especially if a high number of amines is grafted on the catalyst surface, this grafting occurs in a clustered manner, as discussed further. This is already hypothesized in literature [43-45].

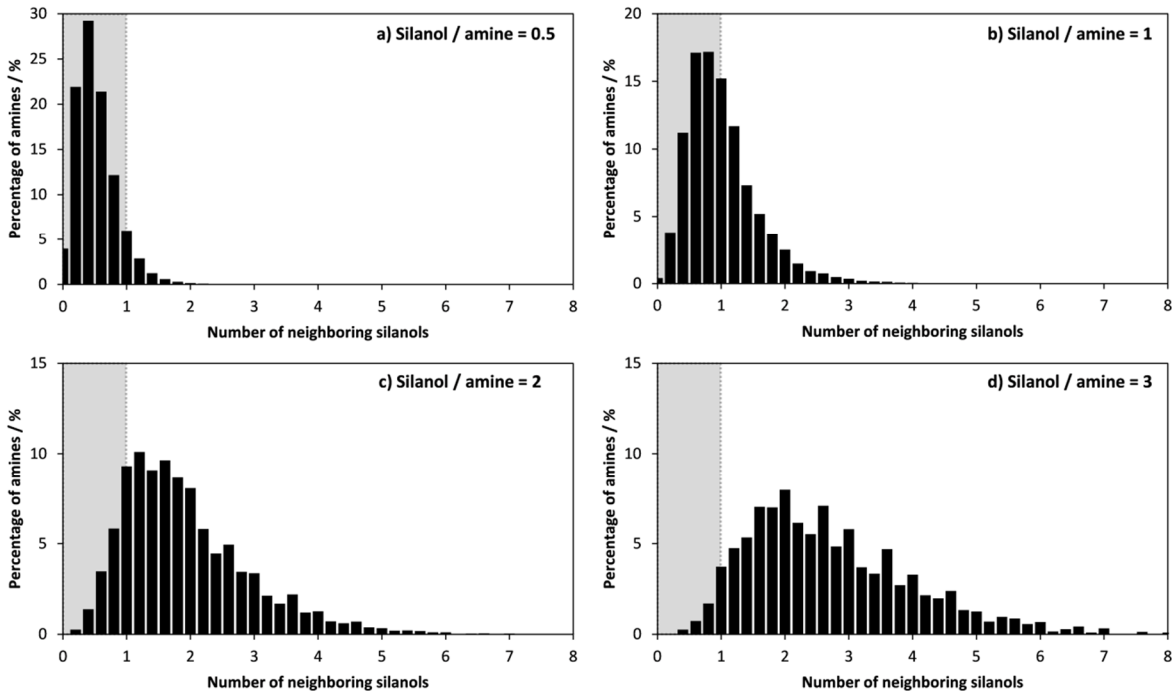

Figure 2-7. Distribution of the number of neighboring silanols for different molar silanol-to-amine ratios; the gray shadowing indicates not fully promoted amines

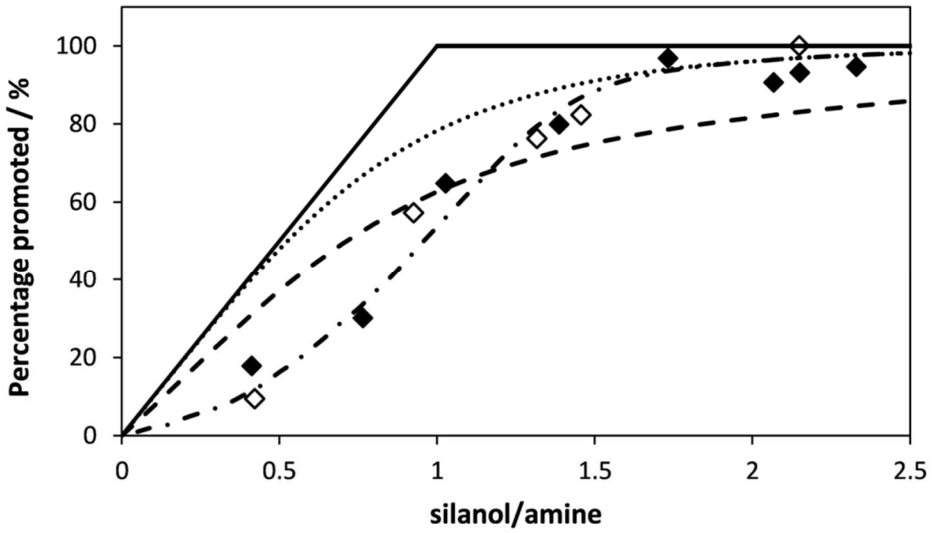

Figure 2-8. Percentage of promoted amines as a function of the silanol-to-amine ratio; catalysts functionalized using APTES (◆, APTES 1–8); catalysts functionalized using APDMES (◊, APDMES 1–5); theoretical maximum percentage promoted amines (full line); calculated percentage by means of randomly generated surfaces (dotted line); calculated percentage accounting for clustering upon grafting (dashed line); calculated percentage accounting for clustering in the synthesis mixture (dash-dotted line)

2.3.4.2 Clustering upon grafting

In the literature, the so-called flip mechanism [29, 46, 47] is used to describe the reactions occurring during the grafting procedure. In this mechanism it is proposed that an amine from the liquid phase forms a hydrogen bond with a surface silanol or an amine that is already grafted on the surface, prior to its actual grafting upon a neighboring silanol. Simulating the arrangement of the amine sites according to this mechanism requires using a grafting probability which is function of the number of amines surrounding the grafting position. More details about the grafting probability function can be found in Appendix A. In this modeling procedure, a first position is initially randomly selected. Subsequently, it is decided whether an amine is grafted on this position depending on the number of neighboring amines and the corresponding grafting probability. It can be seen from the dashed line in Figure 2-8 that the percentage of promoted amines on a surface generated according to the flip mechanism exhibits a qualitatively similar trend with the silanol-to-amine ratio to that obtained from a randomly generated surface. However, the point at which the maximum percentage of promoted amines is obtained shifts to significantly higher silanol-to-amine ratios, in contrast to what was observed experimentally.

2.3.4.3 Clustering in the synthesis mixture

Alternatively to the flip mechanism, hydrogen bonding can already occur between two amines in the catalyst synthesis mixture. Thermodynamic nonideality calculations for an *n*-propylamine–toluene mixture resulted in positive deviations from ideality. This indicates that propylamine–propylamine interactions occur preferentially to propylamine–toluene interactions, for example, through hydrogen bonding. The probability for two *n*-propylamine molecules to form a hydrogen bond is proportional to the concentration of *n*-propylamine molecules in the synthesis mixture. Hence, if sufficient amines are present in the synthesis mixture, they can be considered to move in a clustered manner during the grafting procedure and to be positioned on the surface in each other's vicinity. At low amine concentrations in the synthesis mixture the probability that two amines effectively come and stay together through hydrogen bonding is lower, such that grafting rather occurs in a random manner than in a clustered manner. This can be modeled using a grafting probability function depending on the amine concentration in the synthesis mixture. The experimental data indicate that amine clustering occurs above a threshold value of 1 mol% APTES in the synthesis mixture. The model based upon this threshold leads to a good agreement with the experimental data, see the dash-dotted line in Figure 2-8. In Figure 2-9, a few examples of catalytic surfaces modeled by this method are shown. At a silanol-to-amine ratio amounting to 2.0 the amines are randomly arranged on the catalyst surface, whereas at a ratio of 1.5 some clustering can be observed. A catalyst with a silanol-to-amine ratio of 1.0 has an average cluster diameter of 6.3 amines, whereas at a ratio of 0.5 an average cluster diameter of 23.5 amines is obtained.

In order to distinguish between the formation of hydrogen bonds, as described above, and the possible condensation of two silane molecules in the synthesis mixture, see Scheme 2-5, a series of aminopropyl–silanol cooperative catalysts has also been synthesized by using (3-aminopropyl)dimethylethoxysilane (APDMES) as a precursor for the amine functions. The condensation product of two APDMES molecules does not contain any ethoxy groups, see Scheme 2-5, and, hence, cannot be grafted on the silica surface. The amine and silanol concentrations and corresponding silanol-to-amine ratios are reported in Table 2-3. A similar evolution of the percentage of promoted amine functions as a function of the silanol-to-amine ratio was obtained for APDMES and APTES as amine precursor, see Figure 2-8. It

illustrates that a similar clustering occurs for both precursors and, hence, excludes the condensation of two silane molecules of the APTES precursor as cause of the clustering.

Table 2-3. Number of active sites determined through CHNS elemental analysis for the APDMES-functionalized silica materials

Catalyst	Amine[a] [mmol g^{-1}]	Silanol[b] [mmol g^{-1}]	Silanol/amine[c]
APDMES 1	0.31	0.66	2.15 ± 0.11
APDMES 2	0.41	0.60	1.46 ± 0.06
APDMES 3	0.43	0.57	1.32 ±0.06
APDMES 4	0.51	0.47	0.93 ± 0.04
APDMES 5	0.73	0.31	0.42 ± 0.02

[a] The amine concentrations on the catalysts is equal for catalysts of type AB and type B. The error on this measurement is for all samples ±0.01 $mmolg^{-1}$. [b] The silanol concentrations given in the table is only valid for catalysts of type AB, catalysts of type B have no silanols on the surface. The error on this measurement amounts for all to samples ±0.01 $mmolg^{-1}$. [c] The ratio of silanols to amines given in the table is only valid for catalysts type AB, catalysts of type B have a silanol-to-amine ratio equal to zero.

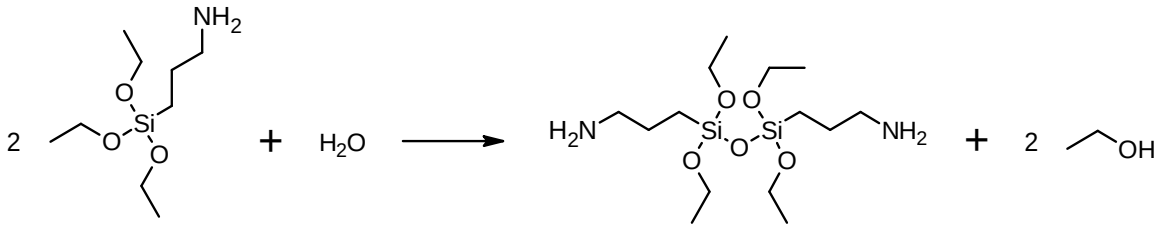

Scheme 2-4. Condensation of two (3-aminopropyl)triethoxysilane (APTES) molecules in the presence of water

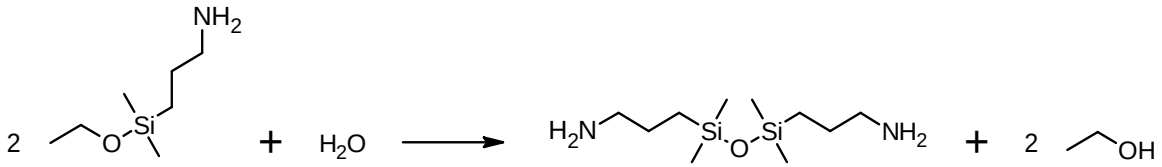

Scheme 2-5. Condensation of two (3-aminopropyl)dimethylethoxysilane (APDMES) molecules in the presence of water

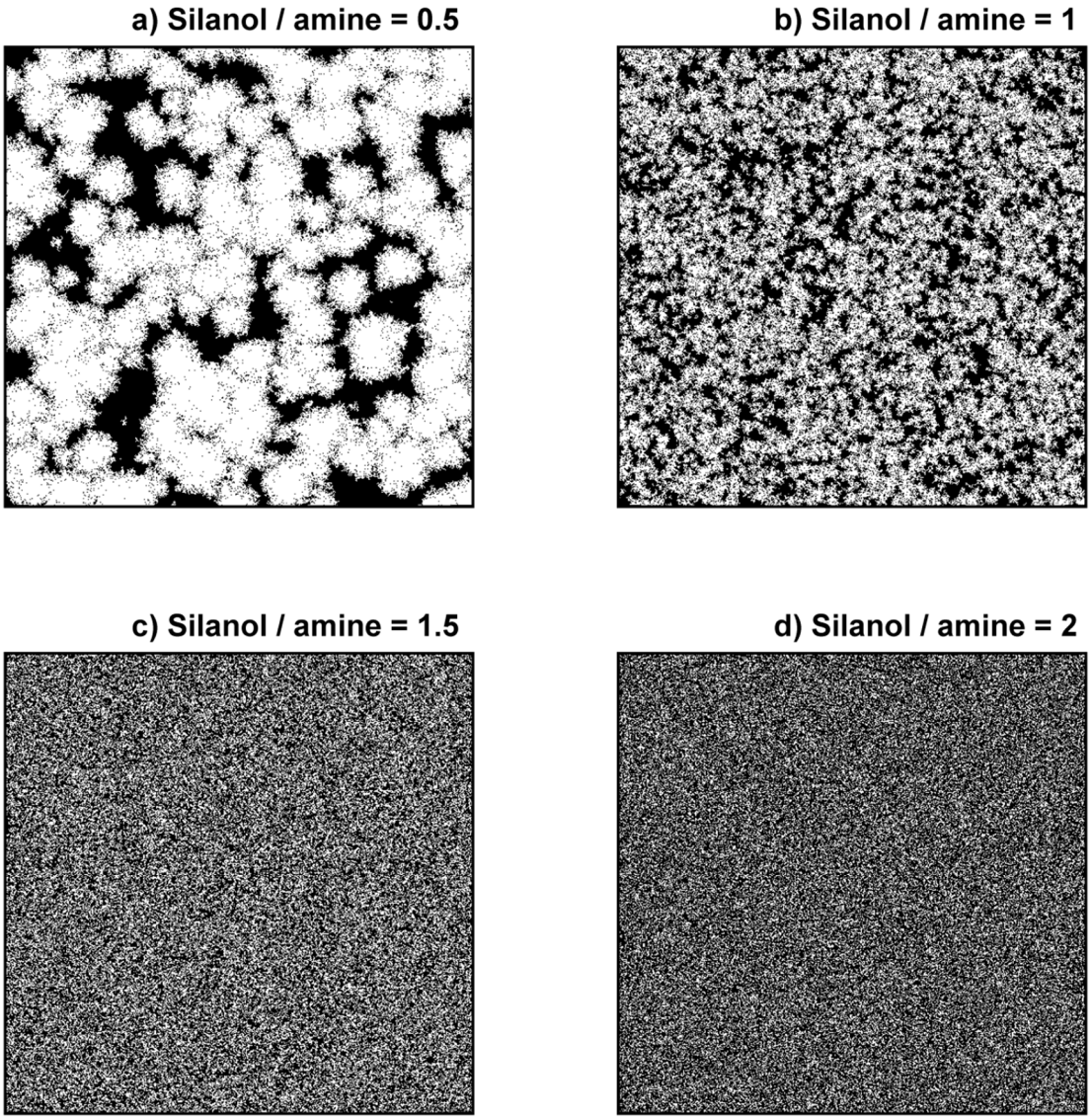

Figure 2-9. Representations of catalytic surfaces with a two hundred fifty thousand sites for different molar silanol-to-amine ratios; white, amine; black, silanol

2.4 Conclusions

The turnover frequencies obtained in the aldol condensation of 4-nitrobenzaldehyde and acetone can be enhanced up to a factor of 5 by the presence of free silanols next to the actually active sites, *i.e.*, the amines. The promotion of amine active sites by silanols does not affect the selectivity in aldol condensation between acetone and 4-nitrobenzaldehyde. Acetone first forms an enamine that subsequently reacts with 4-nitrobenzaldehyde. The promotion by silanol groups originates from hydrogen-bridge interactions between the carbonyl moiety of the reactants and these silanol groups, which makes the former more

susceptible to nucleophilic reactions. If amine groups are grafted from a dilute synthesis mixture, a random positioning occurs whereas if more concentrated synthesis mixtures are employed, the amine groups are grafted as clusters on the silica surface because of the preferential propylamine–propylamine interactions compared to propylamine–toluene interactions, for example, for hydrogen bonding.

2.5 References

1. Y. Q. Shao, J. Q. Guan, S. J. Wu, H. Liu, B. Liu, Q. B. Kan, Microporous Mesoporous Mat., **2010**, 128, 120-125
2. R. K. Zeidan, M. E. Davis, J. Catal., **2007**, 247, 379-382
3. R. K. Zeidan, S. J. Hwang, M. E. Davis, Angew. Chem.-Int. Edit., **2006**, 45, 6332-6335
4. Y. Kubota, H. Yamaguchi, T. Yamada, S. Inagaki, Y. Sugi, T. Tatsumi, Top. Catal., **2010**, 53, 492-499
5. S. F. Cheng, X. G. Wang, S. Y. Chen, Top. Catal., **2009**, 52, 681-687
6. N. A. Brunelli, K. Venkatasubbaiah, C. W. Jones, Chem Mater, **2012**, 24, 2433-2442
7. N. A. Brunelli, S. A. Didas, K. Venkatasubbaiah, C. W. Jones, J. Am. Chem. Soc., **2012**, 134, 13950-13953
8. K. Kandel, S. M. Althaus, C. Peeraphatdit, T. Kobayashi, B. G. Trewyn, M. Pruski, I. I. Slowing, ACS Catal., **2013**, 3, 265-271
9. K. Kandel, S. M. Althaus, C. Peeraphatdit, T. Kobayashi, B. G. Trewyn, M. Pruski, I. I. Slowing, J. Catal., **2012**, 291, 63-68
10. S. Huh, H. T. Chen, J. W. Wiench, M. Pruski, V. S. Y. Lin, Angew. Chem.-Int. Edit., **2005**, 44, 1826-1830
11. N. Solin, L. Han, S. Che, O. Terasaki, Catal. Commun., **2009**, 10, 1386-1389
12. B. Voit, Angew. Chem.-Int. Edit., **2006**, 45, 4238-4240
13. F. P. Shang, J. R. Sun, S. J. Wu, Y. Yang, Q. B. Kan, J. Q. Guan, Microporous Mesoporous Mat., **2010**, 134, 44-50
14. S. Shylesh, A. Wagner, A. Seifert, S. Ernst, W. R. Thiel, Chem.-Eur. J., **2009**, 15, 7052-7062
15. Y. Kubota, K. Goto, S. Miyata, Y. Goto, Y. Fukushima, Y. Sugi, Chemistry Letters, **2003**, 32, 234-235

16. J. D. Bass, A. Solovyov, A. J. Pascall, A. Katz, J. Am. Chem. Soc., **2006**, 128, 3737-3747
17. M. Sahoo, S. Singha, K. M. Parida, New J. Chem., **2011**, 35, 2503-2509
18. P. Van Der Voort, E. F. Vansant, J. Liq. Chromatogr. Relat. Technol., **1996**, 19, 2723-2752
19. L. T. Zhuravlev, Colloids and Surfaces a-Physicochemical and Engineering Aspects, **1993**, 74, 71-90
20. L. T. Zhuravlev, Colloids and Surfaces a-Physicochemical and Engineering Aspects, **2000**, 173, 1-38
21. E. F. Vansant, P. Van Der Voort, *Characterization and Chemical Modification of the Silica Surface. 2 ed. Studies in Surface Science and Catalysis*, **1997**
22. P. Van Der Voort, S. Vercauteren, K. Peeters, E. F. Vansant, J Colloid Interf Sci, **1993**, 157, 518-519
23. S. Brunauer, P. H. Emmett, E. Teller, J. Am. Chem. Soc., **1938**, 60, 309-319
24. E. P. Barrett, L. G. Joyner, P. P. Halenda, J. Am. Chem. Soc., **1951**, 73, 373-380
25. M. E. Davis, R. J. Davis, *Fundamentals of Chemical Reaction Engineering*, McGraw-Hill, **2003**
26. A. Fredenslund, R. L. Jones, J. M. Prausnitz, Aiche J., **1975**, 21, 1086-1099
27. B. E. Poling, J. M. Prausnitz, J. P. O'Connell, *The properties of gases and liquids*, McGraw-Hill, New York, **2001**
28. K. C. Vrancken, P. Van Der Voort, I. Gillisdhamers, E. F. Vansant, P. Grobet, Journal of the Chemical Society-Faraday Transactions, **1992**, 88, 3197-3200
29. K. C. Vrancken, P. Van Der Voort, K. Possemiers, E. F. Vansant, J Colloid Interf Sci, **1995**, 174, 86-91
30. I. Shimizu, A. Yoshino, H. Okabayashi, E. Nishio, C. J. Oconnor, Journal of the Chemical Society-Faraday Transactions, **1997**, 93, 1971-1979
31. H. Okabayashi, I. Shimizu, E. Nishio, C. J. Oconnor, Colloid and Polymer Science, **1997**, 275, 744-753
32. R. Pena-Alonso, F. Rubio, J. Rubio, J. L. Oteo, Journal of Materials Science, **2007**, 42, 595-603
33. N. A. Bhore, M. T. Klein, K. B. Bischoff, Ind. Eng. Chem. Res., **1990**, 29, 313-316
34. B. List, R. A. Lerner, C. F. Barbas, J. Am. Chem. Soc., **2000**, 122, 2395-2396
35. K. Sakthivel, W. Notz, T. Bui, C. F. Barbas, J. Am. Chem. Soc., **2001**, 123, 5260-5267

36. H. Hart, L. E. Craine, D. J. Hart, C. M. Hadad, *Organic Chemistry: A Short Course*, **2007**
37. R. V. Hoffman, John Wiley & Sons., *Organic chemistry an intermediate text*, 2004, Wiley-Interscience: Hoboken, N.J.
38. B. Liu, H. Liu, C. H. Wang, L. L. Liu, S. J. Wu, J. Q. Guan, Q. B. Kan, Appl. Catal. A-Gen., **2012**, 443, 1-7
39. B. Liu, S. J. Wu, X. F. Yu, J. Q. Guan, Q. B. Kan, J Colloid Interf Sci, **2011**, 362, 625-628
40. M. B. Schmid, K. Zeitler, R. M. Gschwind, Angew. Chem.-Int. Edit., **2010**, 49, 4997-5003
41. S. Bahmanyar, K. N. Houk, J. Am. Chem. Soc., **2001**, 123, 11273-11283
42. Y. W. Xie, K. K. Sharma, A. Anan, G. Wang, A. V. Biradar, T. Asefa, J. Catal., **2009**, 265, 131-140
43. J. C. Hicks, R. Dabestani, A. C. Buchanan, C. W. Jones, Chem Mater, **2006**, 18, 5022-5032
44. J. C. Hicks, C. W. Jones, Langmuir, **2006**, 22, 2676-2681
45. M. W. McKittrick, C. W. Jones, Chem Mater, **2003**, 15, 1132-1139
46. H. G. Linde, J. Appl. Polym. Sci., **1990**, 40, 613-622
47. C. W. Chu, D. P. Kirby, P. D. Murphy, J. Adhes. Sci. Technol., **1993**, 7, 417-433

Chapter 3

Effects of Amine Structure and Base Strength on Acid-Base Cooperative Aldol Condensation

---

Aminated silica materials are known to efficiently catalyse aldol condensations, especially when silanol groups are neighbouring the amine function. The effect of the amine structure and corresponding base strength has been analyzed experimentally as well as by kinetic modelling. Commercially available precursors were used to graft primary, secondary and tertiary amines on the silica support. While primary amines are arranged in a clustered manner (see also Chapter 2), secondary amines are arranged randomly which results in a higher percentage of promoted amines in the low silanol-to-amine ratio range. An enamine compound formed by the reaction between the amine active site and acetone has been identified as the key intermediate to explain the experimental observations. In the case of a primary amine this enamine intermediate suffers from interconversion into an inhibiting imine with which it is in equilibrium. As a secondary amine only has a single hydrogen atom bonded to the nitrogen atom, this inhibiting imine cannot be formed, resulting in a comparatively higher concentration of reactive enamines on the catalyst surface. In case of a tertiary amine the formation of the reactive intermediate is impossible due to the absence

of any hydrogen atom bonded to the nitrogen atom. The activation entropies of all reaction steps occurring on the amine sites, *i.e.*, the enamine formation, the desorption of the intermediate, the ketone formation and the reverse reaction with the aldol formation, as obtained by regression, could be correlated to the deprotonation entropies of the amine sites. As steric effects impact on the deprotonation enthalpy, no such correlation could be established between the activation energies of these reaction steps and the deprotonation enthalpies of the amine sites.

3.1 Introduction

Aminated silica supports are known to catalyze aldol condensations, especially when weak acid sites, such as the surface silanols, are present [1-7]. Previous research has shown that some types of amines, *i.e.*, methyl substituted secondary amines have a higher turnover frequency than other types of amines [5, 7]. This has already been attributed to the possibility to form inhibiting species [7]. However, an unambiguous explanation for this observation is still unavailable. Kinetic modeling of catalytic reactions can contribute to the elucidation of the reaction mechanism and the establishment of fundamental relations between catalyst properties and behavior. Subsequently, the insights and relations obtained from the kinetic models can be used to more efficiently design new and optimize existing catalysts.

In this chapter, a kinetic model is developed for the acid-base cooperatively catalyzed aldol condensation reaction. The focus is on the effect of the structure and the base strength of the amine functional groups on the aldol condensation kinetics. A catalyst library comprising both base and acid-base catalysts was synthesized by functionalization of a commercial, mesoporous silica, Silicagel 60, with different commercially available primary, secondary and tertiary amine containing silanes. The effect of the reaction conditions as well as the structure and base strength of the active site on the catalyst activity is investigated by means of both an experimental kinetic study and kinetic modeling.

3.2 Procedures

3.2.1 Catalyst synthesis and characterization

Figure 3-1 shows the 5 cooperative, acid-base and 5 unpromoted base catalysts which were prepared using the commercially available amine containing silanes, (3-aminopropyl)triethoxysilane (98%, APTES, ABCR), N-methylaminopropyltrimethoxysilane (MAPTMS, ABCR), N-cyclohexylaminopropyltrimethoxysilane (CAPTMS, ABCR), N-phenylaminopropyltrimethoxysilane (95% PAPTMS, ABCR) and (N,N-diethyl-3-aminopropyl)trimethoxysilane (DEAPTMS, ABCR). These aminosilanes were grafted on a mesoporous silica, Silicagel 60 (Grade 7734, Sigma-Aldrich) using the synthesis procedures described in section 2.2.1.

The materials were characterized by means of nitrogen adsorption-desorption measurements, elemental (CHNS) analysis and Diffuse Reflectance Infrared Fourier Transform (DRIFT) spectroscopy according to the procedures described in section 2.2.2.

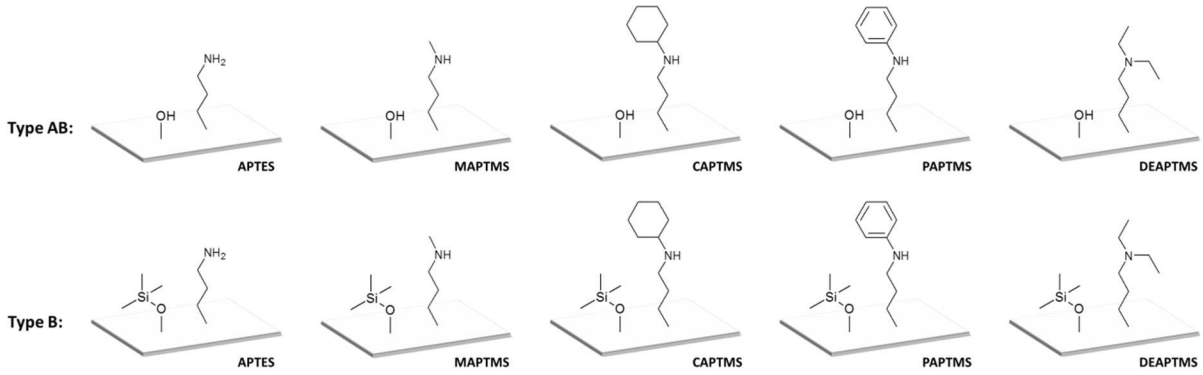

Figure 3-1. Representation of the catalyst surfaces

3.2.2 Catalyst performance testing

Catalysts performance has been assessed via the aldol condensation of acetone (99.6%, Acros) and 4-nitrobenzaldehyde (99%, Acros) towards the primary aldol product 4-hydroxy-4-(4-nitrophenyl)butan-2-one and the secondary ketone product 4-(4-nitrophenyl)-3-buten-2-one, the latter being formed after elimination of water from the aldol (Scheme 2-1). The experiments are performed based on the procedures described in section 2.2.4.

The experiments with the APTES functionalized catalysts are carried out in the Parr 4560 mini reactor as discussed in the previous Chapter. The experiments with the other catalysts are carried out in a three-necked glass flask of 180 ml, which is also operated as a batch type reactor. The flask is equipped with a reflux condenser, a thermocouple and a sampling port. The temperature in this reactor is maintained using a Lauda Proline RP845 PID controller and the reaction mixture is stirred with a magnetic stirrer rotating at 500 rpm. Some experiments were carried out in both reactors to confirm that the deviations on the kinetic data due to the differences in the setup are negligible.

The range of experimental conditions in which the catalyst performance has been evaluated is given in Table 3-1. An acetone excess is used in all experiments in order to suppress the direct interaction between 4-nitrobenzaldehyde and the amine site which would yield an inhibiting imine [6, 7]. In order to investigate the effect of the catalyst properties on the aldol condensation performance, all catalysts were subject to identical operating conditions, *i.e.*, 318K with 0.79 mol acetone, 3.31 mmol 4-nitrobenzaldehyde, 0.39 mol *n*-hexane (solvent) and 1.44 mmol methyl 4-nitrobenzoate (IS). Note that, due to the different amine loading on the different catalysts, the added catalyst mass has to be adjusted in order to keep the concentration of amine groups in the reactor identical in all experiments.

Table 3-1. Range of experimental conditions

Variable	Purpose	Range
Amine groups	Active site	1 mmol/L
Silanol groups	Active site promotion	0 – 2.6 mmol/L
4-nitrobenzaldehyde	Reactant 1	15 – 177 mmol/L
Acetone	Reactant 2	1.4 – 7.0 mol/L
Methyl 4-nitrobenzoate	Internal standard	13 mmol/L
n-hexane	Solvent	3.7 – 6.4 mol/L
Temperature		15 – 55°C

3.2.3 Thermodynamic non-ideality of the liquid mixture

As the experiments are performed in a liquid phase comprising components with different polarities, it is important for the model to explicitly account for the non-ideality of the liquid phase via so-called activity coefficients, γ_i [8-10]. The Universal Quasichemical (UNIQUAC) method and its extension, the UNIQUAC Functional-group Activity Coefficients (UNIFAC)

method are widely accepted methods to calculate activity coefficients and other thermodynamic data of compounds in liquid multi-component mixtures without explicit use of experimental data. Both methods make use of binary interaction parameters to describe the interactions between two molecules or two functional groups in the mixture. More detailed information about the calculation strategy used by these methods can be found in Appendix B.

A large number of the interaction parameters used in these models can be found in literature [11], however, even today some of the parameters remain unreported. The thermodynamic non-ideality of the liquid toluene – amine precursor mixtures used during catalyst synthesis could be described using the UNIFAC method but some interaction parameters necessary to describe the non-ideality of the reaction mixture are unknown. Another limitation of this model is the fundamental assumption that a contribution made by one group is independent of that made by another group. This assumption is only valid when neighboring effects are absent, which is unlikely when, *e.g.*, a carbon-carbon double bond is conjugated with an aromatic ring.

An alternative to the above described methods is the Conductor-like Screening Model for Real Solvents (COSMO-RS) [12-15] which involves a statistical thermodynamics treatment of the solute-solvent interactions. In a first step an individual quantum chemical COSMO calculation is performed for each molecule in the mixture to determine the molecular surface polarity distributions. In this work, these quantum chemical COSMO calculations are performed using RI-DFT with the TURBOMOLE package with B88-VWN-P86 as functional and def-TZVP basis set. COSMO is an implicit solvent model which means that in these calculations the molecules are considered to be in an environment with an infinite conductivity. In this environment, the solute molecule induces a polarization charge density on the interface between the molecule and the conductor. These charges act back on the solute and generate a more polarized electron density than in vacuum. In a second step, this polarization charge density is used by the COSMOthermX program for the calculation of the interaction energy of the most important molecular interaction modes, *i.e.*, electrostatic interactions and hydrogen bonding.

In this chapter, the activity coefficients of all components in the reaction mixture are, in the first instance, calculated using the COSMO-RS method, in order to overcome the limitations

of the UNIQUAC and UNIFAC models. In these calculations the liquid phase composition and temperature are varied in the range of the experimental conditions in order to calculate a reference set of activity coefficients This set is subsequently used to estimate the binary interaction parameters as required for the UNIQUAC method. Due to the presence of the solvent, i.e., *n*-hexane, and the use of an acetone excess in the aldol condensation experiments, a component is only assumed to interact with *n*-hexane or acetone and all other binary interaction parameters are neglected. Finally, the UNIQUAC model with the estimated binary interaction parameters is implemented in the kinetic model to account for the thermodynamic non-ideality of the reaction mixture.

3.2.4 Thermodynamic equilibrium

The Joback method [16] is a relatively simple group contribution method which can be used to estimate the enthalpy of formation, the enthalpy of vaporization, the Gibbs free energy of formation and the heat capacity of individual molecules. In this chapter, this method is used to determine the equilibrium coefficient between the enamine intermediate and the inhibiting imine as well as the difference between the activation energies of the forward and reverse reaction steps between the aldol and the ketone products, see section 3.4.3.

In 1969 Christensen [17] et al. developed a group contribution method to determine the ΔH°, ΔS° and $pK_{a,298K}$ values for deprotonation of amines. This method is used to determine the base strength of the amines studied in this chapter.

3.2.5 Reactor model

Since the experiments have been performed in a batch type reactor, which is considered to be spatially uniform in both composition and temperature, the mass balance for species i is given by equation 1. With t representing the time and C_i and R_i representing, respectively, the concentration and the net rate of formation of component i.

$$\frac{dC_i}{dt} = R_i \tag{1}$$

3.2.6 Regression analysis

The model parameters were estimated based on Bayes' theorem (eq. 2) using Athena Visual Studio [18].

$$p(\beta|y) = \frac{p(y|\beta)\,p(\beta)}{p(y)} \quad (2)$$

The function $p(\beta|y)$ represents the Bayesian posterior probability distribution and expresses the probability of the parameter values, β, given the observed data, y. $p(y|\beta)$ is often called the likelihood function and quantifies the information contained in the acquired data. $p(\beta)$ is the prior probability distribution and describes the information available with respect to the parameter values prior to any modelling. The denominator, $p(y)$, is constant when the data and model are given and, hence, merely serves as a normalizing factor. The estimated parameters are obtained by maximizing $p(\beta|y)$.

In case of an unprejudiced prior probability distribution $p(\beta)$, the Bayesian posterior probability distribution is proportional to the likelihood function (eq. 3).

$$p(\beta|y) \sim p(y|\beta) \quad (3)$$

Assuming that errors, ε (eq. 4), between the dependent variables, y, and the simulated values, $\hat{y}(\beta)$, are normally distributed, the likelihood can be expressed as equation 5. In this work the dependent variables, y, were, either experimentally measured concentrations or activity coefficients calculated based on quantum chemistry, while the simulated values, $\hat{y}(\beta)$, are calculated, respectively, with the kinetic model (see section 3.4.2) or the UNIQUAC model (see section 3.4.1).

$$y = \hat{y}(\beta) + \varepsilon \quad (4)$$

$$p(y|\beta) = \frac{1}{(2\pi\sigma^2)^{n/2}} \exp\left(-\frac{1}{2\sigma^2}\left(y - \hat{y}(\beta)\right)^2\right) \quad (5)$$

The maximizing of the likelihood was achieved by the quadratic programming method as implemented in the GREGPLUS package, included in Athena Visual Studio [18].

Apart from the physical significance of the model and the individual model parameters, the regression results were also evaluated on a statistical basis. The F test for the global significance of the regression was performed. The individual statistical significance of the parameter estimates was assessed with the Student t-test. The binary correlation coefficients between the estimated parameters were calculated [19-21].

3.3 Experimental results

3.3.1 Catalyst characterization

After grafting the precursor on the silica material the presence of amine groups is demonstrated via Diffuse Reflectance Infrared Fourier Transform (DRIFT) measurements, see Figure 3-2. The spectra of the unfunctionalized pretreated silica and the materials functionalized with primary amines have already been shown in Figure 2-2 but are repeated for the reader's convenience. The unfunctionalized pretreated silica exhibits a narrow vibration band at 3745 cm^{-1} which is characteristic for the free silanol groups (Si-OH), see Figure 3-2.1. After treatment with the aminosilane several new bands appear in the range of 2800-3000 cm^{-1}, which can be attributed to the C-H stretch of the grafted functional groups. The spectrum of the silica material functionalized with phenylaminopropane active sites (Figure 3-2.5), also shows two additional bands at 1505 and 1603 cm^{-1} due to stretching of the C-C bonds in the aromatic ring. The primary amine group in aminopropane (Figure 3-2.2) exhibits two small but significant bands at 3314 and 3380 cm^{-1}. The secondary amines methylaminopropane (Figure 3-2.3) and cyclohexylaminopropane (Figure 3-2.4) give only one N-H stretching band, which can be found at 3314 cm^{-1}, while the N-H stretching of phenylaminopropane (Figure 3-2.5) can be found at 3417 cm^{-1}. Figure 3-2.6 exhibits no N-H stretching due to the absence of any hydrogen on the nitrogen atom of diethylaminopropane. The successful endcapping of the silanol groups after threatment with 1,1,1,3,3,3-hexamethyldisilazane (HMDS) is demonstrated by the complete disappearence of the –OH stretching band at 3745 cm^{-1}.

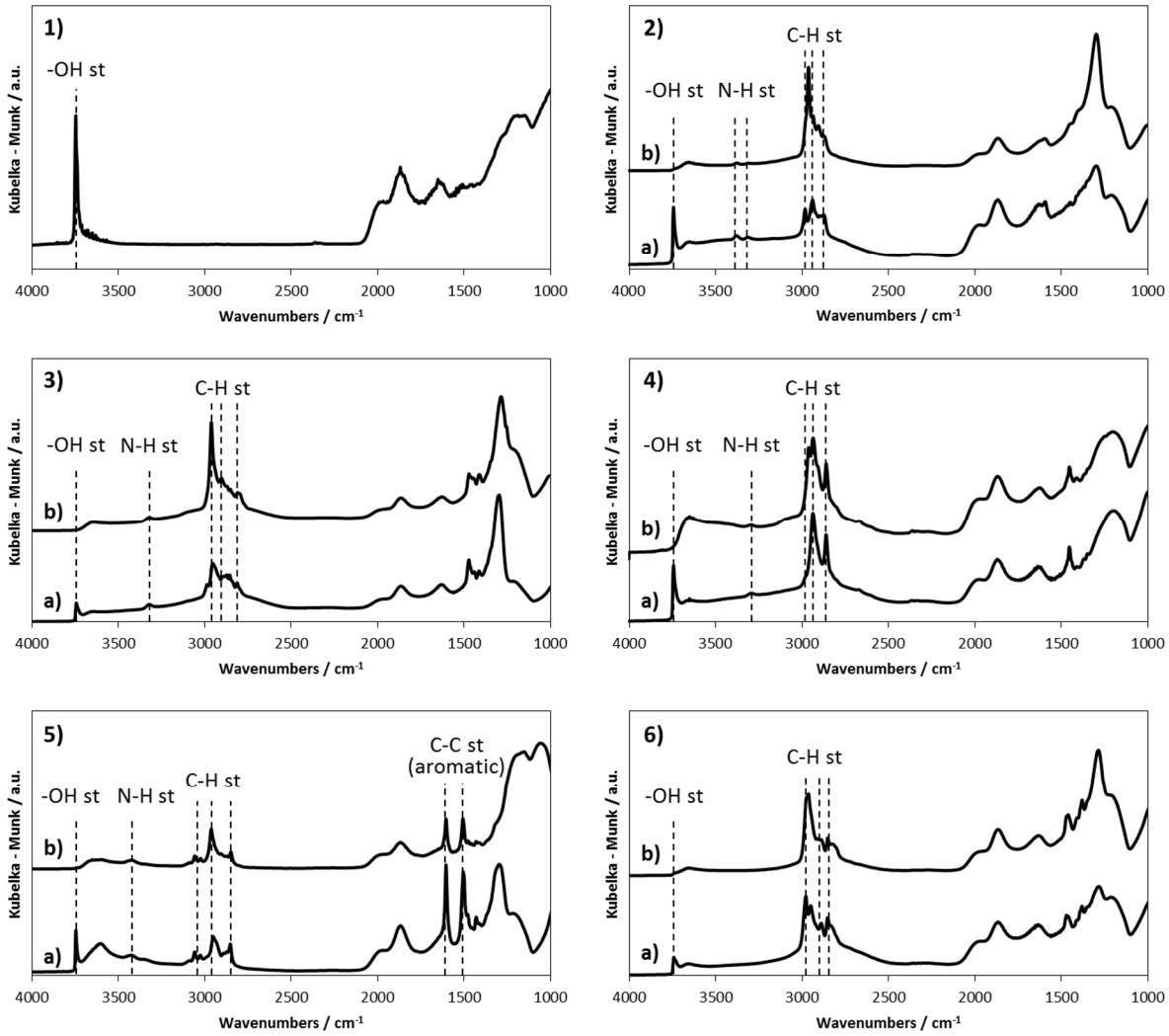

Figure 3-2. Typical DRIFT spectra of 1) pretreated silica; and amine functionalized catalysts using 2) APTES 6; 3) MAPTMS 3; 4) CAPTMS 2; 5) PAPTMS 1; 6) DEAPTMS 3; a) cooperative acid-base catalysts (type AB); and b) unpromoted base catalysts (type B)

The active site concentrations, as determined from CHNS elemental analysis, are reported in Table 3-2. The APTES type of materials are already reported in Table 2-2 but are repeated for the reader's convenience. The concentrations of amine groups on cooperative acid-base (AB) as well as on unpromoted base (B) samples are calculated from the obtained nitrogen weight percentage and are found to be identical. The free silanol concentration on the cooperative acid-base samples is determined from the increase in carbon after HMDS treatment, as one silanol is capped by one trimethylsilyl moiety and, hence, is equivalent with a mass increase corresponding to three carbon atoms. The experimental error was found to be independent of concentration and active site type and equal to 0.02 w%. By

applying the rules of error propagation, it is found that the experimental error in the molar silanol-to-amine ratio decreases with decreasing ratios.

Table 3-2. Concentration of active sites determined from CHNS elemental analysis

Catalyst	Amine[a] [mmol g^{-1}]	Silanol[b] [mmol g^{-1}]	Silanol/amine[c]
APTES 1	0.29	0.67	2.33 ± 0.13
APTES 2	0.32	0.69	2.15 ± 0.11
APTES 3	0.33	0.67	2.07 ± 0.11
APTES 4	0.35	0.61	1.73 ± 0.09
APTES 5	0.40	0.56	1.39 ± 0.07
APTES 6	0.49	0.50	1.03 ± 0.04
APTES 7	0.59	0.45	0.77 ± 0.04
APTES 8	0.65	0.27	0.42 ± 0.03
MAPTMS 1	0.34	0.67	1.96 ± 0.10
MAPTMS 2	0.35	0.67	1.90 ± 0.10
MAPTMS 3	0.41	0.66	1.60 ± 0.08
MAPTMS 4	0.47	0.51	1.09 ± 0.05
MAPTMS 5	0.61	0.35	0.57 ± 0.03
MAPTMS 6	0.70	0.31	0.44 ± 0.02
MAPTMS 7	0.80	0.13	0.17 ± 0.02
CAPTMS 1	0.30	0.67	2.20 ± 0.14
CAPTMS 2	0.43	0.60	1.40 ± 0.06
CAPTMS 3	0.56	0.40	0.72 ± 0.04
CAPTMS 4	0.74	0.25	0.35 ± 0.03
PAPTMS 1	0.29	0.66	2.23 ± 0.16
PAPTMS 2	0.58	0.37	0.63 ± 0.04
DEAPTMS 1	0.33	0.66	2.03 ± 0.12
DEAPTMS 2	0.52	0.48	0.93 ± 0.04
DEAPTMS 3	0.55	0.42	0.77 ± 0.04
DEAPTMS 4	0.60	0.45	0.76 ± 0.04

[a] The amine concentration on the cooperative acid-base (Type AB) and the corresponding base (Type B) catalysts is identical. The error on this measurement amounts for all samples to ±0.01 $mmolg^{-1}$. [b] The reported silanol concentration is only valid for cooperative acid-base catalysts (type AB). The error on this measurement amounts to ±0.01 $mmolg^{-1}$ for all samples. [c] The ratio of silanols to amines given in the table is only valid for cooperative acid-base catalysts (type AB).

3.3.2 Catalytic performance evaluation and interpretation

In chapter 2 [22], a reaction mechanism has been proposed for the primary-amine-catalyzed aldol condensation between 4-nitrobenzaldehyde and acetone. Scheme 3-1 represents a further elaborated version of this reaction mechanism which will allow assessing the amine structure and base strength effects investigated as part of the present chapter. It shows the reaction steps occurring in absence as well as in presence of promoting silanol groups. When no promoting silanol groups are available, the first step of the reaction mechanism is the formation of an enamine (**1**) through a nucleophilic addition of acetone to the amine active site. For the aldol condensation to take place, the enamine reacts with 4-nitrobenzaldehyde yielding an iminium ion (**3**). The primary reaction product (**Aldol**) is formed by a water-assisted desorption of this iminium ion. Finally, the aldol product releases water and forms the secondary reaction product (**Ketone**). In the presence of promoting silanol groups, the nucleophilic reactions will be facilitated due to the formation of hydrogen-bridge interactions between carbonyl moieties and the silanol groups, represented by the species indicated by (**1a**), (**3a**), (**4a**) and (**5a**). In contrast to the mechanism in Scheme 2-3, the mechanism in Scheme 3-1 also includes the equilibrium between the enamine and the imine (**6**) which inhibits the further reaction. The carbinolamine (**1**), on the other hand, is no longer included as it is not kinetically significant, see further.

In the following paragraphs the effects of the presence of silanol groups, the arrangement of the sites on the silica surface, the nature of the amine active sites and the reaction conditions on the catalytic performance is investigated.

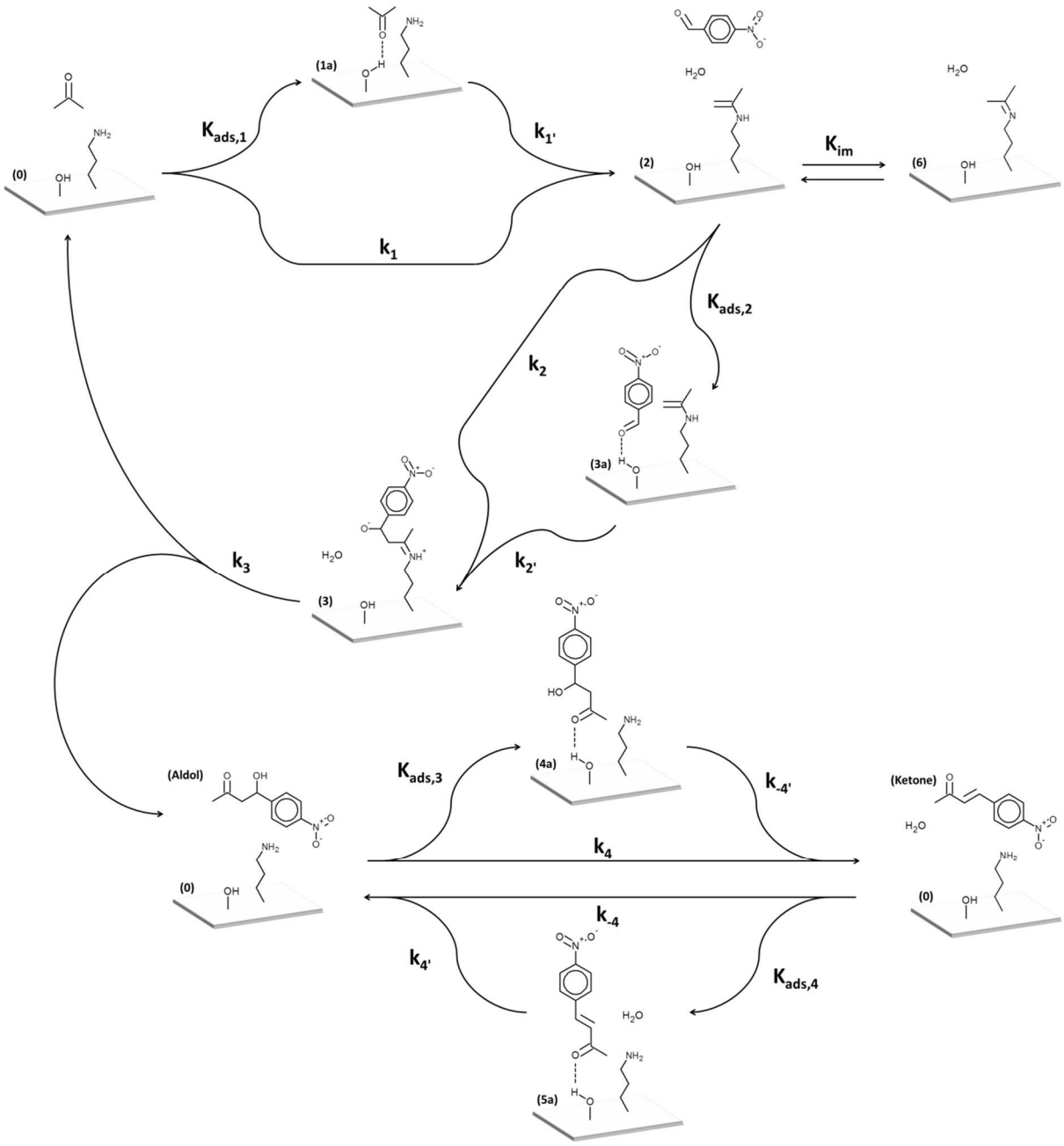

Scheme 3-1. Proposed reaction mechanism for the aldol condensation of 4-nitrobenzaldehyde with acetone

3.3.2.1 Operating conditions

Irrespective of the actual catalyst used the same qualitative trends were observed during the catalyst performance evaluation. In accordance with the Arrhenius law, a higher temperature results in a higher turnover frequency. The selectivity towards the secondary ketone product at a given 4-nitrobenzaldehyde conversion increases with increasing temperature. At low 4-nitrobenzaldehyde concentrations the turnover frequency increases with increasing 4-nitrobenzaldehyde concentration, however, above an initial 4-nitrobenzaldehyde to amine ratio of 50 the turnover frequency remains constant. In

literature, a decreasing reaction rate has been observed at high 4-nitrobenzaldehyde concentrations when using a primary amine as active site [7]. This result suggested that an inhibiting imine could be formed between a primary amine and 4-nitrobenzaldehyde. In the present work an acetone excess has been used, suppressing the direct interaction between 4-nitrobenzaldehyde and the active sites and correspondingly, also the formation of the inhibiting imine from 4-nitrobenzaldehyde [6, 7]. The acetone excess used also results in a rather limited effect of the initial acetone concentration on the turnover frequency. Moreover, a variation in the initial reactant concentrations does not impact on the reaction product selectivities at a given conversion.

3.3.2.2 Catalyst properties

In order to investigate the effect of the catalyst properties on the aldol condensation, all catalysts were subject to identical operating conditions. Pronounced differences in turnover frequency (TOF) are observed as a function of the base that was grafted on the silica, see Table 3-3. While primary amines exhibit a moderate TOF, that observed with tertiary amines does not significantly exceed the noise level, which is consistent with literature reported results [5, 7]. The TOF obtained with secondary amines depended on the substituent. Cyclohexyl and phenyl substituents both lead to a low TOF, while the overall highest turnover frequencies were obtained with N-methylaminopropyltrimethoxysilane as precursor.

At high conversions a selectivity towards the secondary ketone product amounting to 16% is obtained with the aminopropane active site while a selectivity of about 10% is obtained with the methylaminopropane active site. Hence, the nature of the active site somehow affects the obtained product distribution.

Table 3-3. Turnover frequencies obtained with both the unpromoted base as the corresponding cooperative acid-base catalysts

Amine active site	TOF_{unprom} (s^{-1})[a]	TOF_{prom} (s^{-1}) [b]
Aminopropane	$2.0\ 10^{-4}$	$7.8\ 10^{-4}$
Methylaminopropane	$1.0\ 10^{-3}$	$3.3\ 10^{-3}$
Cyclohexylaminopropane	$9.6\ 10^{-6}$	$3.1\ 10^{-5}$
Phenylaminopropane	-	$7.0\ 10^{-6}$
Diethylaminopropane	$1.2\ 10^{-5}$	$3.9\ 10^{-5}$

[a] Turnover frequencies calculated by averaging the TOF's obtained using the unpromoted base catalysts (samples B); [b] Turnover frequencies calculated by extrapolating the TOF's obtained using the cooperative acid-base catalysts (samples AB) towards a molar silanol-to-amine ratio of infinity

The promoting effect of the silanol groups and the active site positioning

It was already shown in Chapter 2 how the cooperativity not only depends on the ratio of both types of active sites but also on the arrangement of these active sites on the catalyst surface [22]. Thermodynamic calculations for a *n*-propylamine-toluene mixture revealed positive deviations from ideal liquid behavior, *i.e.*, propylamine-propylamine interactions preferentially occur as compared to propylamine-toluene interactions. Hydrogen bonding between the primary amines is deemed to be responsible for this and results in primary amines which are positioned in a clustered manner on the silica surface. This is reflected in the percentage of amines which is promoted by silanols as shown in Figure 3-3. The same figure also shows percentage of amines promoted by silanols when using N-methylaminopropyltrimethoxysilane as precursor. It is evident from Figure 3-3 that this precursor leading to a secondary amine is grafted in a random manner on the silica surface, irrespective of the precursor concentration in the grafting procedure. Thermodynamic calculations for a N-methylaminopropane-toluene mixture indeed show no significant deviations from ideality. This indicates that methylaminopropane-methylaminopropane interactions are similar to methylaminopropane-toluene interactions and that the precursor has no tendency to cluster in the synthesis mixture nor on the silica surface. This also results in a higher percentage of promoted secondary amines in the silanol-to-amine ratio range of 0 to 1.7 in comparison to the primary amines. Due to the low activities obtained using the other types of active sites, especially in the low silanol-to-amine ratio range, no conclusive experimental evidence could be obtained about the arrangement of these types of amines on the silica surfaces.

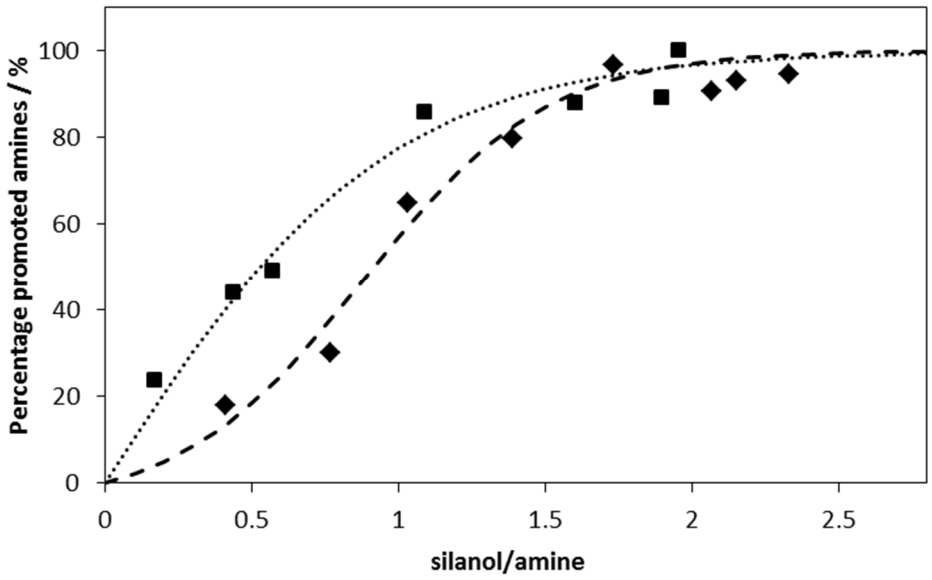

Figure 3-3. Percentage of amines promoted as a function of the silanol-to-amine ratio; ◆ catalysts functionalized using APTES; ■ catalysts functionalized using MAPTMS; dotted line calculated percentage by means of randomly generated surface; dashed line calculated percentage accounting for clustering in the synthesis mixture [22]

Base strength

Table 3-4 shows the base strength of the amine active sites, expressed as pK_a of the corresponding ammonium ion at 298K, that have been used in the present work. These values were obtained from the enthalpy and entropy values calculated using the group contribution method described by Christensen et al. [17] It can be expected that the base strength influences all nucleophilic reactions occurring on the amine site itself, *i.e.*, the nucleophilic addition of acetone with the formation of the enamine intermediate (**1**), the formation of the ketone product and the reverse reaction with the formation of the aldol product. However, except for phenylaminopropane, the differences in basicity of the amines are limited. The low basicity for phenylaminopropane is the result from the stabilization of the nitrogen lone electron pair by its conjugation with the aromatic π cloud. This low base strength limits nucleophilic reactions and explains the low TOF obtained with this active site. However, the limited differences in basicity of the other amines do not explain the experimentally observed TOFs and, hence, other factors, such as the inherent possibility to form the reactive enamine intermediate or an inhibiting imine on the catalyst surface, are expected to exert a dominant effect.

Table 3-4. ΔH°, ΔS° and corresponding pKa,298K values for deprotonation [22]

Amine active site	ΔH° (kJ. mol^{-1})	ΔS° (J. mol^{-1}.K^{-1})	$pK_{a,298K}$ of the ammonium ion
Aminopropane	57.91	-8.37	10.58
Methylaminopropane	52.59	-30.12	10.79
Cyclohexylaminopropane	57.49	-17.15	10.97
Phenylaminopropane	33.39	3.56	5.66
Diethylaminopropane	43.43	-60.67	10.78

Amine structure effects

As shown in Scheme 3-1 the first step in the aldol condensation reaction mechanism is the nucleophilic addition of acetone to the amine group with concomitant formation of an enamine. This reaction happens in two steps: first a carbinolamine is formed which, subsequently, dehydrates with formation of the enamine, see Scheme 3-2. In the case of a primary amine the carbinolamine can also dehydrate with formation of an imine, which is an inhibiting species on the catalyst surface. The acetone excess used, makes that the imine corresponding with acetone is the only one which is formed whereas the formation of the one corresponding with 4-nitrobenzaldehyde is suppressed [6, 7]. In case of a secondary amine the formation of any imine is prevented due to the lack of a second hydrogen on the nitrogen atom. For a similar carbinolamine concentration, this results in a higher enamine concentration when the active site is a secondary rather than a primary amine. Hence, also a higher reaction rate for the subsequent reaction steps is established in the case of secondary amine. Tertiary amines cannot give rise to carbinolamine formation due to the absence of hydrogen atoms on the nitrogen atom. This constitutes a convincing explanation for the low activity of the tertiary amine.

The cyclohexylaminopropane site has a low activity, despite it having the highest base strength and being unable to from the inhibiting imine. This can be attributed to steric hindrance induced by the bulky cyclohexyl group close to the amine.

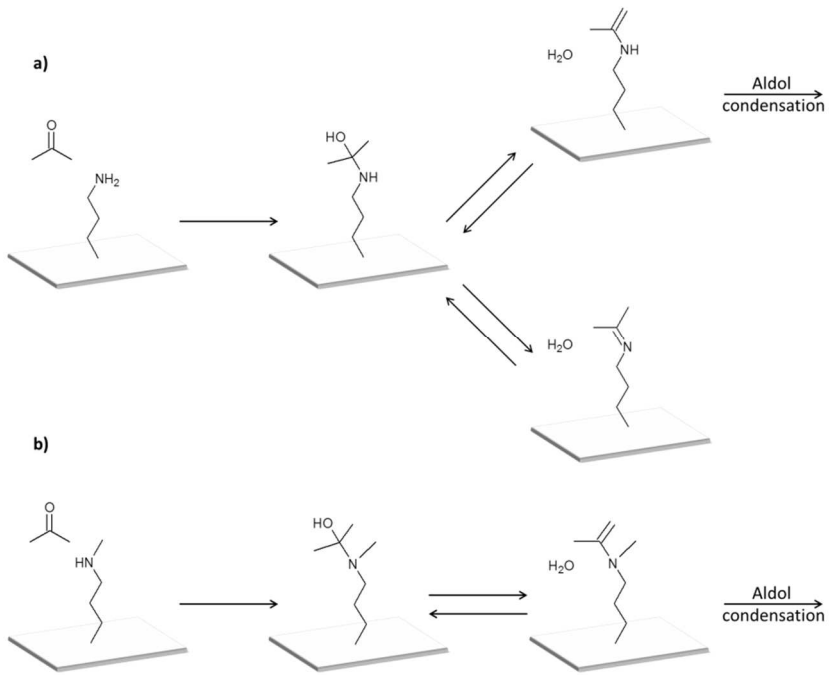

Scheme 3-2. Nucleophilic addition of acetone to a) a primary amine and b) a secondary amine

3.4 Kinetic model based analysis of the amine catalysed aldol condensation

3.4.1 Interaction parameter estimation and activity coefficient calculation

The activity coefficients which were determined using COSMO-RS are used to estimate the binary interaction parameters of the UNIQUAC model. The obtained F value for the global significance of the regression amounts to 7476, which exceeds the tabulated value by 4 orders of magnitude. Hence, the model behaviour can be considered to be acceptable. The binary interaction parameters and corresponding 95% confidence intervals are shown in Table 3-5.

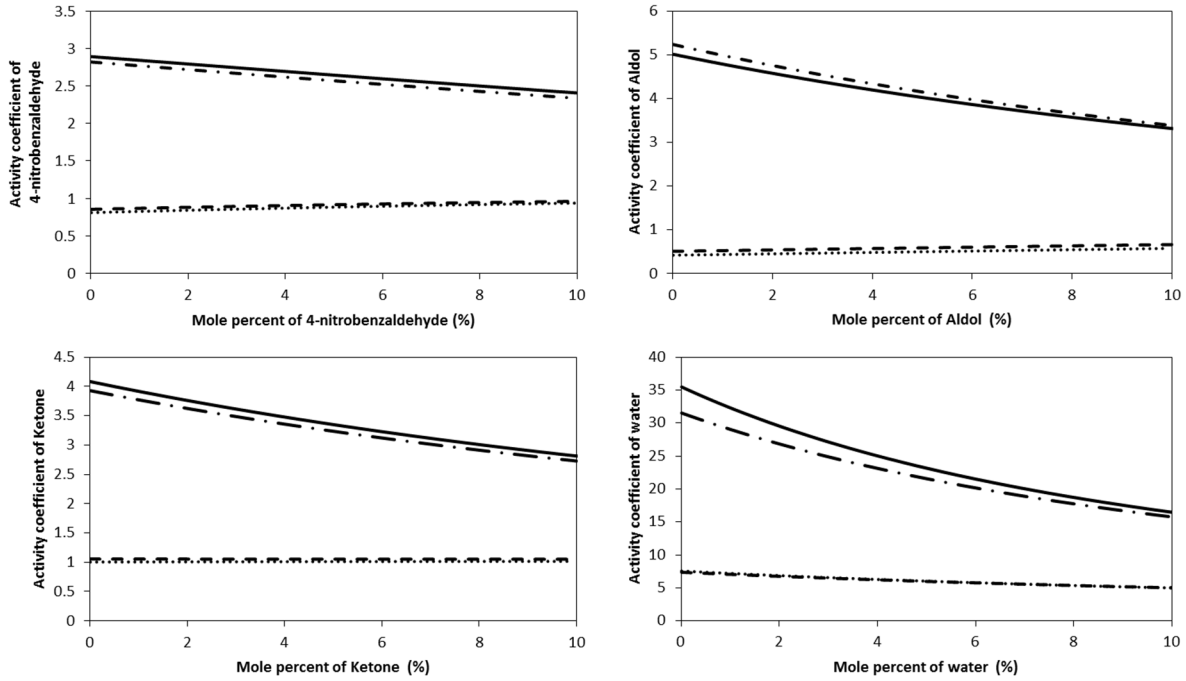

Figure 3-4. Activity coefficients as function of the mole percentage in an acetone/*n*-hexane mixture calculated with the UNIQUAC model using the parameters shown in Figure 3-4; full line: molar ratio of acetone/*n*-hexane of 1:2 and a temperature of 20°C; dotted line: molar ratio of acetone/*n*-hexane of 2:1 and a temperature of 20°C; dash-dotted line: molar ratio of acetone/*n*-hexane of 1:2 and a temperature of 40°C; dashed line: molar ratio of acetone/*n*-hexane of 2:1 and a temperature of 40°C

Figure 3-4 shows the effects of the liquid composition and temperature on the activity coefficients. The activity coefficient of water is the most sensitive to both the composition and the temperature and deviates most significantly from the ideal value of 1. If acetone is the most abundant component in the liquid (ratio 2:1 with respect to *n*-hexane), the activity coefficients of 4-nitrobenzaldehyde and the ketone product are close to 1, while the activity coefficient of the aldol product is only about 0.5. If *n*-hexane is the most abundant component in the liquid, (ratio of 2:1 with respect to acetone) the activity coefficients of 4-nitrobenzaldehyde, the aldol product and the ketone product increase to values around, respectively, 2.5, 4.0 and 3.0. Moreover, in this case, the effect of the mole percentage of the component in the liquid on the activity coefficient is more pronounced. In the investigated range of operating conditions, the activity coefficient of acetone is not much affected by the presence of other components except for *n*-hexane. An increasing amount of *n*-hexane leads to an increasing activity coefficient of acetone.

Table 3-5. UNIQUAC binary interaction parameters estimated based upon COSMO-RS calculations and corresponding 95% confidence intervals

j / *i*	Acetone		*n*-Hexane	
	Δu_{ij} (kJ/mol)	Δu_{ji} (kJ/mol)	Δu_{ij} (kJ/mol)	Δu_{ji} (kJ/mol)
Acetone	0.0	0.0	-0.07 ± 0.04	1.71 ± 0.06
4-nitrobenzaldehyde	-0.98 ± 0.15	0.56 ± 0.21	0.22 ± 0.08	1.51 ± 0.09
Aldol	3.47 ± 0.16	-2.50 ± 0.04	0.66 ± 0.10	1.69 ± 0.11
Ketone	1.97 ± 0.18	-1.59 ± 0.09	0.38 ± 0.10	1.23 ± 0.11
Water	-1.08 ± 0.18	0.90 ± 0.03	0.76 ± 0.13	1.45 ± 0.12

3.4.2 Kinetic model construction and descriptor identification

The reaction mechanism shown in Scheme 3-1 is used for kinetic model construction. Note that the carbinolamine intermediate was found not to be kinetically significant and, hence, is not explicitly accounted. Correspondingly, the enamine (**2**) formation is described by a composite reaction step. Moreover, also the intermediates in the aldol product dehydration to form the ketone and the reverse reaction are not explicitly considered. This is done in order to reduce the number of parameters to be estimated during regression. The reactions resulting in the formation of hydrogen-bridge interactions between carbonyl moieties and silanol groups (**1a**), (**3a**), (**4a**) and (**5a**) and the reactions between the enamine (**2**) and the inhibiting imine (3) are considered to be quasi-equilibrated while all other reactions are taken as irreversible forward reactions.

If the amine is promoted by the presence of a silanol, the net rate of the enamine (**2**) formation is given by equation 6. In this equation a_{ace} and a_{benz}, represent, respectively, the activity of acetone and of 4-nitrobenzaldehyde. In case of an unpromoted amine, both the first and the fourth term of equation 6 disappear. The reaction rate coefficients follow the Arrhenius law, which is reparameterized in order to avoid strong binary correlation between the pre-exponential factor and the activation energy [23].

In this work, the primary amine is considered to be the reference active site. Changing this active site to another type of amine has an effect on all the reaction steps occurring on the amine itself, *i.e.*, the enamine (**2**) formation, the desorption of the intermediate (**3**), the imine (**6**) formation, the product ketone formation and the reverse reaction with the

product aldol formation. As already described in section 3.2.2, the imine can only be formed when the active site is a primary amine. In all other cases the equilibrium coefficient K_{im} equals zero. The effect on the other reaction steps as discussed above is described by a change in activation entropy ΔS_{amine} and activation energy ΔE_{amine} between the reference primary amine and the considered active site. For the rate coefficient k_1 this is illustrated in equation 7. The changes in reaction entropy and reaction enthalpy are assumed to be identical for all affected reaction rate coefficients, *i.e.,*. k_1, k_3, k_4 an k_{-4}. The presence of silanol groups can have a twofold effect on the reaction enthalpy of the four adsorption steps, namely a first one due to the prior adsorption of the reactant on a silanol group and a second one which is related to the higher susceptibility of species (**1a**) and (**3a**) to nucleophilic reactions compared to bulk acetone and 4-nitrobenzaldehyde (eq. 8). As it is impossible to distinguish between these two effects based on the experimentation performed as part of the present work, both effects have been combined into a single parameter $\Delta E_{OH'}$. The adsorption on a silanol group induces also a change in the reaction entropy, *i.e.* $\Delta S_{OH'}$. Also in this case, the shift in reaction entropy and reaction enthalpy is assumed to be identical for all adsorption steps.

$$R_{1,prom} = k_{1'}K_{ads,1}C_{0,prom}a_{ace} + k_1C_{0,prom}a_{ace} - k_2C_{1,prom} - k_{2'}K_{ads,2}C_{1,prom}a_{benz} \quad (6)$$

$$k_1 = A_{1,ref}e^{\frac{-\Delta S_{amine}}{R}}e^{\frac{-(E_1+\Delta E_{amine})}{R}\left(\frac{1}{T}-\frac{1}{T_{ref}}\right)} \quad (7)$$

$$k_{1'}K_{ads,1} = k_1e^{\frac{\Delta S_{ads,1}}{R}}e^{\frac{-\Delta E_{OH}-\Delta H_{ads,1}}{R}\left(\frac{1}{T}-\frac{1}{T_{ref}}\right)} = k_1e^{\frac{\Delta S_{OH'}}{R}}e^{\frac{-\Delta E_{OH'}}{R}\left(\frac{1}{T}-\frac{1}{T_{ref}}\right)} \quad (8)$$

3.4.3 Determination of the descriptors and discussion of the reaction mechanism

Due to the very low activity of phenylaminopropane resulting from a low base strength and the inability of diethylaminopropane to form the carbinolamine intermediate, a kinetic model assessment of the aldol condensation kinetics is only relevant for the catalysts obtained by grafting APTES, MAPTMS and CAPTMS, *i.e.*, a primary amine, an accessible secondary amine and a sterically hindered secondary amine.

The equilibrium coefficient K_{im} and the reaction enthalpy of the reaction forming the ketone, which is equal to difference between the activation energies E_4 and E_{-4}, are

determined using the Jobac method [16], while the other parameters are estimated by means of regression. The obtained parameter values and the corresponding 95% confidence intervals are reported in Table 3-6 and Table 3-7. Notably, the rate coefficient of the water-assisted desorption exceeds the other rate coefficients by far. As a result the exact value of this rate coefficient is only having a limited impact on the obtained results and its temperature dependence, *c.q.*, activation energy cannot be significantly determined. Hence, the corresponding activation energy E_3 is set equal to zero. The other estimated activation energies are in the range of 11 to 51 kJ/mol which is rather low for a chemical reaction, however, this is a result of their composite character, *i.e.*, they combine (at least) 2 elementary steps, see above. If a silanol group is present these activation energies decrease by about 9 kJ/mol due to the formation of a hydrogen bond between the silanol and the reactant. This leads to an apparent activation energy for the formation of the enamine intermediate which is very low. The formation of a hydrogen bond between a silanol and a carbonyl moiety induces an entropy decrease of about 8 J/(mol.K).

The model performance is visualized by the parity diagrams in Figure 3-6. Independently of type of catalyst, *i.e.*, unpromoted or promoted and primary or secondary amine, the simulated concentrations of the reactants and both reaction products agree well with the observed concentrations.

Using the parameter estimates the model simulates similar amounts of free active sites (**0**) and inhibiting imines (**6**) on the surface of a fully promoted primary amine catalyst, *i.e.*, respectively 43% and 45% at typical operating conditions. The remainder of the surface is mainly occupied by the enamine intermediate (**1**). The iminium ion (**3**) occupies less than 1% of the surface. For a fully promoted primary amine catalyst 74% of the reactants are transformed via the promoted pathway, *i.e.*, via intermediates (**1a**) and (**3a**), while the other 26% of the reactants are transformed without the aid of a silanol group.

The effect of the nature of the amine active site is assessed by a change in activation entropy and activation energy between the reference primary amine and the considered active site. In Figure 3-5 these changes are plotted as a function of the reaction entropies and enthalpies for deprotonation of the corresponding active sites, *i.e.*, amine base strength. The decrease of the activation entropy induced by changing the active site exhibits an apparent proportionality to the decrease in reaction entropy for deprotonation while for

the activation energies no such proportionality is observed. When the sterically hindered secondary amine (CAPTMS) is used as active site the activation energies are about 17 kJ/mol higher than expected from the results obtained with the other two amines. This high activation energy can be related to the steric hindrance induced by the bulky cyclohexyl group close to the amine.

For the accessible secondary amine (MAPTMS) type of catalysts the model shows that at typical operating conditions used, the surface of a fully promoted catalyst is mainly covered with the enamine intermediate (**2**), leaving only 1% of active sites free (**0**) and results in a lower production of the unsaturated ketone product. The sterically hindered secondary amine (CAPTMS) sites are mainly free (**0**). The percentage of reactants which are transformed via the promoted pathway remains the similar as with the primary amine (APTES) reference catalysts.

Table 3-6. Estimated values for the kinetic descriptors with their 95% confidence intervals obtained after regression of the kinetic model (see section 3.4.2) to the experimental data (see section 3.3.2)

	Pre-exponential factor	Activation energy
k_1	5.04 10^{-5} ± 0.23 10^{-5} L/(mol.s)	11.7 ± 1.4 kJ/mol
k_2	5.81 10^{-2} ± 0.14 10^{-2} L/(mol.s)	34.1 ± 1.7 kJ/mol
k_3	20.4 ± 9.6 L/(mol.s)	0.0 kJ/mol [b]
k_4	2.02 10^{-2} ± 0.37 10^{-2} L/(mol.s)	39.8 ± 5.8 kJ/mol
k_{-4}	4.60 ± 1.12 L²/(mol².s)	50.6 kJ/mol [a]

[a] Value determined using the Jobac method. [b] Non-significantly estimated parameter.

Table 3-7. Estimated catalyst descriptors with their 95% confidence intervals obtained after regression of the kinetic model (see section 3.4.2) to the experimental data (see section 3.3.2)

Entropic difference		Reaction enthalpy / Activation energy difference	
Promotional effect of silanols			
$\Delta S_{OH'}$	8.25 ± 0.16 J/(mol.K)	$\Delta E_{OH'}$	-8.7 ± 1.8 kJ/mol
Nature of the amine sites			
ΔS_{im}	13.5 J/(mol.K) [a]	ΔH_{im}	43.8 kJ/mol [a]
ΔS_{MAPTMS}	-46.4 ± 2.6 J/(mol.K)	ΔE_{MAPTMS}	10.4 ± 1.0 kJ/mol
ΔS_{CAPTMS}	-23.7 ± 5.0 J/(mol.K)	ΔE_{CAPTMS}	17.6 ± 3.2 kJ/mol

[a] Value determined using the Jobac method.

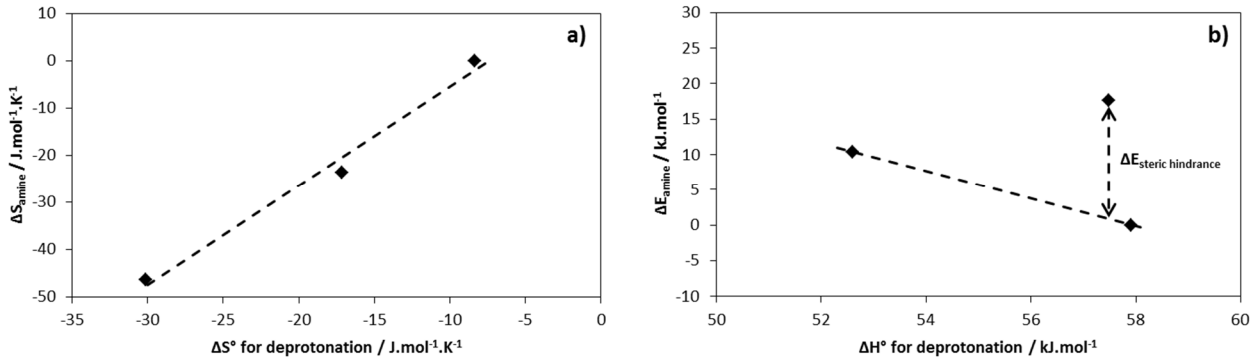

Figure 3-5. a) ΔS_{amine} as a function of ΔS° for deprotonation and b) ΔE_{amine} as a function of ΔH° for deprotonation; the dashed lines are intended as visual aids only

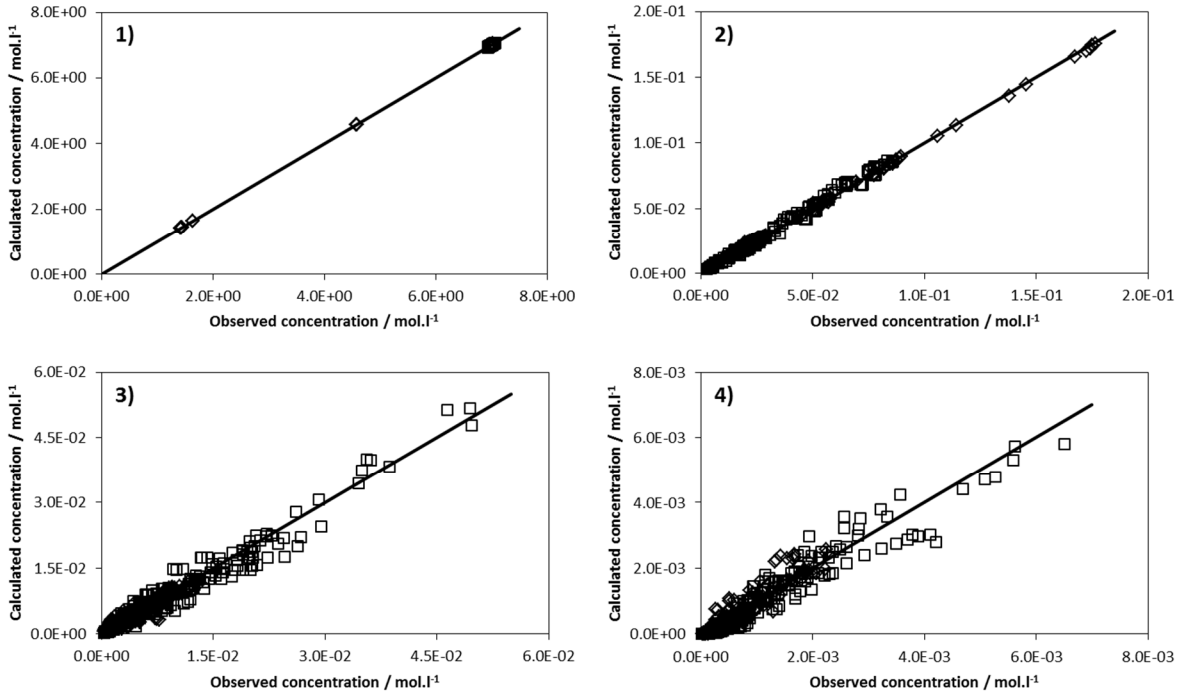

Figure 3-6. Parity diagrams for the responses of the kinetic model for aldol condensation on ◊ APTES catalysts; □ MAPTMS catalysts and Δ CAPTMS catalysts; 1) acetone; 2) 4-nitrobenzaldehyde; 3) aldol and 4) ketone

3.5 Conclusions

Distinct differences in turnover frequency (TOF) were obtained when different types of amines were used to catalyse the aldol condensation between acetone and 4-nitrobenzaldehyde. The activity of all amine active sites could be enhanced by incorporating silanol groups in the catalyst. In contrast with primary amine active sites

which were found to be positioned in a clustered manner, secondary amine active sites were randomly distributed over the silica surface.

While primary amines exhibited a reasonable TOF, that observed with tertiary amines was not exceeding the noise level. The TOF obtained with secondary amines depended on the substituent. Cyclohexyl and phenyl substituents both lead to a low TOF, while the highest turnover frequencies among all investigated catalyst were obtained with secondary amine active sites with a methyl substituent. Activity differences are explained by an interplay of the following three factors, *i.e.*, (i) the possibility of forming a reactive enamine intermediate and inhibiting imine species with the amine active site, (ii) the base strength of the amine active site and (iii) steric hindrance effects. The possibility to form a reactive intermediate and inhibiting species was the most important factor determining the observed TOFs. While the crucial enamine reactive intermediate cannot be formed on a tertiary amine, the inhibiting imine can only be formed on primary amine active sites. As a result, a secondary amine active site which can yield the reactive enamine intermediate without inhibiting imine formation can exhibit the highest TOFs, provided that it is not subject to steric hindrance or unfavourable basicity effects. The latter is quantified via differences in activation entropies and energies of all the reaction steps occurring on the amine sites themselves, *i.e.*, the enamine formation, the water assisted desorption with the product aldol formation, the product ketone formation and the reverse reaction with product aldol formation. A low base strength, such as that of phenylaminopropane results in a low TOF. The steric hindrance effect was exemplified by a cyclohexyl substituted on the amine results in an increase in activation energy of about 17 kJ/mol. Hence, a secondary amine with a small substituent avoiding steric hindrance seems to be the optimal amine type to catalyse the aldol condensation between acetone and 4-nitrobenzaldehyde.

3.6 References

1. N. A. Brunelli, K. Venkatasubbaiah, C. W. Jones, Chem Mater, **2012**, 24, 2433-2442
2. N. A. Brunelli, C. W. Jones, J. Catal., **2013**, 308, 60-72
3. N. A. Brunelli, S. A. Didas, K. Venkatasubbaiah, C. W. Jones, J. Am. Chem. Soc., **2012**, 134, 13950-13953

4. Y. Kubota, K. Goto, S. Miyata, Y. Goto, Y. Fukushima, Y. Sugi, Chemistry Letters, **2003**, 32, 234-235
5. Y. Kubota, H. Yamaguchi, T. Yamada, S. Inagaki, Y. Sugi, T. Tatsumi, Top. Catal., **2010**, 53, 492-499
6. K. Kandel, S. M. Althaus, C. Peeraphatdit, T. Kobayashi, B. G. Trewyn, M. Pruski, I. I. Slowing, ACS Catal., **2013**, 3, 265-271
7. K. Kandel, S. M. Althaus, C. Peeraphatdit, T. Kobayashi, B. G. Trewyn, M. Pruski, I. I. Slowing, J. Catal., **2012**, 291, 63-68
8. B. E. Poling, J. M. Prausnitz, J. P. O'Connell, *The properties of gases and liquids*, McGraw-Hill, New York, **2001**
9. D. S. Abrams, J. M. Prausnitz, Aiche J., **1975**, 21, 116-128
10. A. Fredenslund, R. L. Jones, J. M. Prausnitz, Aiche J., **1975**, 21, 1086-1099
11. H. K. Hansen, P. Rasmussen, A. Fredenslund, M. Schiller, J. Gmehling, Ind. Eng. Chem. Res., **1991**, 30, 2352-2355
12. A. Klamt, J. Phys. Chem., **1995**, 99, 2224-2235
13. A. Klamt, F. Eckert, Fluid Phase Equilib., **2000**, 172, 43-72
14. F. Eckert, A. Klamt, Aiche J., **2002**, 48, 369-385
15. A. Klamt, F. Eckert, Fluid Phase Equilib., **2004**, 217, 53-57
16. K. G. Joback, R. C. Reid, Chem. Eng. Commun., **1987**, 57, 233-243
17. J. J. Christensen, R. M. Izatt, D. P. Wrathall, L. D. Hansen, Journal of the Chemical Society a -Inorganic Physical Theoretical, **1969**, 1212-1223
18. W. E. Stewart, M. Caracotsios, *Computer-Aided Modeling of Reactive Systems*, Wiley-Interscience, Hoboken, New Jersey, **2008**
19. G. F. Froment, L. H. Hosten, *Chap. 3*, in *Catalysis Science and Technology*, J.R. Anderson and B. M., Editors. 1981, Springer Verlag: Berlin.
20. L. H. Hosten, G. F. Froment, *Kinetic Modeling of Complex Reactions*, in *Recent Advances in the Engineering Analysis of Chemically Reaction Systems*, L.K. Doraiswamy, Editor 1984, Wiley Eastern. p. 68-92.
21. Y. Bard, *Nonlinear Parameter Estimation*, Academic Press, New York, **1974**
22. J. Lauwaert, E. De Canck, D. Esquivel, J. W. Thybaut, P. Van Der Voort, G. B. Marin, ChemCatChem, **2014**, 6, 255-264
23. M. Schwaab, J. C. Pinto, Chem. Eng. Sci., **2007**, 62, 2750-2764

Chapter 4

Acid Strength and Spatial Arrangement Effects on Cooperative Aldol Condensation

Weak acids are known to enhance the activity of amines in aldol condensation reactions on silica-based catalysts. The effects of acid strength and arrangement of the promoting site with respect to a secondary amine have been investigated in the aldol condensation of 4-nitrobenzaldehyde with acetone. Changing the substituent of this secondary amine from a methyl to an ethyl group decreases its aldol condensation activity. An intramolecular OH function as provided by a primary alcohol incorporated on the β-carbon of the amine substituent exhibits a similar cooperativity as an intermolecular OH function provided by neighboring surface silanols. A maximum activity was achieved when the secondary amine with the same primary alcohol containing substituent was surrounded by surface silanols, indicating the potential advantage of simultaneously activating both reactants by the formation of a hydrogen bond in contrast to the consecutive activation when there is only a single promoting site in the vicinity of the amine. Changing the alcohol to stronger acids resulted in a reduced cooperativity with increasing acid strength. After endcapping the silanols, 68 % to 83 % of the activity of the intramolecularly promoted catalysts was retained

while that of the conventional, secondary amine was reduced by a factor four compared to its intermolecularly cooperative counterpart.

4.1 Introduction

Aminated silica materials are known to efficiently catalyze carbon-carbon coupling reactions, especially when weak acid sites are neighboring the amine function [1-13]. An adequate understanding of the cooperativity between the two types of sites is crucial for the rational design of an optimal acid-base cooperative catalyst. One can think of several catalyst properties that have an important effect on the catalytic performance of the material, such as the proximity of the promoting sites to the amines [5-8], the structure and base strength of the amine site [3-5], and the acid strength of the promoting site [8-10].

Post-synthetic grafting by means of a stirring or reflux procedure is a popular technique to functionalize silica materials with amines. During the functionalization, a fraction of the weakly acidic silanols, that are intrinsically present on the silica surface, is replaced with an amine-containing silane [6, 14]. It has been shown that the presence of the remaining silanols on the surface enhances the catalytic activity of the amines in the aldol condensation [1, 2, 5-9]. This cooperative effect does not only depend on the concentrations of both types of sites but also on their spatial arrangement with respect to each other [5, 6]. As demonstrated in Chapter 2, primary amine precursors have the tendency to form hydrogen bonds between each other during the grafting procedure [5, 6, 15-19]. Commonly used solvents such as toluene are typically unable to break these hydrogen bonds and, hence, primary amines remain associated to each other and are grafted in a clustered manner on the silica surface [5, 6, 15-17]. In contrast, secondary amines have a lower tendency to form such hydrogen bonds in the same solvents and are more randomly distributed over the silica surface [5]. Both the clustered and the random arrangement deviate from the ideal checkerboard pattern, meaning that at a silanol-to-amine ratio of 1, not every amine has a neighboring silanol and, hence, that the amines are not fully promoted. It has also been demonstrated that the cooperativity between amines and silanols can be tuned by controlling the alkyl chain length of the amine active site as well as the silica support pore size [7, 8]. It was found that with short alkyl chains the catalyst behaves as if the amine groups were isolated, irrespective of the presence of silanol groups.

The catalytic cooperativity increases with the alkyl chain length up to a propyl chain, before leveling off for longer alkyl chains. For smaller silica pore sizes, however, the same maximum cooperativity is already established for an ethyl chain and, significantly decreases for longer chains, suggesting that the long alkyl chain in the small pores perturbs the cooperativity.

To obtain an even better control of the spacing of the cooperating sites, one can draw inspiration from homogeneous catalysis. A series of homogeneous amino acids, in which the amine and the carboxylic acid are separated by 2 to 7 methylene groups, exhibits an increase in catalytic activity with decreasing distance between the two functions [8, 20]. In addition, homogeneous amino acids such as proline and glycine are known to perform well as aldol condensation catalysts [21, 22]. In both amino acids, the amine and the carboxylic acid groups are separated by a single carbon atom. Moreover, a recent study showed that L-proline could be immobilized on mesoporous silica that contained alternating hydrophilic and hydrophobic blocks to catalyze aldol condensations and Knoevenagel-Michael cascade reactions with higher yields and enantioselectivities when compared to their homogeneous precursors [23].

As demonstrated in Chapter 3, primary, secondary and tertiary amines exhibit significant differences in catalytic activities for the aldol condensation, although they have similar base strengths [2-5]. It was concluded that a secondary amine active site that can produce the reactive enamine intermediate without forming the inhibiting imine exhibits the highest catalytic activity, provided that it is not subject to steric hindrance [5]. A recent study examined the ability of several organocatalysts to form enamine and iminium intermediates in the cross condensation of isobutyraldehyde and acetone. Organocatalysts that could form Seebach's oxazolidinones during the reaction were found to favor the formation of aldol-type products instead of Mannich-type products, demonstrating that the intermediates can also affect the product selectivity and not only the activity [24]. The promoting effect of the weak acid sites is often ascribed to hydrogen bond interactions between the acid and the carbonyl moiety of the reactant, which results in a higher susceptibility of the electrophilic reactant for the nucleophilic attack of the amine [1, 2, 5-9]. Replacing the weakly acidic silanols with a stronger acid site seems to have a negative impact on the activity of primary amines [8-10], which could be explained by a more favorable protonation of the amines by the strong acids than by the very weakly acidic silanols. As a result, the lone electron pair of

the amine, necessary for the catalytic aldol condensation cycle, is no longer available for reaction with the reactants.

Previous investigations of acid strength effects were performed on catalysts that were synthesized using an amine-containing silane and a different acid-containing silane [8-10]. Besides the protonation of the amines, differences in surface arrangements of the amine and acid sites may have interfered with the targeted effects of the base and acid strength. In this chapter, the effect of the acid strength of the promoting site is investigated while carefully controlling the arrangement of the sites with respect to each other. A catalyst library comprising different acid-base catalysts was synthesized by functionalizing an SBA-15 support with (3-iodopropyl)trimethoxysilane. The iodo-group is subsequently replaced with the desired functional groups, *i.e.,* a secondary amine and an acid site separated by one carbon atom. As the iodosilane cannot form hydrogen bonds, it does not have any tendency to be grafted in a clustered manner. In addition, the grafting procedure of the iodosilane aims at a low loading, *i.e.,* 0.3 mmol Iodo/g silica, resulting in isolated sites. This procedure makes it possible to study the intramolecular interactions between the acid and the amine site independent of the intermolecular interactions between sites on different linkers. Intermolecular interactions between the amine site and surface silanols remains possible. The effect of these interactions is assessed by endcapping the surface silanols using hexamethyldisilazane. The effect of the acid strength of the intramolecular promoting site on the catalyst activity is investigated in the aldol condensation of acetone with 4-nitrobenzaldehyde.

4.2 Procedures

4.2.1 Catalyst Synthesis

4.2.2 Synthesis of the mesoporous silica support

Two SBA-15 batches are synthesized according to the following recipe: 24.0 g pluronic P123 EO-PO-EO triblock copolymer (poly(ethylene glycol)-poly(propylene glycol)-poly(ethylene glycol), Mn ≈ 5800, Sigma-Aldrich), is dissolved in a mixture of 120 mL of 12.1 M hydrochloric acid (HCl, ACS grade reagent, Sigma-Aldrich) and 636 mL distilled water. Afterwards, 46.26 g of tetraethylorthosilicate (TEOS, 98% Sigma-Aldrich) is added and the mixture is stirred at

40 °C for 20 h. Subsequently, the magnetic stir bar is removed and the mixture is heated to 100 °C for 24 h. The resulting solid is separated from the mixture by filtration and is subsequently washed with several liters of water. The material is dried overnight at 75 °C prior to being calcined according to the following temperature program: (1) ramp to 200 °C at 1.2 °C min^{-1}, (2) hold at 200 °C for 1h, (3) ramp to 550 at 1.2 °C min^{-1}, (4) hold at 550 °C for 12 h, (5) cool to room temperature. The material is further dried overnight at 100 °C under reduced pressure. Nitrogen adsorption-desorption measurements confirmed that the average pore size of both batches of SBA-15 were equal to 8.0 nm and the BET surface areas and the total pore volumes deviated less than 7% from the average value. Therefore, it is concluded that the two SBA-15 batches could be considered as identical. Both batches are mixed thoroughly and used in the next synthesis step as a single source of SBA-15.

4.2.3 Grafting of (3-iodopropyl)trimethoxysilane on the silica surface and endcapping of the remaining silanol groups

In order to ensure homogeneity of the synthesis mixture, the grafting is performed on SBA-15 batches of maximum 4 g. As a result, the procedure described below is repeated three times. The SBA-15 is functionalized with (3-iodopropyl)trimethoxysilane (>95%, Sigma-Aldrich), see Scheme 4-1. The material is diluted in 100 mL of toluene (anhydrous, 99.8%, Sigma-Aldrich). The iodosilane (6.6 mmol, 1.3 mL) is subsequently added and the mixture is refluxed under a nitrogen atmosphere at 110 °C for 24 h. The solid is recovered by filtration and is subsequently washed with 200 mL toluene, 200 mL hexane (ACS grade, BDH) and 200 mL ethanol (ACS grade, BDH). After drying under reduced pressure with heating to 100 °C the three batches are thoroughly mixed.

About half of the mixed batch of grafted SBA-15 is treated with 1,1,1,3,3,3-hexamethyldisilazane (HMDS, ReagentPlus, 99.9%, Sigma-Aldrich) to endcap the remaining silanol groups. This is done according to the procedure described in section 2.2.1.

4.2.4 Replacing the iodo-group with the desired functional groups

Different catalysts are prepared by replacing the iodo-group with ethylamine, ethanolamine, glycine or aminomethylphosphonic acid, see Scheme 4-1. These functionalizations are

performed on both the SBA-15 grafted with the iodosilane as well as on the one that is subsequently treated with HMDS. About 1.5 g of the solid material is diluted in 25 mL of dimethyl sulfoxide (DMSO, ACS Grade, 99.9%, BDH) and 20 mmol of the functional group precursor, *i.e.,* ethylamine hydrochloride (98% Sigma-Aldrich), methyl 2-aminoacetate hydrochloride (>96%, Fisher Scientific), ethanolamine (ACS Reagent, >99.0%, Fluka) or diethyl aminomethylphosphonate (97%, Epsilon Chimie) is added. Next, 6 mL of N,N-diisopropylethylamine (DIPEA, 99%, Alfa Aesar) is added as a catalyst and the mixture is heated to 110 °C for 48 h. Afterwards, the solid is recovered by filtration and washed with 100 mL of DMSO, 100 mL of hexane, and 100 mL of ethanol. After drying the solid overnight at 100°C under reduced pressure, the materials functionalized with ethylamine, *i.e.,* SBA-A and SBA-HMDS-A, are ready for kinetic experiments. The other materials are subsequently diluted in 100 mL of a 2 M HCl solution and stirred at room temperature for 6 h to deprotect the acid site. Afterwards, the solid is recovered by filtration and washed with 100 mL water and 100 mL of a 2 M ammonium hydroxide (Alfa Aesar) solution. Finally, these materials are dried again overnight at 100 °C under reduced pressure and are also ready for kinetic experiments.

The following convention is used for labeling the various samples. The first term, *i.e.*, 'SBA', refers to the supporting material. In case where the remaining silanols groups are endcapped, a second term 'HMDS' is added referring to the corresponding treatment. The final term refers to the functional group. The following abbreviations are used for the different functional groups: 'I' for the iodo-group, 'A' for the secondary amine, 'AL' for the alcohol group, 'CA' for the carboxylic acid and 'PA' for the phosphoric acid. Suffix 'pr' is used for the materials in which the acid group is still protected.

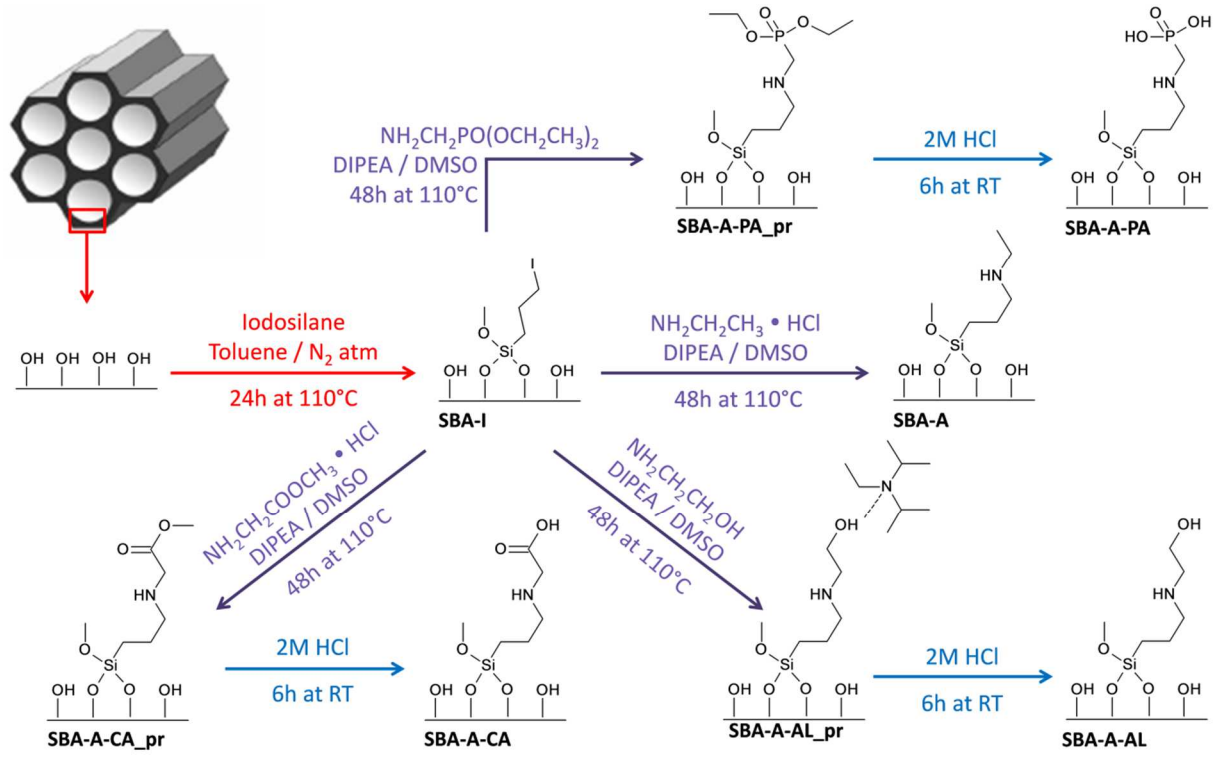

Scheme 4-1. Schematic representation of the synthesis of SBA-X. A similar scheme can be drawn for the synthesis of SBA-HMDS-X. In this case, an HMDS-treatment is included between the grafting of the iodosilane (step 1) and the replacement of the iodo-group with the desired functional group (steps 2).

4.2.5 Catalyst characterization

Nitrogen adsorption-desorption experiments are performed at 77 K on a Micromeritics Tristar 2030. The surface areas are determined by the Brunauer-Emmet-Teller (BET) method. The total pore volumes and pore sizes are calculated using the Broekhoff-de Boer method with the Frenkel-Halsey-Hill modification (BdB-FHH) [25]. The X-ray diffraction (XRD) patterns are measured on a Thermo Scientific ARL X'TRA X-ray diffractometer. Fourier transform infrared (FTIR) spectroscopy is performed using a Bruker Vertex 80v with dual FTIR and FT-Raman benches and KBr and CaF_2 beamsplitters, respectively. The solid-state CP-MAS ^{13}C and ^{31}P NMR spectra are recorded on a Bruker 300 MHz. Elemental analysis is performed by Atlantic Microlab, Inc (Norcross, GA).

4.2.6 Catalyst performance testing

The activity of each catalyst is assessed via the aldol condensation of acetone (ACS Grade, 99.5%, BDH) and 4-nitrobenzaldehyde (99% Alfa Aesar), as shown in Scheme 2-2. It is a frequently used model reaction. To compare the reference catalyst, SBA-A, with data

obtained in Chapter 2 [5], the performance of this material is tested using 4 mol% of amines with respect to the concentration of 4-nitrobenzaldehyde in the reaction mixture (0.03 M). Due to the comparatively lower activities of the other materials, their catalytic performance is assessed using 15 mol% of amines with respect to the concentration of 4-nitrobenzaldehyde. This led to higher conversions and lower experimental errors, although lower turnover frequencies (TOFs) are achieved.

The experiments are performed in a 25 mL two-neck round-bottom flask equipped with a condenser and a septum. First, the supported catalyst is added to the flask such that the desired amount of amines is present, *i.e.,* 4 or 15 mol% with respect to the 4-nitrobenzaldehyde concentration. Afterwards, 3 mL of a mixture consisting of 50 vol% acetone, 50 vol% *n*-hexane, 0.03 mmol/mL 4-nitrobenzaldehyde and 0.03 mmol/mL 1,4-dimethoxybenzene (TCI) is injected into the flask and the flask was immediately placed in an oil bath at 45 °C. The moment the flask is placed in the oil bath is taken as the start of the reaction (t=0). The reaction is monitored for 5 h by taking a sample of the reaction mixture (about 100 µL) every hour. Every sample is passed through a short silica gel bed in a cotton-plugged pipet to remove any catalyst. Approximately 2 mL of acetone is used to wash the syringe needle and to transfer the sample to a GC vial. The samples are analyzed using a Shimadzu GCMS-QP2010S gas chromatograph equipped with an Agilent DB-1701 column (30 m x 0.25 mm internal diameter x 0.25 µm thickness). Quantification of the conversion is performed by relating the peak surface area of 4-nitrobenzaldehyde to the amount of the internal standard, 1,4-dimethoxybenzene. All data are obtained at differential conditions, which means that the conversion depended linearly on the batch time and the TOF could be determined from the slope of the observed straight line [26]. This also means that any product, *c.q.*, water, inhibition is absent. The conversion versus time plots are shown in Figure 4-1. The experimental error (EE) on the TOF is determined from repeat experiments and calculated using equation (1). With N representing the number of repeat experiments, TOF_i the turnover frequency observed in experiment i and TOF_{av} the average TOF. The experimental error is found to be below 5%.

$$EE = \frac{1.96}{TOF_{av}} \sqrt{\frac{1}{N-1} \sum_{i=1}^{N} (TOF_i - TOF_{av})^2} \quad (1)$$

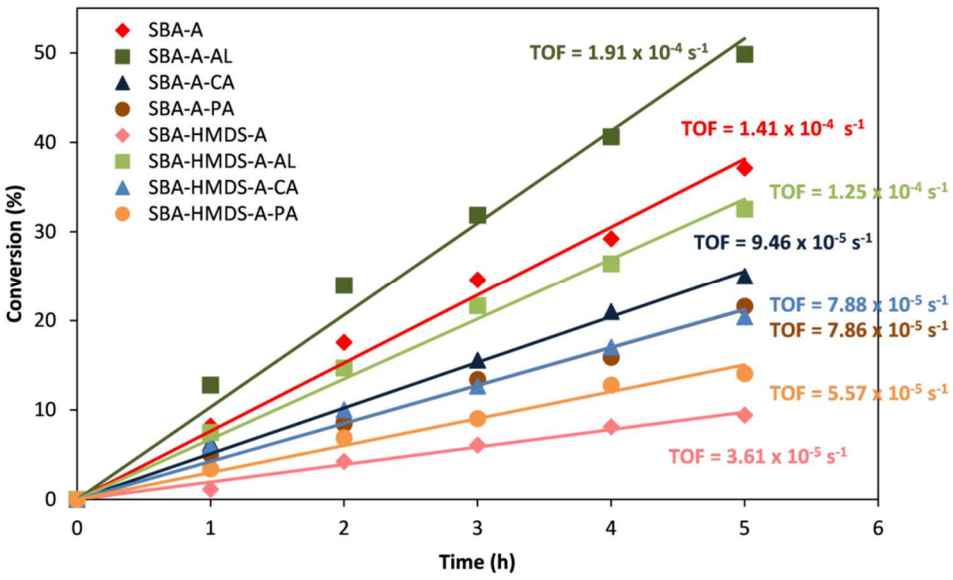

Figure 4-1: Conversion versus time plots with corresponding TOFs

4.3 Results and discussion

4.3.1 Catalyst characterization

The specific BET surface areas, average pore sizes, and total pore volumes of the SBA-15 support and the different catalysts were determined from nitrogen adsorption-desorption isotherms and are listed in Table 4-1. After functionalization of the SBA-15 support, a small decrease in surface area and total pore volume, resulting from the loss in free volume and the increase in catalyst mass, was observed. The average pore size of the materials that were treated with HMDS were about 1 nm smaller than the parent SBA-15, while that of the other materials remained unaltered. Moreover, all materials retained their mesoporosity. Therefore it can be assumed that the catalysts are not subject to pore blocking and most of the sites are accessible. The small-angle XRD patterns of all materials, shown in Figure 4-2, exhibit three peaks that could be attributed to the (100), (110) and (200) reflections associated with the hexagonal symmetry of the SBA-15 structure [27]. These results indicate that the structure of the support remained intact after the functionalization.

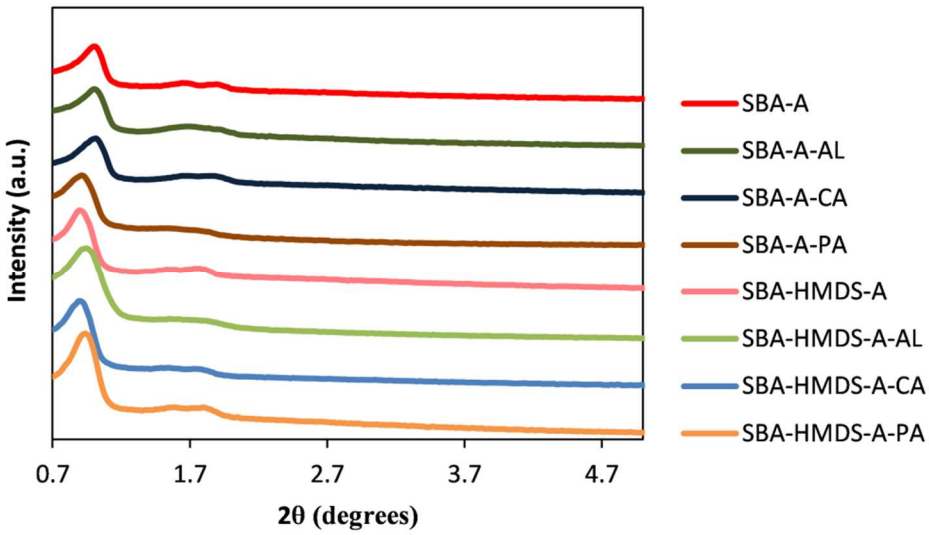

Figure 4-2: Small-angle XRD patterns

The presence of the desired functional groups on the final catalytic materials was qualitatively confirmed by CP-MAS ^{13}C NMR, as shown in Figure 4-3. All materials exhibit three peaks around **(a)** 9, **(b)** 20 and **(c)** 45 ppm, which can be attributed to the propyl chains and one peak at **(f)** 58 ppm, corresponding to the methoxy group [6, 28]. SBA-A also exhibits two peaks at **(d)** 51 and **(e)** 17 ppm, which can be attributed to the ethyl substituent [29]. SBA-A-AL exhibits two peaks at **(g)** 51 and **(h)** 60 ppm, which can be assigned to the ethanol substituent [29]. The carboxylic acid substituent of SBA-A-CA shows two characteristic peaks at **(i)** 49 and **(j)** 171 ppm [30]. Moreover, the FTIR spectrum of SBA-A-CA, shown in Figure 4-5, also exhibits a clear carbonyl peak at 1745 cm^{-1}, indicating the presence of the carboxylic acid. In the CP-MAS ^{13}C NMR spectrum, SBA-A-PA exhibits a peak at **(k)** 32 ppm corresponding to the carbon between the amine and the phosphoric acid [31, 32]. In CP-MAS ^{31}P NMR, shown in Figure 4-4, the phosphoric acid exhibits a peak at 9 ppm, while no peak is observed at 28 ppm, indicating that the deprotection of the acid site was successful [33, 34].

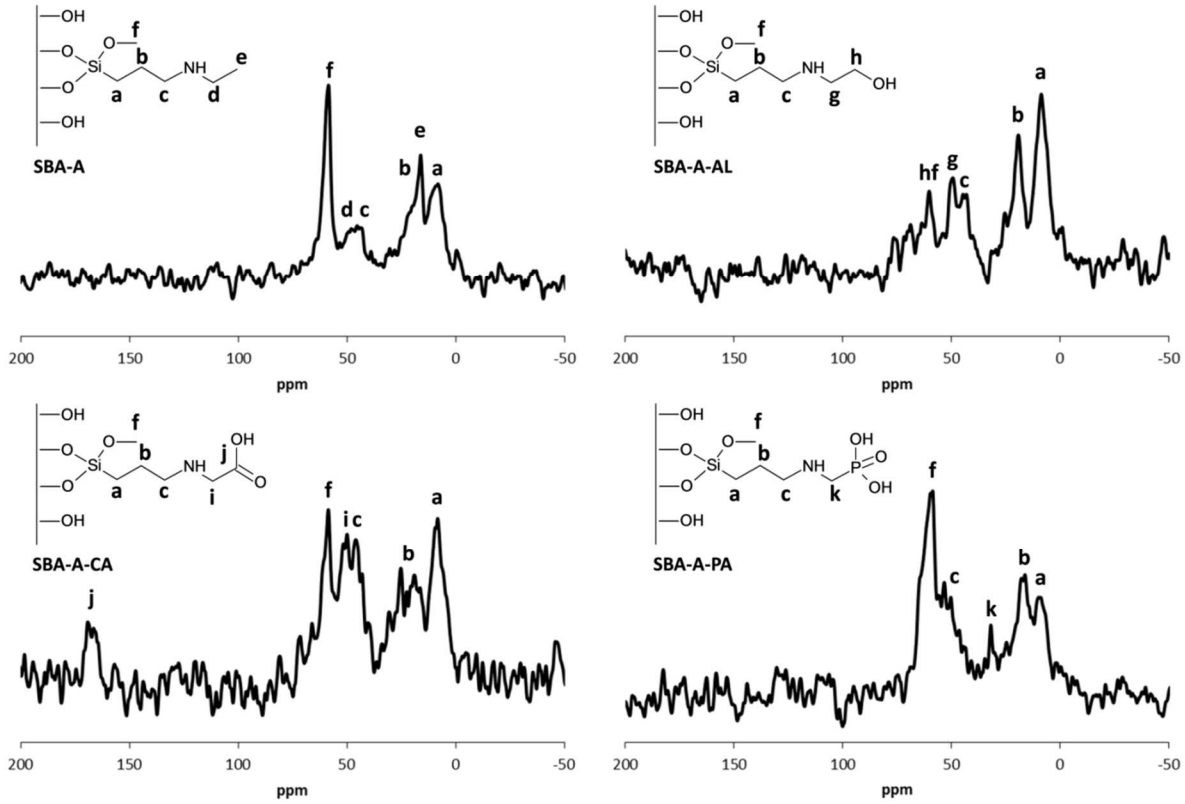

Figure 4-3: ^{13}C CP/MAS NMR spectra and assignment to chemical groups of SBA-A, SBA-A-AL, SBA-A-CA and SBA-A-PA

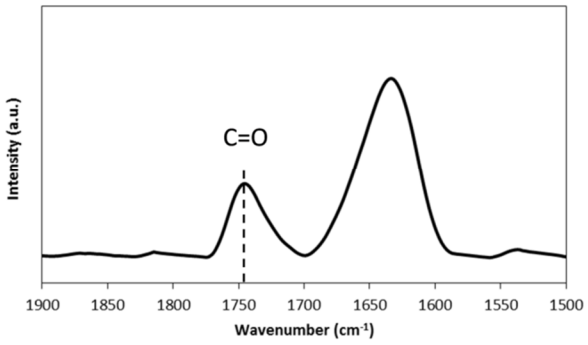

Figure 4-5: FTIR spectrum of SBA-A-CA showing a carbonyl peak at 1745 cm^{-1}

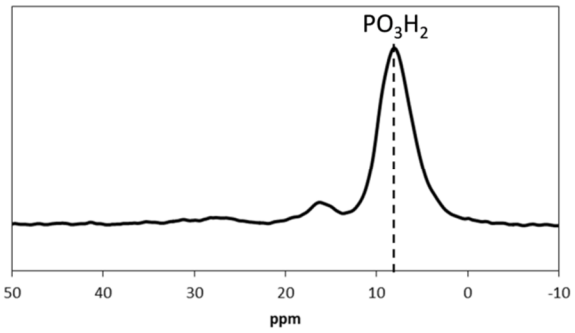

Figure 4-4: CP-MAS ^{31}P NMR spectrum of SBA-A-PA showing a phosphoric acid

The amine loadings were determined by means of nitrogen and iodine elemental analysis and are also reported in Table 4-1. No iodine was detected in the final materials, indicating that the replacement of the iodine with the desired functional groups was complete. The nitrogen content of the silanol containing materials corresponds to an amine site density ranging between 0.24 and 0.31 mmol/g. This corresponds to an average site density of 0.18

acid-base pairs per nm². As the iodosilane has the tendency to be grafted randomly on the silica surface, the low average site density indicates that the amines will most likely interact with the acid groups on the same linker and potentially also with surrounding silanols but not with the acid groups on a neighboring linker. The HMDS-treated materials have somewhat lower amine loadings than the silanol containing materials. This could be explained by ammonia formation the HMDS treatment, see Scheme 1-11. Ammonia is able to catalyze the removal of iodine leading to lower amine loadings. These lower amine loadings and the absence of nitrogen in sample SBA-HMDS-I indicate that there are no primary amines formed during the HMDS treatment. The iodine lost by this ammonia formed during the HMDS treatment, is most likely replaced by an inert trimethylsilyl group. Hence, no effect on the obtained turnover frequency (TOF) is expected by this undesired side reaction during the HMDS treatment. The SBA-A-AL_pr and SBA-HMDS-A-AL_pr samples contain respectively, 0.65 mmol N/g and 0.46 mmol N/g, which is about twice the amount of nitrogen as expected from the iodine loading of SBA-I and SBA-HMDS-I, indicating that DIPEA was hydrogen bonded to the alcohol group of the catalyst as shown in Scheme 4-1, or physisorbed on the catalyst surface. After consecutively treating these samples with HCl and ammonium hydroxide solutions, the samples SBA-A-AL and SBA-HMDS-A-AL contained the expected amounts of nitrogen, demonstrating that the excess nitrogen was effectively removed.

Table 4-1: Catalyst properties determined via nitrogen adsorption-desorption measurements and elemental analysis

Catalyst	BET surface area (m^2/g)	Average pore size (nm)	Total pore volume (cm^3/g)	Amine loading (mmol/g)
SBA-15 support	912	8.0	1.10	0.00
SBA-A	704	8.1	0.96	0.27
SBA-A-AL	644	8.1	0.96	0.31
SBA-A-CA	693	7.9	0.93	0.31
SBA-A-PA	662	7.6	0.89	0.24
SBA-HMDS-A	506	7.0	0.81	0.21
SBA-HMDS-A-AL	608	7.0	0.93	0.23
SBA-HMDS-A-CA	603	7.0	0.90	0.15
SBA-HMDS-A-PA	612	7.0	0.91	0.15

4.3.2 Catalytic performance evaluation and interpretation

4.3.2.1 Reference catalysts

No conversion was observed if unmodified SBA-15 or SBA-I, were used as catalysts. This means that neither pristine, nor a iodo-group are active in aldol condensation and the incorporation of other functional groups is necessary to catalyze the reaction. In Chapter 3 [5], the catalytic performance of different, commercially available amine-containing silanes, including (3-aminopropyl)triethoxysilane (APTES), N-methylaminopropyl-trimethoxysilane (MAPTMS), and N-cyclohexylaminopropyl-trimethoxysilane (CAPTMS), grafted upon Silicagel 60 was studied. These materials were respectively labeled Silicagel APTES, Silicagel MAPTMS and Silicagel CAPTMS. All TOFs were obtained in the low amine loading range, ensuring that the majority of amines has a silanol in the vicinity and, hence, is fully intermolecularly promoted. The catalytic activity of the reference catalyst in this chapter, SBA-A, was determined at the same operating conditions as used in the previous chapter. Although all four amines have very similar base strengths [5, 35], the materials exhibit significant

differences in catalytic activity for aldol condensation of acetone with 4-nitrobenzaldehyde, as shown in Figure 4-6. The primary amine-functionalized material Silicagel APTES exhibits a TOF of 7.80 x 10^{-4} ± 0.34 x 10^{-4} s^{-1}. The TOFs obtained with the materials that were functionalized with secondary amines depend on the substituent of the secondary amine. A cyclohexyl substituent (Silicagel CAPTMS) leads to a much lower TOF of 3.10 x 10^{-5} ± 0.14 x 10^{-5} s^{-1}. A secondary amine with an ethyl substituent (SBA-A) exhibits a TOF of 2.87 x 10^{-4} ± 0.13 x 10^{-4} s^{-1}, which is in the same order of magnitude as the TOF obtained with a primary amine. The highest TOF of 3.30 x 10^{-3} ± 0.15 x 10^{-3} s^{-1} is obtained using a secondary amine with a methyl substituent (Silicagel MAPTMS). The high activity of a secondary amine with a methyl substituent compared to that of a primary amine can be attributed to the ability of primary amines to form inhibiting imine species [3-5]. Primary amines are able to form two imines, one by reaction with 4-nitrobenzaldehyde [3-5] and one by reaction with acetone [5]. The formation of the former can be suppressed by using an acetone excess while the latter is in equilibrium with the reactive enamine intermediate. These species lower the concentrations of free active sites and reactive intermediates on the surface. As a result, a secondary amine active site that can yield the reactive enamine intermediate while simultaneously avoiding the formation of inhibiting imines can exhibit a higher catalytic activity. Moreover, the difference in activity between primary and secondary amines will be even much more pronounced when using equimolar amounts of both reactants. Changing the substituent of the secondary amine from a methyl group to a more bulky cyclohexyl group increases the steric hindrance and lowers the activity by two orders of magnitude. The TOF obtained with a secondary amine with an ethyl substituent is about one order of magnitude lower than the TOF obtained with a methyl-substituted secondary amine. These observations suggest that the previously observed steric hindrance matters even for relatively small substituents.

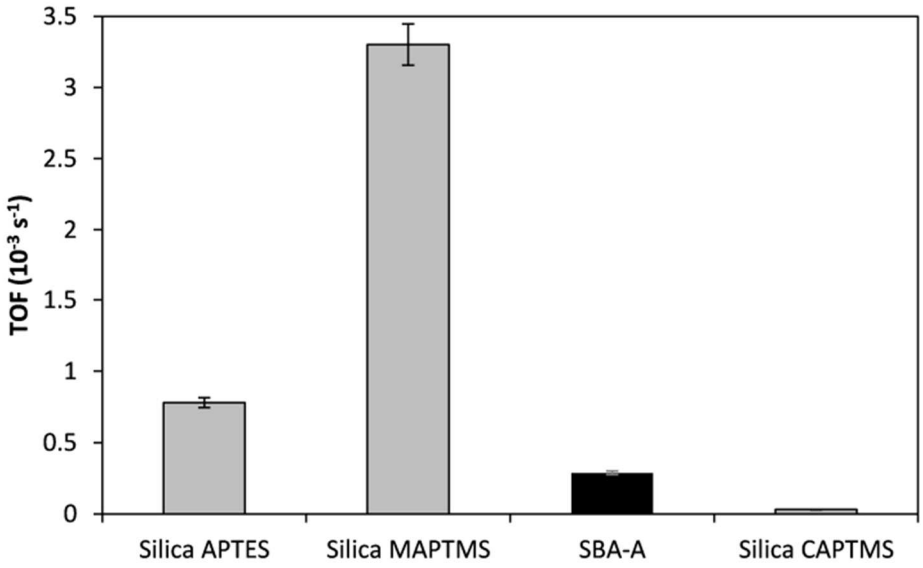

Figure 4-6: Comparison of the turnover frequency of SBA-A (black) with the turnover frequencies of (3-aminopropyl)triethoxysilane (APTES), N-methylaminopropyltrimethoxysilane (MAPTMS) and N-cyclohexylaminopropyltrimethoxysilane (CAPTMS) grafted on Silicagel 60 (grey) at 45 °C using 4 mol% of amines with respect to the concentration of 4-nitrobenzaldehyde [5].

4.3.2.2 Intramolecular acid strength effects and spatial arrangement

To investigate the intramolecular acid strength effects on the cooperativity, the newly synthesized materials were also assessed through aldol condensation experiments with 4-nitrobenzaldehyde and acetone as reactants. The black bars in Figure 4-7 correspond to the TOFs obtained using the silanol-containing materials. At the investigated operating conditions the reference catalyst (SBA-A) exhibits a TOF of $1.41 \times 10^{-4} \pm 0.06 \times 10^{-4}$ s^{-1}. Incorporating an intramolecular alcohol on the amine site increases the TOF to $1.91 \times 10^{-4} \pm 0.08 \times 10^{-4}$ s^{-1} (SBA-A-AL), indicating that, in this case, the active and promoting sites are in a more favorable conformation to catalyze the aldol condensation compared to a conformation in which only intermolecular surface silanols promote the activity of an amine site on a long carbon chain. However, changing the alcohol to a stronger acid site such as a carboxylic acid or a phosphoric acid decreases the TOF to $9.46 \times 10^{-5} \pm 0.42 \times 10^{-5}$ s^{-1} (SBA-A-CA) and $7.86 \times 10^{-5} \pm 0.35 \times 10^{-5}$ s^{-1} (SBA-A-PA), respectively, confirming that stronger acid sites have a negative impact on the activity of the amines [8-10]. These results suggest that the optimal promoting sites for the aldol condensation are H-bond donors, such as alcohols and silanols, and not strong acid sites.

The grey bars in Figure 4-7 correspond to the TOFs obtained using the HMDS treated materials, hence, exhibiting exclusively intramolecular cooperativity, if any. In this case, the reference secondary amine exhibits a TOF of 3.61 x 10^{-5} ± 0.16 x 10^{-5} s^{-1} (SBA-HMDS-A), which corresponds to a decrease in activity of a factor four. This decrease in activity is similar to the activity decrease observed with primary amines and other secondary amines when silanols were endcapped [5]. Endcapping these silanols while the amine is still in close proximity of an alcohol, a carboxylic acid, or a phosphoric acid results in TOFs of 1.25 x 10^{-4} ± 0.55 x 10^{-4} s^{-1} (SBA-HMDS-A-AL), 7.88 x 10^{-5} ± 0.35 x 10^{-5} s^{-1} (SBA-HMDS-A-CA) and 5.57 x 10^{-5} ± 0.25 x 10^{-5} s^{-1} (SBA-HMDS-A-PA), respectively. This corresponds to a more limited decrease in TOFs by a factor 1.2 to 1.5 maximum. In the absence of silanols, even the amines adjacent to a 'strong' acid site are more active than the unpromoted amines (SBA-HMDS-A), indicating that, indeed, also stronger acids exert a promoting effect on the activity of the amines, albeit less pronounced than silanols. Figure 4-7 also shows that in the absence of silanols, the secondary amine combined with an alcohol (SBA-HMDS-A-AL) exhibits a similar TOF as the secondary amine combined with surface silanols (SBA-A), indicating that an intramolecular, primary alcohol is as efficient as an intermolecular surface silanol as promoting site for the aldol condensation. The highest TOF is obtained when the secondary amine is combined with both an alcohol and surface silanols (SBA-A-AL). This observation can be attributed to the joint movement of the amine and promoting alcohol site when they are located on the same linker. Due to this concerted movement the amine and alcohol can bend together towards a neighboring silanol on the silica surface, resulting in two promoting sites in the vicinity of the same amine active site, *i.e.*, the intramolecular alcohol function and the intermolecular surface silanol. Subsequently, the two reactants can simultaneously be activated by the formation of a hydrogen bond instead of the consecutive activation when there is only a single promoting site in the vicinity of the amine and lead to an increase in catalytic activity. Figure 4-8 shows that, regardless the reactant concentration in the liquid phase, the probability that the necessary activated reactant is in proximity of the amine site increases with increasing number of promoting sites in vicinity of the amine. Moreover, both in the presence and absence of surface silanols, the materials that intramolecularly combine the amine with an alcohol exhibit the highest TOFs. The results obtained in this work suggest that a methyl-substituted secondary amine with one or more intramolecular alcohol functions on the β-carbons would be optimal for the aldol condensation of acetone with

4-nitrobenzaldehyde, provided that the inclusion of such intramolecular alcohol functions does not significantly increase steric hindrance.

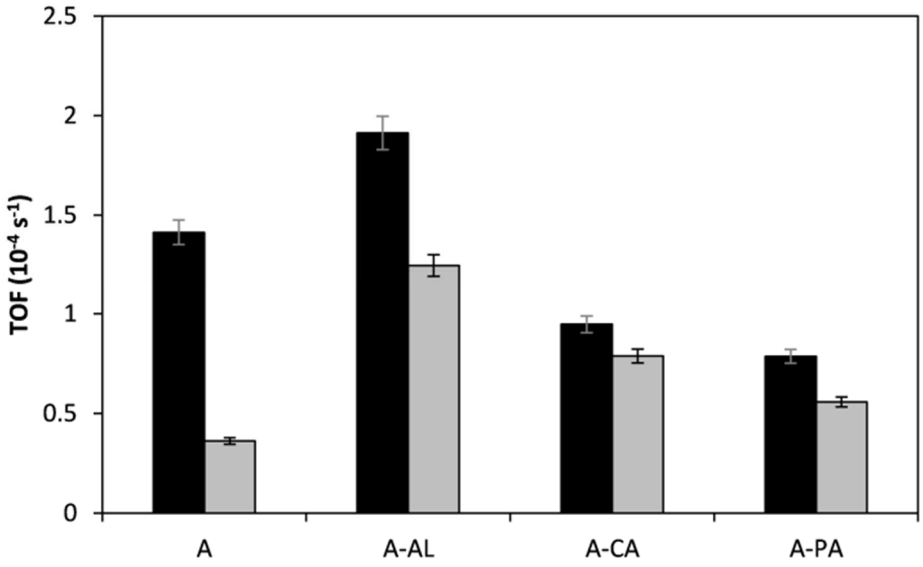

Figure 4-7: Turnover frequencies of the different catalysts at 45 °C using 15 mol% of amines with respect to the concentration of 4-nitrobenzaldehyde; black: catalysts without HMDS treatment combining intra- and intermolecular cooperativity (SBA-X), grey: catalysts treated with HMDS exhibiting exclusively intramolecular cooperativity (SBA-HMDS-X)

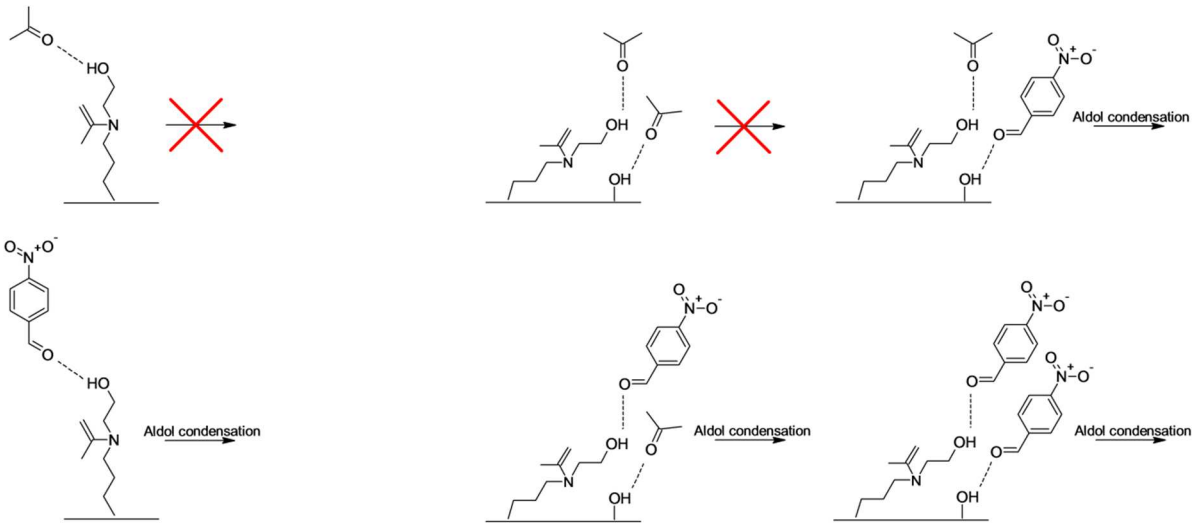

Figure 4-8: Comparison of the probability to activate 4-nitrobenzaldehyde in consecutive (left) and simultaneous (right) activation of the reactants

4.4 Conclusions

In this work, an SBA-15 support was successfully functionalized with a secondary amine and different acid groups, carefully positioned with respect to each other. Changing the

substituent of a secondary amine from a methyl to an ethyl group decreased the catalytic activity in aldol condensation. The activity of the secondary amine could be increased by incorporating an alcohol group close to the amine, showing the importance of the arrangement of the cooperative sites. However, incorporating stronger acids in the catalyst showed that intermolecular amine-silanol cooperativity or intramolecular amine-alcohol cooperativity outperforms the intramolecular amine-carboxylic acid or amine-phosphoric acid cooperativity. These results further support the notion that the optimal promoting sites for the aldol condensation are H-bond donors and not stronger acid sites [9]. After endcapping the silanols, the preserved intramolecular cooperativity of the catalysts consisting of an amine and an acid site on the same linker resulted only in a minor activity loss, while the activity of the reference acid-free secondary amine decreased by a factor of 4 due to the loss of all intermolecular activity. The insights obtained in this work suggest that a silica support functionalized with a methyl-substituted secondary amine with one or more alcohol functions on the β-carbons would be optimal aldol condensation catalysts, provided that the inclusion of additional alcohol functions does not significantly increase the steric hindrance.

4.5 References

1. Y. Kubota, K. Goto, S. Miyata, Y. Goto, Y. Fukushima, Y. Sugi, Chemistry Letters, **2003**, 32, 234-235
2. Y. Kubota, H. Yamaguchi, T. Yamada, S. Inagaki, Y. Sugi, T. Tatsumi, Top. Catal., **2010**, 53, 492-499
3. K. Kandel, S. M. Althaus, C. Peeraphatdit, T. Kobayashi, B. G. Trewyn, M. Pruski, I. I. Slowing, J. Catal., **2012**, 291, 63-68
4. K. Kandel, S. M. Althaus, C. Peeraphatdit, T. Kobayashi, B. G. Trewyn, M. Pruski, I. I. Slowing, ACS Catal., **2013**, 3, 265-271
5. J. Lauwaert, E. De Canck, D. Esquivel, P. Van der Voort, J. W. Thybaut, G. B. Marin, Catal Today, **2015**, 246, 35-45
6. J. Lauwaert, E. De Canck, D. Esquivel, J. W. Thybaut, P. Van Der Voort, G. B. Marin, ChemCatChem, **2014**, 6, 255-264
7. N. A. Brunelli, S. A. Didas, K. Venkatasubbaiah, C. W. Jones, J. Am. Chem. Soc., **2012**, 134, 13950-13953

8. N. A. Brunelli, C. W. Jones, J. Catal., **2013**, 308, 60-72
9. N. A. Brunelli, K. Venkatasubbaiah, C. W. Jones, Chem Mater, **2012**, 24, 2433-2442
10. R. K. Zeidan, M. E. Davis, J. Catal., **2007**, 247, 379-382
11. R. K. Zeidan, S. J. Hwang, M. E. Davis, Angew. Chem.-Int. Edit., **2006**, 45, 6332-6335
12. J. A. Ma, D. Cahard, Angew. Chem.-Int. Edit., **2004**, 43, 4566-4583
13. J. D. Bass, A. Solovyov, A. J. Pascall, A. Katz, J. Am. Chem. Soc., **2006**, 128, 3737-3747
14. P. Van Der Voort, E. F. Vansant, J. Liq. Chromatogr. Relat. Technol., **1996**, 19, 2723-2752
15. J. C. Hicks, C. W. Jones, Langmuir, **2006**, 22, 2676-2681
16. J. C. Hicks, R. Dabestani, A. C. Buchanan, C. W. Jones, Chem Mater, **2006**, 18, 5022-5032
17. M. W. McKittrick, C. W. Jones, Chem Mater, **2003**, 15, 1132-1139
18. L. D. White, C. P. Tripp, J Colloid Interf Sci, **2000**, 227, 237-243
19. S. A. Kanan, W. T. Y. Tze, C. P. Tripp, Langmuir, **2002**, 18, 6623-6627
20. E. L. Margelefsky, *Cooperative Catalysis by Bifunctionalized Mesoporous Silica*, 2008, California Institute of Technology.
21. B. List, R. A. Lerner, C. F. Barbas, J. Am. Chem. Soc., **2000**, 122, 2395-2396
22. F. Tanaka, R. Thayumanavan, N. Mase, C. F. Barbas, Tetrahedron Lett., **2004**, 45, 325-328
23. Z. An, Y. Guo, L. W. Zhao, Z. Li, J. He, ACS Catal., **2014**, 4, 2566-2576
24. P. D. de Maria, P. Bracco, L. F. Castelhano, G. Bargeman, ACS Catal., **2011**, 1, 70-75
25. W. W. Lukens, P. Schmidt-Winkel, D. Y. Zhao, J. L. Feng, G. D. Stucky, Langmuir, **1999**, 15, 5403-5409
26. G. F. Froment, K. B. Bischoff, *Chemical reactor analysis and design*, Wiley series in chemical engineering, Wiley, New York, **1990**, xxxiv, 664 p.
27. D. Y. Zhao, J. L. Feng, Q. S. Huo, N. Melosh, G. H. Fredrickson, B. F. Chmelka, G. D. Stucky, Science, **1998**, 279, 548-552
28. S. Radi, S. Tighadouini, Y. Toubi, M. Bacquet, Journal of hazardous materials, **2011**, 185, 494-501
29. J. E. Sarneski, H. L. Surprenant, F. K. Molen, C. N. Reilley, Analytical Chemistry, **1975**, 47, 2116-2124

30. C. Ye, R. Fu, J. Hu, L. Hou, S. Ding, Magnetic Resonance in Chemistry, **1993**, 31, 699-704
31. F. K. Kalman, M. Woods, P. Caravan, P. Jurek, M. Spiller, G. Tircso, R. Kiraly, E. Brucher, A. D. Sherry, Inorganic Chemistry, **2007**, 46, 5260-5270
32. Z. Glowacki, M. Topolski, Magnetic Resonance in Chemistry, **1989**, 27, 897-899
33. M. L. Rueppel, J. T. Marvel, Organic Magnetic Resonance, **1976**, 8, 19-20
34. Z. Glowacki, M. Hoffmann, M. Topolski, J. Rachon, Phosphorus Sulfur and Silicon and the Related Elements, **1991**, 60, 67-71
35. J. J. Christensen, R. M. Izatt, D. P. Wrathall, L. D. Hansen, Journal of the Chemical Society a -Inorganic Physical Theoretical, **1969**, 1212-1223

Chapter 5

From Model Reaction to Practical Application: Feedstock and Catalyst Support Effects

The aldol condensation of furfural with acetone is investigated in the present chapter as a societally more relevant reaction compared to the conventionally used model reaction for aldol condensation, *i.e.*, 4-nitrobenzaldehyde and acetone that was employed in the preceding chapters. More particularly, the effects of water in the reaction mixture and the hydrophobicity of the catalyst support have been focused on. In contrast to 4-nitrobenzaldehyde, furfural does not contain an electron withdrawing group such as the nitro function, which makes the partial, negative charge on its carbonyl group less pronounced. As a result, furfural is less susceptible for nucleophilic reactions. Therefore, relatively high temperatures, *i.e.*, exceeding the boiling point of acetone, are necessary to obtain measurable reaction rates and the aldol product dehydration becomes more prevalent such that the main observed reaction product is the α,β-unsaturated ketone. An apparent activation energy amounting to 106 kJ/mol was derived from the kinetic data. It also appears that the absence of an electron withdrawing group on furfural, gives rise to a predominance of furfural bounded to the silanols. As a result, acetone is unable to reach the silanols and the enamine formation from acetone has to occur directly, rather than going via

the promoted route. This hypothesis is in agreement with the decreasing TOF observed with increasing furfural concentration, which is in strong contrast with the increasing 4-nitrobenzaldehyde concentration leading to an increased TOF. Adding 2 vol% water to the furfural-acetone mixture resulted in a drastic decrease of the catalytic activity of a 'hydrophilic' catalyst such as silicagel. Hydrophobicity can be tuned by synthesizing organosilica materials making use of different organic bridges. Preliminary experiments confirm that physical adsorption effects determine the observed aldol condensation kinetics.

5.1 Introduction

The depletion of world petroleum reserves and increased environmental concern have stimulated recent interest in alternative sources for typical petroleum derivates or, at least, products with similar properties. Lignocellulosic biomass constitutes such an interesting renewable resource which can be converted to liquid hydrocarbon fuels via furanic intermediates [1]. *E.g.*, furfural can be obtained by dehydration of C_5 sugars such as xylose and, subsequently, converted into heavier components by means of aldol condensations, see Figure 1-2 [1-4]. After oxygen removal from the condensation product liquid hydrocarbon fuels obtained [1].

It is important to note that starting from lignocellulosic biomass, the sugars and, subsequently, furfural are produced in an aqueous phase. Complete separation of furfural and water would most probably not be cost effective and, hence, the presence of water should be taken into account in the design of novel aldol condensation catalysts. It is known that water has a negative effect on the catalytic activity of hydrophilic acid-base cooperative silica materials due to a pronounced shift in the equilibrium from the free acid and free base towards the resulting neutralized ion pair [5]. As a result, the free electron pair of the amine, necessary for the catalytic aldol condensation cycle, is no longer available for reaction. However, the hydrophobicity of the support can be manipulated by incorporating organic components into the pore walls [6]. The resulting, enhanced hydrophobicity is expected to impact on these acid-base equilibria such that the aldol condensation catalysis can be preserved.

Recently, the catalytic activity of functionalized periodic mesoporous organosilicas (PMOs) has been assessed using the aldol condensation of 4-nitrobenzaldehyde with acetone with *n*-

hexane as solvent as model reaction, see Figure 5-1 [7]. No cooperativity between primary amines and surface silanols is observed if an ethene-PMO is functionalized with cysteamine [7]. This could be due to the short linker length of cysteamine [8]. A carboxylic acid site can be incorporated close to the primary amine, *i.e.*, on a single 'linker', by functionalizing the ethene-PMO with cysteine [7]. This carboxylic acid has a promoting effect on the activity of amines, albeit less pronounced than that of the surface silanols [9-11]. The study also shows that at high active site densities the activity of the catalyst decreases [7]. This is most likely because at high densities, the intermolecular interactions between two cysteine groups result in a protonation of the amine function by the carboxylic acid located on a different cysteine.

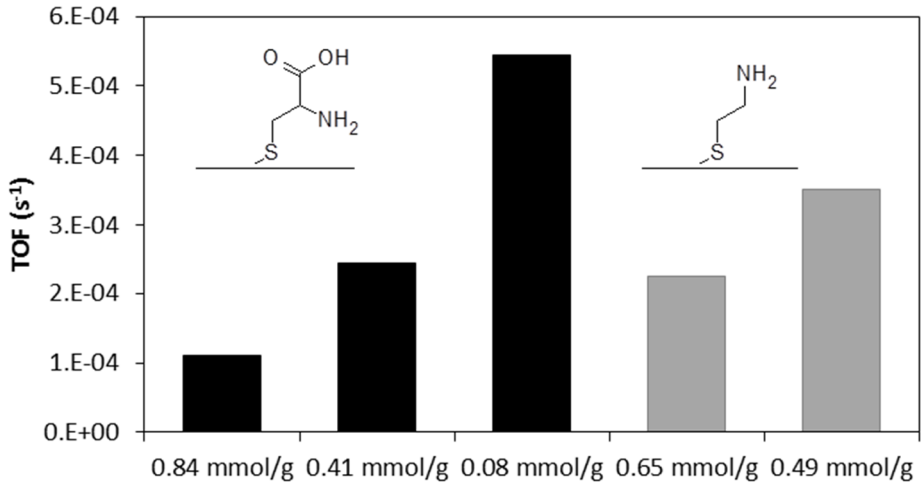

Figure 5-1. Turnover frequencies in the aldol condensation of 4-nitrobenzaldehyde with acetone at 45°C using 4 mol% of amines with respect to the concentration of 4-nitrobenzaldehyde as a function of the site density obtained with cysteine functionalized ethene-PMOs (black) and cysteamine functionalized ethene-PMOs (grey) [7]

In this chapter, the aldol condensation of furfural with acetone is investigated using a traditional silica support functionalized with a methyl substituted secondary amine. Additionally, the effect of water and the hydrophobicity of the catalyst support is investigated. Two organosilicas are functionalized with a low amount of cysteine in order to avoid the unwanted intermolecular interactions between different cysteine groups. Subsequently, the catalytic performance of the materials are assessed in the aldol condensation of 4-nitrobenzaldehyde with acetone using *n*-hexane and water as solvents.

5.2 Procedures

5.2.1 Catalyst preparation and characterization

Silica MAPTMS is synthesized by grafting N-methylaminopropyltrimethoxysilane (MAPTMS, ABCR) on Silicagel 60 (Grade 7734, Sigma-Aldrich) using the synthesis procedures described in section 2.2.1.

Two hydrophobic organosilica materials are synthesized, *i.e.*, one consisting of 1,2-bis(triethoxysilyl)ethane (BTEE, 97%, ABCR) and one consisting of 1,4-bis(triethoxysilyl)benzene (BTEB, 95%, ABCR). A small amount of vinyltriethoxysilane (VTES, 98% ABCR) is added to both materials in order to be able to functionalize them with cysteine such that a site density of about 0.06 mmol/g is obtained. The silane composition used in the synthesis is shown in Table 5-1. The organosilica materials are synthesized according to the recipe shown in Figure 5-2. About 3 g Brij S10 ($C_{18}H_{37}(OCH_2CH_2)_nOH$, n∼10, Sigma-Aldrich) is dissolved in a mixture of 138 mL distilled water and 10 mL of 12.1 M hydrochloric acid (HCl, ACS grade reagent, Sigma-Aldrich). The mixture is stirred for 4 h at 50 °C in order to form micelles. Afterwards, $2.5x10^{-2}$ mol of Si atoms in the form of the (organo)silanes is added and the mixture is stirred at 50 °C for 24 h. Subsequently, the magnetic stir bar is removed and the mixture was heated to 90 °C for 24 h. The resulting solid is separated from the mixture by filtration and is subsequently washed three times by stirring at 80 °C for 24 h in a 98 vol% ethanol (96%, Fiers)– 2 vol% HCl mixture. The material is dried overnight at 100 °C under reduced pressure. Afterwards, 2 g L-cysteine (99+%, Acros) and 1g of 2-hydroxy-4'-(2-hydroxyethoxy)-2-methylpropiophenone (98%, Sigma-Aldrich) is dissolved in 50 ml of distilled water, 1 g of the solid material is added and the mixture is stirred for 24 h in a UV reactor. The material is recovered by filtration and subsequently washed four or five times by stirring at 85°C for 3 h. Finally, the material is dried under reduced pressure with heating to 100 °C.

Table 5-1. Silane composition used in the synthesis of the organosilica materials

Catalyst	Mole fraction BTEE (%)	Mole fraction BTEB (%)	Mole fraction VTES (%)
BTEE	97	0	3
BTEB	0	90	10

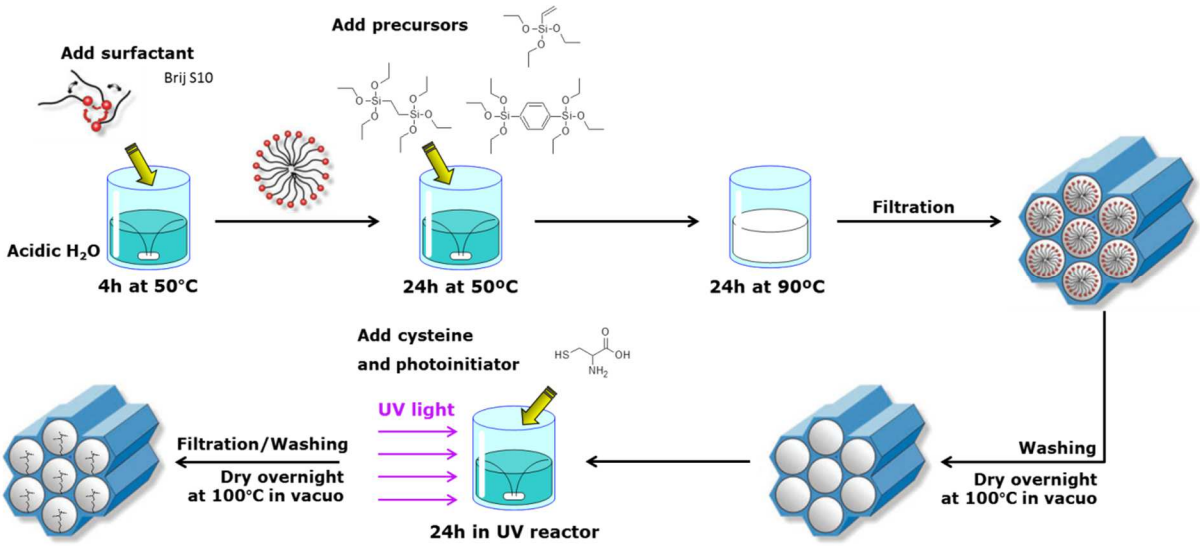

Figure 5-2. Representation of the catalyst synthesis procedure

The materials were characterized by means of nitrogen adsorption-desorption measurments, elemental (CHNS) analysis and Diffuse Reflectance Infrared Fourier Transform (DRIFT) spectroscopy according to the procedures described in section 2.2.2 and by means of X-ray diffraction (XRD) according to the procedure described in section 4.2.5.

5.2.2 Aldol condensation kinetics

The aldol condensation of furfural with acetone, see Scheme 5-1, is investigated using Silica MAPTMS as a catalyst. The range of experimental conditions used in this study is shown in Table 5-2. At these conditions, secondary reactions leading to low concentrations of components such as 1,4-pentandien-3-on-1,5-di-2-furanyl, come into play. The temperature effect is investigated using furfural and acetone concentrations amounting to 0.04 mol/l and 12 mol/l respectively. The experiments are performed in a Parr 4560 mini reactor as described in section 2.2.4. The reactor is first loaded with the catalyst and the reaction mixture, *i.e.,* furfural, acetone and toluene (internal standard). Then, the mixture is heated to the reaction temperature. The heating phase takes up to 10 minutes. The concentrations of products formed during this heating period do not significantly exceed the noise level and,

hence, it can be concluded that the heating phase has a negligible effect on the obtained turnover frequency (TOF), see section 2.2.4. A fraction of the acetone evaporates during this heating phase which leads to a pressure increase in the reactor. Vapor-liquid equilibrium calculations, see section 5.2.3, show that an acetone excess of about 1 to 2 percent is necessary to obtain the desired liquid phase concentrations. In the current configuration of the set-up, the increased pressure is used during sampling to push a liquid sample out of the reactor. Because the sample flashes during the sampling procedure a fraction of the acetone is lost. Hence, the acetone concentration cannot be determined correctly. The samples taken during these experiments are analyzed using a FID-equipped gas chromatograph (6850 Series II, Agilent Technologies), loaded with a non-polar capillary column (HP-PONA, 50 m x 200 µm x 0.5 µm polydimethylsiloxane).

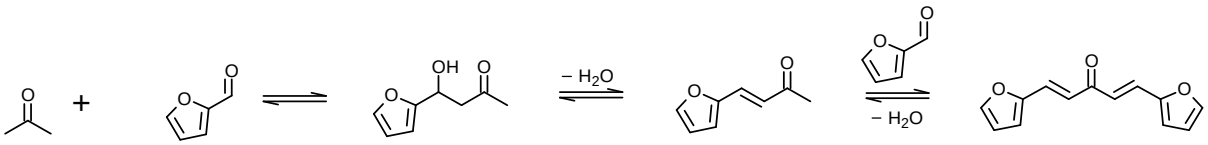

Scheme 5-1. Aldol condensation of acetone and furfural

Table 5-2. Range of experimental conditions

Variable	Range
Amine groups	1 mmol/L
Silanol-to-amine ratio	3.89
Furfural	0.04 – 1.4 mol/L
Acetone	10.9 – 12.8 mol/L
Toluene	57 – 75 mmol/L
Water	0 – 4.6 mol/L
Temperature	60 – 100 °C

The activity of the organosilica materials are assessed via the aldol condensation of acetone (99.6%, Acros) and 4-nitrobenzaldehyde (99 %, Acros). The experiments are performed in a 25 mL two-neck round-bottom flask equipped with a condenser and a septum. First, the supported catalyst is added to the flask so that the desired amount of amines is present, *i.e.,* 4 mol% with respect to the 4-nitrobenzaldehyde concentration. The reaction mixture is prepared separately by mixing the desired amounts of acetone (50 vol%),

4-nitrobenzaldehyde (0.03 mmol/mL), methyl 4-nitrobenzoate (internal standard, 0.022 mmol/mL, >99 %, Aldrich) and the relevant solvents, *i.e. n*-hexane (40 or 50 vol%, Extra Pure, Acros) and distilled water (none or 2 vol%). Afterwards, 5 mL of the reaction mixture is injected into the flask which contains the catalyst and the flask is immediately placed in an oil bath at 45 °C. The moment the flask is placed in the oil bath is taken as the start of the reaction. The reaction is monitored for 5 h by taking samples (about 50 µL) of the reaction mixture. Approximately 0.5 mL of acetone is used to wash the syringe needle and to transfer the sample to a vial. Subsequently, the catalyst is separated from the sample by means of centrifugation. Finally, the samples are analyzed using a reversed-phase high-performance liquid chromatograph as described in section 2.2.4.

5.2.3 Determination of the vapor-liquid equilibrium and thermodynamic non-ideality

As explained above, furfural is less susceptible to nucleophilic reactions such as aldol condensations and, hence, relatively high reaction temperatures, *i.e.*, exceeding the boiling point of acetone, are necessary in order to obtain measurable reaction rates. Correspondingly a non-negligible amount of acetone is vaporized, which has to be accounted for in the assessment of the acquired data.

A vapor liquid equilibrium is established in a mixture when the chemical potential of each component i in the liquid phase is equal to the chemical potential of that component in the vapour phase. If the chemical potentials of all components are expressed with respect to the ideal gas phase, the condition expressing the establishment of equilibrium reduces to an equality of fugacities such as in eq. 1. Using the definitions of vapor and liquid phase fugacities, the ratio of each component in vapor and liquid phase can be obtained from eq. 2. The saturation pressures in eq. 2 are determined using the Antoine equation [12]. The liquid-vapor ratios, K_i, combined with the molar balances in eq. 3 and the trivial conditions in equations 4 and 5, results in a set of equations which has to be solved to the unknown x_i, y_i, n_L and n_G.

$$f_i^L = f_i^G \tag{1}$$

$$K_i = \frac{y_i}{x_i} = \frac{\gamma_i \Phi_i^S P_i^S \exp\left(\frac{V_i^L\left(P - P_i^S\right)}{RT}\right)}{\Phi_i P} \tag{2}$$

$$n_i = n_L x_i + n_G y_i \quad (3)$$

$$X = \sum_i x_i - 1 = 0 \quad (4)$$

$$Y = \sum_i y_i - 1 = 0 \quad (5)$$

In order to solve this set of equations, the thermodynamic non-ideality of both phases has to be calculated. The Non-Random Two-Liquid (NRTL) method [13] and the Universal Quasichemical (UNIQUAC) method [14] together with its extension, *i.e.*, the UNIQUAC Functional-group Activity Coefficients (UNIFAC) method [15] are widely accepted methods to calculate activity coefficients, γ_i, and other thermodynamic data of compounds in liquid multi-component mixtures without explicit use of experimental data [12]. These methods make use of binary interaction parameters to describe the interactions between two molecules or two functional groups in the mixture. Equations of state such as, the Soave modification of Redlich-Kwong (SRK) [16], Peng-Robinson (PR) [17] or Hayden-O'Connell (HOC) [18] are used to calculate the fugacity coefficient, Φ_i, of a gas phase. Because of the availability of binary interaction parameters and the good performance of the NRTL-HOC model to describe polar components at low pressures, this model is chosen in this chapter to describe the thermodynamically non-ideality of the system is described, see appendix B.

5.3 Results and discussion

5.3.1 Catalyst characterization

The specific BET surface areas, average pore sizes, and total pore volumes of the unfunctionalized materials were determined from the nitrogen adsorption-desorption isotherms and are listed in Table 5-3. The BET surface areas of the organosilicas are approximately 950 m²/g, which is much higher than that of silicagel 60. However, the average pore size of silicagel 60 is larger than those of the organosilicas, *i.e.*, 5.60 nm versus 3 to 3.7 nm. The total pore volumes all range between 0.7 and 0.95 cm³/g.

Table 5-3. Catalyst properties determined via nitrogen adsorption-desorption measurements

Catalyst	BET surface area (m^2/g)	Average pore size (nm)	Total pore volume (cm^3/g)
Silicagel 60	497	5.60	0.69
BTEE	928	3.68	0.94
BTEB	971	3.04	0.70

The small-angle XRD patterns of the organosilica materials, exhibit three peaks that can be attributed to the (100), (110) and (200) reflections associated with the hexagonal symmetry similar to the structure of SBA-15 [19]. Silicagel 60 is amorphous and does not exhibit any XRD peaks. Silica MAPTMS contains 0.148 mmol/g amines and a silanol-to-amine ratio of 3.9, while BTEE and BTEB have a cysteine site density of 0.064 and 0.069, respectively.

5.3.2 Feedstock effects in the aldol condensation

5.3.2.1 Furfural versus 4-nitrobenzaldehyde

In accordance with Arrhenius law, the reaction rate and, correspondingly, the turnover frequency increases with increasing temperature. The apparent rate coefficient is determined from eq. 6. At the reaction conditions used, a_{ace}, independently from the temperature, amounts to 0.99, while a_{fur} decreases from 1.0×10^{-2} at 60 °C to 4.1×10^{-3} at 100 °C. This leads to the Arrhenius diagram shown in Figure 5-2 from which an apparent activation energy amounting to 106 kJ/mol is derived.

$$TOF = k a_{ace} a_{fur} \tag{6}$$

Because of the high temperatures required for the aldol condensation with furfural to occur, the aldol product dehydration is more pronounced compared to aldol condensation with 4-nitrobenzaldehyde and the corresponding ketone selectivity amounts to 90%, approximately. Additionally, also low concentrations of difuranyl components, such as 1,4-pentandien-3-on-1,5-di-2-furanyl, see Scheme 5-1, are observed.

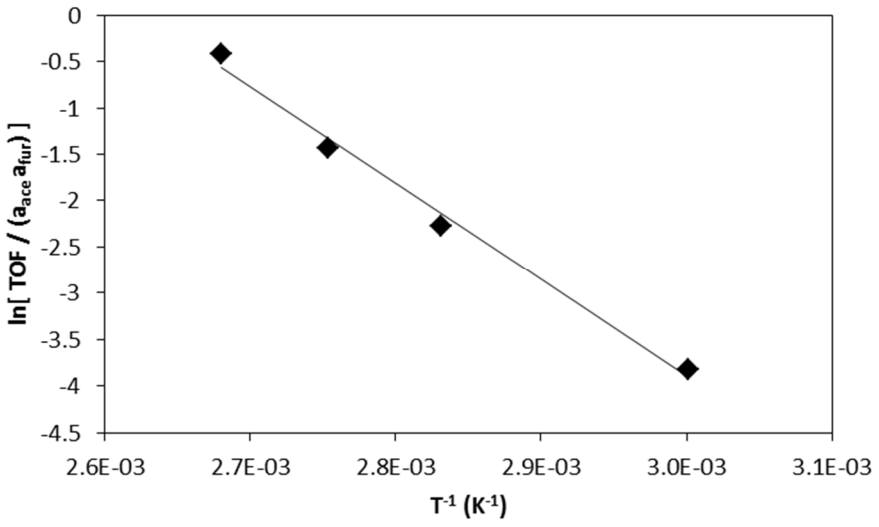

Figure 5-3. Arrhenius diagram of the data obtained with silicagel MAPTMS type AB

An increase of the initial molar furfural-to-acetone ratio from $4.0x10^{-3}$ to $1.2x10^{-1}$ results in a decrease of the turnover frequency from $1.26x10^{-3}$ s^{-1} to $8.4x10^{-4}$ s^{-1}, *i.e.*, a decrease of about 34%. The increased furfural concentration results in a corresponding increase of its thermodynamic activity by 30% while that of acetone decreases by 10%. Figure 5-4 demonstrates that the decrease in TOF indicates that the apparent rate coefficient decreases with increasing furfural-to-acetone ratio. This indicates that the apparent rate coefficient contains an important adsorption contribution. As a result, higher furfural concentration exert an inhibiting effect, in the investigated range of operating conditions. Similar experiments performed at 45°C using 4-nitrobenzaldehyde and acetone as reactants exhibited an increase in TOF from $2.05x10^{-3}$ s^{-1} at a molar 4-nitrobenzaldehyde-to-acetone ratio of $4.0x10^{-3}$ to $5.91x10^{-3}$ s^{-1} at a ratio of $5.4x10^{-2}$. Assuming that, despite the significantly different temperature, similar phenomena are involved the hydrogen bond formation is much more pronounced in the case of furfural than in the case of 4-nitrobenzaldehyde. Figure 5-4 also shows that the inhibition phenomena are not observed when using the unpromoted base version of the silicagel MAPTMS catalyst (type B). Moreover, as secondary amines are unable to form inhibiting imine species, see Chapter 3, the observed inhibition cannot be caused by interactions of furfural with the amine active site. This suggests that the inhibition is originating from a strong hydrogen bond formation between furfural and the promoting silanol causing a predominance of furfural bounded to the silanols. As a result, at high furfural concentrations the silanols are unable to promote the enamine formation of acetone and the turnover frequency decreases. The carbonyl group in 4-nitrobenzaldehyde is less susceptible to hydrogen bond formation due to presence of the electron withdrawing nitro-group. Therefore, an increase of 4-nitrobenzaldehyde concentration leads to an increase in 4-nitrobenzaldehyde bounded to the silanols without significantly affecting the concentration of hydrogen bounded acetone and, subsequently, an increase of turnover frequency.

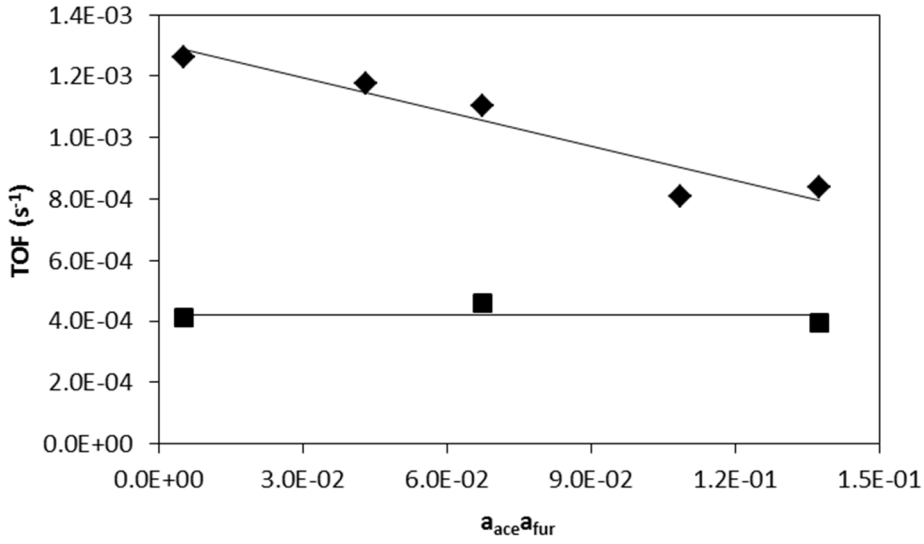

Figure 5-4. Turnover frequency in the aldol condensation of acetone with furfural obtained at a temperature of 90°C as a function of the product of thermodynamic activities of acetone and furfural; ◆ cooperative acid-base catalyst (silicagel MAPTMS type AB); ■ HMDS-treated catalyst (silicagel MAPTMS type B); the lines are intended as visual aids only

5.3.2.2 Effect of water addition

Adding 2 vol% water to the furfural-acetone mixture drastically decreases the catalytic activity, resulting in a TOF which amounts to only 29% of the TOF obtained in the absence of water, *i.e.*, 3.70×10^{-4} s^{-1} versus 1.26×10^{-3} s^{-1}. This can be attributed to poisoning of the amine group by water after which it is no longer available for reaction with the reactants. In the framework of the conversion of lignocellulosic biomass inhibiting effects by water should be avoided, which can be pursued by tuning the properties of the support, see also the next section.

5.3.3 Effect catalyst support

Two organosilicas, *i.e.*, BTEE and BTEB, have been used to investigate variations in support hydrophobicity in the aldol condensation of 4-nitrobenzaldehyde and acetone. The former support contains ethane bridges in the support leading to an increased hydrophobicity compared to the traditional silicagel while the latter introduces an aromatic character into the support by means of benzene bridges. BTEE exhibits a TOF of 1.92×10^{-4} s^{-1} while BTEB exhibits a TOF of 1.83×10^{-5} s^{-1}, which is about an order of magnitude lower. The low activity of the benzene containing support, *i.e.*, BTEB could be attributed to a strong physisorption of 4-nitrobenzaldehyde in the pore structure originating from the like-likes-like principle [20,

21]. This strong physisorption could result in a decrease in acetone concentration in the pores and, subsequently, in the TOF for aldol condensation.

In the remainder of this investigation, other organosilica materials combining BTEE or BTEB with tetraethyl orthosilicate (TEOS) will be investigated to further tune the hydrophobicity of the material. These materials will also be assessed via the traditional aldol condensation of 4-nitrobenzaldehyde and acetone and, subsequently via the same aldol condensation in an aqueous environment. Due to its high silanol content, it is expected that in the absence of water, a hydrophilic material consisting solely of TEOS, will exhibit the highest TOF. However, in the presence of water, it is expected that the TEOS-BTEE mixtures will exhibit the highest TOF for a certain TEOS-to-BTEE ratio. Due to strong physisorption of 4-nitrobenzaldehyde on the benzene support it is expected that the materials combining TEOS with BTEB will not exhibit high TOFs.

5.4 Conclusions

Due to the absence of an electron withdrawing group such as the nitro function, temperatures exceeding the boiling point of acetone, *i.e.*, 56°C, are necessary to obtain measurable aldol condensation rates with furfural. These higher temperatures also result in more pronounced aldol product dehydration such that the main observed reaction product is the α,β-unsaturated ketone. Additionally, secondary reactions come into play leading to low concentrations of difuranyl components, such as 1,4-pentandien-3-on-1,5-di-2-furanyl. An apparent activation energy amounting to 106 kJ/mol was obtained from the kinetic data. It was also suggested that the absence of an electron withdrawing group on furfural, gives rise to a predominance of furfural bounded to the silanols. As a result, acetone is unable to reach these silanols and enamine formation from acetone has to occur directly rather than via the promoted route, in strong contrast with what was observed for 4-nitrobenzaldehyde. Adding 2 vol% of water to the reaction mixture decreases the catalytic activity to only 29% of the TOF obtained in the absence of water. Support properties critically impact on reactant physical adsorption and, hence, on the observed aldol condensation kinetics. An organosilica with benzene bridges in its structure functionalized with cysteine exhibits a TOF which is an order of magnitude lower than that exhibited by an organosilica with ethane bridges and the same functional group. In the presence of water the enhanced hydrophobicity of the

organosilicas is expected to impact on these acid-base equilibria such that the aldol condensation catalysis can be preserved.

5.5 References

1. J. C. Serrano-Ruiz, J. A. Dumesic, Energy Environ. Sci., **2011**, 4, 83-99
2. K. J. Zeitsch, *The chemistry and technology of furfural and its many by-products*, Sugar series, Elsevier, Amsterdam ; New York, **2000**, xv, 358 p.
3. C. Moreau, M. N. Belgacem, A. Gandini, Top. Catal., **2004**, 27, 11-30
4. J. N. Chheda, G. W. Huber, J. A. Dumesic, Angew. Chem.-Int. Edit., **2007**, 46, 7164-7183
5. R. K. Zeidan, S. J. Hwang, M. E. Davis, Angew. Chem.-Int. Edit., **2006**, 45, 6332-6335
6. Z. An, Y. Guo, L. W. Zhao, Z. Li, J. He, ACS Catal., **2014**, 4, 2566-2576
7. J. Ouwehand, *Internal discussions*, 2015.
8. N. A. Brunelli, S. A. Didas, K. Venkatasubbaiah, C. W. Jones, J. Am. Chem. Soc., **2012**, 134, 13950-13953
9. N. A. Brunelli, K. Venkatasubbaiah, C. W. Jones, Chem Mater, **2012**, 24, 2433-2442
10. N. A. Brunelli, C. W. Jones, J. Catal., **2013**, 308, 60-72
11. J. Lauwaert, E. G. Moschetta, P. Van der Voort, J. W. Thybaut, C. W. Jones, G. B. Marin, J. Catal., **2015**, 325, 19-25
12. B. E. Poling, J. M. Prausnitz, J. P. O'Connell, *The properties of gases and liquids*, McGraw-Hill, New York, **2001**
13. H. Renon, Prausnit.Jm, Aiche J., **1968**, 14, 135-&
14. D. S. Abrams, J. M. Prausnitz, Aiche J., **1975**, 21, 116-128
15. A. Fredenslund, R. L. Jones, J. M. Prausnitz, Aiche J., **1975**, 21, 1086-1099
16. G. Soave, Chem. Eng. Sci., **1972**, 27, 1197-&
17. D. Peng, D. B. Robinson, Industrial & Engineering Chemistry Fundamentals, **1976**, 15, 59-64
18. J. G. Hayden, J. P. Oconnell, Industrial & Engineering Chemistry Process Design and Development, **1975**, 14, 209-216
19. D. Y. Zhao, J. L. Feng, Q. S. Huo, N. Melosh, G. H. Fredrickson, B. F. Chmelka, G. D. Stucky, Science, **1998**, 279, 548-552

20. R. P. Feynman, R. Leighton, M. Sands, *The Feynman Lectures on Physics*, Addison-Wesley, Reading, MA, USA, **1970**, 1552

21. K. L. Williamson, K. M. Masters, *Macroscale and Microscale Organic Experiments*, (Eds.: S. Kiselica), Hartford, C., Bemont, CA, USA, **2011**, 802

Chapter 6

Conclusions and Future Work

Aldol condensations constitute an interesting route for new C-C bond creation, yielding larger and more complex molecules. It is widely used in the pharmaceutical industry as well as for the preparation of fine chemicals, perfumes and synthetic flavors. Furthermore, aldol condensation provides promising perspectives with respect to the transition from a fossil to renewable resources based society, e.g., via its role in the conversion of lignocellulosic biomass into liquid hydrocarbon fuels. At present, at the industrial scale, a homogenous, base catalyst such as NaOH or Na_2CO_3 is used to catalyze aldol condensations. However, in a search for more sustainable chemical processes, heterogeneous alternatives for these homogenous catalysts are being pursued. Inspired by enzymatic catalyzed aldol condensations, this work aimed at the further investigation of the cooperativity between acids and bases on heterogeneous silica supports.

It has been elucidated in more detail how the turnover frequency obtained in a model reaction, *i.e.*, the aldol condensation of 4-nitrobenzaldehyde, can be enhanced up to a factor of five by the presence of surface silanols next to the actual, active sites, *i.e.*, the amines. The reaction mechanism of amine catalyzed aldol condensations has been unraveled: acetone first forms an enamine with the amine site that subsequently reacts with 4-nitrobenzaldehyde from the liquid phase yielding an iminium ion. The primary reaction product, *i.e.,* the aldol species, is obtained by a water-assisted desorption of this iminium ion. Finally, the aldol product releases water and forms the secondary reaction product, *i.e.,* the unsaturated ketone. The promotion by silanol groups originates from hydrogen-bridge interactions between the carbonyl moiety of the reactants and these silanol groups, which makes the former more susceptible to nucleophilic reactions. The promotion of amine active

sites by silanols does not affect the selectivity in aldol condensation between acetone and 4-nitrobenzaldehyde.

From the reaction mechanism it is clear that the cooperativity does not only depend on the concentrations of both types of sites but also on their spatial arrangement with respect to each other. It has been shown how the spatial arrangement is strongly affected by the type of amine-containing silane and its concentration in the synthesis mixture: if primary amines are grafted from a dilute synthesis mixture, a random positioning occurs whereas if more concentrated synthesis mixtures are employed, the primary amines are grafted as clusters on the silica surface because of the preferential propylamine–propylamine interactions by means of hydrogen bonding, compared to propylamine–toluene interactions. In contrast to primary amine active sites, secondary and tertiary amine active sites were found to be randomly distributed over the silica surface, due to a lower tendency to form hydrogen bonds.

In line with the identified reaction mechanism, activity differences between different amines are determined by an interplay of the following three factors, *i.e.*, (i) the possibility of forming a reactive enamine intermediate and inhibiting imine species with the amine active site, (ii) the base strength of the amine active site and (iii) steric hindrance effects. The crucial enamine reactive intermediate cannot be formed with a tertiary amine as active site and, hence, the turnover frequency observed with tertiary amines is extremely low. Inhibiting imine species can only be formed with a primary amine. As a result, a secondary amine active site which can yield the reactive enamine intermediate without competition with inhibiting imine formation will exhibit the highest turnover frequencies, provided that it does not suffer from steric hindrance or unfavorable basicity effects. Both the base strength of the amine site as well as the steric effects strongly depend on the substituent on the secondary amine. The base strength is captured via differences in both the activation entropies and energies of all adsorption and desorption steps involving the lone electron pair of the nitrogen atom. A low base strength, such as of phenylaminopropane results in a low turnover frequency. A final factor which has been considered is steric hindrance. A cyclohexyl substituted on the amine results in an increase in activation energy of about 17 kJ/mol. Moreover, it was observed that steric hindrance matters even for small substituents,

such as an ethyl compared to a methyl group. Hence, it seems that a methyl substituted secondary amine is the best amine type to catalyze the aldol condensation.

In addition to base properties effects on aldol condensation behavior also acid strength and arrangement effects of the promoting site with respect to a secondary amine have been investigated. It was observed that an intramolecular OH function, provided by a primary alcohol incorporated on the β-carbon of the amine substituent is as efficient as an intermolecular OH function provided by neighboring surface silanols as promoting site for the aldol condensation. However, incorporating stronger acids in the catalyst showed that intermolecular amine-silanol cooperativity or intramolecular amine-alcohol cooperativity exhibits higher catalyst performances than intramolecular amine-carboxylic acid or amine-phosphoric acid cooperativity. Nevertheless, intramolecularly promoted catalysts, even those with the stronger acids, retain up to 83% of their original activity when the intermolecular promotional effects are cancelled by endcapping the surface silanol groups, while the activity of a conventional amine reduces by a factor of four upon endcapping the surface silanols. These results further support the notion that the optimal promoting sites for the aldol condensation are H-bond donors and not strong acid sites. They also demonstrate that, indeed, stronger acids do exert a promoting effect on the activity of the amines, albeit less pronounced than silanols. A maximum activity was achieved when the secondary amine with a primary alcohol containing substituent was surrounded by surface silanols. This observation can be attributed to the concerted mobility of the amine and the intramolecularly promoting alcohol site when they are located on the same linker. Due to this concerted movement the amine and alcohol can bend together towards a neighboring silanol on the silica surface, resulting in two promoting sites in the vicinity of a single amine active site, *i.e.*, the intramolecular alcohol function and the intermolecular surface silanol. This results in a simultaneous activation of both reactants by the formation of a hydrogen bond and an increase in activity compared to the consecutive activation when there is only one promoting site in the vicinity of the amine. This suggests that a methyl-substituted secondary amine with one or more intramolecular alcohol functions on the β-carbons would be optimal for the aldol condensation, provided that the inclusion of such intramolecular alcohol functions does not significantly increase steric hindrance.

After the studies which were focused on the active and promoting sites, the effect of the feedstock has been examined. In the framework of the conversion of lignocellulosic biomass into liquid hydrocarbon fuels, it was decided to investigate the aldol condensation of furfural and acetone catalyzed by a methyl substituted secondary amine grafted on silicagel 60. Due to the absence of an electron withdrawing group such as the nitro function, the furfural carbonyl group is less susceptible to nucleophilic reactions, compared to 4-nitrobenzaldehyde. Therefore, somewhat more elevated temperatures are necessary to obtain measurable reaction rates. As a result, aldol product dehydration becomes more pronounced and the main observed reaction product is the α,β-unsaturated ketone. It also appears that the absence of an electron withdrawing group on furfural, gives rise to a predominance of furfural bounded to the silanols. As a result, acetone is unable to reach the silanols at high furfural concentrations and the enamine formation step rather occurs directly and, hence, slower, then via the promoted pathway. This is in strong contrast with the increasing aldol condensation TOF when increasing the 4-nitrobenzaldehyde concentration. If 2 vol% water is added to the reaction mixture the catalytic activity of a hydrophilic catalyst drastically decreased which has been related to the poisoning of the amine group, after which it is no longer available for reaction. An organosilica comprising a pronounced aromatic character in its structure functionalized with cysteine exhibits a TOF which is an order of magnitude lower than that exhibited by an organosilica with an aliphatic character functionalized with the same functional group. A strong 4-nitrobenzaldehyde physisorption is deemed responsible for this observation. It originates from the 'like-likes-like' principle which results in a decrease in acetone concentration in the pores and, subsequently, a decrease in TOF. The above results demonstrate the crucial interplay between the reactant and support properties in achieving the desired catalyst performance.

The TOFs obtained with weak basic amines grafted on heterogeneous supports are rather modest while the TOFs observed with homogeneous strong bases can be up to two orders of magnitude higher. Therefore it might be interesting to incorporate stronger bases, such as guanidine, into silica supports.

In the near future, the investigation of the effects of water and the catalyst support hydrophobicity should be continued. The hydrophobicity of the support could be tuned by co-condensation of tetraethyl orthosilicate and bridged organosilanes. The catalytic

performance of the materials could be assessed in the traditional aldol condensation of 4-nitrobenzaldehyde and acetone and, subsequently via the same aldol condensation in an aqueous environment. It will be necessary, in this pursuit of the most suited support, to account for the reactant properties such as aromaticity, nucleophilicity, etc.

There are still some other directions in which the present work can be further extended. For example, the fundamental effects that give rise to the steric hindrance for secondary amines with relatively small substituents are not yet fully understood. This could be further investigated by performing ab initio calculations which are aimed at clarifying the interaction of acetone with the various types of amines. Since the reaction is performed in a mixture of acetone and *n*-hexane, the effect of the solvent on the calculations could also be assessed. Additionally, the results of these calculations could be used to further expand the kinetic model.

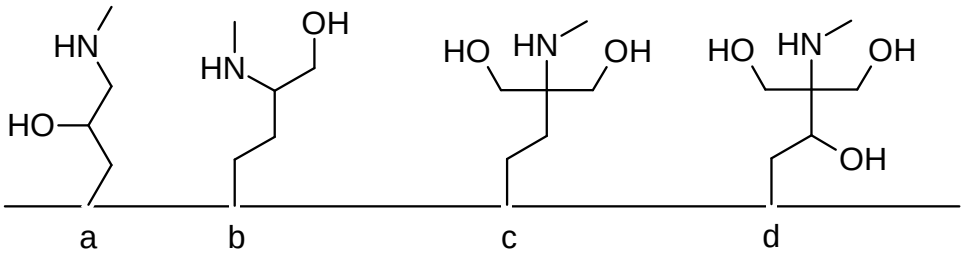

Figure 6-1. Interesting structures to catalyze the aldol condensation

The results obtained in this work suggest that a silica support functionalized with methyl-substituted secondary amine with one or more intramolecular alcohol functions on the β-carbons would be the ideal aldol condensation catalysts. The synthesis, characterization and testing of the structures which are shown in Figure 6-1 could provide more insights on this type of materials. Comparison of structures **(a)** and **(b)** could reveal the difference between primary and secondary alcohols, while comparison of structures **(b)**, **(c)** and **(d)** could confirm the effect of the simultaneous activation of the reactants and indicate the potential steric hindrance of the inclusion of multiple alcohol functions.

Appendix A

Grafting Probabilities

As described in section 2.2.5, the modeling of the arrangement of active sites on the catalytic surfaces has been done based upon random number generation and grafting probabilities (GPs), see Scheme 2-1. These grafting probabilities represent the probability that an amine is grafted on a given position and determine the degree of clustering of the amines on the generated surfaces. In the following sections the grafting probabilities used to model the three types of grafting mechanisms, *i.e.*, random positioning, clustering upon grafting and clustering in the synthesis mixture, are discussed in more detail.

A.1. Random positioning

If the grafting of the amines on the catalytic surface occurs in a random manner, the probability that an amine is grafted on a given position is independent of the number of amines in a neighboring position and the amine concentration in the synthesis mixture. The exact value of this constant grafting probability is then irrelevant.

A.2. Clustering upon grafting

A mechanism that has been invoked to explain the clustered arrangement of the active sites is the so-called flip mechanism [1-3]. In this mechanism, also denoted as 'clustering upon grafting', while being grafted the amine forms an hydrogen bond with either a surface silanol or an amine that has already been grafted on the surface. Subsequently, the amine is grafted upon a neighboring silanol. Potential differences in hydrogen bonding with a surface silanol or a previously grafted amine may result in specific grafting patterns of the amines on the catalyst surface.

Amine clusters will be obtained on the catalyst surface if the probability that an amine is grafted next to another amine exceeds the probability that an amine is grafted on a location surrounded by silanols. In other words, a clustered surface arrangement of the amines will occur when hydrogen bonding with a previously grafted amine is stronger than with a surface silanol. In this work, several different grafting probability functions were tested: (i) step functions which only differentiate between locations without neighboring amines and locations next to another amine but do not account for the number of neighboring amines (Figure A-1.a), (ii) grafting probability functions which linearly increase with increasing number of neighboring amines (Figure A-1.b) and (iii) quadratic grafting probability functions which account for steric hindrance effects when the number of neighboring amines is too high (Figure A-1.c). However, as discussed in section 2.3.4.2, the percentage of promoted amines on the surfaces generated using these grafting probability functions exhibits qualitatively similar trends with the silanol-to-amine ratio to that obtained from a randomly generated surface. Only the point at which the maximum percentage of promoted amines is obtained shifts towards significantly higher silanol-to-amine ratios. Hence, it could be concluded that these types of grafting probability functions are unable to describe the experimental observations.

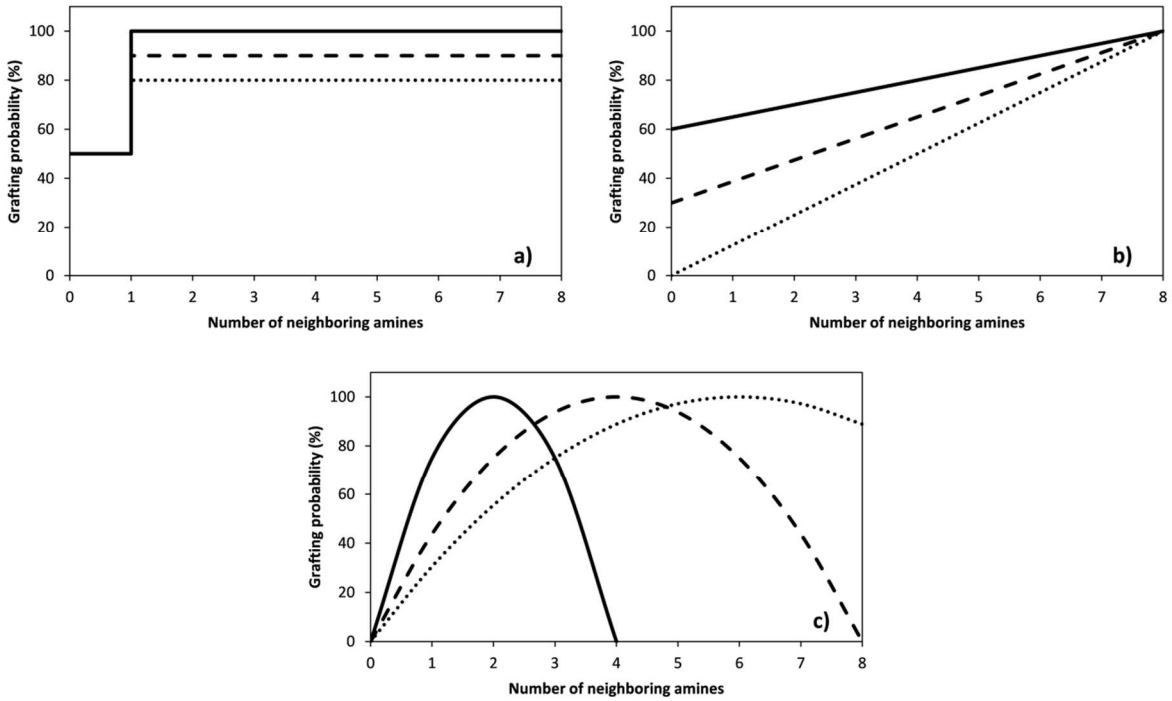

Figure A-1. Grafting probabilities as a function of the number of neighboring amines; a) step functions; b) linearly increasing functions; c) quadratic functions

A.3. Clustering in the synthesis mixture

Another possible cause for the clustering of the amines on the catalyst surface is the self-association of the amines in the synthesis mixture due to the formation of hydrogen bonds [4-6]. In this case, also denoted as 'clustering in the synthesis mixture', the probability that amines are grafted at neighboring positions depends on the amine concentration in the synthesis mixture instead of the number of amines which are previously grafted on neighboring position. Note that the catalysts with varying silanol-to-amine ratios are synthesized by varying the amine concentration in the synthesis mixture. Figure A-2 shows that the silanol-to-amine ratio of the final catalysts correlates with mole fraction of 3-aminopropyltriethoxysilane (APTES) in the synthesis mixture according to the power law shown in equation 1.

$$\frac{silanol}{amine} = 1.65\ {x_{APTES}}^{-0.63} \quad (1)$$

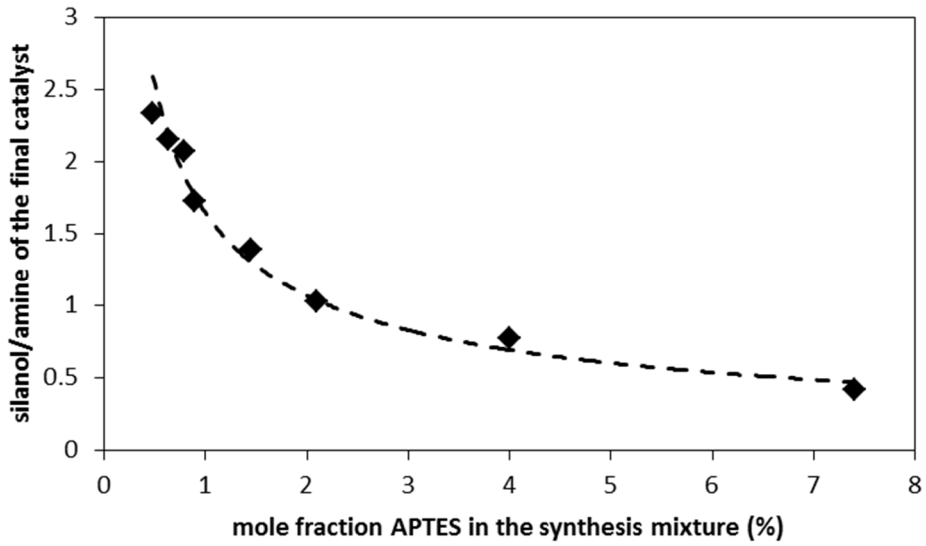

Figure A-2. Silanol-to-amine ratio of the final catalysts as a function of the mole fraction 3-aminopropyltriethoxysilane (APTES) in the synthesis mixture

At low amine concentrations in the synthesis mixture the probability that two amines effectively collide and stay together through hydrogen bonding is low. Hence, low amine concentrations in the synthesis mixture, that will inherently lead to materials with a high silanol-to-amine ratio, will result in a random amine arrangement. This means that, at these synthesis conditions, the probability that an amine is grafted on a position is independent of the number of amines neighboring this position, *i.e.*, $GP_{silanol}$ is equal to GP_{amine}, see Figure A-3. However, if sufficient amines are present in the synthesis mixture, the amines are able to form hydrogen bonds and can be considered to move in a clustered manner. At these synthesis conditions, inherently leading to lower silanol-to-amine ratios, the amines will be grafted in each other's vicinity which means that GP_{amine} should exceed $GP_{silanol}$, see Figure A-3. The number of neighboring amines is not accounted for in this assessment. A transition area occurs between low and high amine concentrations. It can be deduced from Figure A-4 together with Figure A-2 that amine clustering occurs above a threshold value of 1 mol% of APTES in the synthesis mixture. This threshold concentration corresponds to a catalyst with a silanol-to-amine ratio of 1.65, see equation 1. Ultimately, these insights led to the grafting probability functions shown in equations 2 and 3 and Figure A-3.

$$GP_{silanol} = \frac{4925}{97 + 1.61 \text{ x } 10^{7} \exp\left(-8.25 \frac{silanol}{amine}\right)} \quad (2)$$

$$GP_{amine} = 50 + \frac{9040}{178 + 1.02 \text{ x } 10^{-3} \exp\left(8.25 \frac{silanol}{amine}\right)} \quad (3)$$

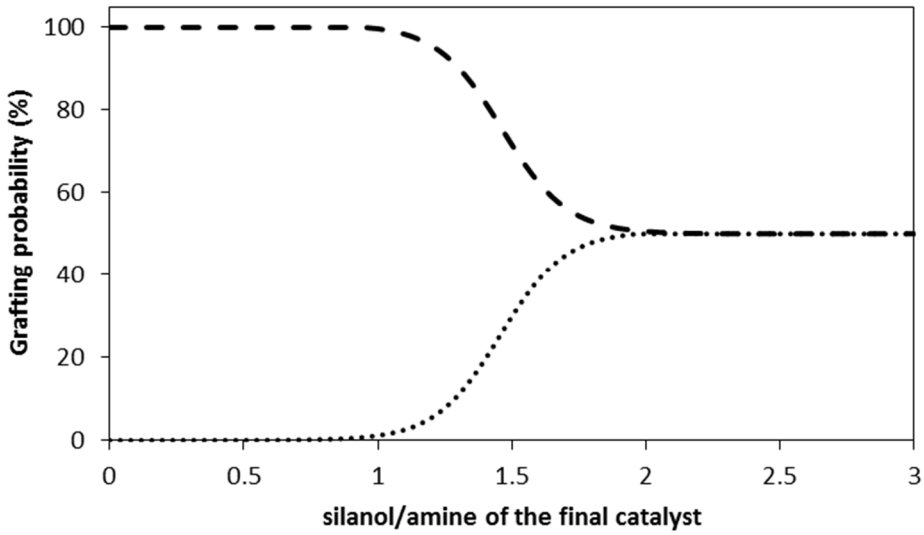

Figure A-3. Grafting probabilities as a function of the silanol-to-amine ratio of the final catalysts; dashed line: probability that an amine is grafted next to another amine; dotted line: probability that an amine is grafted on a position without neighboring amines

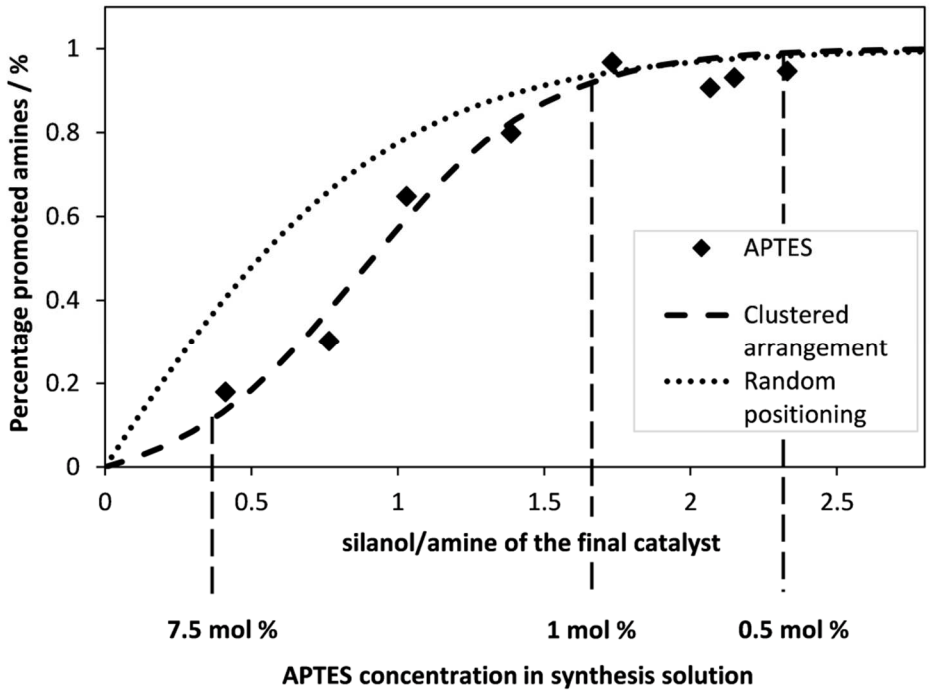

Figure A-4. Percentage of amines promoted as a function of silanol to amine ratio of the final catalyst and the 3-aminopropyltriethoxysilane (APTES) concentration in the synthesis solution; (◆) catalysts functionalized using APTES (APTES 1-8); dotted line: calculated percentage by means of randomly generated surfaces; dashed line: calculated percentage accounting for clustering in the synthesis mixture

A.4. References

1. K. C. Vrancken, P. Van Der Voort, K. Possemiers, E. F. Vansant, J Colloid Interf Sci, **1995**, 174, 86-91
2. H. G. Linde, J. Appl. Polym. Sci., **1990**, 40, 613-622
3. C. W. Chu, D. P. Kirby, P. D. Murphy, J. Adhes. Sci. Technol., **1993**, 7, 417-433
4. J. C. Hicks, R. Dabestani, A. C. Buchanan, C. W. Jones, Chem Mater, **2006**, 18, 5022-5032
5. J. C. Hicks, C. W. Jones, Langmuir, **2006**, 22, 2676-2681
6. M. W. McKittrick, C. W. Jones, Chem Mater, **2003**, 15, 1132-1139

Appendix B

Thermodynamics Calculations

The reaction mixtures of both the model reaction, *i.e.*, the aldol condensation of 4-nitrobenzaldehyde and acetone, as well as the more practical application, *i.e.*, the aldol condensation of furfural and acetone exhibit pronounced polarity effects. As a result, the mixtures are significantly thermodynamic non ideal. The thermodynamic non-ideality of a liquid phase can be accounted for via so-called activity coefficients, γ_i, which can be calculated using various methods such as, the Non-Random Two-Liquid (NRTL) method [1] and the Universal Quasichemical (UNIQUAC) method [2] and its extension, the UNIQUAC Functional-group Activity Coefficients (UNIFAC) method [3]. These methods make use of binary interaction parameters to describe the interactions between two molecules or two functional groups in the mixture. UNIQUAC is mathematically more complex than NRTL and, correspondingly, has three advantages: (i) it relies on one (adjustable) parameters less, *i.e.*, the nonrandomness parameter α_{ij} is not required in this method, (ii) UNIQUAC's parameters often have a more limited temperature dependence, and (iii) because the primary concentration variable is a surface fraction instead of a mole fraction, UNIQUAC is applicable to solutions containing small or large molecules, including polymers [4]. A large number of the parameters used in the models can be found in literature [4, 5], however, even today some of the parameters remain unreported. Therefore, in addition to the performance of the model, the availability of the parameters for the necessary components is an important factor in the decision to use the one or the other methodology.

In addition to the thermodynamic non-ideality of the liquid phase, the thermodynamic non-ideality of the vapor phase has to be calculated in order to determine a vapor-liquid equilibrium. This can be accounted for using fugacity coefficients, Φ_i, which can be determined by equations of state such as, the Soave modification of Redlich-Kwong (SRK)

[6], Peng-Robinson (PR) [7] or Hayden-O'Connell (HOC) [8]. The HOC equation of state performs well for polar components at low pressures because it attempts to filter out polarity and associating effects from the critical properties and uses an effective acentric factor for shape and globularity so that more appropriate characteristics are used for the non-polar contributions [4]. Additionally, it is applicable to components which exhibit strong intermolecular hydrogen bonding, such as carboxylic acids, because it relates the equilibrium coefficient for dimerization to the estimated virial coefficient according to the ''chemical theory'' of non-ideal gas behavior [4].

Several models are used in this work. In Chapters 2 and 3, the UNIQUAC model and its extension UNIFAC are used to describe the non-ideality of both the catalyst synthesis and the reaction mixture. In Chapter 5, the NRTL-HOC model is used to determine the vapor-liquid equilibrium and thermodynamic non-ideality of the acetone-furfural mixture.

B.1. The Universal Quasichemical model and its extension

The Universal Quasichemical (UNIQUAC) model (eq. 1) [2, 4] contains a combinatorial part (eq. 2), which accounts for the contribution due to differences in molecular size and shape of the different compounds in the liquid mixture, and a residual part (eq. 3), which accounts for the contribution due to energetic interactions.

$$\ln \gamma_i = \underbrace{\ln \gamma_i^C}_{combinatorial} + \underbrace{\ln \gamma_i^R}_{residual} \tag{1}$$

$$\ln \gamma_i^C = \ln \frac{\Phi_i}{x_i} + \frac{z}{2} q_i \ln \frac{\theta_i}{\Phi_i} + l_i - \frac{\Phi_i}{x_i} \sum_j x_j l_j \tag{2}$$

$$\ln \gamma_i^R = q_i \left[1 - \ln\left(\sum_j \theta_j \tau_{ji}\right) - \sum_j \left(\theta_j \tau_{ij} / \sum_k \theta_k \tau_{kj}\right)\right] \tag{3}$$

$$l_i = \frac{z}{2}(r_i - q_i) - (r_i - 1) \tag{4}$$

$$\theta_i = \frac{q_i x_i}{\sum_j q_j x_j}; \quad \Phi_i = \frac{r_i x_i}{\sum_j r_j x_j} \tag{5}$$

$$\tau_{ij} = \exp\left(-\frac{\Delta u_{ij}}{RT}\right) \tag{6}$$

In these equations x_i represents the mole fraction of component i, r_i and q_i pure-component parameters which are, respectively, measures of molecular van der Waals volumes and molecular surface areas of component i, with θ_i and Φ_i the corresponding

area and segment fractions. The binary parameters Δu_{ij} and Δu_{ji} describe the interactions between two molecules in the mixture. The parameter z is the coordination number which is typically equal to 10.

The UNIFAC method [3, 4] is a group-contribution extension of the UNIQUAC method and is used when the binary interaction parameters Δu_{ij} and Δu_{ji} between the molecules are unknown. By assuming that a physical property of a fluid component can be determined from the sum of contributions corresponding to the component's functional groups it becomes possible to correlate the properties of a large number of liquid compounds and mixtures in terms of a much smaller number of parameters which characterize individual group contributions. The parameters used in this work are reported in Table 3-5.

B.2. Non-Random Two-Liquid model

The NRTL model [1, 4] is based on Scott's two-liquid model [9] and on an assumption of nonrandomness similar to that used by Wilson [10]. The activity coefficient can be determined from eq. 7. The NRTL model contains three parameters, a_{ij}, b_{ij} and c_{ij}, eq. 9, which describe the binary interactions between two components in the liquid mixture and a parameter α_{ij}, eq. 8, which describes the nonrandomness. These parameters are obtained from the commercial simulation software Aspen Plus.

$$\ln \gamma_i = \frac{\sum_j \tau_{ji} G_{ji} x_j}{\sum_l G_{li} x_l} + \sum_j \frac{x_j G_{ij}}{\sum_l G_{lj} x_l} \left(\tau_{ij} - \frac{\sum_r x_r \tau_{rj} G_{rj}}{\sum_l G_{lj} x_l} \right) \quad (7)$$

$$G_{ij} = \exp\left(-\alpha_{ij} \tau_{ij}\right) \quad (8)$$

$$\tau_{ij} = a_{ij} + \frac{b_{ij}}{T} + c_{ij} \ln(T) \quad (9)$$

B.3. Hayden-O'Connell equation of state

The virial equation of state relates the compressibility factor to the composition, temperature and pressure [4]. In the Hayden-O'Connell method [8] the virial equation is terminated at the second coefficient, see eq. 10. It is a simple but accurate method for conditions up to a density of about one-half of the critical one. The second virial coefficient is determined by the mole fractions and the binary interactions of all the components in the gas mixture, see eq. 11. The fugacity coefficient is given by eq. 12.

$$Z = \frac{Pv}{RT} = 1 + \frac{BP}{RT} \quad (10)$$

$$B = \sum_i \sum_j y_i y_j B_{ij}(T) \quad (11)$$

$$\ln(\Phi_i) = \left(2\sum_j y_j B_{ij}(T) - B\right)\frac{P}{RT} \quad (12)$$

The second virial coefficient consists of various contributions, which can be described as bound, metastable bound, free pairs and an association contribution, eq. 13. The bound and metastable bound second virial coefficents are expressed in equations 14 to 20 as a function of temperature and reduced dipole moment.

$$B_{total} = B_{free} + B_{metastable} + B_{bound} + B_{chem} \quad (13)$$

$$B_{metastable} + B_{bound} = b_0 A \exp\left(\frac{\Delta H}{k_B T/\epsilon}\right) \quad (14)$$

$$b_0 = \frac{2\pi}{3} N_0 \sigma^3 \quad (15)$$

$$A = -0.3 - 0.05\mu^* \quad (16)$$

$$\Delta H = 1.99 + 0.2\mu^{*2} \quad (17)$$

$$\mu^* = \mu^2/\epsilon\sigma^3 \quad (18)$$

$$\frac{\epsilon}{k_B T_c} = 0.748 + 0.91\omega - \frac{0.4\eta}{2+20\omega} \quad (19)$$

$$\sigma = (2.44 - \omega)\left(\frac{T_c}{P_c}\right)^{1/3} \quad (20)$$

In case of nonpolar components, the free contribution of the second virial coefficient is determined by equations 21 and 22.

$$B_{free-nonpolar} = b_0\left(0.94 - 1.47/T^{*\prime} - 0.85/T^{*\prime 2} + 1.015/T^{*\prime 3}\right) \quad (21)$$

$$1/T^{*\prime} = \epsilon/k_B T - 1.6\omega \quad (22)$$

The critical properties of polar components with large dipole moments, *i.e.* $\mu > 1.45$, are affected by the polarity. This is accounted for in the potential parameters ϵ and σ by means of equations 24 and 25. The values of ϵ' and σ' are obtained from equations 19 and 20 ,respectively. Finally, the free contribution of the second virial coefficients is determined by eq. 23.

$$B_{free} = B_{free-nonpolar} - b_0\mu^{*\prime}\left(0.75 - 3/T^{*\prime} + 2.1/T^{*\prime 2} + 2.1/T^{*\prime 3}\right) \quad (23)$$

$$\epsilon = \epsilon'/(1+\xi)^{n/(n-6)} \approx \epsilon'\left(1 - \left(\frac{n}{n-6}\right)\xi\left(1 - \left(\frac{n}{n-6}+1\right)\frac{\xi}{2}\right)\right) \quad (24)$$

$$\sigma^3 = \sigma'^3(1+\xi)^{3/(n-6)} \approx \sigma'^3(1+3\,\xi/(n-6)) \quad (25)$$

$$\xi = \frac{4\mu^4}{3C\epsilon\prime\sigma\prime^6 k_B T_c} = \frac{k_B\mu^4}{5.723 \text{ x } 10^{-8}\, C\epsilon\prime\sigma\prime^6 T_c} \quad (26)$$

$$n = 16 + 400\omega \quad (27)$$

$$C = 2.882 - \frac{1.882\omega}{0.03+\omega} \quad (28)$$

$$\begin{aligned} \mu^{*\prime} &= \mu^* - 0.25 \qquad \mu^* \geq 0.25 \\ \mu^{*\prime} &= 0 \qquad 0.25 > \mu^* \geq 0.04 \\ \mu^{*\prime} &= \mu^* \qquad 0.04 > \mu^* \geq 0 \end{aligned} \quad (29)$$

For associating components such as water, alcohols, esters, amines, mercaptans and ketones is another contribution to the second virial coefficient given in eq. 30.

$$\begin{aligned} B_{chem} &= b_0 \exp\big(\eta(650/(\epsilon/k_B + 300) - 4.27)\big)\big(1 - \exp(1500\eta/T)\big) \quad \eta \neq 4.5 \\ B_{chem} &= b_0 \exp\big(\eta(42.8/(\epsilon/k_B + 22.4) - 4.27)\big)\big(1 - \exp(1500\eta/T)\big) \quad \eta = 4.5 \end{aligned} \quad (30)$$

When the system is a mixture of several components, the mixing rules expressed by equations 31 to 34 should be used.

$$\epsilon_{ij} = 0.7\big(\epsilon_i\epsilon_j\big)^{1/2} + 0.6\big(1/\epsilon_i + 1/\epsilon_j\big)^{-1} \quad (31)$$

$$\sigma_{ij} = \big(\sigma_i\sigma_j\big)^{1/2} \quad (32)$$

$$\omega_{ij} = 0.5\big(\omega_i + \omega_j\big) \quad (33)$$

$$\mu^*_{ij} = \mu_i\mu_j/\big(\epsilon_{ij}\sigma^3_{ij}\big) \quad (34)$$

In the gas phase molecules which exhibit strong intermolecular hydrogen bonding exists, such as carboxylic acids, have a molar volume which is less than that corresponding to an ideal gas at the same temperature and pressure. These vapour imperfections can be accounted for by assuming an equilibrium association where dimers are being formed [11, 12]. The dimerization equilibrium coefficient of an associating component is given in, eq 35. The true mole fraction of the associating component i can be calculated with eq. 36, while the true mole fractions of the non-associating components can be determined from eq. 37.

These true mole fractions has to be used in calculations above and, finally, the obtained fugacity coefficients has to be rescaled according to eq. 38.

$$\log\left(K_i^{CT}\right) = \Omega_1 + \frac{\Omega_2}{T} \tag{35}$$

$$y_i^{True} = \frac{-1+\sqrt{1+4K_i^{CT}P\exp\left(\frac{B_{free,i}P}{RT}\right)y_i(2-y_i)}}{2K_i^{CT}P\exp\left(\frac{B_{free,i}P}{RT}\right)(2-y_i)} \tag{36}$$

$$y_{j\neq i}^{True} = \frac{y_j}{1-(y_i-y_i^{True})/(2-y_i^{True})} \tag{37}$$

$$\Phi_i^{True} = \frac{y_i^{True}}{y_i}\Phi_i \tag{38}$$

The critical temperature, critical pressure, molecular dipole moment, acentric factor and the association and solvation parameters of the components in the system are obtained from the commercial simulation software Aspen Plus.

B.4. References

1. H. Renon, Prausnit.Jm, Aiche J., **1968**, 14, 135-&
2. D. S. Abrams, J. M. Prausnitz, Aiche J., **1975**, 21, 116-128
3. A. Fredenslund, R. L. Jones, J. M. Prausnitz, Aiche J., **1975**, 21, 1086-1099
4. B. E. Poling, J. M. Prausnitz, J. P. O'Connell, *The properties of gases and liquids*, McGraw-Hill, New York, **2001**
5. H. K. Hansen, P. Rasmussen, A. Fredenslund, M. Schiller, J. Gmehling, Ind. Eng. Chem. Res., **1991**, 30, 2352-2355
6. G. Soave, Chem. Eng. Sci., **1972**, 27, 1197-&
7. D. Peng, D. B. Robinson, Industrial & Engineering Chemistry Fundamentals, **1976**, 15, 59-64
8. J. G. Hayden, J. P. Oconnell, Industrial & Engineering Chemistry Process Design and Development, **1975**, 14, 209-216
9. R. L. Scott, J. Chem. Phys., **1956**, 25, 193-205
10. G. M. Wilson, J. Am. Chem. Soc., **1964**, 86, 127-&
11. K.-H. Nothnagel, D. S. Abrams, J. M. Prausnit, Industrial & Engineering Chemistry Process Design and Development, **1973**, 12, 25-35
12. L. Li, Y. He, Y. X. Wu, W. H. Zou, Chin. J. Chem. Eng., **2013**, 21, 759-765

Appendix C

Experimental Data

Table C-1. Reaction conditions at which the APTES catalysts were assessed with the corresponding turnover frequencies

Exp#	Catalyst	C_{amine}(mol/l)	C^0_{ace} (mol/l)	C^0_{benz} (mol/l)	$C^0_{nC_6}$ (mol/l)	Temp (°C)	TOF (s^{-1})
1	APTES 1 (type AB)	1.01E-03	7.03E+00	2.96E-02	3.70E+00	55	1.02E-03
2	APTES 1 (type AB)	9.83E-04	7.03E+00	2.96E-02	3.70E+00	55	1.01E-03
3	APTES 2 (type AB)	1.01E-03	7.03E+00	2.96E-02	3.70E+00	55	1.01E-03
4	APTES 3 (type AB)	1.01E-03	7.03E+00	2.96E-02	3.70E+00	55	9.83E-04
5	APTES 4 (type AB)	1.01E-03	7.03E+00	2.96E-02	3.70E+00	55	1.03E-03
6	APTES 4 (type AB)	1.01E-03	7.03E+00	2.96E-02	3.70E+00	55	1.03E-03
7	APTES 4 (type AB)	1.01E-03	7.03E+00	2.96E-02	3.70E+00	55	1.02E-03
8	APTES 4 (type AB)	1.01E-03	7.03E+00	2.96E-02	3.70E+00	55	1.02E-03
9	APTES 4 (type AB)	1.01E-03	7.03E+00	2.96E-02	3.70E+00	55	1.07E-03
10	APTES 4 (type AB)	1.01E-03	7.03E+00	2.96E-02	3.70E+00	55	1.05E-03
11	APTES 4 (type AB)	1.01E-03	7.03E+00	2.96E-02	3.70E+00	55	1.06E-03
12	APTES 5 (type AB)	1.01E-03	7.03E+00	2.96E-02	3.70E+00	55	9.07E-04
13	APTES 5 (type AB)	1.01E-03	7.03E+00	2.95E-02	3.70E+00	55	8.90E-03
14	APTES 6 (type AB)	9.35E-04	7.03E+00	2.95E-02	3.70E+00	55	7.58E-04
15	APTES 7 (type AB)	1.01E-03	7.03E+00	2.96E-02	3.70E+00	55	4.57E-04

16	APTES 8 (type AB)	1.01E-03	7.03E+00	2.96E-02	3.70E+00	55	3.50E-04
17	APTES 1 (type B)	9.83E-04	7.03E+00	2.96E-02	3.70E+00	55	2.18E-04
18	APTES 2 (type B)	1.01E-03	7.03E+00	2.96E-02	3.70E+00	55	2.09E-04
19	APTES 3 (type B)	1.01E-03	7.03E+00	2.96E-02	3.70E+00	55	2.30E-04
20	APTES 4 (type B)	1.01E-03	7.03E+00	2.96E-02	3.70E+00	55	2.61E-04
21	APTES 5 (type B)	1.01E-03	7.03E+00	2.96E-02	3.70E+00	55	2.21E-04
22	APTES 6 (type B)	9.37E-04	7.03E+00	2.96E-02	3.70E+00	55	1.85E-04
23	APTES 7 (type B)	1.01E-03	7.03E+00	2.96E-02	3.70E+00	55	1.44E-04
24	APTES 7 (type B)	1.01E-03	7.03E+00	2.96E-02	3.70E+00	55	1.43E-04
25	APTES 7 (type B)	1.01E-03	7.03E+00	2.96E-02	3.70E+00	55	1.45E-04
26	APTES 8 (type B)	9.58E-04	7.03E+00	2.96E-02	3.70E+00	55	1.45E-04
27	APTES 8 (type B)	1.01E-03	7.03E+00	2.96E-02	3.70E+00	55	1.41E-04
28	APTES 8 (type B)	9.40E-04	7.03E+00	2.96E-02	3.70E+00	55	1.37E-04
29	APTES 3 (type AB)	1.01E-03	7.03E+00	5.92E-02	3.70E+00	55	1.26E-03
30	APTES 4 (type AB)	1.01E-03	7.03E+00	5.90E-02	3.70E+00	55	1.35E-03
31	APTES 5 (type AB)	1.01E-03	7.03E+00	5.92E-02	3.70E+00	55	1.13E-03
32	APTES 7 (type AB)	9.40E-04	7.03E+00	5.92E-02	3.70E+00	55	6.01E-04
33	APTES 3 (type B)	9.40E-04	7.03E+00	5.92E-02	3.70E+00	55	1.93E-04
34	APTES 1 (type AB)	1.01E-03	7.03E+00	8.87E-02	3.70E+00	55	1.28E-03
35	APTES 3 (type AB)	1.01E-03	7.03E+00	8.87E-02	3.70E+00	55	1.22E-03
36	APTES 3 (type AB)	1.01E-03	7.03E+00	8.87E-02	3.70E+00	55	1.36E-03
37	APTES 5 (type AB)	6.67E-04	4.59E+00	5.85E-02	5.11E+00	55	1.25E-03
38	APTES 6 (type AB)	1.00E-03	7.03E+00	9.11E-02	3.70E+00	55	8.75E-04
39	APTES 7 (type AB)	1.00E-03	7.03E+00	9.01E-02	3.70E+00	55	5.65E-04
40	APTES 8 (type AB)	1.02E-03	7.03E+00	9.07E-02	3.70E+00	55	4.37E-04
41	APTES 3 (type AB)	1.01E-03	7.03E+00	1.18E-01	3.70E+00	55	1.39E-03
42	APTES 3 (type AB)	1.01E-03	7.03E+00	1.48E-01	3.70E+00	55	1.39E-03
43	APTES 3 (type AB)	1.01E-03	7.03E+00	1.77E-01	3.70E+00	55	1.33E-03

44	APTES 3 (type AB)	1.01E-03	7.03E+00	1.48E-02	3.70E+00	55	8.81E-04
45	APTES 3 (type AB)	1.01E-03	7.03E+00	2.96E-02	3.70E+00	45	8.22E-04
46	APTES 4 (type AB)	1.01E-03	7.03E+00	2.96E-02	3.70E+00	45	7.77E-04
47	APTES 5 (type AB)	1.01E-03	7.03E+00	2.96E-02	3.70E+00	45	6.71E-04
48	APTES 7 (type AB)	9.40E-04	7.03E+00	2.96E-02	3.70E+00	45	4.12E-04
49	APTES 3 (type B)	9.40E-04	7.03E+00	2.96E-02	3.70E+00	45	9.85E-05
50	APTES 6 (type AB)	1.01E-03	7.03E+00	1.48E-02	3.70E+00	45	4.81E-04
51	APTES 6 (type AB)	1.01E-03	7.03E+00	5.92E-02	3.70E+00	45	6.06E-04
52	APTES 6 (type AB)	1.01E-03	7.03E+00	1.77E-01	3.70E+00	45	6.03E-04
53	APTES 2 (type AB)	1.01E-03	7.03E+00	3.03E-02	3.70E+00	40	5.75E-04
54	APTES 1 (type AB)	1.01E-03	7.03E+00	2.96E-02	3.70E+00	40	5.58E-04
55	APTES 1 (type AB)	1.29E-03	7.03E+00	3.03E-02	3.70E+00	40	6.20E-04
56	APTES 4 (type AB)	1.01E-03	7.03E+00	2.96E-02	3.70E+00	40	5.88E-04
57	APTES 5 (type AB)	1.01E-03	7.03E+00	2.95E-02	3.70E+00	40	5.03E-04
58	APTES 7 (type AB)	1.01E-03	7.03E+00	2.96E-02	3.70E+00	40	3.14E-04
59	APTES 6 (type AB)	1.01E-03	7.03E+00	1.55E-02	3.70E+00	40	3.99E-04
60	APTES 6 (type AB)	1.01E-03	7.03E+00	5.92E-02	3.70E+00	40	4.23E-04
61	APTES 6 (type AB)	1.01E-03	7.03E+00	1.77E-01	3.70E+00	40	4.51E-04

Table C-2. Reaction conditions at which the APDMES catalysts were assessed with the corresponding turnover frequencies

Exp#	Catalyst	C_{amine}(mol/l)	C^0_{ace} (mol/l)	C^0_{benz} (mol/l)	$C^0_{nC_6}$ (mol/l)	Temp (°C)	TOF (s^{-1})
1	APDMES 1 (type AB)	9.91E-04	6.97E+00	2.90E-02	3.72E+00	45	7.51E-04
2	APDMES 1 (type B)	9.99E-04	6.97E+00	2.93E-02	3.72E+00	45	2.14E-04
3	APDMES 2 (type AB)	1.01E-03	7.03E+00	2.94E-02	3.69E+00	45	6.45E-04
4	APDMES 2 (type B)	9.99E-04	6.98E+00	2.92E-02	3.72E+00	45	2.06E-04
5	APDMES 3 (type AB)	1.00E-03	7.00E+00	2.93E-02	3.70E+00	45	6.44E-04
6	APDMES 3 (type B)	9.96E-04	7.03E+00	2.91E-02	3.69E+00	45	1.98E-04
7	APDMES 4 (type AB)	9.95E-04	6.99E+00	2.91E-02	3.71E+00	45	5.15E-04
8	APDMES 4 (type B)	9.95E-04	6.98E+00	2.91E-02	3.72E+00	45	1.85E-04
9	APDMES 5 (type AB)	9.98E-04	7.03E+00	2.92E-02	3.69E+00	45	3.73E-04
10	APDMES 5 (type B)	9.99E-04	6.98E+00	2.92E-02	3.72E+00	45	2.08E-04
11	APDMES 5 (type AB)	9.98E-04	7.03E+00	2.92E-02	3.69E+00	45	3.59E-04
12	APDMES 5 (type B)	9.99E-04	6.98E+00	2.92E-02	3.72E+00	45	2.00E-04

Table C-3. Reaction conditions at which the MAPTMS catalysts were assessed with the corresponding turnover frequencies

Exp#	Catalyst	C_{amine}(mol/l)	C^0_{ace} (mol/l)	C^0_{benz} (mol/l)	$C^0_{nC_6}$ (mol/l)	Temp (°C)	TOF (s^{-1})
1	MAPTMS 3 (type AB)	1.03E-03	7.08E+00	2.92E-02	3.66E+00	45	3.66E-03
2	MAPTMS 3 (type B)	1.03E-03	7.02E+00	2.91E-02	3.69E+00	45	8.11E-04
3	MAPTMS 1 (type AB)	6.87E-04	7.03E+00	2.93E-02	3.69E+00	45	1.14E-03
4	MAPTMS 2 (type B)	8.81E-04	7.00E+00	2.92E-02	3.71E+00	45	6.99E-04
5	MAPTMS 4 (type B)	1.17E-03	6.99E+00	2.91E-02	3.71E+00	45	7.95E-04
6	MAPTMS 2 (type AB)	8.86E-04	6.97E+00	2.93E-02	3.72E+00	45	3.32E-03
7	MAPTMS 4 (type AB)	1.17E-03	7.00E+00	2.92E-02	3.71E+00	45	3.42E-03
8	MAPTMS 1 (type AB)	1.00E-03	7.02E+00	2.94E-02	3.69E+00	45	3.30E-03
9	MAPTMS 1 (type B)	1.00E-03	7.03E+00	2.93E-02	3.69E+00	45	1.00E-03
10	MAPTMS 1 (type AB)	1.01E-03	6.99E+00	2.95E-02	3.71E+00	35	2.62E-03
11	MAPTMS 1 (type B)	1.00E-03	7.03E+00	2.93E-02	3.69E+00	35	6.44E-04
12	MAPTMS 2 (type AB)	9.97E-04	7.07E+00	2.91E-02	3.67E+00	35	2.40E-03
13	MAPTMS 2 (type B)	1.01E-03	7.01E+00	2.95E-02	3.70E+00	35	4.59E-04
14	MAPTMS 3 (type AB)	9.95E-04	6.96E+00	2.90E-02	3.73E+00	35	2.38E-03
15	MAPTMS 3 (type B)	1.01E-03	7.01E+00	2.94E-02	3.70E+00	35	5.24E-04
16	MAPTMS 4 (type AB)	1.00E-03	6.98E+00	2.93E-02	3.72E+00	35	2.34E-03
17	MAPTMS 4 (type B)	9.95E-04	7.06E+00	2.92E-02	3.67E+00	35	5.46E-04
18	MAPTMS 1 (type AB)	9.94E-04	6.96E+00	2.91E-02	3.73E+00	25	1.79E-03
19	MAPTMS 1 (type B)	9.92E-04	7.00E+00	2.91E-02	3.71E+00	25	6.36E-04
20	MAPTMS 2 (type B)	9.96E-04	7.03E+00	2.90E-02	3.69E+00	25	4.53E-04
21	MAPTMS 3 (type B)	1.00E-03	7.00E+00	2.92E-02	3.70E+00	25	4.46E-04
22	MAPTMS 4 (type AB)	1.00E-03	7.04E+00	2.92E-02	3.68E+00	25	1.68E-03
23	MAPTMS 4 (type B)	9.97E-04	7.04E+00	2.91E-02	3.68E+00	25	4.50E-04
24	MAPTMS 4 (type AB)	9.99E-04	7.01E+00	2.93E-02	3.70E+00	15	1.11E-03
25	MAPTMS 4 (type B)	9.99E-04	6.98E+00	2.93E-02	3.72E+00	15	3.15E-04
26	MAPTMS 1 (type AB)	9.93E-04	7.01E+00	2.90E-02	3.70E+00	15	1.15E-03
27	MAPTMS 1 (type B)	9.98E-04	7.01E+00	2.91E-02	3.70E+00	15	3.33E-04
28	MAPTMS 3 (type AB)	9.97E-04	6.98E+00	2.91E-02	3.72E+00	15	1.24E-03

29	MAPTMS 3 (type B)	9.97E-04	6.96E+00	2.91E-02	3.73E+00	15	3.30E-04
30	MAPTMS 1 (type B)	1.00E-03	6.97E+00	2.93E-02	3.73E+00	45	7.08E-04
31	MAPTMS 3 (type B)	1.00E-03	7.02E+00	2.93E-02	3.69E+00	35	5.63E-04
32	MAPTMS 4 (type B)	9.99E-04	7.07E+00	2.92E-02	3.67E+00	35	5.23E-04
33	MAPTMS 1 (type AB)	1.00E-03	7.04E+00	5.85E-02	3.68E+00	45	4.32E-03
34	MAPTMS 1 (type B)	1.00E-03	6.99E+00	5.85E-02	3.71E+00	45	8.90E-04
35	MAPTMS 3 (type AB)	1.00E-03	7.01E+00	5.86E-02	3.70E+00	45	4.35E-03
36	MAPTMS 3 (type B)	9.95E-04	7.03E+00	5.82E-02	3.69E+00	45	9.25E-04
37	MAPTMS 1 (type AB)	9.92E-04	7.02E+00	8.70E-02	3.69E+00	45	5.56E-03
38	MAPTMS 1 (type B)	9.98E-04	7.00E+00	8.77E-02	3.70E+00	45	1.18E-03
39	MAPTMS 4 (type AB)	1.00E-03	7.01E+00	5.86E-02	3.70E+00	45	4.07E-03
40	MAPTMS 4 (type B)	1.00E-03	7.01E+00	5.88E-02	3.70E+00	45	1.01E-03
41	MAPTMS 3 (type AB)	1.00E-03	7.04E+00	8.76E-02	3.68E+00	45	4.90E-03
42	MAPTMS 3 (type B)	9.98E-04	7.03E+00	8.73E-02	3.69E+00	45	1.16E-03
43	MAPTMS 4 (type AB)	1.00E-03	7.04E+00	8.77E-02	3.68E+00	45	5.36E-03
44	MAPTMS 4 (type B)	1.00E-03	6.98E+00	8.76E-02	3.72E+00	45	1.23E-03
45	MAPTMS 6 (type AB)	9.99E-04	7.04E+00	2.92E-02	3.68E+00	45	1.79E-03
46	MAPTMS 6 (type B)	1.00E-03	7.04E+00	2.93E-02	3.68E+00	45	1.02E-03
47	MAPTMS 7 (type AB)	9.97E-04	6.99E+00	2.92E-02	3.71E+00	45	1.32E-03
48	MAPTMS 7 (type B)	1.00E-03	7.05E+00	2.92E-02	3.68E+00	45	9.20E-04
49	MAPTMS 5 (type B)	9.95E-04	7.05E+00	2.92E-02	3.68E+00	45	8.15E-04
50	MAPTMS 6 (type AB)	1.00E-03	6.98E+00	2.92E-02	3.72E+00	35	1.51E-03
51	MAPTMS 6 (type B)	1.00E-03	7.05E+00	2.92E-02	3.68E+00	35	8.46E-04
52	MAPTMS 5 (type AB)	1.00E-03	7.04E+00	2.94E-02	3.68E+00	35	1.61E-03
53	MAPTMS 5 (type B)	1.00E-03	6.96E+00	2.93E-02	3.73E+00	35	7.66E-04
54	MAPTMS 7 (type AB)	1.00E-03	6.99E+00	2.93E-02	3.71E+00	35	1.10E-03
55	MAPTMS 7 (type B)	9.95E-04	7.01E+00	2.92E-02	3.70E+00	35	7.83E-04
56	MAPTMS 6 (type AB)	9.98E-04	6.98E+00	2.92E-02	3.72E+00	25	1.11E-03
57	MAPTMS 6 (type B)	9.96E-04	7.03E+00	2.91E-02	3.69E+00	25	6.97E-04
58	MAPTMS 5 (type AB)	9.94E-04	7.03E+00	2.91E-02	3.69E+00	25	1.17E-03

59	MAPTMS 5 (type B)	1.00E-03	6.99E+00	2.94E-02	3.71E+00	25	5.67E-04
60	MAPTMS 7 (type AB)	9.94E-04	7.00E+00	2.91E-02	3.71E+00	25	8.14E-04
61	MAPTMS 7 (type B)	1.00E-03	6.97E+00	2.93E-02	3.72E+00	25	6.27E-04
62	MAPTMS 6 (type AB)	9.88E-04	6.98E+00	2.89E-02	3.72E+00	15	7.84E-04
63	MAPTMS 6 (type B)	9.98E-04	6.98E+00	2.92E-02	3.72E+00	15	4.82E-04
64	MAPTMS 5 (type AB)	9.95E-04	7.05E+00	2.91E-02	3.68E+00	15	8.02E-04
65	MAPTMS 5 (type B)	9.95E-04	7.05E+00	2.91E-02	3.69E+00	15	4.06E-04
66	MAPTMS 7 (type AB)	9.99E-04	6.97E+00	2.93E-02	3.72E+00	15	5.38E-04
67	MAPTMS 7 (type B)	1.00E-03	6.96E+00	2.92E-02	3.73E+00	15	4.18E-04
68	MAPTMS 5 (type AB)	9.99E-04	6.98E+00	2.92E-02	3.71E+00	45	2.08E-03
69	MAPTMS 5 (type B)	1.00E-03	6.98E+00	2.94E-02	3.72E+00	45	1.05E-03
70	MAPTMS 6 (type AB)	9.93E-04	6.99E+00	5.80E-02	3.71E+00	45	2.57E-03
71	MAPTMS 6 (type B)	9.94E-04	7.02E+00	5.81E-02	3.69E+00	45	1.73E-03
72	MAPTMS 5 (type AB)	9.90E-04	7.00E+00	5.81E-02	3.70E+00	45	2.95E-03
73	MAPTMS 5 (type B)	1.00E-03	7.01E+00	5.88E-02	3.70E+00	45	1.46E-03
74	MAPTMS 7 (type AB)	9.98E-04	7.03E+00	5.84E-02	3.69E+00	45	2.24E-03
75	MAPTMS 7 (type B)	9.99E-04	7.04E+00	5.83E-02	3.68E+00	45	1.63E-03
76	MAPTMS 7 (type AB)	9.91E-04	7.03E+00	8.71E-02	3.69E+00	45	2.62E-03
77	MAPTMS 7 (type B)	9.99E-04	7.03E+00	8.74E-02	3.69E+00	45	1.91E-03
78	MAPTMS 6 (type AB)	9.99E-04	7.00E+00	8.75E-02	3.71E+00	45	3.16E-03
79	MAPTMS 7 (type B)	1.01E-03	7.00E+00	8.82E-02	3.70E+00	45	2.12E-03
80	MAPTMS 5 (type AB)	9.96E-04	7.03E+00	8.76E-02	3.69E+00	45	3.68E-03
81	MAPTMS 5 (type B)	9.97E-04	7.04E+00	8.77E-02	3.68E+00	45	1.70E-03

Table C-4. Reaction conditions at which the CAPTMS catalysts were assessed with the corresponding turnover frequencies

Exp#	Catalyst	C_{amine}(mol/l)	C^0_{ace} (mol/l)	C^0_{benz} (mol/l)	$C^0_{nC_6}$ (mol/l)	Temp (°C)	TOF (s^{-1})
1	CAPTMS 1 (type AB)	9.91E-04	6.97E+00	2.91E-02	3.73E+00	45	2.97E-05
2	CAPTMS 1 (type B)	9.91E-04	7.01E+00	2.90E-02	3.70E+00	45	9.44E-06
3	CAPTMS 2 (type AB)	9.91E-04	7.03E+00	2.93E-02	3.69E+00	45	4.99E-05
4	CAPTMS 1 (type AB)	9.90E-04	6.96E+00	2.92E-02	3.73E+00	45	3.24E-05
5	CAPTMS 1 (type B)	9.90E-04	6.99E+00	2.93E-02	3.71E+00	45	9.67E-06
6	CAPTMS 3 (type AB)	9.92E-04	7.04E+00	2.93E-02	3.69E+00	45	1.90E-05
7	CAPTMS 3 (type B)	9.90E-04	6.99E+00	2.89E-02	3.71E+00	45	1.01E-05
8	CAPTMS 4 (type AB)	9.93E-04	7.03E+00	2.94E-02	3.69E+00	45	1.40E-05
9	CAPTMS 4 (type B)	9.93E-04	6.94E+00	2.92E-02	3.74E+00	45	1.22E-05
10	CAPTMS 2 (type AB)	9.91E-04	7.02E+00	2.93E-02	3.69E+00	45	2.08E-05
11	CAPTMS 2 (type B)	9.90E-04	7.00E+00	2.90E-02	3.71E+00	45	7.08E-06
12	CAPTMS 3 (type AB)	9.91E-04	7.03E+00	2.92E-02	3.69E+00	50	3.43E-05
13	CAPTMS 3 (type B)	9.92E-04	7.00E+00	2.94E-02	3.70E+00	50	1.30E-05
14	CAPTMS 4 (type AB)	9.93E-04	6.96E+00	2.93E-02	3.73E+00	50	1.35E-05
15	CAPTMS 4 (type B)	9.92E-04	7.01E+00	2.90E-02	3.70E+00	50	1.74E-05
16	CAPTMS 1 (type AB)	9.90E-04	6.95E+00	2.92E-02	3.73E+00	45	3.09E-05
17	CAPTMS 1 (type B)	9.90E-04	6.95E+00	2.91E-02	3.73E+00	45	9.46E-06

Table C-5. Reaction conditions at which the PAPTMS catalysts were assessed with the corresponding turnover frequencies

Exp#	Catalyst	C_{amine}(mol/l)	C^0_{ace} (mol/l)	C^0_{benz} (mol/l)	$C^0_{nC_6}$ (mol/l)	Temp (°C)	TOF (s^{-1})
1	PAPTMS 1 (type AB)	1.01E-03	7.01E+00	2.95E-02	3.70E+00	45	7.00E-06
2	PAPTMS 2 (type AB)	1.01E-03	6.96E+00	2.92E-02	3.73E+00	45	4.07E-06

Table C-6. Reaction conditions at which the DEAPTMS catalysts were assessed with the corresponding turnover frequencies

Exp#	Catalyst	C_{amine}(mol/l)	C^0_{ace} (mol/l)	C^0_{benz} (mol/l)	$C^0_{nC_6}$ (mol/l)	Temp (°C)	TOF (s^{-1})
1	DEAPTMS 1 (type AB)	9.92E-01	6.99E+00	2.90E-02	3.71E+00	45	3.89E-05
2	DEAPTMS 1 (type B)	1.00E+00	7.02E+00	2.93E-02	3.70E+00	45	1.19E-05
3	DEAPTMS 2 (type AB)	9.97E-01	6.99E+00	2.92E-02	3.71E+00	45	1.96E-05
4	DEAPTMS 2 (type B)	1.00E+00	7.04E+00	2.93E-02	3.69E+00	45	8.14E-06
5	DEAPTMS 3 (type AB)	9.89E-01	6.99E+00	2.89E-02	3.71E+00	45	1.83E-05
6	DEAPTMS 3 (type B)	9.96E-01	7.04E+00	2.91E-02	3.68E+00	45	1.40E-05
7	DEAPTMS 4 (type AB)	9.94E-01	7.02E+00	2.91E-02	3.69E+00	45	1.39E-05
8	DEAPTMS 4 (type B)	1.00E+00	6.97E+00	2.93E-02	3.72E+00	45	1.28E-05

Table C-7. Reaction conditions at which the SBA catalysts were assessed with the corresponding turnover frequencies

Exp#	Catalyst	C_{amine}(mol/l)	C^0_{ace} (mol/l)	C^0_{benz} (mol/l)	$C^0_{nC_6}$ (mol/l)	Temp (°C)	TOF (s^{-1})
1	SBA-A	1.00E-03	7.00E+00	3.00E-02	3.70E+00	45	2.83E-04
2	SBA-A	1.00E-03	7.00E+00	3.00E-02	3.70E+00	45	2.83E-04
3	SBA-A	1.00E-03	7.00E+00	3.00E-02	3.70E+00	45	2.94E-04
4	SBA-A	3.75E-03	7.00E+00	3.00E-02	3.70E+00	45	1.37E-04
5	SBA-A	3.75E-03	7.00E+00	3.00E-02	3.70E+00	45	1.43E-04
6	SBA-A	3.75E-03	7.00E+00	3.00E-02	3.70E+00	45	1.42E-04
7	SBA-HMDS-A	3.75E-03	7.00E+00	3.00E-02	3.70E+00	45	3.56E-05
8	SBA-HMDS-A	3.75E-03	7.00E+00	3.00E-02	3.70E+00	45	3.65E-05
9	SBA-A-AL	3.75E-03	7.00E+00	3.00E-02	3.70E+00	45	1.88E-04
10	SBA-A-AL	3.75E-03	7.00E+00	3.00E-02	3.70E+00	45	1.93E-04
11	SBA-HMDS-A-AL	3.75E-03	7.00E+00	3.00E-02	3.70E+00	45	1.27E-04
12	SBA-HMDS-A-AL	3.75E-03	7.00E+00	3.00E-02	3.70E+00	45	1.23E-04
13	SBA-A-CA	3.75E-03	7.00E+00	3.00E-02	3.70E+00	45	9.47E-05
14	SBA-A-CA	3.75E-03	7.00E+00	3.00E-02	3.70E+00	45	9.45E-05
15	SBA-HMDS-A-CA	3.75E-03	7.00E+00	3.00E-02	3.70E+00	45	7.80E-05
16	SBA-HMDS-A-CA	3.75E-03	7.00E+00	3.00E-02	3.70E+00	45	7.95E-05
17	SBA-A-PA	3.75E-03	7.00E+00	3.00E-02	3.70E+00	45	7.75E-05
18	SBA-A-PA	3.75E-03	7.00E+00	3.00E-02	3.70E+00	45	7.96E-05
19	SBA-HMDS-A-PA	3.75E-03	7.00E+00	3.00E-02	3.70E+00	45	5.50E-05
20	SBA-HMDS-A-PA	3.75E-03	7.00E+00	3.00E-02	3.70E+00	45	5.63E-05

Table C-8. Reaction conditions at which the organosilica catalysts were assessed with the corresponding turnover frequencies

Exp#	Catalyst	C_{amine}(mol/l)	C^0_{ace} (mol/l)	C^0_{benz} (mol/l)	$C^0_{nC_6}$ (mol/l)	Temp (°C)	TOF (s^{-1})
1	BTEE	1.00E-03	7.00E+00	3.00E-02	3.70E+00	45	1.92E-04
2	BTEB	1.00E-03	7.00E+00	3.00E-02	3.70E+00	45	1.83E-05

Table C-9. Reaction conditions used to investigate the feedstock effects with the corresponding turnover frequencies

Exp#	Catalyst	C_{amine}(mol/l)	C^0_{ace} (mol/l)	C^0_{furf} (mol/l)	C^0_{water} (mol/l)	Temp (°C)	TOF (s^{-1})
1	MAPTMS 8 (type AB)	1.00E-03	1.27E+01	4.13E-02	0.00E+00	60	2.24E-04
2	MAPTMS 8 (type AB)	1.00E-03	1.24E+01	4.97E-02	0.00E+00	80	7.17E-04
3	MAPTMS 8 (type AB)	1.00E-03	1.22E+01	4.90E-02	0.00E+00	90	1.26E-03
4	MAPTMS 8 (type AB)	1.00E-03	1.20E+01	4.85E-02	0.00E+00	100	2.67E-03
5	MAPTMS 8 (type AB)	1.00E-03	1.20E+01	4.33E-01	0.00E+00	90	1.18E-03
6	MAPTMS 8 (type AB)	1.00E-03	1.20E+01	6.88E-01	0.00E+00	90	1.10E-03
7	MAPTMS 8 (type AB)	1.00E-03	1.20E+01	1.15E+00	0.00E+00	90	8.10E-04
8	MAPTMS 8 (type AB)	1.00E-03	1.20E+01	1.47E+00	0.00E+00	90	8.37E-04
9	MAPTMS 8 (type B)	1.00E-03	1.22E+01	4.90E-02	0.00E+00	90	4.12E-04
10	MAPTMS 8 (type B)	1.00E-03	1.20E+01	6.88E-01	0.00E+00	90	4.59E-04
11	MAPTMS 8 (type B)	1.00E-03	1.20E+01	1.47E+00	0.00E+00	90	3.93E-04
12	MAPTMS 8 (type AB)	1.00E-03	1.20E+01	4.90E-02	5.51E+00	80	4.42E-05
13	MAPTMS 8 (type AB)	1.00E-03	1.20E+01	4.90E-02	1.10E+00	90	3.70E-04